

Sheffield Hallam University

Laser ablation for sample introduction in inductively coupled plasma spectrometry.

BOOTH, Peter.

Available from the Sheffield Hallam University Research Archive (SHURA) at:

<http://shura.shu.ac.uk/19368/>

A Sheffield Hallam University thesis

This thesis is protected by copyright which belongs to the author.

The content must not be changed in any way or sold commercially in any format or medium without the formal permission of the author.

When referring to this work, full bibliographic details including the author, title, awarding institution and date of the thesis must be given.

Please visit <http://shura.shu.ac.uk/19368/> and <http://shura.shu.ac.uk/information.html> for further details about copyright and re-use permissions.



7 OCT 17.59
1/2/95 17.03
~~17/3/95 - 17.59~~

Sheffield City Polytechnic Library

REFERENCE ONLY

ProQuest Number: 10694249

All rights reserved

INFORMATION TO ALL USERS

The quality of this reproduction is dependent upon the quality of the copy submitted.

In the unlikely event that the author did not send a complete manuscript and there are missing pages, these will be noted. Also, if material had to be removed, a note will indicate the deletion.



ProQuest 10694249

Published by ProQuest LLC (2017). Copyright of the Dissertation is held by the Author.

All rights reserved.

This work is protected against unauthorized copying under Title 17, United States Code
Microform Edition © ProQuest LLC.

ProQuest LLC.
789 East Eisenhower Parkway
P.O. Box 1346
Ann Arbor, MI 48106 – 1346

**LASER ABLATION FOR SAMPLE INTRODUCTION IN
INDUCTIVELY COUPLED PLASMA SPECTROMETRY**

by

PETER BOOTH BSc

A thesis submitted to the Council for National Academic Awards in partial fulfilment of the requirements for the degree of Doctor of Philosophy.

Sponsoring Establishment:

Sheffield City Polytechnic

Collaborating Establishment: Ministry of Defence

RARDE

Fort Halstead

Kent

November 1991

SUMMARY

LASER ABLATION FOR SAMPLE INTRODUCTION IN INDUCTIVELY COUPLED PLASMA SPECTROMETRY

Peter Booth

The aim of this research was to investigate laser ablation as a means of sample introduction for the Inductively Coupled Plasma (ICP). This involved the configuration of an ICP spectrometer, a laser and a novel laser ablation chamber. The latter offered the facility of electrothermally heating samples before or during laser ablation.

Several operating conditions associated with the ablation process were investigated and optimised. These optimisation studies utilised a variety of metallurgical materials. It was found that the Q-Switched mode of laser operation provided greater sensitivity than long pulsed operation.

This research reports the first laser ablation ICP studies on paints and polymers. Ablation of paints was found to provide good precision. This was attributed to a combination of homogeneity and viscosity effect. Operating conditions associated with the ablation process were again examined and found to be independent of sample type.

Calibration studies were performed using laser ablation of synthetic aqueous standards. This research includes the first reports of such an approach to calibration. The wide dynamic range associated with conventional ICP was also evident for laser ablation. Calibration followed by analysis of samples provided semi-quantitative data for paints and polymers. Limits of detection were inferior to solutions nebulisation ICP.

"The whole of science is nothing more than a
refinement of everyday thinking"

Albert Einstein, "Out of my Later Years",
Chapter 12, Thames & Hudson, London, 1950.

ACKNOWLEDGEMENTS

I would like to extend thanks to my supervisor Dr.C.W.McLeod whose guidance and encouragement were invaluable, particularly during the first eighteen months of this research project.

Thanks to Mr.T.Heron and the Ministry of Defence for sponsoring the project and for the award of a studentship. To Mr.B.Didsbury of Sheffield City Polytechnic for machining of all graphite components and constructing the laser ablation chamber.

Finally, a special thank you must go to Sue for all the time and effort spent at a word processor deciphering my writing and putting it into an acceptable format.

CONTENTS

Chapter One

Emission Spectroscopy and the Inductively Coupled Plasma

		Page
1.0	Historical	2
1.1	Quantum Theory and Spectroscopy	10
1.1.1	The Hydrogen Atom	13
1.1.2	Wave Mechanics	18
1.1.3	Quantum Numbers	22
1.1.4	The Periodic Table	25
1.1.5	Energy Levels and Spectra of Atoms	27
1.1.6	Excitation of Line Spectra	38
1.2	The Inductively Coupled Plasma (ICP)	44
1.2.1	ICP Generation	47
1.2.2	Plasma Temperatures	53
1.2.3	Excitation Mechanisms	59
1.2.4	Spectroscopic Detection	62
1.2.5	Performance Characteristics	64
1.2.6	Sample Introduction	68

Chapter Two

The Principles and Applications of Lasers

2.0	Historical	98
2.1	Laser Principles	100
2.1.1	Population Inversion	103
2.1.2	Optical Pumping	108
2.1.3	Optical Feedback	112
2.2	Properties of Laser Radiation	121
2.2.1	Radiance	121
2.2.2	Monochromaticity	123
2.2.3	Laser Modes	127
2.2.4	Divergence	129
2.2.5	Coherence	131
2.2.6	Focusing	137
2.2.7	Q-switching	138
2.3	Laser Applications	143
2.3.1	Metrological Applications	146

		Page
2.3.2	Materials Processing Applications	150
2.3.3	Miscellaneous Applications	153
2.3.4	Lasers in Analytical Spectroscopy	156

Chapter Three

Experimental Instrumentation

3.0	The Laser	167
3.1	Optics	176
3.2	Durr-Jobin Yvon 38-48 ICP	178
3.3	Jarrell Ash ICAP 9000	189
3.4	Laser Ablation Chamber	206
3.5	Perkin-Elmer HGA-2100	211
3.6	Laser Safety	214

Chapter Four

Studies with Metallurgical Samples

4.0	Introduction	217
4.1	Preliminary Studies	218
4.1.1	Laser Sampling	218
4.1.1.1	Experimental	218
4.1.1.2	Observations	219
4.1.1.3	Results	220
4.1.1.4	Discussion	225
4.1.2	Preparation for Laser Ablation Studies	230
4.1.3	Feasibility Studies	231
4.1.3.1	Iron in Stainless Steel	231
4.1.3.2	Chromium in Stainless Steel	232
4.1.3.3	Lens Damage	235
4.1.3.4	Discussion	235
4.2	Experimental (Jobin-Yvon 38-48)	238
4.2.1	Materials	238
4.2.2	Apparatus	238
4.2.3	Spectrometer Resolution	239
4.2.4	Electrothermal Melting	241
4.2.5	The Effects of Laser Focusing	244
4.2.5.1	Results	247

		Page
4.2.5.2	Discussion	248
4.2.6	The Effect of Ablation Period	254
4.2.6.1	Results	255
4.2.6.2	Discussion	256
4.2.7	The Effect of Laser Operating Mode	259
4.2.7.1	Results	259
4.2.7.2	Discussion	261
4.2.8	Conclusions	262
4.3	Experimental (Jarrell Ash ICAP-9000)	265
4.3.1	Materials	265
4.3.2	Apparatus	267
4.3.3	Electrothermal Pretreatment	267
4.3.3.1	Results	268
4.3.3.2	Discussion	268
4.3.4	Melting and Ablation Time Studies	272
4.3.4.1	Results	273
4.3.4.2	Discussion	280
4.3.5	The Effect of Ablation Period	282
4.3.5.1	Results	283
4.3.5.2	Discussion	283
4.3.6	Analyte Erosion	293
4.3.6.1	Results	293
4.3.6.2	Discussion	293
4.4	Concluding Remarks	297

Chapter Five

Studies with Polymeric Samples

5.0	Introduction	299
5.1	Preparation of Paint Samples	301
5.1.1	Electrothermal Drying	301
5.1.2	Direct Measurement	302
5.1.3	Conclusions	307
5.2	Experimental (Paints)	313
5.2.1	Materials	313
5.2.2	Apparatus	313
5.2.3	The Effect of Laser Focusing	313
5.2.3.1	Results	315

	Page	
5.2.3.2	Discussion	322
5.2.4	The Effect of Ablation Period	324
5.2.4.1	Results	325
5.2.4.2	Discussion	329
5.2.5	The Effect of Laser Lamp Energy	331
5.2.5.1	Results	332
5.2.5.2	Discussion	333
5.2.6	The Effect of Carrier Gas Flow	333
5.2.6.1	Results	337
5.2.6.2	Discussion	340
5.2.7	Precision Studies	341
5.2.7.1	Results	342
5.2.7.2	Discussion	343
5.2.8	Comparative Studies	343
5.2.8.1	Results	344
5.2.8.2	Discussion	344
5.2.9	Concluding Remarks	347
5.3	Experimental (Polymers)	350
5.3.1	Materials	350
5.3.2	Apparatus	351
5.3.3	The Effect of Laser Mode	351
5.3.3.1	Results	351
5.3.3.2	Discussion	353
5.3.4	Precision Study	356
5.3.4.1	Results	356
5.3.4.2	Discussion	356
5.3.5	Comparative Studies	358
5.3.5.1	Results	358
5.3.5.2	Discussion	360
5.3.6	An Application	360
5.3.6.1	Results	362
5.3.6.2	Discussion	362
5.4	Concluding Remarks	364

Chapter Six

Laser Ablation of Aqueous Solutions and Calibration Studies

6.0	Introduction	366
-----	--------------	-----

		Page
6.1	Calibration Studies	367
6.1.1	The Effect of Ablation Period	369
6.1.1.1	Results	370
6.1.1.2	Discussion	371
6.1.2	Simple Two Point Calibration	373
6.1.2.1	Results	374
6.1.2.2	Discussion	378
6.1.3	Further Calibration Studies	380
6.1.3.1	Results	381
6.1.3.2	Discussion	390
6.1.4	Precision Study	392
6.2	Laser Ablation and ETV Studies	397
6.2.1	Results	399
6.2.2	Discussion	408

Chapter Seven

Conclusions and Future Work

7.0	Conclusions and Future Work	410
-----	-----------------------------	-----

CHAPTER ONE

EMISSION SPECTROSCOPY AND THE INDUCTIVELY COUPLED PLASMA

1.0 HISTORICAL

Before Newton's investigation of the nature of light, colour was thought to be a property of surfaces of objects. Light was considered to be white or without colour. From his experiments with prisms and sunlight described in his "Opticks", Newton concluded that colour was in the illuminating light, not in reflecting surfaces. He observed a smoothly merging spectrum of colours, but what he did not observe or at least did not report, were the discontinuities in the spectrum. This has puzzled modern scientists [1] who have duplicated Newton's experiments as well as possible and found the discontinuities - now known as the Fraunhofer lines - to be clearly visible. It is assumed that Newton's aperture had been too large or that he did not report the phenomenon because he was unable to explain it.

When considering the nature of light, Newton paid little attention to the study of flames. In 1752 Thomas Melvill [2] examined flames produced by spirits mixed with nitre, sea salt or other materials, by means of a prism illuminated through a circular aperture. Melvill wrote, "Because the hole appears thro' the prism quite circular and uniform in colour; the bright yellow which prevails so much over the other colours, must be of one determined degree of refrangibility; and the transition from it to the fainter colour adjoining, not gradual, but immediate." Had he used

a slit aperture and not died in the following year, emission spectra from flames may have been discovered much earlier than they were.

In 1802 Wollaston [3] repeated Newton's experiments and observed dark, irregularly spaced lines in the sun's spectrum. These were almost certainly what were to become the Fraunhofer lines, now known to be due to atomic absorption. At about this time Dolland constructed the first achromatic lens and Young and Fresnel demonstrated diffraction and interference by means of an assemblage of narrow slits. Consequently the equipment available for the study of the sun's spectrum was vastly improved. In 1814, Fraunhofer utilised these improvements when constructing the first spectroscopy. He used this instrument to map approximately 600 dark lines in the sun's spectrum and assigned letters of the alphabet to the most prominent. He also recognised the doublet nature of the sodium D line. This was published in 1817 [4].

Wollaston's observations were of sunlight using a prism. When he examined candle-light he observed a bright yellow line and a series of five broad images of different colours, these were the sodium doublet and the Swan C_2 bands. Wollaston was also aware that the spectrum extended into the ultra-violet and that this could be shown by the effect on silver chloride. The origin of atomic emission and atomic absorption studies can be considered to have been in 1802 although

the significance of the findings was not fully appreciated.

In 1826 Talbot [5] almost related the yellow colour of flames to the presence of sodium, but he did not realise how sensitive the test was. Discussing the light from the Brewster [6] alcohol flame, Talbot wrote, "But the most remarkable quality of this light is its homogeneity, which is perfect as far as I have been able to ascertain. I speak of the yellow rays which form the mass of the light and quite overpower the feeble effect of the blue and the green. The origin of this homogeneous light appears to be difficult to explain. I have found that the same effect takes place whether the wick of the lamp is steeped in the muriate, sulphate or carbonate of soda, while the nitrate, chlorate, sulphate and carbonate of potash agree in giving a blueish-white tinge to the flame. Hence the yellow rays may indicate the presence of soda, but they, nevertheless, frequently appear where no soda can be supposed to be present." Talbot concluded his paper, "If this opinion should be correct and applicable to other definite rays, a glance at the prismatic spectrum of a flame may show it to contain substances, which it would otherwise require a laborious chemical analysis to detect."

In 1860, Bunsen and Kirchhoff using an improved spectroscope showed that the lines in spectra were fixed, enabling identification of the rays. They also

showed that spectral lines did not change when different compounds of a metal were used and concluded that they were due to cations not anions. The discovery of the elements caesium and rubidium soon followed this work. In a letter to Sir Henry Roscoe, Bunsen explained that he had called the element caesium from the Latin caesius (blue) due to "the splendid blue line in its spectrum" [7]. The advances made by Bunsen and Kirchhoff may be considered as the birth of chemical analysis by observation of a flame and soon practical applications began to appear in the literature. Simmler [8] considered the determination of alkali and alkaline earth metals in Swiss rocks, minerals, waters and wine. Champion [9] determined the levels of sodium in plant ashes.

In the late 19th century several advances in spectroscopy occurred. In 1869 Angstrom mapped about 1000 lines in the solar spectrum and assigned them wavelengths in terms of the standard meter. In 1879 Gouy [10] addressed the irreproducibility of sample introduction and developed the first pneumatic nebuliser which was the prototype of those used in modern instruments. In 1880 dry photographic plates became available and practical spectrography became possible although analytical flames were limited to the alkali and alkaline earth elements. In 1882 Rowland produced the first high quality grating surpassed only by today's interferometric gratings.

After investigation of the emission spectrum of H_2 in 1885, Balmer reported the first indication of regularity. Adopting improved wavelength measurements made by Angstrom, he was able to derive a simple formula which allowed prediction of the wavelengths of the lines in the spectrum. The search for regularity continued and it was found that the spectra could be arranged in series which were given the names, "principal", "sharp", "diffuse" and "fundamental" according to their supposed appearance. This nomenclature is still used, the letters S,P,D and F being used to denote series of energy levels.

Until 1913 there was no explanation of how atomic spectra were produced, but this was to change when Bohr proposed his model for atomic theory. The model incorporates Plank's theory that energy is absorbed and emitted in discrete quanta. Bohr's model assumes a positively charged nucleus around which negatively charged electrons rotate in fixed circular orbits. If the atom absorbs energy, an electron is driven to an orbit of greater radius. As the electron falls back to its original or ground state the absorbed energy is emitted. As this emitted energy is fixed, the orbits between which excitation and relaxation occur must also be fixed. Hence the energy of the spectral line is equal to the energy difference of the two states involved.

This work catalysed a great deal of understanding in atomic structure; selection rules for the emission of allowed and forbidden lines were announced; rules for the intensity relations of spectral lines were formulated; the energy states of the known elements were determined; energy data were collected. Such work also led to chemists having a fundamental physical explanation of the Periodic Table.

From 1928 onwards Lundegardh [11,12,13] developed the first methods of quantitative analysis. He used a microphotometer to measure spectral line density, and appears to have been the first to realise the value of such measurements. He also made the first allowance for background density by using the ratio of galvanometer deflections for the line plus background and background only. An air-acetylene flame replaced air-coal gas flames and the number of elements determinable rose to 40, and improvements in photographic emulsions allowed ultra-violet lines such as those of copper and magnesium to be recorded. Lundegardh was the first to use a photoelectric flame photometer using a vacuum photocell. This suffered from the rudimentary amplification then available and stability was difficult to achieve.

Over the next 10 years a variety of developments were made. Monochromators were used [14], new nebuliser and burner designs arose [15], multiple filters capable of isolating narrow spectral bands [16] became available. It was at about this time that the first commercial

filter flame photometers became available. They were used mainly for the determination of potassium but the use of interference filters allowed the determination of all the alkali and alkaline earth elements [17].

Instruments at this time were single-channel models but Ivanov [18] placed a number of filter photometers around a single flame thus creating a multi-channel instrument which allowed internal standardisation and background correction. The first multi-element direct reading instrument was the Lundegardh Robot [19] built in 1940 and based on a spectrographic process. This instrument was also well advanced in terms of automation. The film was automatically developed and scanned in a simple built in microphotometer and sample feed was via a conveyer belt.

Burners and nebulisers followed Lundegardh's design until Barnes [20] used a Meker type burner with indirect sample introduction. Sheathed flames were used [21] to create the fuel rich, reducing conditions required for certain metals normally occurring as oxides. Work with reducing flames was pioneered by several workers [22,23]. It was realised very early that expansion chambers and baffles removed large aerosol droplets and so reduced interference due to compound formation. Rauterberg [24] introduced a baffle directly in front of the nebuliser nozzle which is widely used in modern instruments. A variety of other nebulisation devices have been used such as an electrostatic

nebuliser [25] and an ultrasonic nebuliser [26], but pneumatic nebulisation remains the most popular.

Atomic flame spectroscopy was at this position when in 1955 Walsh [27] and Alkemade [28] independently realised the analytical potential of absorption by neutral atoms in the flame. It was recognised that most elements existing as free atoms in the flame could be determined this way, provided sources of high intensity and narrow line width were available. Walsh noted that the hollow cathode lamp provided such a source. Soon methods had become available for elements not determinable by flame emission, largely because the flame does not provide sufficient energy for emission of lines much shorter than magnesium at 285.2nm. In atomic absorption excellent sensitivity is obtained at the resonance line for zinc at 213.8nm. Consequently, atomic absorption soon became the preferred method.

Today, spectroscopy is an area of high technology which utilises quality optics, electronics and computer systems. It is very widely used in areas such as minerology, metallurgy, archaeology, forensic science, medicine, defence and the determination of a wide range of sample types.

1.1 QUANTUM THEORY AND SPECTROSCOPY

The experiments described earlier, observing the solar spectrum, clearly showed atomic absorption of radiation due to elements present in the sun's atmosphere. Similarly, examination of a flame produced an emission spectrum characteristic of elements in the flame. Emission spectra are generally more complex than absorption spectra, but many lines have a common wavelength and appear in both. To understand how these spectra arise it is necessary to have a clearer understanding of the nature of light.

Light has several wave-like properties; it can be diffracted and interference patterns can be produced. Also different colours correspond to different wavelengths hence different frequencies, the two being related by;

$$\text{WAVELENGTH X FREQUENCY} = \text{VELOCITY}$$

$$\lambda \quad \times \quad \nu \quad = \quad c$$

Wavelength and frequency are clearly wave-like properties of light, but at the turn of the century some experiments suggested that light also had particle-like properties.

If a metal M is placed in an evacuated chamber with a plate P which is maintained at a slight positive potential relative to M, and a gap between M and P prevents the completion of an electrical circuit, no

current flows. If ultraviolet (UV) radiation is focused onto M it is found that electrons flow from M to P and a current is detected. Importantly, current flows only if the frequency of the UV exceeds a certain threshold value specific to the metal. This is known as the Photoelectric Effect.

This phenomenon can only be explained by a particle theory of light, it consisting of a stream of particles called photons. Each photon has an energy E and frequency ν related by;

$$E = h\nu$$

where h is Plank's constant (6.626176×10^{-34} J.s)

The amount of energy required to remove one electron from the metal is called the "work function", and the magnitude of the work function varies from metal to metal. Einstein suggested that an electron could only leave the metal if the energy of the incident photon exceeded the work function. This implies that a single quantum of energy must be transferred to a single electron. Clearly, if the frequency of the photon is too low the photo-electric effect will not occur. The important point is that one electron is emitted by the action of one incident photon.

This conflicting evidence as to the nature of light was compounded by Compton. He demonstrated that it was possible to scatter electrons with a beam

of X-rays and that the laws of conservation of energy and momentum held during the process, as they should for the collision of particles. He also showed that in a scattering experiment, momentum was transferred in discrete amounts not continuously. Consequently, light is considered to exhibit wave-particle duality.

When considering the absorption and emission of light by atoms, light is regarded as a stream of photons. An atom can only absorb particular wavelengths of light which correspond to a particular photon energy. Consequently, the atom can exist in a number of well defined energy states. Normally, an atom exists in a state of lowest energy, the ground state. If the atom absorbs a photon, it jumps to a higher energy state or excited state and the energy of the photon is equal to the energy difference of the ground and excited states involved. The absorption spectrum therefore contains lines of particular wavelengths which correspond to the atomic energy transition's involved.

In the case of emission, the atoms are raised to various excited states using a flame for example. The atoms may lose their energy, or relax, by emitting photons. If an atom emits a photon and in so doing returns to the ground state then the emission line produced in the spectrum will correspond to an absorption line. Atoms may, however, relax to intermediate energy levels before finally falling to the ground state.

In this case the emission line would not correspond to a line in the absorption spectrum.

1.1.1 The Hydrogen Atom

The emission spectrum of hydrogen gas consists of several series of lines. One series, called the Balmer series after its discoverer, lies in the visible region. Other series lie in the ultraviolet (Lyman series) and the infrared (Paschen, Brackett and Pfund series).

It was shown that all the emission lines in all the series could be fitted to a general formula;

$$E = hv = R \left(\frac{1}{n_1^2} - \frac{1}{n_2^2} \right) \quad (1.1)$$

where R is the Rydberg constant, v is the frequency and n_1 and n_2 are both integers. For a given series n_1 is a constant; in the Lyman series $n_1 = 1$ and in the Paschen series $n_1 = 3$. As n_2 increases the separation between transition lines decreases as the frequency corresponding to the series limit is approached. In principle an infinite number of lines lie at the series limit. This point also corresponds to the ionisation potential and is given by;

$$E = hv = \frac{R}{n_1^2} \quad (1.2)$$

Equation (1.1) describes the energy involved in a transition from n_1 to n_2 and is easily rearranged to give the frequency (ν) of the photon emitted which was the experimental observation Bohr made.

Bohr explained equation (1.1) in terms of a simple model based on three postulates;

- (i) The electron in the hydrogen atom moves in a circular orbit around the positive nucleus.
- (ii) Only certain discrete orbits are allowed and the electrons do not emit radiation when they are in these orbits.
- (iii) A single photon is emitted or absorbed when an electron passes from one allowed orbit to another.

Bohr's postulations seemed arbitrary at the time particularly the second which is contrary to classical theory. An orbiting electron is continuously accelerating towards the nucleus and according to classical electrodynamics should radiate and lose energy. Bohr's success was that he made his model quantitative, and obtained agreement with experimental observations.

If an electron of mass m and velocity v rotates about the nucleus in an orbit of radius r , then the force required to maintain that orbit is,

$$\frac{mv^2}{r} \quad (1.3)$$

This force arises from the electrostatic attraction between the electron and proton, hence;

$$\frac{e^2}{4\pi\epsilon_0 r^2} = \frac{mv^2}{r} \quad (1.4)$$

Where e is the charge of the proton and ϵ_0 is the permittivity of a vacuum.

Bohr made the revolutionary assumption that the angular momentum of the electron (mvr) could only have certain values and that it was quantised in units of $h/2\pi$ where h is Plank's constant.

Thus,

$$mvr = \frac{nh}{2\pi} \quad n = 1, 2, 3, \dots \quad (1.5)$$

Equations (1.4) and (1.5) may be combined to give a value of r ;

$$r = \frac{\epsilon_0 n^2 h^2}{\pi m e^2} \quad (1.6)$$

Equation (1.6) gives a value r for the ground state ($n = 1$) of 0.052917nm. This is in very good agreement with viscosity measurements of hydrogen gas which show that the H_2 molecule has a diameter of about 0.1nm. This value of r became the Bohr radius a_0 .

Even more notable is the expression for frequencies of the lines in the H atom spectrum. The energy E of the atom is given by;

$E = \text{Kinetic energy} + \text{potential energy}$

$$E = \frac{mv^2}{r} - \frac{e^2}{4\pi\epsilon_0 r} \quad (1.7)$$

Combining equations (1.4) and (1.7);

$$\begin{aligned} E &= \frac{e^2}{8\pi\epsilon_0 r} - \frac{e^2}{4\pi\epsilon_0 r} \\ &= - \frac{e^2}{8\pi\epsilon_0 r} \\ &= - \left(\frac{me^4}{8\epsilon_0^2 h^2} \right) \times \frac{1}{n^2} \\ &= - (\text{constant}) \times \frac{1}{n^2} \end{aligned}$$

Thus the energy emitted in a transition from state n_1 to n_2 is;

$$\Delta E = E_2 - E_1 = hv = \text{constant} \times \left(\frac{1}{n_1^2} - \frac{1}{n_2^2} \right) \quad (1.8)$$

The value of the constant in equation (1.8) may be calculated using the known values of m, e and h . It is found that this constant equals the Rydberg constant almost exactly!

The electron rotates about the common centre of gravity of the electron and proton, and this can

be taken into account by replacing the electron mass by the reduced mass u ;

$$u = \frac{M \times m}{M + m}$$

where M is the mass of the proton. This brings the agreement between the experimental and calculated Rydberg constants to better than 1 part in 10^4 .

In Bohr's theory there is a single quantum number which quantises angular momentum (n);

$$mvr = \frac{nh}{2\pi}$$

and energy;

$$E = - \frac{R}{n^2}$$

The theory had considerable success with a one electron system but failed with more complicated ones such as the alkali metal spectra. The whole theory was too arbitrary and the work of Heisenberg led to Bohr's theory being discarded. Heisenberg's Uncertainty Principle showed that it was not possible in principle to know simultaneously the position and momentum of an electron with complete accuracy. This was a direct contradiction of Bohr's theory.

Wave mechanics takes into account the work of Heisenberg and may be used to describe the spectra of all atoms. This is the basis of the new Quantum Theory.

1.1.2 Wave Mechanics

The Schrodinger wave equation given in 1926 ascribes wave-like properties to electrons and may be regarded as the basis of modern quantum theory. It is commonly written as;

$$\frac{1}{2} \left(\frac{\partial^2}{\partial x^2} + \frac{\partial^2}{\partial y^2} + \frac{\partial^2}{\partial z^2} \right) \Psi + (E-V) \Psi = 0 \quad (1.9)$$

It is possible to give some form of rationale to this equation which follows on from some of the work involved in the Old Quantum Theory.

Plank related the energy E of a photon to a wave-like property, frequency ν ;

$$E = h\nu$$

Einstein's work on relativity produced the well known equation;

$$E = mc^2$$

relating energy to particle-like properties mass m, and velocity c.

De Broglie in 1924 combined these properties and obtained;

$$h\nu = mc^2$$

Since momentum $p = mc$ and $\nu = c/\lambda$;

$$p = h/\lambda$$

where the momentum p is a particle property and wavelength λ is a wave property.

To obtain the common form of the Schrodinger equation consider the equation for a simple standing wave,

$$\Psi = A \sin 2\pi x/\lambda$$

Where Ψ is the property whose value changes with distance x in a wave-like manner. A is the amplitude. Differentiating twice;

$$\frac{d\Psi}{dx} = \frac{2\pi}{\lambda} A \cos 2\pi x/\lambda$$

and,

$$\frac{d^2\Psi}{dx^2} = -\frac{4\pi^2}{\lambda^2} A \sin 2\pi x/\lambda = -\frac{4\pi^2}{\lambda^2} \Psi$$

The Kinetic energy T of a particle of mass m and velocity c is given by;

$$T = \frac{1}{2} mc^2 = \frac{1}{2m} p^2$$

Using the De Broglie equation;

$$T = \frac{1}{2m} \cdot \frac{h^2}{\lambda^2}$$

And therefore;

$$\frac{d^2\psi}{dx^2} = - \frac{8\pi^2 m \cdot T \cdot \psi}{h^2} \quad (1.10)$$

If the particle has potential energy V, then its total energy $E = T + V$. Schrodinger postulated that for a system that does not change with time, the kinetic energy T in equation (1.10) could be replaced by (E-V). Hence the Schrodinger equation for one dimension may be written;

$$\frac{d^2\psi}{dx^2} + \frac{8\pi^2 m}{h^2} (E-V) \psi = 0$$

and in three dimensions;

$$\frac{\partial^2\psi}{\partial x^2} + \frac{\partial^2\psi}{\partial y^2} + \frac{\partial^2\psi}{\partial z^2} + \frac{8\pi^2 m}{h^2} (E-V) \psi = 0$$

This may be simplified by using atomic units. The mass m and electronic charge e are put to unity

and the unit of length is chosen to be the Bohr radius a_0 . In these units $h = 2\pi$. If double differentiation with respect to each of the three co-ordinates is denoted by ∇^2 , the equation becomes;

$$\frac{1}{2} \nabla^2 \Psi + (E-V) \Psi = 0$$

which is the form given in equation (1.9). ∇^2 is the Laplacian operator.

The quantity Ψ is called the wave function and the value Ψ^2 is considered as a probability. For a single particle system, $\Psi^2 dx$ is the probability of finding the particle in the region defined by dx .

This interpretation allows Heisenbergs Uncertainty Principle to be incorporated into the new quantum theory.

The wave function has three conditions which must be applied to it; Ψ must always be finite at any point - if it were infinite at any point in space, this would correspond to a certainty of finding the particle there, which would conflict with the Uncertainty Principle; Ψ must be single valued at any point in space and must be continuous.

Solution of the Schrodinger wave equation for a spherically symmetrical system such as the hydrogen atom gives rise to three quantum numbers. Each quantum number is related to one of the three polar co-ordinates required to define a point on a sphere. The quantum numbers so derived are n , the principle quantum number,

l the azimuthal quantum number and m_l the magnetic quantum number.

1.1.3 Quantum Numbers

It has been shown that wave functions can be obtained for the electron in a hydrogen atom and that the hydrogen atom wave functions require three quantum numbers n, l and m_l to describe them. These wave functions are often called orbitals.

The quantum number n is called the principle quantum number. It corresponds exactly to Bohr's n given in his theory;

$$E_n = - R/n^2$$

The quantum number l is called the azimuthal quantum number. It may have a maximum value of $(n-1)$. All integral values of l from 0 to $(n-1)$ are allowed. This quantum number also specifies the orbital angular momentum of the electron p_e ;

$$p_e = \sqrt{l(l+1)} h/2\pi$$

Thus angular momentum is quantised as well as energy.

For historical reasons electrons with values of $l = 0, 1, 2, 3, 4$ are designated s, p, d, f and g. Hence, if an electron is in an orbital $n=2$ and $l=1$ it is called a 2p electron; if $n=2$ and $l=2$ it is called a 2d electron.

The third quantum number m_l is called the magnetic quantum number and refers to the orientation of an orbital. It specifies the component of the angular momentum in a particular direction. m_l can have integral values of $-l, (-l + 1) \dots (l-1)$, and thus has $(2l + 1)$ values.

It has been shown that the number of quantum numbers required is equal to the number of dimensions in the problem. One might assume therefore, that the three quantum numbers described are sufficient for the three dimensional hydrogen atom. In Einsteins celebrated work on relativity, time became the fourth dimension. He showed that four quantum numbers were needed.

The need for a fourth quantum number was realised experimentally rather than from theory and Uhlenbeck and Gaudsmit introduced the electron spin angular momentum s . s has the value;

$$s = \sqrt{\frac{1}{2}(\frac{1}{2}+1)} h/2\pi$$

and can have components of this intrinsic angular momentum as it spins about its own axis, given by the fourth quantum number $m_s = \pm \frac{1}{2}$ corresponding to the two possible directions of spin. With the extra quantum number m_s , the total angular momentum can take two possible values $(l + \frac{1}{2})$ and $(l - \frac{1}{2})$.

The Schrodinger equation does not account for electron-electron repulsions in polyelectronic systems.

Consequently, it may only be used analytically for systems having one nucleus and one electron, ie hydrogen-like atoms.

For polyelectronic atoms it is necessary to make the so-called "orbital approximation" to understand electronic structure. This involves considering the wave function of the atom as a product of orbitals or functions which apply individually to each of the electrons. Each electron then has its own set of four quantum numbers n, l, m_l and m_s .

One more point must be considered before the electronic structure of polyelectronic atoms may be rationalised. This is the Pauli Principle. In its simplest form this principle states that, "No two electrons in the same atom may have the same set of all four quantum numbers". The square of the wave function Ψ^2 is a probability function describing the probability of locating an electron at a particular point in space. If electrons are labelled 1,2,3...n and then the labels are exchanged, the electron density cannot change if electrons are all identical particles. Therefore, Ψ^2 must be invariant to changes of labelling the electrons, and therefore Ψ must either remain the same or merely change sign. It is universal in nature that particles with spin $\frac{1}{2}$, such as electrons, behave such that interchange of identical particles causes the wave function to change sign. This is called antisymmetric behaviour.

The Pauli Principle may now be more fundamentally stated, "Wave functions must be antisymmetric with respect to interchange of electrons". If there is one quantum number different between two electrons, then it is always possible to form a wave function that satisfies the Pauli Principle.

1.1.4 The Periodic Table

It is now possible to consider the electronic structures of all ground state atoms. The hydrogen atom has a single electron in the 1s orbital. Proceeding to helium, the nuclear charge increases by one and the total number of electrons becomes two. The second electron occupies the same 1s orbital but has opposite spin thus satisfying the Pauli Principle. The configuration of H is 1s and of He is 1s².

In He the 1s orbital is full so the extra electron in the Li atom must occupy an orbital with n = 2. This is a 2s orbital and Li has the configuration 1s²2s. The first ten elements in the periodic table have the following configurations;

H	1s	C	1s ² 2s ² 2p ²
He	1s ²	N	1s ² 2s ² 2p ³
Li	1s ² 2s	O	1s ² 2s ² 2p ⁴
Be	1s ² 2s ²	F	1s ² 2s ² 2p ⁵
B	1s ² 2s ² 2p	Ne	1s ² 2s ² 2p ⁶

The order in which the sub-levels are filled is given by Hund's rule which states that the electrons shall have as many parallel spins as the Pauli Principle allows. Thus the quantum numbers of the seven electrons in the nitrogen atom may be assigned;

n	l	m_l	m_s
1	0	0	$\frac{1}{2}$
1	0	0	$-\frac{1}{2}$
2	0	0	$\frac{1}{2}$
2	0	0	$-\frac{1}{2}$
2	1	-1	$\frac{1}{2}$
2	1	0	$\frac{1}{2}$
2	1	+1	$\frac{1}{2}$

The most important point is that the electrons occupy the orbitals of lowest energy compatible with the Pauli Principle. Orbitals usually have the following energy sequence;

$$1s < 2s < 2p < 3s < 3p < 4s < 3d < 4p < 5s < 4d < 5p < 6s < 4f$$

The 1s level accounts for the electronic configurations of H and He. The first period of the Periodic Table, from Li to Ne, involves filling the 2s and 2p orbitals, and similarly the third period involves 3s and 3p orbitals. When the 4s orbital has been filled, the lowest energy orbital unfilled becomes the 3d. This corresponds to the transition metals

and the filling of the 4f orbital accounts for the lanthanides.

The Schrodinger equation and relativity gave rise to four quantum numbers which describe the periodic Table. They also account for the shapes of orbitals and electron configurations. The latter helps to rationalise much of the basic chemistry and physics of the elements.

1.1.5 Energy Levels and Spectra of Atoms

It has been shown that wave mechanics and the four quantum numbers provide an explanation of the spectra of single electron systems. Polyelectronic systems require more detail. The energies and angular momenta of the individual electrons must be considered but so must the energy and angular momenta of the atom as a whole. It is necessary to consider the coupling of angular momenta, either orbital angular momentum l , or spin angular momentum s . Since l and s are quantised it is necessary for the resultant to be quantised.

The different energy levels of an atom arise primarily because of the different electrostatic energies of the various electronic configurations. There are also magnetic effects which arise due to the motions of the electrons. In Russell-Saunders coupling the magnetic effects are regarded as being of secondary importance, as a first approximation.

For Russell-Saunders coupling there are a series of rules:

- (i) The individual spin angular momenta s_i combine to give a resultant S which must be either integral or half-integral.

Therefore;

$$\sum s_i = S$$

and for two electrons $S = 1$ or 0 . Two spins of $\frac{1}{2}$ couple to produce $S = 1$ but if they have opposite spins then $S = 0$.

- (ii) The individual orbital angular momenta of the electrons l_i (each of which may be $0, 1, 2, 3, \dots$ for s, p, d, f electrons) combine to give a resultant L which must be quantised $L = 0, 1, 2, 3, \dots$. Therefore;

$$\sum l_i = L \quad L = 0, 1, 2, 3, \dots$$

referred to as S, P, D, F, \dots

- (iii) An orbiting electronic charge produces a magnetic field perpendicular to the plane of the orbit, so both the total orbital angular momentum L and the total spin angular momentum S have corresponding magnetic field vectors. Consequently, L and S can interact magnetically to give

a total angular momentum J. J is quantised in units of $h/2\pi$ and may have integral or half-integral values.

Therefore;

$$J = (L + S), (L + S - 1) \dots (L - S).$$

It was shown earlier that the work of Balmer produced the following equation;

$$E = hv = \frac{R}{n_1^2} - \frac{R}{n_2^2}$$

this may be written as:

$$hv = T_1 - T_2$$

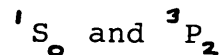
where it is understood that these "terms" represent different energy levels. The word "term" is frequently used for an energy level and the name or label of an atomic energy level is called a "term symbol".

Each term of an atom is described by its quantum numbers L, S and J. The notation used is;

$$^{2S+1}L_J$$

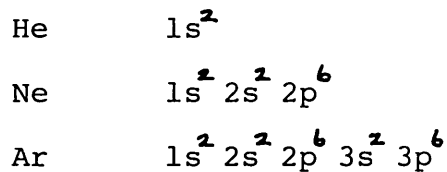
where the value of L is represented by the capital letter S, P, D etc. The left superscript takes

the value $(2S + 1)$, so if $S=1$ the left superscript becomes 3. The value of J appears as a right subscript. Term symbols that may be encountered are;



which are read "singlet S naught" and "triplet p two" respectively.

This system of nomenclature is simplified when an atom has a complete shell of electrons or even a complete sub-shell such as s^2 , p^6 , d^{10} or f^{14} . Such a set of electrons have resultant spin and orbital angular momenta equal to zero. Consequently, all atoms whose ground states are closed shells, such as the noble gases;



will have term symbols 1S_0 (singlet S zero). They have no resultant orbital angular momentum, no resultant spin angular momentum and hence no resultant total angular momentum.

A second consequence of this simplification is that even for atoms with many electrons, it is seldom necessary to consider the angular momenta of more than a few electrons. Electrons in full sub-shells contribute

nothing to the values of L, S and J and may be disregarded. Thus elements such as Li ($1s^2 2s$), Na ($1s^2 2s^2 2p^6 3s$) and K ($1s^2 2s^2 2p^6 3s^2 3p^6 4s$) all reduce to one electron problems, provided the atom is not excited.

It is now possible to consider the term symbols of some simple atoms. In the hydrogen atom, the electron occupies the $1s$ orbital therefore,

$$L=0, S=\frac{1}{2} \text{ and } J=\frac{1}{2}.$$

The term symbol is thus $^2S_{\frac{1}{2}}$. If the electron is excited to the $2s$, $3s$, $4s$ etc. levels then the values for L, S and J remain the same as does the term symbol. If the electron is excited to the $2p$ orbital the situation is different,

$$L=1, S=\frac{1}{2} \text{ and } J=\frac{1}{2} \text{ or } \frac{3}{2}$$

hence there are two states with term symbols $^2P_{\frac{1}{2}}$ and $^2P_{\frac{3}{2}}$. In the absence of magnetic fields these states are degenerate, the splitting of these states is 0.1 cm^{-1} . The same term symbols arise for excitation to the $3p$, $4p$, $5p$ etc. orbitals.

If the electron is excited to the $3d$ orbital then,

$$L=2, S=\frac{1}{2} \text{ and } J=1\frac{1}{2} \text{ or } 2\frac{1}{2}$$

and the term symbols are ${}^2D_{3/2}$ and ${}^2D_{5/2}$. These are also degenerate. From this information it is possible to construct an energy level diagram for hydrogen, labelling the states with the correct term symbols (figure 1).

The ground state of the lithium atom has the electron configuration $1s^2 2s$ and so becomes a single electron consideration. For the ground state,

$$L=0, S=\frac{1}{2} \text{ and } J=\frac{1}{2}$$

and the term symbol is ${}^2S_{1/2}$. If excited states $1s^2 3s$, $1s^2 4s$ etc. are considered then a series of ${}^2S_{1/2}$ states is obtained each having a higher energy than the previous one. As with hydrogen, terms for other excited states arise when considering $1s^2 2p$ etc. and $1s^2 3d$ etc. electron configurations.

Helium in the ground state has the closed shell configuration of $1s^2$ and hence the term symbol 1S_0 . The simplest excited state has the configuration $1s 2s$ which makes the problem more complicated since there are two electrons to consider,

$$\begin{aligned} l_1 = 0 \quad l_2 = 0 & \text{ therefore } L=0 \\ s_1 = \frac{1}{2} \quad s_2 = \frac{1}{2} & \text{ therefore } S=0 \text{ or } 1 \\ & \text{ and } J=0 \text{ or } 1 \end{aligned}$$

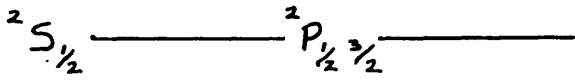
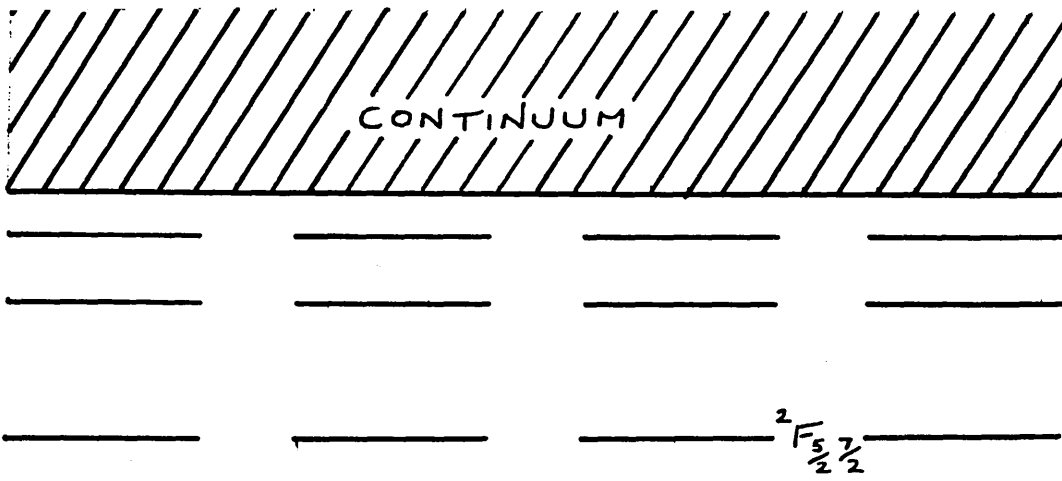


Figure 1. Energy Level Diagram for Hydrogen

There are two terms, 1S_0 and 3S_1 , which are not degenerate. The same argument holds for the excited configurations of $1s\ 3s$, $1s\ 4s$ etc.. The states with the configuration $1s\ np$ have,

$$l_1 = 0 \quad l_2 = 1 \quad \text{therefore } L=1$$

$$s_1 = \frac{1}{2} \quad s_2 = \frac{1}{2} \quad \text{therefore } S=0 \text{ or } 1$$

$$\text{and } J=1 \text{ or } 0,1,2.$$

If $S=0$ and $J=1$ the term symbol is 1P_1 . But if $S=1$ then there are three possible values of J . There are thus three triplet terms 3P_2 , 3P_1 and 3P_0 .

For the $1s\ nd$ states, there is a 1D_2 state and three triplet terms 3D_3 , 3D_2 and 3D_1 .

It has been shown how the energy levels of atoms arise and how term symbols can be used to describe the coupling of angular momenta for each energy level. It is still not possible to predict the appearance of atomic spectra because the so called "selection rules" have not been taken into account. It is found experimentally that transitions between all possible states are not allowed. Only a limited number of transitions are allowed and these are governed by the selection rules.

The selection rules are as follows;

- (i) There is no selection rule governing changes in the value of n . Thus the transitions $1s-2p$, $1s-3p$ and $1s-4p$ are all allowed.

(ii) The selection rule for the total orbital angular momentum is,

$$\Delta L = +/- 1$$

consequently, transitions such as $^1S - ^1P$ and $^2D - ^2P$ are allowed but $^3D - ^3S$ where $\Delta L = -2$ is forbidden.

(iii) The selection rule for the spin angular momentum is,

$$\Delta S = 0$$

so transitions such as $^2S - ^2P$ and $^3D - ^3F$ are allowed but $^1S - ^3P$ is not.

(iv) The selection rule for the total angular momentum J, is,

$$\Delta J = 0 \text{ or } +/- 1$$

thus transitions such as $^2P_{1/2} - ^2D_{3/2}$ and $^2P_{3/2} - ^2D_{3/2}$ are allowed but $^2P_{1/2} - ^2D_{5/2}$ is forbidden.

Using a knowledge of an atoms electronic states and the selection rules, it is possible to predict the experimental spectra of atoms. It is very important to obtain the correct term symbols as they govern whether a particular transition is allowed or forbidden.

Consider now the spectrum of lithium. The ground state lithium atom has the configuration $1s^2 2s$ and the term symbol $^2S_{1/2}$. There is a series of excited states with the configuration $1s^2 ns$ which all have the term symbol $^2S_{1/2}$. Transitions between these excited states and the ground state are not observed since they all have the same value of the L quantum

number($\Delta L=0$).

Transitions between the ground state and excited states of the type $1s^2 2p$ are possible. These excited states have term symbols $^2P_{1/2}$ and $^2P_{3/2}$. These levels are not exactly degenerate which gives rise to two closely spaced lines in the spectrum called a doublet. Similarly, transitions to all states of the $1s^2 np$ type are allowed which produces a series of doublets.

Transitions from the ground state to $1s^2 nd$ orbitals whose term symbols are $^2D_{3/2}$ and $^2D_{5/2}$ are not allowed ($\Delta L=2$). The same argument holds for transitions to orbitals of the type $1s^2 nf$ which are forbidden ($\Delta L=3$).

The discussion has only considered transitions from the ground state which constitute the absorption spectrum at relatively low temperatures. In the emission spectrum at higher temperatures, transitions which do not involve the ground state occur. The emission spectrum is consequently more complicated.

There are four important series of lines which are known as,

SHARP series	ns-mp
PRINCIPAL series	np-ms
DIFFUSE series	nd-mp
FUNDAMENTAL series	nf-md.

It was stated earlier that the 2P states of the alkali metals eg. Li, produce doublets due to a splitting of energy states. This splitting is a

consequence of a magnetic effect called spin-orbit coupling. The spinning electron acts as a tiny magnet which interacts with the field created by virtue of its motion around the nucleus. The splitting is roughly proportional to Z^4 where Z is the effective nuclear charge. Hence, moving down group 1 of the Periodic Table shows increasing splitting of the $^2P_{1/2}$ and $^2P_{3/2}$ levels. For lithium the splitting is 0.3cm^{-1} and for caesium it is 554.1cm^{-1} . It is spin-orbit coupling that allows a transition from a singlet to a triplet state - a transition forbidden by the selection rules. The coupling of spin and orbital angular momenta mixes the multiplicities of terms, and singlet terms acquire some triplet characteristics as a consequence. It follows that L and S as quantum numbers are imperfect.

When considering atomic energy levels, the coupling scheme used has been the Russell-Saunders scheme in which electrostatic interactions between electrons dominate. In a second coupling scheme, jj coupling, the magnetic effects dominate the term differences and the electrostatic interactions play a minor role.

In jj coupling, the rules for coupling angular momenta are,

- (i) for each electron i , the orbital and spin angular momenta l_i and s_i combine to give the total angular momentum j_i .
- (ii) the individual j_i then couple to give

a resultant J , the total angular momentum of the atom.

The two coupling schemes described represent two extreme cases. In one magnetic effects predominate over electrostatic effects, and in the other the reverse is true. Reality always lies somewhere between these cases and in general light atoms are best treated by Russell-Saunders coupling and very heavy atoms by jj coupling.

Having considered atomic energy levels in some detail, along with the relevant nomenclature and the transitions that may and may not occur, it is possible to examine the population of excited states which is a prerequisite of atomic emission spectroscopy.

1.1.6 Excitation of Line Spectra

Atomic spectroscopy involves the transition of atoms between electronic energy levels. The intensity of radiation ν_{12} emitted by an atom as a result of a radiative transition between two states 2 and 1 is determined by the probability of finding the atom in the initial state 2 and the probability of the transition $2 \rightarrow 1$ occurring.

It can be shown that for a system in thermal equilibrium at temperature T , the ratio of the numbers of atoms occupying the two energy levels E_2 and E_1 , is given by Boltzmann's formula,

$$\frac{N_2}{N_1} = \frac{g_2}{g_1} e^{-(E_2 - E_1)/kT}$$

where N_2 and N_1 are the numbers of atoms in levels 2 and 1 respectively. The statistical weighting factor g of a level is equal to its degeneracy. This formula shows that as the energy of the transition $E_2 - E_1$ increases, the population in the upper level decreases exponentially.

At room temperature the population of even the lowest excited state is very small. Consider a transition at 500nm, this corresponds to an excitation energy of $20,000 \text{ cm}^{-1}$, and assume g_1 is unity;

$$\begin{aligned} \Delta E = E_2 - E_1 &= 20,000 \text{ cm}^{-1} \\ &= 20,000 \times 1.98 \times 10^{-23} \text{ J} \\ &= 3.96 \times 10^{-19} \text{ J} \\ k &= 1.38 \times 10^{-23} \text{ JK}^{-1} \end{aligned}$$

Therefore at a temperature of 300K,

$$\begin{aligned} \Delta E/kT &= \frac{3.96 \times 10^{-19}}{1.38 \times 10^{-23} \times 300} \\ &= 95 \\ N_2 &= N_1 e^{-95} \\ N_2/N_1 &= 5 \times 10^{-42} \end{aligned}$$

Thus at room temperature, population of the excited

state may be neglected. Even at 3000K N_2/N_1 is only 7×10^{-5} . Consequently, atomic spectra will be in absorption unless energy is supplied to populate excited states from which emission is possible.

The intensity of a particular spectral line produced by a particular transition depends not only on the population of the initial level but also on the intrinsic probability of this transition occurring. The latter is defined by the Einstein Coefficients.

Consider two energy levels E_1 and E_2 ($E_2 > E_1$), populated by N_1 and N_2 atoms cm^{-3} respectively. There are three possible radiative processes connecting the two levels;

- (i) an atom in level E_2 may undergo a spontaneous transition to level E_1 , emitting a photon of energy $h\nu_{12}$. The probability of this occurring in unit time is denoted by the coefficient A_{12} .
- (ii) an atom in level E_1 may absorb a photon of energy $h\nu_{12}$, when irradiated by radiation of density $\rho(\nu_{12})$, and jump to level E_2 . The probability of this process is denoted by $B_{12} \rho$. The number of such transitions is then $B_{12} N_1 \rho \text{ sec}^{-1} \text{ cm}^{-3}$.
- (iii) an atom in level E_2 may undergo an induced transition to level E_1 in the presence of radiation $\rho(\nu_{12})$, with the emission of energy $h\nu_{12}$. The probability of this

occurring is denoted by $B_{12} p$. The number of such transitions is then $B_{21} N_2 p$.

Scheme (i) represents spontaneous emission, (ii) spontaneous absorption and (iii) stimulated emission where the emitted radiation has the same phase and direction as the stimulating radiation. This is the basis of laser action.

In equilibrium, the rate at which atoms enter level E_2 must be equal to the rate at which they leave it. The rate of transitions upwards from E_1 to E_2 must equal the rate downward from E_2 to E_1 . Hence the relationship between the three Einstein coefficients is given by,

$$B_{12} N_1 p(\nu_{12}) = A_{21} N_2 + B_{21} N_2 p(\nu_{12})$$

Rearranging gives,

$$p(\nu_{12}) = \frac{A_{21}}{B_{12} (N_1/N_2) - B_{21}}$$

By Boltzmann's equation,

$$\frac{N_1}{N_2} = \frac{g_1}{g_2} e^{h\nu/kT}$$

where $E_2 - E_1$ has been set equal to $h\nu$.

Therefore,

$$p(\nu) = \frac{A_{21}}{B_{12} (g_1/g_2) e^{h\nu/kT} - B_{21}}$$

This is identical to the Plank expression,

$$p(\nu) = \frac{8\pi h\nu^3/c^3}{e^{h\nu/kT} - 1}$$

for arbitrary T if and only if

$$g_1 B_{12} = g_2 B_{21}$$

$$A_{21} = \frac{8\pi h\nu^3}{c^3} B_{21}$$

The Einstein coefficients are intrinsic atomic properties which can in principle be calculated from knowledge of the wave functions for both the energy levels involved in a particular transition. The radiative decay rate for a real atomic transition is exactly equivalent to the Einstein A coefficient for that transition.

The study of emission spectra requires that the atoms of interest be excited to upper electronic energy levels. In the early days of emission spectroscopy a flame was used to achieve this. Flames have relatively low excitation energy so they are only useful for the intrinsically strong transitions of the alkali and

alkaline earth elements. Flames are most often used in the study of the molecules and radicals formed during the combustion process and in atomic absorption spectroscopy.

Electrical arcs may be used and typically produce temperatures of around 5000K. This is sufficient to excite neutral spectra of atoms and a number of ionic lines. Some arcs have been developed to produce temperatures as high as 30 000K. High voltage electrical sparks can achieve around 10 stages of ionisation of atoms forming the electrodes or of the atoms of the gas through which the spark passes.

Another emission source is a glow discharge such as a hollow cathode lamp. The cathode of the lamp is made of the element of interest and the lamp is filled with a noble gas at low pressure. Application of a voltage produces positive ions from the noble gas which are accelerated towards the hollow cathode. Atoms are sputtered from the cathode and become excited and consequently emit radiation. The emission spectrum produced consists of lines due to the cathode element and the filler gas.

The source of excitation and emission of interest in this work is the Inductively Coupled Plasma. An electrodeless discharge sustained by a radiofrequency power supply, which reaches temperatures of approximately 10,000 K.

1.2 THE INDUCTIVELY COUPLED PLASMA

One of the most significant advances in atomic spectroscopy occurred during the 1960's when the Inductively Coupled Plasma (ICP) became an alternative excitation source for atomic emission spectroscopy (AES). Prior to this, AES using flames, arcs and sparks had undergone a decline in usage as a general analytical technique. The main reason for this decline was the wide acceptance of atomic absorption spectroscopy (AAS). However, AES offered a very attractive advantage over AAS, namely the capability of simultaneous multi-element analysis. Consequently, scientists strove to find a more suitable source for AES and this they found in the ICP.

Babat [27,28] is recognised as being the first to establish and sustain a plasma at atmospheric pressure by induction heating. He used input powers of 30-50kW and generated plasmas in closed systems.

Reed [29-31] developed an open ended plasma torch through which gases could flow. He was able to initiate and sustain atmospheric pressure plasmas by induction heating within this torch. Reeds interest was refractory crystal growth but he did speculate that induction heated plasmas may be useful in spectroscopic applications.

The investigation of the ICP as a possible source for AES began concurrently with Reed's work. At the laboratories of Albright and Wilson Ltd.,

Birmingham, England, Stanley Greenfield began his work with ICP's in 1962. Unknown to him, Velmer Fassel at the Ames Laboratory, Iowa, U.S.A., also began experimenting with ICP's in the same year. Both were working towards the same goal, an atomisation-excitation source for emission spectroscopy.

Greenfield was investigating a toroidal plasma operating at high frequency (36MHz). He used relatively large diameter torches for his argon-nitrogen ("nitrogen cooled") ICP [32]. He postulated that his system offered higher sensitivity, fewer interference's and better precision than lower powered all argon ICP's [33].

Fassel's early work involved all argon ICP's operating at low frequency (3.4MHz). He used a smaller diameter torch than Greenfield and utilised laminar gas flow [34].

Perhaps the most significant similarity between these research groups was that both were considering the introduction of solutions to the plasma for analysis. This was due in part to the fact that solution nebulisation technology was already well established in AAS. Now, almost thirty years later there is a general requirement that the sample be in liquid form for analysis by ICP-AES.

During the early years of work with ICP's, one of the most important criteria in assessing the progress of the technique was improvements in detection limits. Dickinson and Fassel [35] published a very

significant paper in 1969 reporting detection limits two or more orders of magnitude better than previously achieved.

By 1971, extensive research had established the viability of the ICP as a source for spectroanalytical measurements. Fassel [36] summarised the ICP's major advantages;

- (i) effective injection of the sample into the hot portion of the plasma;
- (ii) relatively long residence time of the sample in the plasma;
- (iii) higher temperature than combustion flames;
- (iv) continuous temperature gradient from 9000K to room temperature, allowing greater latitude in selecting optimal temperature;
- (v) free atoms may be generated in the hottest zones of the plasma and then observed in lower temperature zones where background emission is lower;
- (vi) chemical environment may be manipulated within limits;
- (vii) no electrode contamination.

The potential of the low power argon ICP as an emission source for simultaneous multi-element analysis using compromised operating conditions was soon firmly established [37-40]. Further exploration and development of the low power argon ICP led to the exploitation of the exceptionally high sensitivity of ionic lines

in spectra [39,41]. Other performance characteristics such as relatively low interference levels, large dynamic range and good stability were also documented. Similar characteristics were found by a variety of experimental research groups. This work, along with that of the early researchers, forms the basis of present day ICP-AES.

1.2.1 ICP Generation

A plasma is defined as a volume of gas in which a significant fraction of its atoms or molecules is ionised. Consequently, magnetic fields may readily interact with plasmas, and one such interaction is an inductive coupling of time varying magnetic fields with the plasma.

A basic ICP torch, such as that used by Reed [29], consists of a tube, most frequently made of silica, placed inside a water cooled copper coil connected to a high frequency generator (figure 2). The generator is operated in the 4-50MHz frequency range at output powers of 2-5KW. With argon (Ar) gas flowing through the tube and the power switched on there is no interaction since Ar gas is a non-conductor. To initiate a plasma it is necessary to plant a "seed" of electrons in the coil space. Modern instruments use a Tesla coil. When the seed electrons are supplied a pear shaped plasma forms spontaneously and locates itself within and above the coil space.

The radio-frequency (rf) current flowing in

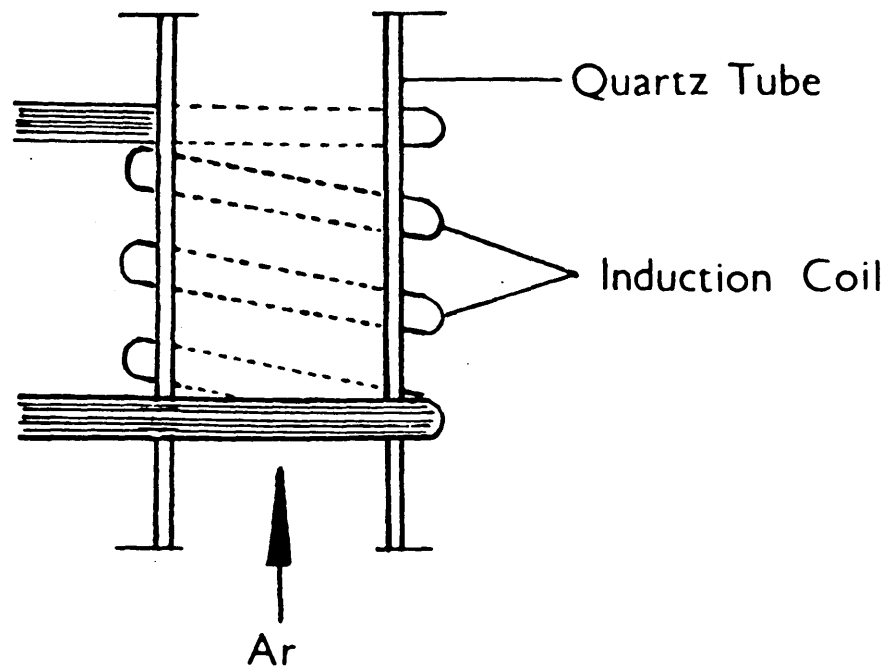


Figure 2. Basic ICP Torch

the coil generates oscillating magnetic fields whose lines of force are axially oriented inside the silica tube and follow elliptical paths outside the coil. The induced axial magnetic fields cause the seed electrons to flow in closed annular paths inside the coil space. Since the induced magnetic fields are time varying in direction and strength, the electrons are accelerated in each half cycle. These electrons and ions meet resistance to their flow resulting in Joule or Ohmic heating and additional ionisation occurs. These steps lead to the almost instantaneous formation of a plasma whose properties and characteristics are extremely useful for emission spectroscopy.

A plasma formed in this way will have a gas temperature of about 9,000-10,000K so some form of thermal isolation from the tubing is necessary. This is achieved by Reed's vortex stabilisation technique [29] whereby the Ar gas is introduced tangentially. The gas streams helically upwards cooling the tube and centering the plasma radially in the tube. This gas flow will be referred to as "coolant gas".

Most modern ICP torches consist of three concentric silica tubes. The outermost tube has been described and allows the tangential introduction of coolant Ar gas. The intermediate tube allows for the introduction of an optional gas flow called the "plasma gas" which may be used to adjust the vertical position of the plasma. Finally, the innermost tube allows

the introduction of a sample to the plasma. This "nebuliser gas" is usually Ar and it is mixed with an aerosol of the sample. Such an arrangement creates an annular or toroidal plasma where the sample is restricted to a central axial channel (figure 3).

The most commonly used gas for ICP's is Ar but a variety of other gases have been examined for ICP-AES. These include the nitrogen-cooled ICP where nitrogen is used as the coolant gas and the all helium ICP [42].

The tangential introduction of coolant and plasma gases is a highly significant characteristic in ICP generation. This technique produces a low pressure area at the centre of the torch which causes the ions to recirculate within the coil region. Furthermore, it creates a toroidal discharge in which the central sample carrier gas "punches" a hole through the centre of the plasma. This is a result of the so called skin-depth effect. The high frequency field does not penetrate the plasma uniformly because the outer electrons act as a shield. Consequently, the largest currents flow in the periphery of the plasma. The sample carrier gas bores a hole through this "weak spot" without disturbing the stability of the plasma. The temperature of this central axial channel is about 4000-5000K. This temperature coupled with the residence time of a few milliseconds create an environment suitable for the volatilisation and atomisation of aerosols during

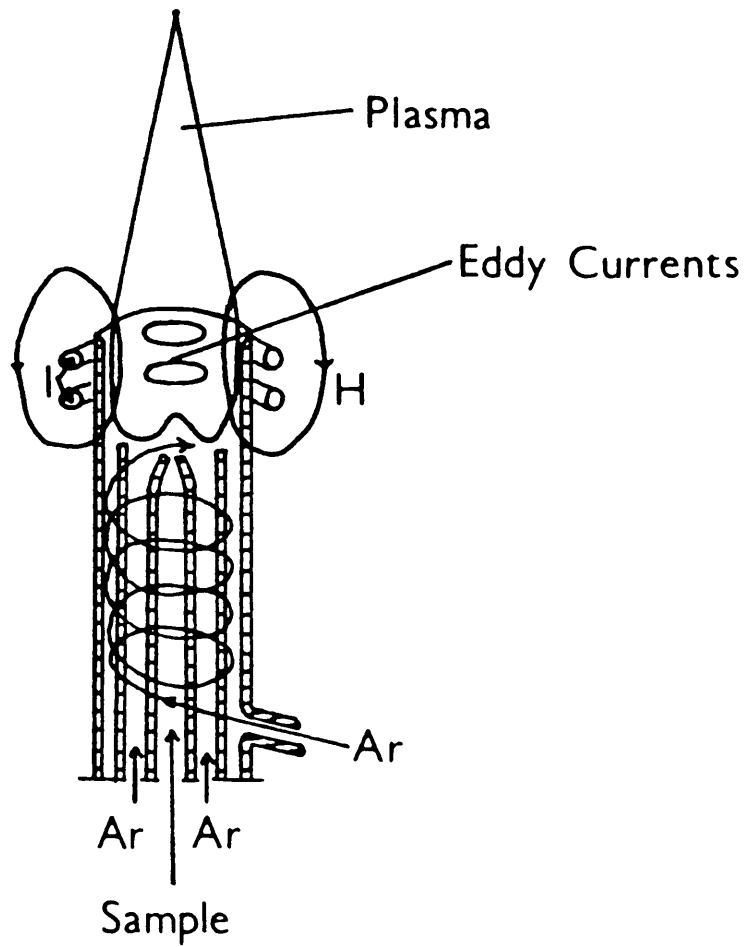


Figure 3. Modern Fassel ICP Torch

their passage through the coil space. Atomic spectra are then produced above the coil. The efficiency of atomisation depends on the power input to the ICP and on the flow rate and velocity of the sample carrier gas.

The appearance of the ICP may be divided into three main regions, the core, core tail and the tail flame. The intensely luminous core fills the coil space and usually extends a few millimeters above and below it. Very intense continuum emission along with the spectra of hydrogen, argon and some band spectra such as OH, NO and CN arise from this region. Above the coil the discharge becomes conical and less intense. This is the core tail located 10-20mm above the coil. It is generally the best area for analytical measurements as it provides best signal to background ratios and low flicker noise. Above this area is the tail flame which is usually invisible when aspirating deionised water but becomes coloured, similar to a flame, when solutions of metals are introduced.

Koirtzmann et al [43] have proposed a form of nomenclature for the zones in the ICP. A preheating zone (PHZ) is found at the base of the plasma core. Here the sample aerosol is dry but the atoms unexcited. The normal analytical zone (NAZ) occurs in the core tail and has the highest temperature outside the induction region at the centre of the core. The greatest ionic emissions occur in this region. In the tail plume

(tail flame) the temperatures are decreasing and emission intensity is also decreasing. Air is becoming entrained thus increasing spectral background. The importance of these viewing zones is in identifying the best viewing heights and in understanding how to avoid interferences.

A great deal of development work has been done on ICP torch design. Torches used in modern instrumentation are usually hybrids of either the Greenfield torch [33] or the Fassel torch [38]. Reviews covering torch design have been published by Greenfield [44] and Barnes [45].

Typical operating conditions for an all argon ICP are given in table 1 (see overleaf).

1.2.2 Plasma Temperatures

Characterisation of the ICP requires the examination of its fundamental parameters. Plasma temperatures, electron number densities, atom and ion emission intensities, number densities of argon and analyte species and spectral line widths are regarded as fundamental properties. Since the ICP is heterogeneous it is necessary to study the spatial distributions of these parameters if the physical nature of the ICP is to be understood.

The toroidal nature of the ICP allows efficient introduction of sample aerosols into the central axial channel. This structure also provides important analytical characteristics, namely, wide dynamic range,

Table 1. Operating Conditions for Conventional Argon

ICP

Frequency (MHz)	27-50
Power (KW)	1-2
Coolant gas flow (L/min)	15-20
Plasma gas flow (L/min)	0-1
Carrier gas flow (L/min)	0.5-1
Observation height above coil (mm)	12-18
Sample uptake rate (mL/min)	1-2

low detection limits and relative freedom from chemical and physical interferences and from self-absorption. The high temperatures and large electron number densities provide higher emission intensities for ionic species than for atomic species. However, ionic and neutral atom species are not necessarily in local thermodynamic equilibrium (LTE) and such non-LTE phenomena have been the subject of many major studies on the characterisation and on excitation mechanisms of the ICP.

A range of excitation mechanisms have been proposed for the ICP, and a variety of parameters must be measured before such a proposal can be made. These include, temperature measurements, electron number density measurements, spatial distributions of various species, spectral line profiles and gas flow dynamics. Most of these are major study areas in their own right and beyond the scope of this thesis but temperature measurements and an understanding of LTE will be considered prior to a discussion of excitation mechanisms.

The different species in a plasma, atoms, ions, molecules and electrons are distributed over many energy states. These states are often defined by different temperatures:

- (i) Excitation temperature. The Boltzmann distribution describes the population density of an excited atomic energy level and the temperature governing this population is the excitation temperature T_{exc} . If the absolute

transition probability from an excited energy level to a lower energy level and the total concentration of a particular atom in the ICP is known, then T_{exc} may be determined from the absolute intensity of an emission line due to the atom undergoing a particular transition. In an Ar ICP this method is only applicable to Ar, literature values for T_{exc} vary in the range 3000-7000K [46]

(ii) Ionisation temperature. If neutral atoms and ions are collisionally equilibrated, their concentration ratio is given by the Saha formula [47]. This concentration ratio can be related to emission line intensity such that the ionisation temperature T_{ion} can be determined from the spectral line intensity ratio of atom to ion and the electron number density. Houk [48] has reported ICP-MS measurements of this sort. Values of T_{ion} vary in the range 6000-9000K [46].

(iii) Rotational temperature. The rotational temperature T_{rot} is generally recognised as the gas kinetic temperature due to the rapid exchange between rotational and kinetic energy of a molecule. T_{rot} is determined by measuring emission intensities of rotational lines emitted from a diatomic molecule. Literature values of T_{rot} are very wide ranging and not easily

interpreted.

(iv) Doppler temperature. The temperature that governs the velocity distribution of heavy particles is the Doppler temperature T_D . The relative motions of atoms in the plasma cause emission line broadening called Doppler broadening. Values of T_D may be derived from measurement of Doppler broadening. It is important to be able to distinguish this process from other line broadening processes such as Stark and Lorentz broadening. T_D has values in the range 4000-6000K [46].

(v) Electron temperature. The transition of an electron from the free to the bound state, accompanied by the emission of continuum radiation is called radiative recombination. The intensity of the continuum depends on the electron number density and the Kinetic temperature of the electrons ie. electron temperature T_e . T_e can be derived from the emission intensity ratio of an Ar atomic line and the adjacent continuum. T_e is in the range 8000-10000K [46].

The above ICP temperatures can be summarised as follows;

$$T_{rot} < T_D \approx T_{exc} < T_{ion} < T_e$$

and this suggests a deviation from LTE.

If every energy exchange process occurring

in a system is exactly balanced by its reverse process, the system is said to be in complete thermodynamic equilibrium (CTE) [47] and all energy distributions are described by one temperature. The energy exchange processes include not only collisional processes but radiative processes, so that emitted photons must be completely absorbed in the CTE system.

In real plasmas the radiative processes are out of balance, since complete absorption of photons requires high optical densities for all the radiative transitions. When collisional processes are dominant in a system, each point of the system can be described by an individual temperature which is governed by the various distribution laws. This state is known as LTE and the criteria for the presence of LTE is that collisional excitation and ionisation processes exceed radiative processes. Mathematically [49],

$$n_e \gg 1.6 \times 10^{12} \times T_e^{1/2} (\Delta E)^3 \quad (\text{cm}^{-3})$$

where T_e is the electron temperature and ΔE is the energy difference (eV) between the states in question.

Conventional Ar ICP is regarded as not being in LTE as various measured temperatures differ from each other. Analytically, the relationship $T_{exc} < T_{ion}$ is important because it means higher sensitivities of ionic lines or overpopulation of ions.

1.2.3 Excitation Mechanisms

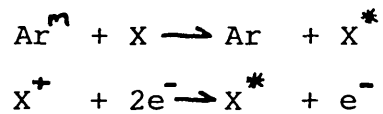
The first excitation mechanism proposed for analyte excitation [50] was the Penning ionisation reaction in which argon metastable atoms ionise analyte atoms with their high excitation energies, 11.55 and 11.76eV;



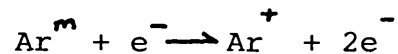
It is assumed that Ar^m are overpopulated so the reverse processes are ignored. This mechanism clearly provides the higher population of ions, but it does not account for the ionic levels for which the ionisation energy plus excitation energy is higher than the excitation energy of Ar^m . In this case, a two step reaction including electron collision is considered;



The overpopulation of higher atomic levels can be interpreted in terms of direct excitation by Ar^m or by the recombination of the overpopulated ionic ground state with electrons in a three body recombination;



Boumans [51] further postulated that Ar^m was overpopulated due to its inflow from the surrounding zone and played a dual role in the plasma, as an ioniser causing the Penning processes and as an ionisant acting as follows;



This allows a quantitative understanding of the high electron number density in the ICP and thus, the relatively small ionisation interference.

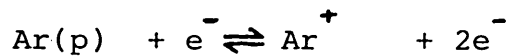
This excitation mechanism was generally accepted until it was shown that the number density of Ar^m was not significantly different from that predicted by the Boltzmann equation and the ideal gas law and by the Saha and Boltzmann equations [52]. The similarity of these values appears to be the most serious contradiction against the Penning mechanism [53].

Any excitation model must be refined to explain the non-LTE phenomena of the ICP. A recent model which explains the basic properties of the ICP has been proposed by Hasegawa and Haraguchi [54,55]. This collisional-radiative model incorporates the following six processes:

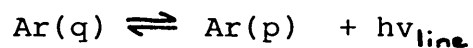
- (i) Electron impact excitation and de-excitation;



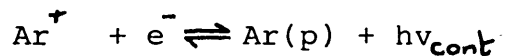
(ii) Electron impact ionisation and three body recombination;



(iii) Spontaneous emission and induced absorption;



(iv) Radiative recombination;



where $\text{Ar}(p)$ is the neutral Ar atom in the lower level p . Processes (i), (ii) and (iv) are governed by reaction rate constants which are a function of T_e . In process (iii), spontaneous emission is a function of the transition probability for spontaneous emission between states p and q and induced absorption is a function of Einsteins B coefficient for absorption and the radiation density. Besides these reactions, the diffusions of electrons and argon ions are also considered:

(v) Ambipolar diffusion;

$$L_a = D_a \nabla^2 n_e$$

(vi) Convection;

$$L_c = -v \nabla n_e$$

where L is the number of electron-Ar ion pairs flowing into a unit volume at the location (x,y,z) per second, D_a is the ambipolar diffusion coefficient, v is the gas velocity and ∇ is the Laplacian operator. In this model T_e and n_e (the electron number density) are the most important fundamental parameters for characterising the ICP.

The collisional-radiative model seems very promising as a method to elucidate the excitation mechanisms in the ICP though it is yet to be verified experimentally. The electron temperature is the most important parameter in the proposed model, hence the precise measurement of T_e will greatly assist its verification.

1.2.4 Spectroscopic Detection

A multi-element capability of an analytical method denotes the potential for simultaneous determination of a range of elements in one sample. Multi-element capability is inherent in AES where the temperature of the source is sufficient to achieve virtually complete atomisation. Under these conditions

atomic and ionic species predominate.

For alkali metals such temperatures can be too high. The atoms are ionised to a high degree so that atomic emission is weak and ionic emission is negligible or absent because alkali ions behave as noble gases. Consequently, the best source for alkali metals is a flame.

Flames did not really become very popular for multi-element AES. Flames are not suited to those elements that form stable compounds (oxides) as they are not sufficiently atomised at flame temperatures. Chemical interferences can also be a problem. Plasma sources provide an inert high temperature environment and excellent excitation characteristics.

A disadvantage of AES is the problem of line coincidences which can cause major problems in trace analysis of samples whose matrix constituents have line rich spectra. In such situations high resolution spectroscopic equipment is required.

Utilisation of the multi-element capability of AES requires the use of spectroscopic equipment that can measure intensities of spectral lines at several different wavelengths using either a simultaneous or rapid scanning sequential mode of operation.

The use of solid state detectors has not been very successful. Photo-diode arrays and vidicon tubes are limited by poor signal to noise ratios in the UV and poor resolution. The photomultiplier tube (PMT)

remains the detector of choice and is used almost exclusively in commercial instruments. Several PMT's are used in polychromators each with its own exit slit corresponding to a particular wavelength. This facilitates simultaneous multi-element determinations. A monochromator with a single PMT can be used for sequential determinations. Spectrographs utilising photographic detection are still in use, generally for survey analysis.

The characteristics of spectroscopic instrumentation for ICP-AES are given in table 2.

The initial work with ICP's utilised the mechanical monochromators of the day. Later, polychromators that had been used with spark excitation sources were coupled with the ICP but as they had not been designed for trace analysis such spectrometers were soon updated. Improvements included reducing stray light levels, the use of digital electronics, design of vacuum and gas purged spectrometers and automatic background correction at wavelengths close to the line of interest. Monochromators became computer controlled slew-scan instruments providing rapid scanning sequential measurements.

1.2.5 Performance Characteristics

The nature and properties of the ICP give rise to some special performance characteristics as a source for emission spectroscopy. Since the analyte is

POLYCHROMATORS

Routine multielement analysis.

Low sample diversity.

Rapid, high sample throughput.

Inflexible.

Wavelength range 170-900nm.

Resolution may be limited.

Sample size independent of number of analytes.

MONOCHROMATORS

Non-routine analysis.

Very flexible in sample type and line choice.

Relatively slow.

Limited wavelength range but interchangeable gratings and PMT's improve this.

High speed slewing and accurate wavelength positioning.

Sample size dependent on number of analytes.

Table 2. Characteristics of Spectroscopic Instrumentation.

restricted to the central axial channel of the plasma rather than its cooler edges, self-absorption is negligible. This, coupled with the naturally low particle density of the ICP compared with many other sources, produces extended linear calibration curves. Excitation and emission zones are spatially resolved in the ICP, producing a relatively simple background spectrum consisting of mainly argon lines and some weak band emission from OH, NO and CN molecules. The low background and high signal to background ratio (SBR) of analyte emission gives rise to low detection limits, typically in the parts per billion (ppb) range. The ICP discharge is very stable over long periods of operation, thus eliminating the need for frequent restandardisation. Sample excitation in the ICP is highly efficient as it experiences high temperatures and long residence times, thus the system is relatively free from matrix interferences. Also, the inert Ar atmosphere minimises chemical interferences.

A variety of sample types may be determined by ICP-AES but solutions nebulisation is the conventional mode of analysis. Aqueous and organic solutions may be nebulised but the latter requires some adjustment of plasma operating conditions. Solutions with high dissolved solids may also be used but care needs to be taken in the choice of nebuliser and in preventing clogging of the central injection tube of the ICP torch. The direct analysis of solids requires special techniques

which are considered later.

For simultaneous multi-element determinations only a few millilitres of sample is required. Larger volumes are usually required for sequential determinations. Using specialised techniques such as electrothermal vaporisation and flow injection can reduce the sample volume to microliter sizes.

In principle, all metallic elements may be determined by ICP-AES. Low concentrations of alkali elements can pose problems and argon, hydrogen, oxygen and the halides are generally regarded as indeterminable. A vacuum or gas purged spectrometer is required for or greatly improves the determination of boron, carbon, nitrogen, sulphur and phosphorus. The use of hydride generating equipment can improve measurement of hydride forming elements such as arsenic and selenium.

Detection limits in ICP-AES are generally very good but vary depending on several parameters; the ICP, nebuliser, sample type, the spectrometer and the use of special techniques such as hydride generation.

The precision and accuracy are also very good. The former is dependent upon equipment used and sample types. If care is taken throughout sample preparation and analysis, accuracy limited by the precision only can be achieved.

Perhaps the most firmly established feature of ICP-AES is the wide dynamic range of four to six orders of magnitude. This facilitates determination

of trace and major concentrations simultaneously.

A summary of the ICP's performance characteristics is given in table 3.

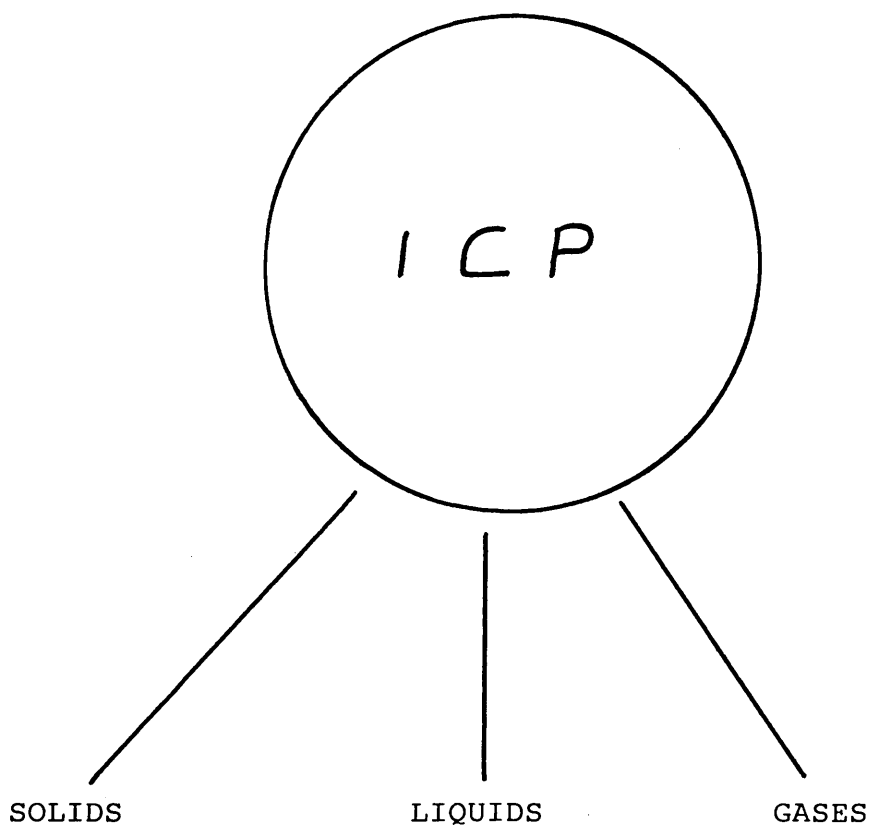
1.2.6 Sample Introduction

Sample introduction has been described as "The Achilles' Heel of Atomic Spectroscopy?" [57]. This is due, in part, to the generally poor efficiency of sample introduction techniques. Ideal sample introduction could be defined as "the reproducible transfer of a representative portion of sample material to the atomiser cell, with high efficiency and with no adverse interference effects" [57]. A summary of the techniques used in ICP-AES is given in figure 4.

The sample introduction technique used in conventional analysis of solutions by ICP-AES is pneumatic nebulisation. There are two basic designs of pneumatic nebuliser, concentric and cross-flow. In the former, the sample solution passes through a capillary surrounded by a high velocity argon gas stream flowing parallel to the capillary axis. In the latter, the capillary carrying the sample solution is set at right angles to that carrying the argon gas stream. In both configurations a reduction in pressure at the sample capillary orifice causes the solution to be drawn up through it due to the Venturi effect. The high velocity gas stream shears the solution and breaks it up into a fine aerosol mist. This aerosol is then transported

Sample types:	Liquids directly. Solids after dissolution. Solids directly using special techniques.
Sample size:	A few ml. A few μ l with special techniques.
Element coverage:	70 elements at least.
Detection limits:	0.1 - 100ng/ml
Multielement capability:	Simultaneous: high Sequential: virtually unlimited.
Precision:	0.5 - 2% RSD
Accuracy:	Reasonable with little effort. Accuracy= precision with effort.
Dynamic range:	4 - 6 orders of magnitude.
Analytical range:	Trace, minor and major levels.
Interferences:	Multiplicative : low. Additive (spectral): severest limitation of the method.

Table 3. Performance Characteristics of ICP-AES [56].



Arc/spark ablation

Electrothermal
vaporisation

Direct insertion

Laser ablation

Nebulisation

Nebulisation

Electrothermal
vaporisation

Flow injection

HPLC effluents

Direct insertion

Hydride generation

GC Effluents.

Figure 4. Sample Introduction for ICP-AES.

to the ICP via a spray chamber.

The Meinhard concentric nebuliser is the most widely used in current ICP spectrometry, but a variety of nebulisers have been designed. The Babington nebuliser is designed for high dissolved solids samples [58] as is the MAK nebuliser which operates at relatively high pressures [59]. Nebulisation can also be achieved using ultrasound. A longitudinal ultrasonic wave is propagated perpendicularly to the liquid sample-air interface where it produces a pressure sufficient to break the surface into an aerosol [60].

Aerosol transport efficiency is defined as the percentage of the mass of nebulised solution that actually reaches the plasma. For this percentage to be high, and for rapid desolvation, volatilisation and atomisation of aerosol droplets when they reach the plasma, a nebuliser must produce droplets less than 10 micrometers in diameter. Nebulisers produce aerosols which are highly polydispersive with droplets upto 100 micrometers in diameter. These large droplets must be removed by a spray chamber such as that described by Scott [61]. The large droplets are removed by turbulent deposition or by gravitational action. Generally, for such nebulisation techniques, the transport efficiency is less than 3%.

There is currently a general requirement that the sample be in liquid form for analysis by ICP. This requirement is a shortcoming in the analytical

application of the plasma since many samples eg. steels occur naturally in the solid state. Several analytical and practical advantages may be realised by direct analysis of solids by ICP-AES without pretreatment or dissolution.

Ideally, the sample is analysed in its natural state; contamination from reagents is minimised; dilution errors are eliminated; sample transfer losses arising from extra sample-handling steps are avoided; the time delay from sample collection to analysis is reduced; the potential for improved absolute detection limits is enabled; analysis of microsamples or localised areas of samples is facilitated and sample vaporisation, atomisation and excitation steps may be separated and optimised.

A variety of solid sample forms have been successfully introduced to an ICP such as powders, conductive and non-conductive solids, homogeneous and heterogeneous solids. When introducing solids to the ICP, sample heterogeneity becomes a major consideration. This is generally not a problem when using a solid that has been put into solution given that a sample size of one gram or more is used. Solid sampling techniques consume much smaller quantities, generally in the microgram to milligram range, which gives rise to poor sample to sample reproducibilities. Some solid sampling techniques can reduce the effects of sample heterogeneity to provide information about localised

concentrations of sample constituents. Let us now consider the solid sampling techniques that have successfully been applied to ICP spectrometry.

Direct sample insertion is achieved, as the name suggests, by inserting the sample on a probe directly into the plasma volume. A number of researchers have shown its feasibility [62-71]. During its initial stages of development liquid samples were used. When using solids the sample is usually ground into a powder or segmented into sufficiently small pieces before being placed into a probe made of graphite, tantalum or tungsten, for insertion into the plasma. Many certified reference materials are supplied in a form suitable for this sort of technique.

The probe is usually inserted axially through the sample injection tube of the plasma torch. This may be done manually or automatically, in one reproducible motion or in a series of specified steps.

Salin and Horlick [62] were the first to report on a direct insertion device (see figure 5). A modified Fassel torch was used, where the central injection tube was used as a guide for a graphite electrode which contained the sample.

The torch was mounted on a PTFE base which also supported the probe. The graphite electrode was mounted on a quartz rod, the lower end of which was attached to a sliding platform whose vertical position was controlled by a lead screw. Rotation of this screw

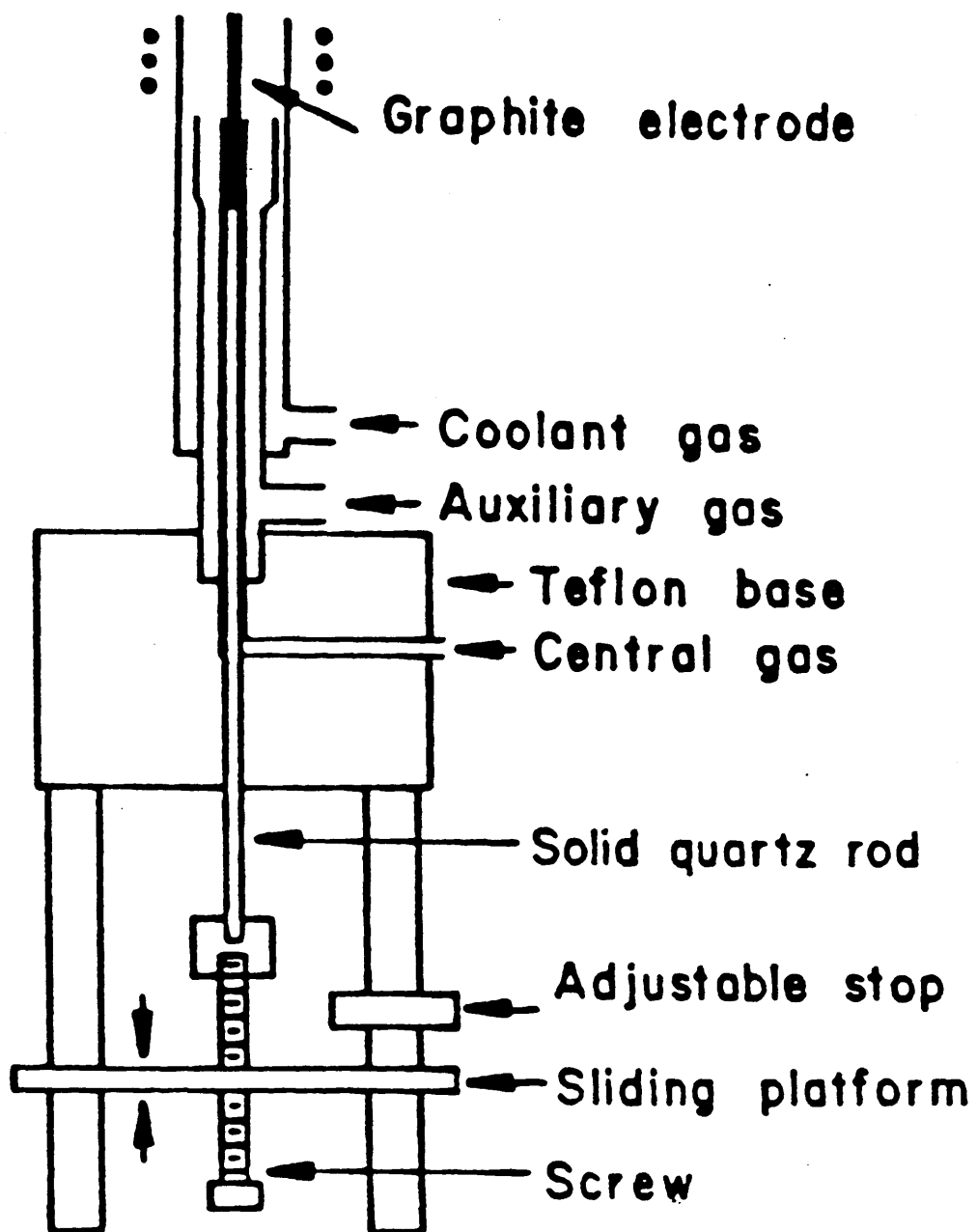


Figure 5. Direct Insertion Device
 (Reproduced with permission Ref. 62)

allowed the insertion and withdrawal of the probe into and from the plasma. During operation the tip of the electrode was placed just below the load coil whilst the plasma was initiated. Once the plasma had stabilised the probe was quickly inserted into the plasma such that the tip of the electrode was positioned just above the load coil.

To facilitate continuous operation of the plasma during direct insertion it is necessary to prevent the entrainment of air. Kirkbright and co-workers [63,64] achieved this by eliminating the central injector argon flow. Utilisation of a high power (3KW) argon nitrogen ICP [65,66] also enables continuous operation. Abdullah [67] described the use of an argon flow stopper placed at the base of the injector tube. An elegant system to prevent air entrainment was devised by Pettit and Horlick [68]. In this system a snuffer gas inlet was used to introduce argon as the probe was withdrawn.

Another major consideration for direct insertion is precise positioning of the sample within the plasma volume to allow reproducible vaporisation and excitation. In the simplest system this is achieved using a mechanical stop which positions the probe in a reproducible position relative to the ICP. More elaborate systems allow control of the final position, any intermediate position(s), duration at each position and the rate of insertion by using an automatic insertion device. These include stepper motors [64], dc motors [69],

car aerial motors [70], combination of pneumatic activators and motor driven assemblies [68], and pneumatic elevators [66].

Several researchers have reported on the automated insertion of a single probe into the ICP, but only recently has a system that allows automatic changing of sample probes been reported [68]. The system incorporates a computer controlled 24-position autosampler carousel which holds the sample probes. The sample probes are pneumatically removed from the carousel for insertion into the plasma. The carousel and the gas flows are controlled thus allowing unattended operation.

Graphite is the most widely used material for direct insertion probes, and a small recess at the end of the probe is usually used as a reservoir for the sample. Although a variety of probes and sample reservoirs have been used there is no exhaustive study detailing the geometry required for optimum analytical performance. Improved results have been reported when using boiler caps [62,66,68], which allow the controlled release of vapours into the central channel of the ICP.

All of the operating parameters important to ICP-AES with solution nebulisation also require optimising for direct probe insertion analysis, but additional parameters such as probe heights, rate and duration of insertion and sample size also require optimisation.

Such variables have been optimised using univariate and simplex optimisation methods but little information exists on the effects of each parameter on analytical results. Integration time is usually established by observing the time dependency of the emission signal which is dependent upon element volatility. Sample sizes used are normally between 5 and 10 mg but depend on weighing constraints and whether the sample is considered to be representative of the bulk sample.

Detection limits for the direct insertion of solids are difficult to compare due to the lack of a well defined definition and procedure for their determination and the scarcity of analytical blanks for solid samples. A wide range of detection limits have been reported in the ppm and sub-ppm range, but it is impossible to make conclusions due to insufficient data. Precision is generally inferior to solution nebulisation being in the range 1-25% RSD. A typical working range would be 7-10% RSD. This is due mainly to sample heterogeneity, vaporisation irreproducibility and imprecise sample insertion.

Calibration curves have been constructed using solid samples of known elemental concentration such as certified reference materials. Calibrations are generally linear over at least three orders of magnitude. A significant point is that it is possible to calibrate using solid materials of different matrix composition, indicating a relative insensitivity to elemental origin

[67,70]. This indicates the possibility of calibrating with solutions for the analysis of solids.

There are three main limitations to the technique, the most significant being sample heterogeneity. Background shifts also cause problems, a situation which is compounded by the transient nature of the signals. Currently, no commercial instrument exists that allows simultaneous multielement quantitation of transient analyte peaks and associated backgrounds. The seriousness of this problem requires greater evaluation. The probe material can also cause problems and graphite has several shortcomings, including reactivity, carbide formation, deterioration and occasional memory effects. The severity of these problems may be reduced by using pyrolytically coated graphite, metal cups and hydrogen gas as an oxygen scavenger. As indicated earlier, boiler caps greatly improve precision by controlling variations in volatility.

Reports on the general accuracy of direct insertion are quite recent [67,70,71]. The results are based on certified reference materials and generally good agreement is attainable, although refractory elements pose difficulties due to carbide formation and retention in the cup.

The technique has been shown to be applicable to a wide variety of sample types such as metallurgical solids and botanical powders. If the problems associated with sample heterogeneity can be overcome then the

analysis of a variety of solids with acceptable accuracy and precision should be possible.

Another solid sampling technique that has been successfully applied to ICP-AES is electrothermal vaporisation (ETV). The detection limits are orders of magnitude better than for solution nebulisation due to improved sample transport. The volatilisation of the sample is achieved by resistance heating of a sample supporting device such as boats, cups and rods which are constructed of either a refractory metal or graphite.

Most ETV-ICP systems utilise a power supply which permits control of the times, rates of heating and temperatures of the vaporiser heating sequence. This allows the optimum conditions for sample drying, ashing or vaporisation to be set, and facilitates selective volatilisation so that the solvent (in liquid samples), matrix and analytes may be temporarily separated from each other as they are volatilised from the heated ETV surface.

A measured weight of sample is placed onto the ETV surface, usually referred to as a furnace, and the heating sequence initiated. The high-temperature environment produces a dry, highly dispersed vapour which is swept to the plasma (usually with argon) via the central injection tube, for excitation and all the processes prerequisite to it. The signal so produced is of a transient nature and quantitation is by peak

height or peak area.

The system requires an atomisation chamber which houses the ETV surface. The chamber has inlet and outlet ports to allow the passage of sample/carrier gas through the chamber and to the ICP torch. A high current power supply is connected to the furnace whose resistance to the flow of current causes it to heat up. An atomisation chamber from a commercial AA instrument has been adapted for the ICP [72].

Some atomisation chambers have been designed to mate with the ICP torch thus reducing transport distances to a minimum [73]. This situation increases sensitivity because diffusion of the analyte peak is reduced and condensation of the vapour on surfaces such as lengths of tubing is minimised. For these reasons also, the atomisation chamber itself has an optimum volume. Too large a volume causes diffusion and too small a volume increases condensation problems.

The original atomisation chamber designs were used for the analysis of solutions but Hull and Horlick [74] adopted one such design for the analysis of solid samples 2-3 mg in weight. The analysis of 0.5 mg of solid samples using a pyrolytically coated graphite microboat has also been reported [72]. The atomisation chamber was originally used for graphite furnace atomic absorption spectrometry (GFAAS)(see figure 6). A commercial ETV-ICP system has recently been introduced to the market place by Thermo Jarrell Ash.

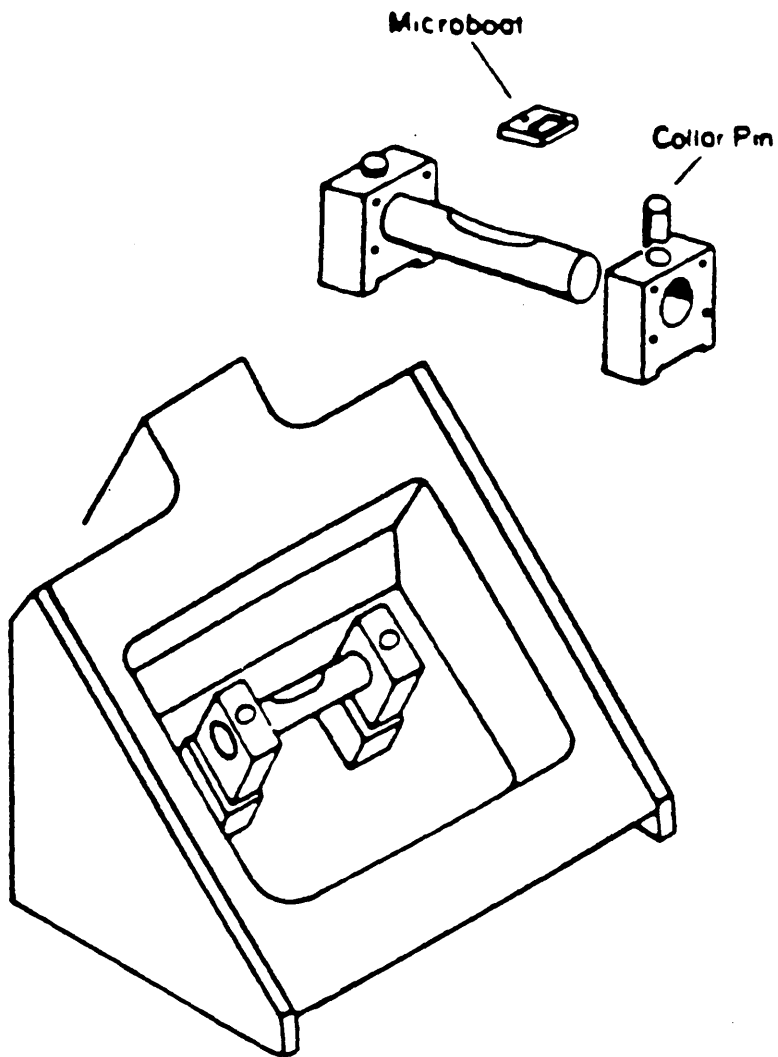


Figure 6. Electrothermal Vaporisation Unit originally used for Atomic Absorption and adapted for ICP (see ref. 72).

Conventional solutions analysis by ICP requires the optimisation of a variety of parameters. The use of ETV-ICP requires the additional optimisation of time, temperature, rate of drying, ashing and vaporisation. Optimisation is usually achieved by observing time resolved spectra. Such responses have shown the occurrence of selective volatilisation hence the more volatile elements arrive at the plasma first. In this manner, it is possible to minimise interferences such as spectral overlap and matrix effects common to solution ICP.

Due to the highly efficient sample utilisation ETV-ICP is an extremely sensitive technique especially for solutions analysis. Detection limits for solutions are in the nanogram to picogram range. Investigations of solids are at the early stages so no detection limits are available, however, since signals produced by solid samples are very similar to those produced by solutions it is expected that detection limits will also be similar.

Blackemore [72] investigated the precision of the technique by determining 10 elements in bovine liver. He reported 11.8% RSD which is inferior to ETV-ICP of solutions and conventional analysis. As with direct insertion, the degradation of precision, detection limits and long term reproducibility is due mainly to sample heterogeneity.

Linear calibrations of at least 3 orders of magnitude have been reported for Zn using internal

standardisation and investigation of a variety of certified reference materials has shown that matrix composition has little effect [74].

There is currently little data on the accuracy of the technique but one report [72] shows good accuracy with the certified values for bovine liver falling within the confidence range of the results. The limitations of ETV-ICP are similar to those for direct insertion. It would be ideal for small sample sizes but that has inherent problems with sample homogeneity.

Perhaps the most successful technique for introducing solid samples to the ICP is arc and spark ablation. In this case an electrical discharge is used to remove material from the sample surface. The removal of material, called ablation or erosion, generates a solid dry aerosol which may be transported to the plasma.

There are two types of discharge used, arcs and sparks [75,76] and both require a conducting sample. If a sample is non-conducting it may be mixed with a conducting matrix such as powdered copper or graphite to produce a homogeneous mixture. The sample may be of any physical form provided that a reproducible discharge is obtained between the sample and an electrode. Thus reproducibility is extremely important as it forms the basis of the assumption that the amount of material ablated per unit time is reproducible for a given sample, discharge conditions and discharge duration. Consequently,

sample weighing is unnecessary.

The ablated material is transported to the ICP by an argon gas flow passing along tubing which may be centimetres or meters in length or via settling chambers. The signals produced have a time dependency which is related to element volatility, discharge conditions, discharge stability and matrix composition.

The first and perhaps the simplest form of electrical discharge used to ablate material from a sample surface was the d.c. arc. The system described by Dahlquist [75] consisted of an air-cooled hollow anode flushed with argon, and a tubular grounded cathode that contacts the sample. A discharge between the anode and the sample ablates material which is transported by the argon gas to the ICP.

Farnsworth and Hieftje [76], reported the use of a radio frequency arc. The system uses a modified torch whose central injection tube has been expanded at the base to form a bell jar which houses the sample. The sample itself is grounded and when the plasma is initiated a filament forms between the plasma and the sample which erodes the sample.

The most common form of discharge used to generate a solid sample aerosol is the spark, which can range from low to high voltage types of varying pulse durations, frequencies and waveform shapes [77-81]. A schematic of a spark aerosol generator that forms the basis of the conductive solids nebuliser (CSN) manufactured

by Applied Research Laboratories is shown in figure 7. A spark source and Petry table of the type used in spark emission spectrometry are used. The spark discharge is formed between the tungsten counter electrode and the sample surface. Ablated material and argon are transported to the plasma via 1 m long tubing. The conventional solution spray chamber may be used as a settlement chamber to remove large aerosol particles which may perturb the plasma. Thermo Jarrell-Ash manufacture a similar system.

For the most sensitive lines, detection limits extend down to the microgram-per-gram level. This is comparable to solution nebulisation when the dilution factor is taken into account. It is also important to remember that only a few micrograms of sample are ablated. Precision is better than for any other solid sampling technique. For most metallurgical samples precision is in the range 0.5-5% RSD. This is attributable to the absence of sample-to-sample variations and the large area of sample that is ablated ($0.2\text{-}1\text{cm}^2$). Briquetting of powdered samples reduces precision due to irreproducibilities in the briquetting procedure.

Calibration curves show linearity over at least three orders of magnitude, element response has been shown to be independent of matrix composition and the sample aerosol may be transported over large distances. Work has also shown that calibration with conventional solutions nebulisation may be feasible prior to spark

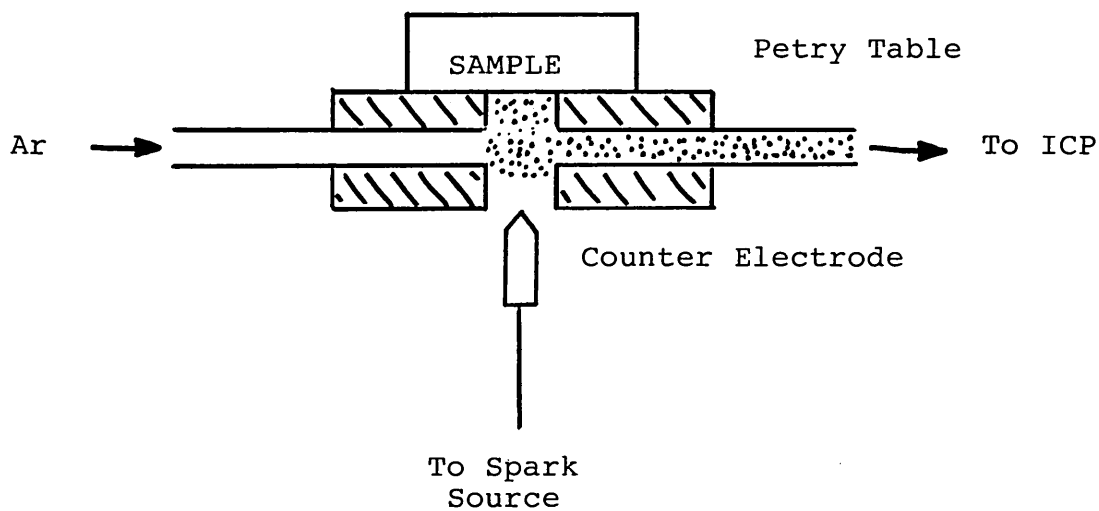


Figure 7. Schematic of Spark Ablation System. A spark generated between the sample and counter electrode ablates the sample and the aerosol produced is transported to the ICP in an argon stream. (Taken from bibliography ref. 5)

ablation of solid samples.

The technique shows minimal interferences and in this respect is very similar to solution nebulisation but there are several limitations. The transport of too much material to the plasma can cause imprecision, calibration curvature, memory effects and plasma instability. Too little spark energy can give rise to differential distillation of elements from the sample and as with all solid sampling methods, sample heterogeneity can cause problems. Some of these effects can be guarded against; memory effects are minimised by flushing the spark chamber with argon and sample heterogeneity is improved by using a pre-burn cycle to reduce the metallurgical structure differences on the sample surface.

Perhaps the most significant limitation of spark ablation is the requirement of the sample to be conductive. Non-conductive samples may be analysed when a conductive matrix is added but this becomes time consuming (especially if samples require grinding) and may cause contamination problems.

The method has been widely used for metallurgical analysis and accuracies have been reported for a variety of materials. Generally, relative accuracies are within a few per cent unless analyte levels are at or below the detection limits.

We may now consider the solid sampling technique which is of central concern to this report, that of

laser ablation. The technique has been investigated by several research groups [82-99]. Similar to the arc and spark, energy, in the form of a focused laser beam, is directed onto the sample surface to remove material from that surface by ablation. The ablated material is transported in an argon stream to the ICP for excitation.

Emission signals may be measured using a monochromator or a polychromator, but the transient nature of the signals requires that a polychromator be used for multi-element determinations. Data may be acquired in the time resolved mode or by total signal integration.

The intensity of emission is directly related to the amount of material ablated. The degree and rate of ablation are related to sample characteristics such as surface condition and reflectivity. A variety of laser conditions and operating parameters are also of importance such as laser focus, energy output, operating mode, shot frequency and duration. The ablation chamber geometry and length of connective tubing can also determine how much ablated material reaches the plasma.

The main attractive feature of laser ablation is its ability to sample conducting and non-conducting materials with a wide variety of geometries and forms. Additionally, focusing of the laser beam permits sampling of such a small area that localised in situ microanalysis

is possible.

The basic requirements for laser ablation (LA) ICP are a laser which can be operated in Q-switched or free running mode, the necessary beam directing optics, the ablation chamber to house the sample in an argon atmosphere and the connections between chamber and ICP torch. Figure 8 shows the system described by Ishizuka and Uwamino [84]. The ablation chamber is a stainless steel cylinder with a pyrex glass window which sits on the sample such that the sample acts as the base of the chamber. A 45-degree prism and a 50 mm focal length lens direct and focus the beam onto the sample surface. Sample aerosol is transported via PVC tubing to the ICP. The emission signal is detected by the photomultiplier tube (PMT) of a monochromator and amplified, converted to frequency, then counted with a multichannel analyser. Laser firing is synchronised to data acquisition with a PMT trigger activated by a xenon flash lamp pulse.

Various sample geometries are used in LA. Researchers have designed ablation chambers for powdered samples [85,86], while Carr and Horlick have configured two chambers, one for rod shaped samples and one for discs [86]. These chambers accommodate a range of metallic industry standards. The chambers are mounted directly below the ICP torch to minimise sample transport distance and a 2 rpm motor is used to rotate the samples to present a fresh surface for ablation. The laser

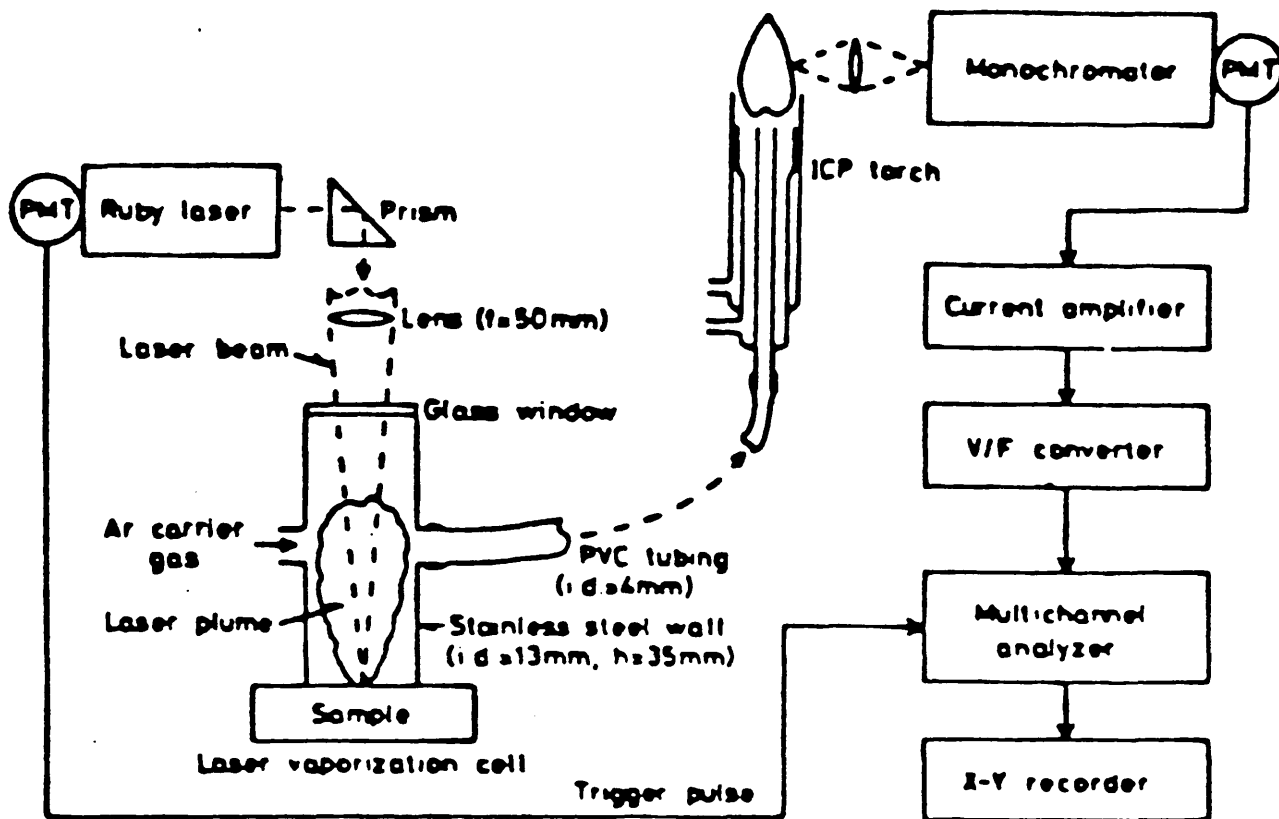


Figure 8. Laser Ablation System

(Reproduced with permission Ref. 84)

used was a Ruby laser of 1-2J output energy which could be dumped in either Q-switched or free running mode. A right angled deflection prism and a 50 mm focussing lens were used to position and focus the beam.

Thompson and co-workers [87,90,91] have described a LA system which utilises a commercially available laser-microprobe. The ablation chamber is a laboratory made glass dome with two side ports for gas connections, a window of optical grade silica and a base formed by mounting the chamber on an inverted rubber bung. The sample to be ablated is positioned on the bung. The laser microprobe consists of a Ruby laser head mounted in a binocular microscope. The target area is selected under the microscope, then the laser is focused and fired. The ablated material is swept to the ICP along PVC tubing. Signals from the plasma are detected by a 1 m polychromator.

In addition to the parameters usually optimised for solution nebulisation ICP, there are a variety of other parameters related to the laser that require optimisation e.g. ablation chamber volume and aerosol transport distance.

Pulsed lasers that may be operated in the Q-switched or free running mode are generally used. The suitability of a laser depends on a wide range of characteristics such as output power, lasing wavelength, repetition rate, shot-to-shot reproducibility, thermal stability, ease of alignment and operation

and the cost of the system.

Most of the research done in this area has been with a solid state Ruby laser. The Ruby laser lases at a wavelength of 694.3 nm. Being visible, this wavelength is easily aligned and monitored during operation, it is also absorbed by most materials with the exception of some glasses and polymers. It does however have a low repetition rate and the shot to shot reproducibility can be poor.

Solid state neodymium:glass and neodymium:YAG (yttrium aluminium garnet) lasers lase at 1064nm a wavelength that is absorbed by most materials but its invisibility can be very hazardous. Such lasers can have repetition rates greater than 1000 pulses per second (pps) but are thermally sensitive and require cooling. Operational ease, size, reasonable cost and good shot to shot reproducibility make this laser a good choice for laser ablation.

A gaseous carbon dioxide laser has been used for laser ablation [85], but the lasing wavelength of 10.6 microns is not optimal for laser ablation as many metals are highly reflective at this wavelength. Also a coaxial alignment laser is required.

The amount of material ablated from a surface is related to the amount of energy incident on it. The effects of Q-switched and free running pulses are documented [84]. When ablating a low-alloy aluminium sample with a Ruby laser (694 nm) it was found that

up to 500 μ g of material could be ablated in the free running mode, but a maximum of 25 μ g was achieved in Q-switched mode from the same sample. Generally, ablation in the free running mode produced 20-30 times more material than Q-switched operation. The larger sample size created by free running operation improves the emission signal and reduces the effects of heterogeneity.

The amount of sample ablated can also be controlled by the laser focus. Defocussing the beam creates a larger diameter spot, decreases the energy density and changes the ablation characteristics. Defocussing appears to have a more significant effect when lasing in the free running mode [84].

As with many discrete sampling processes, time resolved profiles are used to optimise operating conditions. Such methods have shown that increased ablation chamber volume results in broader transient signals [87]. Similarly, the distance of sample transport has been investigated. As tubing length is increased, diffusion of the sample becomes more pronounced resulting in decreased peak heights.

Researchers have shown that detection limits in the free running mode of operation are in the microram-per-gram range. Precisions of 3-11% RSD have been reported for a variety of metal samples. This lack of precision may be accounted for by sample heterogeneity on a micro scale and poor shot to shot reproducibility of Ruby lasers.

Calibration curves are generally linear over two to three orders of magnitude for elements such as chromium and copper in steels.

No comprehensive work has been done to investigate interferences in this technique, though one might expect them to be similar to other solid sampling techniques. The accuracy of LA-ICP is also not very well documented as yet, but good accuracy has been achieved for nickel and a number of other elements in powdered geological reference materials [87].

It is generally accepted that improvements in the analytical capabilities of this technique are dependent on a clearer understanding of the fundamental processes involved. These fundamentals have been the subject of a number of papers by Thompson and co-workers [92-95]. Studies have also been performed using ICP-Mass Spectrometry [96-99].

Laser ablation techniques are applicable to a wide variety of sample types, conducting and non-conducting, but because of the focusing characteristics of the laser beam, localised, in situ microanalysis is the most promising application of the laser ablation ICP excitation technique. A summary of the studies of laser ablation for plasma spectrometry is given in table 4.

A variety of other solid sampling techniques have been investigated. Greenfield and Sutton [100] used a Danielsson tape machine that passed through

a spark gap. Abercrombie used a similar machine in laser ablation studies [85]. A vibrating device has been used to float powders into the ICP [101], and slurry nebulisation has been used for samples such as animal tissues and coals [102,103].

<u>REFERENCE</u>	<u>LASER</u>	<u>MODE</u>	<u>FREQUENCY</u>	<u>SAMPLE</u>	<u>ELEMENTS</u>	<u>PERFORMANCE</u>
[84]	Ruby	Free Running Q-Switched	-	Steels Brass	Al Co Cr Cu Mn Mo Ni V	3-11% RSD
[86]	Ruby	Free Running Q-Switched	-	Aluminium Brass	Cu Zn Pb Fe Sn Ni Ti Si	2-10% RSD
[87]	Ruby	Free Running	-	Steels	Fe Cu Ni Cr Si	2-25% RSD
[88]	Nd:YAG	Free Running	1-20 Hz	Ores Steels	Cu	2-12% RSD
[89]	Nd:YAG	Q-Switched	5 kHz	Steels	P S Ni Cr Fe Mn Cu Si	0.4-12% RSD
[90]	Ruby	Free Running	-	Steels	Fe Ni	-
[91]	Ruby	Free Running	-	Pebble Coatings	Fe Mn Si Zn Co V	-

Table 4. Summary of Studies of Laser Ablation Plasma Spectrometry.

CHAPTER TWO

THE PRINCIPLES AND APPLICATIONS OF LASERS

2.0 HISTORICAL

The laser (light amplification by stimulated emission of radiation) may be considered as one of the most significant technological advances this century since it has led to the rebirth of the science and technology of optics and opened avenues into new areas of science. The variety of lasers and their applications is huge.

In 1917, Einstein showed that the process of stimulated emission must exist. From that point laser action was waiting to be discovered, but it was not until the early 1950's that Charles H Townes demonstrated a device that amplified radiation by stimulated emission [104]. This device was termed a maser (microwave amplification by stimulated emission of radiation) as it operated in the microwave region of the electromagnetic spectrum. Laser action, operating at optical frequencies, was first reported by T.H.Maiman of Hughes Research Laboratories in 1960 [105]. His ruby laser consisted of a pink ruby rod with silvered ends inserted in the helical coil of a photographic flashlamp.

Since the invention of the laser, a variety of media have been used to produce laser action including impure crystals, semiconductors, ionised gases, molecular gases and dye solutions. Consequently, a range of laser wavelengths is available in the infra-red, visible and ultra-violet portions of the spectrum. Intense

research is currently directed at the x-ray laser.

The range of applications of lasers is many and varied; materials processing, communications, optical data processing, holography, optical spectroscopy, distance measurement and medicine to name but a few.

In the future it is reasonable to expect more powerful lasers to be invented covering wider wavelength ranges. This and further modification of laser output beams will lead to new applications which will serve to re-emphasise that the invention of the laser was one of the most important scientific discoveries this century.

2.1 LASER PRINCIPLES

A laser is a device which generates or amplifies light. The term light is used broadly to include infra-red, visible, ultra-violet and even x-ray wavelengths of radiation. Lasers have a variety of different forms, using many different laser materials, many different atomic systems and many different kinds of pumping or excitation techniques. The beams of radiation emitted by lasers have unique properties of directionality, spectral purity and intensity. It is these properties which have led to such an array of applications for laser radiation.

The essential elements of a laser are;

(i) a laser medium consisting of an appropriate collection of atoms, ions, molecules or a semi-conducting crystal;
(ii) a pumping process to excite these atoms to higher energy levels; and (iii) suitable optical feedback components that allow the beam of radiation to pass once through the laser medium (as in a laser amplifier) or bounce back and forth repeatedly through the laser medium (as in a laser oscillator). The components of a typical laser oscillator are shown in figure 9.

To achieve laser action a pumping process is required to excite the atoms (the term atoms will be used to denote the species of the laser medium be they atoms, ions, molecules or semiconductor electrons) to higher energy levels, but a population inversion is also required. That is, there must be a larger

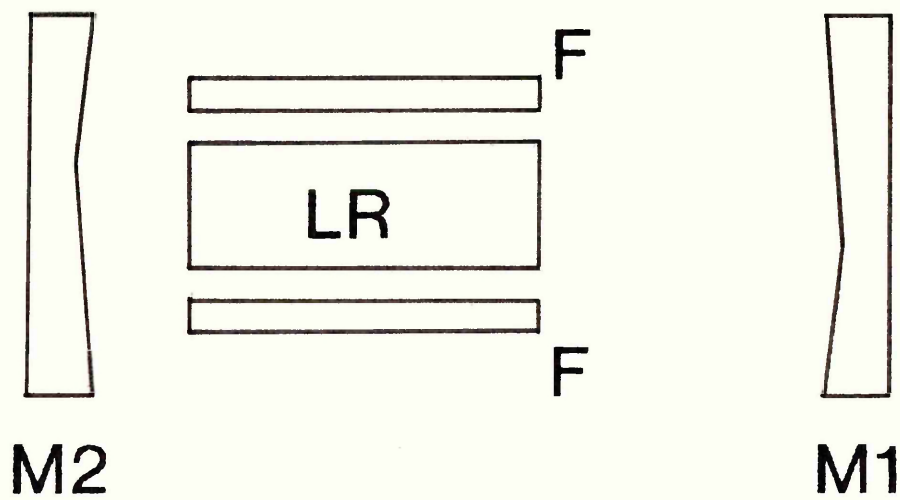


Figure 9. Typical Laser Oscillator showing the active medium or laser rod (LR), the flashlamps (F) used to optically pump the active medium and mirrors (M1, M2) which provide an optical feedback mechanism.

population of atoms in a higher energy level than in some lower energy levels in the laser medium. This condition can be achieved in a variety of ways.

Once population inversion is obtained, radiation within a certain narrow band of frequencies can be coherently amplified if it passes through the laser medium. This amplification bandwidth will extend over the range of frequencies within about one atomic line width on either side of the transition frequency from the more heavily populated upper energy level to the less heavily populated lower energy level. Coherent amplification means that the output signal will almost exactly match the input signal except for a substantial increase in amplitude.

Coherent amplification combined with feedback produces oscillation. The feedback in a laser oscillator is usually supplied by mirrors at both ends of the laser medium. The radiation bounces back and forth between these mirrors with small losses at each reflection. If the net laser amplification between mirrors exceeds the net reflection loss at the mirrors themselves then coherent optical oscillation will build up in the system.

When such coherent oscillation occurs, a highly directional, highly monochromatic beam may be coupled out of the laser oscillator by means of a partially transmitting mirror.

The atomic process of stimulated emission is

a prerequisite for laser action. An excited atom can return to a lower or ground state by one of two possible relaxation mechanisms, spontaneous emission and stimulated emission. These processes are represented schematically in figure 10. The atom may return to its lower atomic level spontaneously and emit a photon $h\nu$. A photon $h\nu$, incident upon an excited atom may stimulate the atom to undergo emission in which case two photons $h\nu$ are emitted. These photons have the same phase and direction. Thus, if an atom is stimulated to emit light energy by a propagating wave, the additional quantum of energy liberated in the process adds to that wave on a constructive basis increasing its amplitude. As indicated in figure 10, the radiation is emitted in the direction defined by the stimulating photon, so both photons leave in the same direction. The emitted radiation has the same wavelength as the stimulating radiation, they are both of the same polarisation and they both have the same phase.

2.1.1 Population Inversion

Consider a group of atoms in thermodynamic equilibrium. The atomic populations of each of the possible energy levels will be governed by Boltzmann's law and may be represented schematically by figure 11, for a simple system of 100 atoms. The immediate conclusion is that no energy level will have a population greater than that of any level beneath it. This is

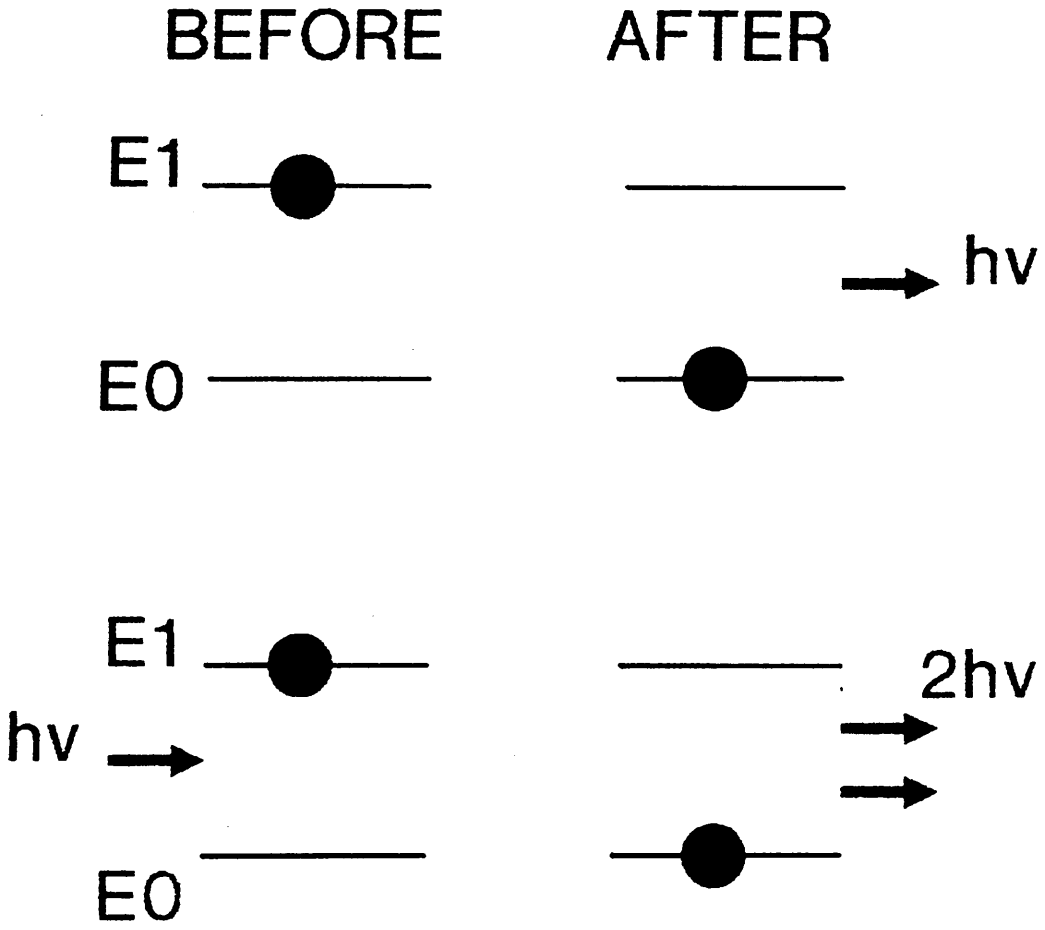


Figure 10. Atomic Emission Processes showing spontaneous emission above and stimulated emission below.

the "normal" situation, but it is possible to induce an abnormal situation for short periods of time.

If energy is added to the system eg. by heating, the distribution changes. There would be fewer atoms in the low lying levels and some of the previously empty upper levels would be populated, but the previous conclusion is still valid. If the system was cooled the reverse would occur and if it were taken to absolute zero, all atoms would be in level E_0 .

Boltzmann's law is applicable to systems in thermal equilibrium but it is possible to create a system in non-thermal equilibrium where the above conclusion is not valid.

If energy is added to the system in precise amounts rather than in the form of random thermal energy it is possible to create a population inversion. If the system was irradiated with a beam of electrons all of the same energy, and that energy was equal to the energy difference between levels E_2 and E_3 , then on collision with an atom in level E_2 it could be excited to E_3 . If the electrons were supplied quickly enough then the atoms could be excited to E_3 quicker than they could spontaneously decay back to E_2 . So a population inversion is created between levels E_2 and E_3 (figure 12). This is a non-equilibrium distribution and will rapidly return to a normal thermal distribution if the exciting electrons are removed.

Consider a system where all the atoms are in

the ground state. Three photons whose energy $h\nu$ correspond to the energy difference between the ground state E_0 and an excited state E_2 irradiate the system. It is highly probable that all three photons will be absorbed putting three atoms into state E_2 . Suppose that half the atoms in the system are in E_0 and half are in E_2 . In this case each of the irradiating photons has a 50:50 chance of interacting with an excited atom and thus stimulating emission. There is also the same probability that a photon will be absorbed by a ground state atom. Hence, for every photon produced by stimulated emission another disappears by absorption, and the number of photons entering the system is equal to the number leaving. If all the atoms were in the excited E_2 state then there is a very high probability that all three photons will stimulate emission so the number of photons leaving the system (perhaps six) will be greater than the number entering. This latter case represents a 100% population inversion.

To achieve this amplification of light, a population inversion is required but not necessarily 100%. A 51% inversion would result in some amplification, but the greater the population inversion the greater the amplification.

The above description assumes that one photon interacts with one atom. In fact the probability of such an interaction occurring is dependent upon the cross-section of the atoms. If the atoms have a large

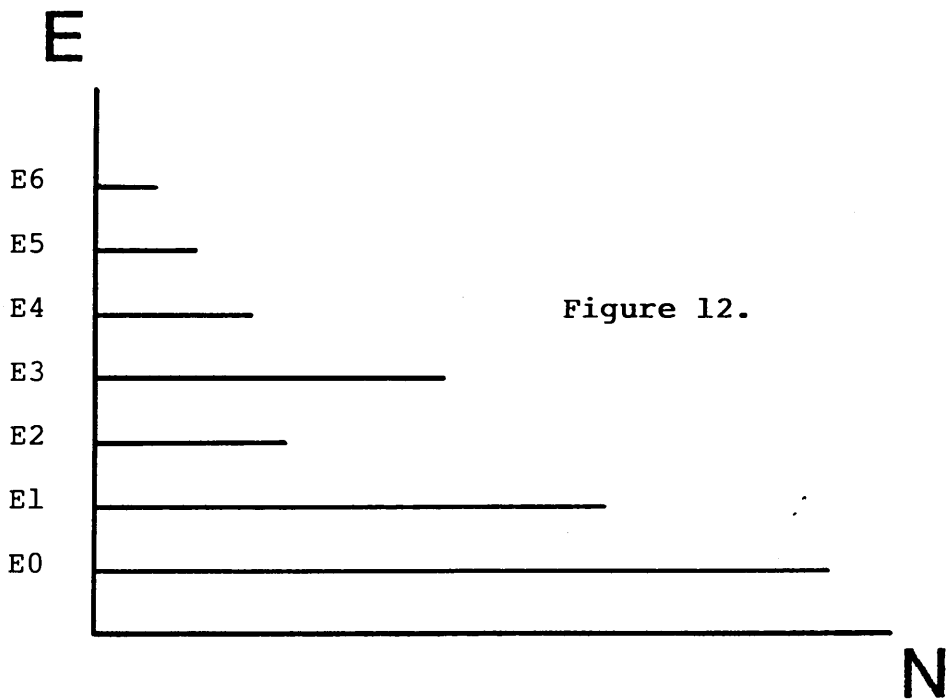
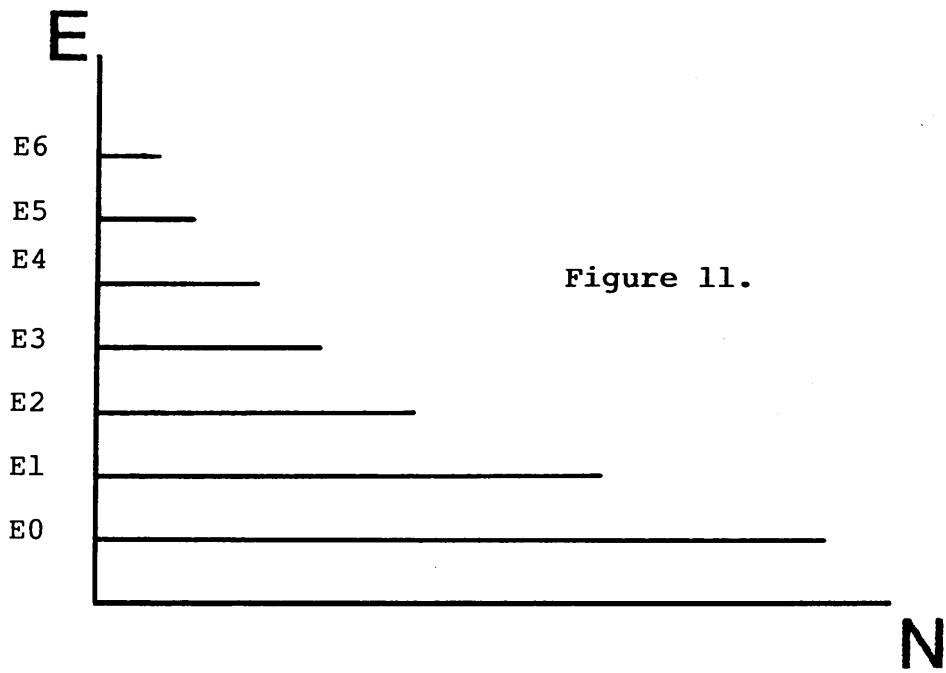


Figure 11. Boltzmann Distribution of Atoms.

Figure 12. Population Inversion.

cross-section, interaction is more likely to occur than if they have a small cross-section. Also, photons produced by stimulated emission may themselves stimulate emission from other atoms. The main point remains that amplification occurs, resulting in more photons leaving the system than entering.

2.1.2 Optical Pumping

Optical pumping is the process of irradiating the laser medium with a light source, usually a xenon flashtube, to achieve a population inversion and induce laser action. This method of pumping is most common with the three and four level energy schemes typical of doped insulator lasers. The atoms are indirectly pumped to the upper level of the laser transition.

A three level scheme is involved for the Ruby laser. Initially, the population distribution among the various energy levels obeys Boltzmann's law. If the ruby is intensely illuminated a large number of atoms can be excited to level E_2 through absorption. From here the atoms decay to level E_1 . With sufficiently intense pumping a significant number of ground state atoms can be pumped to level E_1 . A population inversion occurs when the population of E_1 exceeds that of E_0 (figure 13 a,b and c). For the population inversion to be easily achieved state E_2 must have a very short lifetime (ie decay from E_2 to E_1 is rapid) and state E_1 must be metastable. This allows pumping of ground

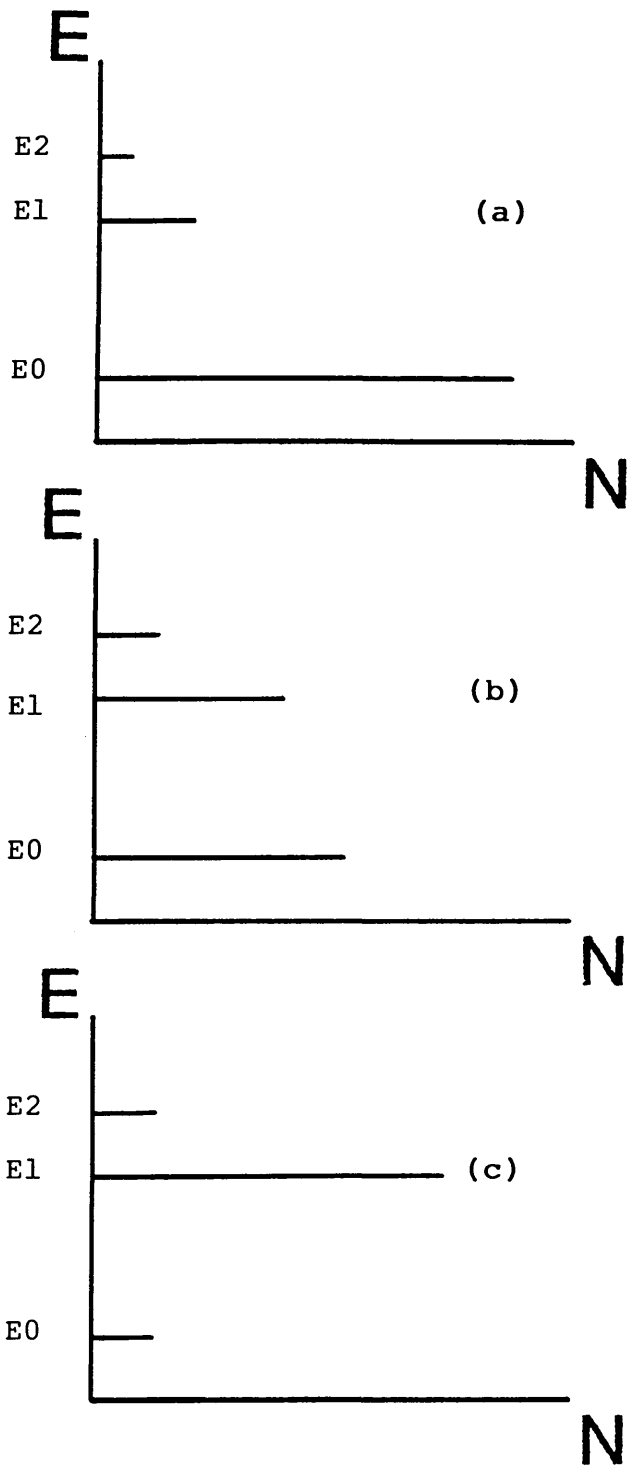


Figure 13. Three Level Pumping Scheme
(see text for further details)

state atoms to level E_1 , where they tend to accumulate.

An important characteristic of three level pumping schemes is that they require very high pump powers. This is due to the fact that the terminal state of the laser transition is the ground state. Consequently, more than one half of the ground state atoms must be pumped to the upper state to achieve population inversion.

The four level pumping scheme, in contrast, is characterised by greatly reduced pumping requirements. Pumping raises ground state atoms to the highest of the four energy levels involved in the process. From here, the atoms decay to the metastable state E_2 whose population grows rapidly. If all the transitions are rapid except for $E_2 - E_1$, then a population inversion between these states is achieved and maintained with only moderate pumping. The populations of levels E_3 and E_1 remain relatively unchanged so only a small number of atoms need to be added to the population of E_2 in order to create the population inversion (figure 14).

The detailed mechanisms involved in pumping lasers can be quite complicated and varied. Frequently, more than three or four levels are involved and complex interactions between energy levels occur. However, the simple pumping schemes given above are adequate representations of the majority of real laser systems. Optical pumping is not the only mechanism by

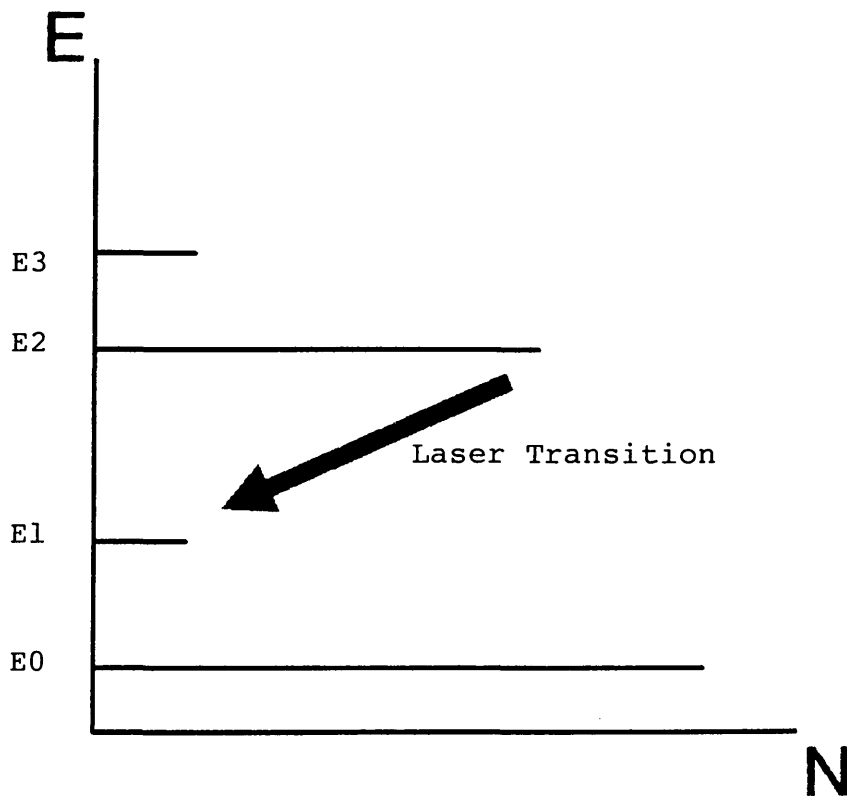


Figure 14. Four Level Pumping Scheme

which population inversion is created. Electrical gas discharges, chemical reactions, electron beams and other lasers may be used to drive the pumping mechanism.

2.1.3 Optical Feedback

Perhaps the most direct application of the amplification by stimulated emission process is the single pass light amplifier. This is a device whose input signal is a collimated beam of narrowband radiation, typically from a laser, which it then amplifies. This direct amplification is practical for only a few select materials because the degree of amplification is of the order of fractions of a percent per centimeter of light travel. This is far too low for a device of reasonable length.

This limitation is overcome in lasers by using reflective mirrors that reflect the radiation back and forth through the laser medium many times. Consequently, the effective length of the active medium becomes many times greater than the actual length of the laser. Whereas a single pass device provides limited amplification, that provided by multiple passes can be substantial.

Placing mirrors at opposite ends of a laser medium produces an optical resonator or optical resonant cavity. If a small amount of spontaneous emission at the laser frequency starts out along the axis of

this device, it will be amplified as it travels. On reflection it will pass back through the laser medium undergoing further amplification and so on. If the round-trip laser gain minus any losses is less than unity then the radiation intensity will decrease and eventually die away. But if the total round-trip gain is greater than unity the radiation amplitude will increase on each round-trip and will become a coherent self-sustained oscillation inside the laser cavity formed by the two mirrors.

It is possible to determine the minimum gain required for operation of a laser by considering the increase of irradiance undergone by laser radiation in traveling a round-trip within the laser. This discussion assumes that the mirrors are in contact with the laser medium and that the pumping excitation is uniform. In traveling from mirror M_1 , to mirror M_2 the initial beam irradiance I_0 increases to a value I given by;

$$I = I_0 e^{(b-a)L}$$

where L is the separation of the mirrors, b is the small signal gain coefficient and a is the distributed loss per unit distance due to scattering and possible absorption in nonactive constituents of the laser medium.

The small signal gain coefficient b is given by;

$$b = B_{01} (N_1 - N_0) \frac{h\nu}{4\pi c} \quad (2.1)$$

where B_{01} is the Einstein coefficient of stimulated absorption, and N_1 and N_0 are the numbers of atoms in state 1 (upper) and state 0 (lower) involved in the laser transition.

After reflection at mirror M_2 , the relative beam irradiance is given by $R_2 \exp((b-a)L)$, where R_2 (the reflectivity of M_2) is the ratio of reflected to incident light irradiance. After a return trip through the laser medium and a reflection at mirror M_1 (which has reflectivity R_1), the final round-trip relative increase in beam irradiance is given by;

$$G = R_1 R_2 \exp(2(b-a)L)$$

$$= \frac{\text{Beam irradiance at end of round trip}}{\text{Beam irradiance at start of round trip}}$$

G , the net round-trip power gain quantifies the build up of oscillations within the laser as a function of b and therefore as a function of the population difference.

If G is greater than unity, any laser transitions resulting from stimulated emission will produce an optical signal that will experience a net round-trip

growth in amplitude and the cavity oscillations increase. If G is less than unity cavity oscillations will die out. Therefore, the threshold condition for laser oscillation may be written as,

$$G = R_1 R_2 \exp(2(b-a)L) = 1$$

In a continuous output laser the small signal gain, which may have increased at the onset of pumping, decreases to b_t , the threshold gain. Only when $G=1$ does the energy in the laser cavity and hence the laser output power become a steady-state value. Therefore, the steady-state value of the small signal gain must equal b_t . This is referred to as gain saturation.

The small signal gain required for steady-state operation is dependant upon the laser medium (via a) and the laser construction (via R_1 , R_2 and L). An expression for the threshold gain b_t as a function of these parameters may be obtained by taking the logarithm of both sides of the above equation;

$$b_t = a + \frac{1}{2L} \ln\left(\frac{1}{R_1 R_2}\right) = a + a'$$

This equation shows the similarity of the two terms, as losses; a represents cavity losses due to absorption and scattering and a' represents cavity losses as useful laser output beam. Thus for

steady-state laser oscillation the gain must be equal to the sum of the losses in the laser.

The small-signal gain b is at least partly dependant upon properties of the laser medium. A laser with a high gain medium can be made to lase comparatively easily, and losses can be greater because a higher threshold gain is allowable. With low gain media losses must be as low as possible before lasing can be initiated.

Optical feedback within the laser cavity is highly dependent on physical properties of the mirrors themselves. It has so far been assumed that radiation within the laser bounces back and forth between the mirrors as a well collimated beam. But due to diffraction effects this is not the case. Some of the cavity radiation passes around the edges of the mirrors. This loss must be balanced by a higher small signal gain (and hence harder pumping) to achieve laser action. For many media this additional loss may mean the difference between sufficient and insufficient gain to reach threshold.

In general, diffraction losses are minimised by using slightly spherical and inwardly concave mirrors. Different combinations of mirrors can give rise to high loss or low loss situations. A simple mathematical relationship can be used to identify these configurations.

Consider a pair of spherically concave mirrors placed a distance L apart such that their centres of curvature lie on a common axis, the optic axis of the

resonator. r_1 is the radius of curvature of mirror M_1 and r_2 that of M_2 . Convention states that the radius of curvature is positive if the centre of curvature lies in the direction of the laser cavity. A particular resonator may then be characterised by considering the movement of a ray of light within the cavity, initially close to the optic axis and inclined at a very small angle to it, a paraxial ray. If the ray is found to move away from the optic axis as the number of reflections increases then the particular resonator configuration would be characterised by high losses. If the ray remains close to the axis the resonator would demonstrate low losses.

It can be shown that a condition called the stability condition is satisfied by a low loss resonator configuration. This condition is expressed in terms of the resonators g-parameters defined as follows,

$$g_1 = 1 - \frac{L}{r_1} \quad \text{and} \quad g_2 = 1 - \frac{L}{r_2}$$

for mirrors M_1 and M_2 respectively. The stability condition then has the form,

$$0 < g_1 g_2 < 1$$

If the resonator satisfies this relationship it is termed stable, as a paraxial ray will continue to remain close to the optic axis even after many

reflections.

If however;

$$g_1, g_2 < 0 \text{ or } g_1, g_2 > 1$$

the resonator is described as unstable and a paraxial ray will diverge away from the optic axis. Where g_1, g_2 equals zero or unity the resonator is on the boundary between stability and instability, it is termed marginally stable.

The most common laser resonator is a nearly planar stable configuration. Such a configuration is relatively easy to align and is also efficient in that it utilises a large fraction of the resonator volume in the amplification process (figure 15).

Unstable resonators can be very useful configurations. They can be very efficient, utilising almost all of the active medium which can then contribute strongly to the amplification process. A confocal or "telescopic" unstable resonator emits an annular beam, but it is still possible to focus the beam to a spot most intense at the centre, similar to a Gaussian beam. Since the unstable resonator exhibits high losses, namely the output beam, it is necessary to use an active medium with a high small signal gain. In such a case, an unstable resonator represents the best practical method for obtaining nearly complete energy extraction from the laser medium in an output beam of high quality.

(figure 16). The laser used in this study utilises an unstable resonator configuration.

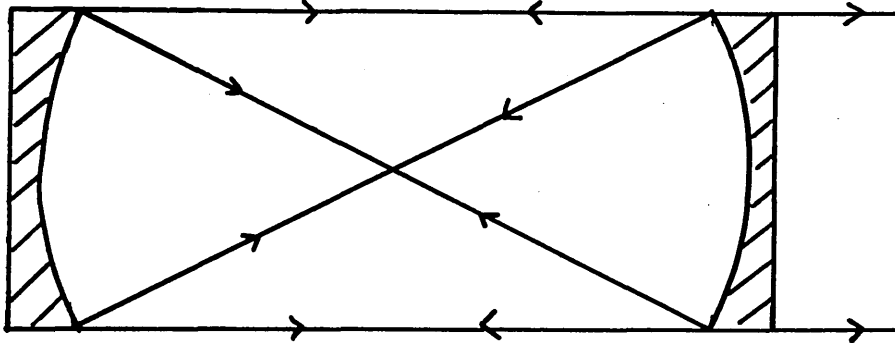


Figure 15. Stable Laser Resonator

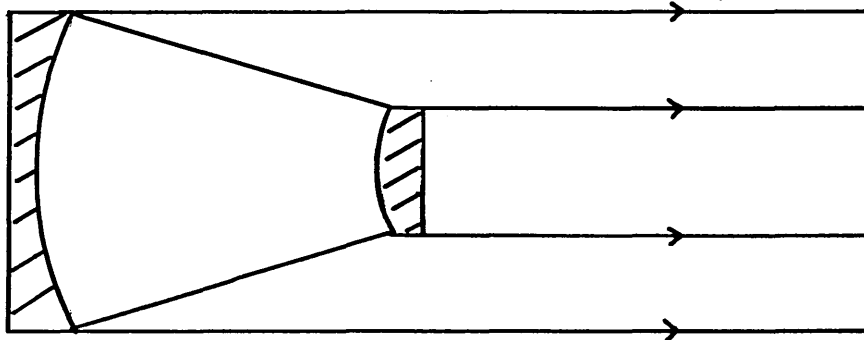


Figure 16. Unstable Laser Resonator

2.2 PROPERTIES OF LASER RADIATION

The radiation emitted by lasers demonstrates some unique properties which are present in lasers to a much greater degree than in any other light source. It is these properties that have made the laser useful in such a wide variety of applications. The most striking properties are those of high radiance and low beam divergence. Laser radiation also exhibits a high degree of monochromaticity and coherence.

2.2.1 Radiance

The radiance of a source of light is defined as the power emitted per unit area of the source per unit solid angle. The units are watts per square metre per steradian. A steradian is the unit of solid angle which is the three dimensional analogue of a two dimensional (planar) angle expressed in radians. For small angles the relationship between a planar angle and the solid angle of a cone with that planar angle is, to a good approximation;

$$s = \frac{\pi}{4} p^2$$

where s is the solid angle and p is the planar angle.

Lasers are generally characterised by a high radiance output. Consider a helium-neon (He-Ne) laser with an output of 1mW, an output spot diameter of 1mm and a beam divergence (angle of the cone into which

the light is spreading) of 1mrad (milliradian);

$$s = \frac{\pi}{4} (\text{1mrad})^2 = 0.8 \times 10^{-6} \text{ sterad}$$

the radiance is;

$$R = \frac{1\text{mW}}{\pi (0.5\text{mm})^2 \cdot 0.8 \times 10^{-6}} = 159 \times 10^7 \text{ W/m}^2 \cdot \text{sterad}$$

The radiance of the sun is only $1.3 \times 10^6 \text{ W/m}^2 \cdot \text{sterad}$ even though it emits a power of $4 \times 10^{26} \text{ W}$.

Radiance is an important concept. It can be high at low powers due to low divergence, another important property of lasers.

The amount of power that can be focused to a spot is directly proportional to the radiance. This introduces another important parameter, the irradiance. Irradiance is the power per unit area falling on a given point. It is expressed in units of watts per square centimeter (W/cm^2). The above He-Ne laser could be focused by a 2.5cm focal length lens to a spot of 25 μm resulting in an irradiance of 200 W/cm^2 . The low divergence of lasers allows focusing of the beam to very small spot sizes which in turn produces high irradiances.

Small spot sizes are required in such applications as integrated circuit manufacture and the recording and reading of optical data storage media. High irradiances are important in materials processing

applications such as welding and cutting.

2.2.2 Monochromaticity

No light source is truly monochromatic but lasers are relatively so. They represent the most monochromatic light sources available. Absolute monochromaticity is an unattainable goal that can be approached by refining laser sources. The single mode laser, which produces the highest degree of monochromaticity yet attained, falls short of the ideal source.

Monochromaticity is characterised by consideration of the spread of frequency of an emission line $\Delta\nu$, the linewidth. The corresponding wavelength spread $\Delta\lambda$ may also be considered.

It has been assumed that atoms in either the upper or lower energy levels of the laser medium interact with a monochromatic input beam. This is not true. All transition lines have a finite frequency and wavelength spread ie. they have a fluorescent or spectral linewidth described by $\Delta\nu$. If the intensity of a spectral line is considered as a function of frequency the result is a Gaussian frequency distribution given by the lineshape function $g(\nu)$. The precise form of $g(\nu)$ depends on the mechanism causing the spectral broadening eg. collision broadening, natural damping and Doppler broadening.

Consequently, when a population of excited

atoms in a laser medium which emit with a given lineshape $g(\nu)$ and halfwidth $\Delta\nu$ are irradiated with an input beam, it must be realised that an input photon $h\nu$ will not necessarily stimulate emission of another photon of energy $h\nu$. The function $g(\nu)$ is the probability that the stimulated photon will have an energy in the range $h\nu$ to $h(\nu+d\nu)$. It can be shown that the small signal gain coefficient b , is proportional to $g(\nu)$. Hence, if the lineshape function is to be taken into account, then the small signal gain coefficient (equation 2.1) must be modified;

$$b = B_{01} (N_1 - N_0) \frac{h\nu}{4\pi c} g(\nu) \quad (2.2)$$

or at the line centre;

$$b = B_{01} (N_1 - N_0) \frac{h\nu}{4\pi c \Delta\nu} \quad (2.3)$$

It can be seen from equation (2.3) that when all other things are equal, the greater $\Delta\nu$ is, the more difficult it is to achieve laser action. For some applications, however, such as mode locking, a laser medium with a wide fluorescent transition curve can be an advantage.

It has been shown that the laser medium can support lasing over a frequency range dictated by the transitions natural linewidth. In practice the frequency

range is less than this, depending on cavity losses and pumping strength. The presence of the optical cavity then serves to limit the oscillating frequencies to certain discrete values within this range, each different frequency being associated with a cavity mode (see next section).

Cavity modes may be separated into two types, axial (or longitudinal) and transverse. Axial modes may be regarded as similar to standing waves on a string and may be designated by an integer p . The frequencies of oscillation are given by $pc/2L$ where L is the cavity length. Normally, values of p are quite large (about 10^6).

Transverse modes are characterised by two integers q and r and designated by $TEM_{q,r}$ (transverse electro-magnetic modes). Values of q and r determine the oscillating frequencies and also the spatial extent of the mode. Higher values of q and r give rise to more complex and more widely spread irradiance patterns across the cross section of the beam. Values of q and r are usually low (<10) and the simplest transverse mode is the $TEM_{0,0}$ mode which exhibits a Gaussian irradiance profile.

If several modes are operating simultaneously, the total frequency spread of the laser radiation will approach the laser gain profile. The frequency spread may then be reduced by reducing the number of modes such that only one can oscillate. This may be done

using a limiting aperture in the cavity. The diameter of this aperture is chosen so that most of the TEM₀₀ mode passes through but those modes of larger spatial spread will experience sufficient losses to prevent them from oscillating. Even when this is achieved there may still be several axial modes operating. The frequency spacing of these modes is inversely proportional to L, the cavity length. The number of axial modes operating may therefore be reduced by decreasing the cavity length which in turn increases the frequency spacing of the modes. When the axial mode separation approaches the width of the gain curve it is possible that only a single mode remains.

Single mode operation produces a laser output whose linewidth can be very narrow indeed. It is directly related to a quantity called the quality factor (Q) of the cavity. Q may be defined as;

$$Q = \frac{\text{resonant frequency}}{\text{linewidth}} = \frac{\nu}{\Delta \nu}$$

and for the calculation of Q the following relationship must be used;

$$\Delta \nu = \frac{\nu}{Q} = \frac{c(1 - R_1 R_2)}{4\pi L}$$

where R₁ and R₂ are the reflectivities of the mirrors.

In theory, Q can be infinite if the cavity

losses are zero. In practice there are always losses that prevent this happening but, even so, linewidths of about 1Hz have been achieved.

Another potential problem is that although the linewidth may be narrow the centre frequency may change with time. This will happen unless the cavity length is kept highly stable. Thus rigid construction and temperature control are necessary.

2.2.3 Laser Modes

If the output beam of a laser is examined with a highly resolving spectrometer it becomes apparent that it consists of a number of closely spaced discrete frequency components covering a moderately broad spectral range. These discrete components are laser modes. They cover a spectral range approximately equal to that of the fluorescent linewidth of the atomic transition producing the laser output. The precise frequencies within this range that are amplified by stimulated emission are dependent on the nature of the mirrors and their separation, the losses in the system and the broadening mechanisms.

For laser oscillations to occur a wave within the cavity must replicate itself so that the waves electric fields add in phase. The mirrors form a resonant cavity and standing waves are set up. The phase change experienced by laser oscillations (ignoring phase changes that may occur on reflection) has the form;

$$d\phi = \frac{2\pi}{\lambda} (2L) = 2p\pi \quad (2.4)$$

or

$$L = p\lambda/2 \quad (2.5)$$

where p is an integer, and L is the separation of the mirrors. Each value of p which satisfies equation (2.5) defines an axial (or longitudinal) mode of the cavity.

Since $v = c/\lambda$ equation (2.5) may be written;

$$v = \frac{pc}{2L} \quad (2.6)$$

and therefore the frequency separation Δv between adjacent modes ($\Delta p = 1$) is given by;

$$\Delta v = c/2L \quad (2.7)$$

The axial modes of the laser cavity consist of a large number of frequencies given by equation (2.6) each separated by $c/2L$. Although there are many modes within the cavity the only ones to oscillate will be those that experience gain at that particular frequency, ie. if the mode frequency lies within the frequency range of the fluorescent line and the gain exceeds the losses.

The axial modes all contribute to a single "spot" of light in the laser output but if a laser

is shone onto a screen a pattern of spots may be observed. These are due to the transverse modes of the cavity. The axial modes are produced by plane waves travelling along the optic axis between the mirrors. Other waves may be travelling off-axis but are still able to undergo amplification by following a more complex closed path within the cavity. Such modes are called transverse electromagnetic modes or TEM modes. They are characterised by two integers q and r and the modes are described as TEM_{qr} . q is the number of minima (or phase reversals) as the beam is scanned horizontally and r the number of minima as it is scanned vertically. The higher order TEM modes can be eliminated by the use of narrow apertures.

The TEM_{00} mode is often described as the uniphase mode as all parts of the propagating wavefront are in phase. It represents the greatest spectral purity and degree of coherence. It is more usual for laser output to consist of a number of discrete frequency components being a complex combination of axial and transverse modes. This not only affects the coherence of the laser but also its divergence and consequently may have limiting effects on the range of applications for a particular laser system.

2.2.4 Divergence

One of the most striking properties of a laser beam is its low divergence. This is apparent from

the sight of a long, thin laser beam which immediately distinguishes the laser from any other light source. The amount of radiation emitted per unit solid angle from say, a thermal light source, is very small compared with even the poorest quality laser.

A laser emitting the TEM₀₀ mode has an output beam that is more or less uniform in amplitude and constant in phase (ie uniphase) across its full output aperture of width or diameter d. Such a beam can propagate for a sizeable distance with very little divergence; will have a very small far-field angle at still larger distances; and can be focused to a spot only a few wavelengths in diameter.

Diffraction theory says for example, that a uniphase plane wave coming from an aperture of diameter d will have a minimum angular diffraction spread $\Delta\theta$ in the far-field given by;

$$\Delta\theta \approx \frac{\lambda}{d} \text{ (in radians)}$$

For a visible laser with $\lambda = 500\text{nm}$ and an output aperture of $d = 0.5\text{cm}$, an angular spread of $\Delta\theta \approx 10^{-4}$ radians is produced.

The axial distance over which this same beam will stay approximately parallel before diffraction spreading begins to significantly increase the beam size (sometimes called the Rayleigh range) is given by;

$$z_R \approx \frac{d^2}{\lambda}$$

the above beam therefore has a Rayleigh range z_R , of approximately 50m.

Suppose this same uniphase beam is expanded by a 20x telescope attached to the laser output and focused to infinity. The source aperture diameter is then $d = 10\text{cm}$ and the above results change to $\Delta\theta \approx 5$ microradians and $z_R \approx 20\text{Km}$. Uniphase beams can be propagated for very large distances with very small divergence.

2.2.5 Coherence

One of the characteristics of stimulated emission is that the stimulated wave is in phase with the stimulating wave, the spatial and temporal variation of the electric field of the two waves are the same. In a perfect laser the electric field varies with time in an identical fashion for every point on the beam cross-section. Such a beam exhibits perfect spatial coherence. Another related property considers the relative phase relationship of the electric field at the same position as a function of time. If the phase changes uniformly with time then the beam is said to show perfect temporal coherence (figure 17).

Coherence can be quantified in terms of the mutual coherence function. This function describes

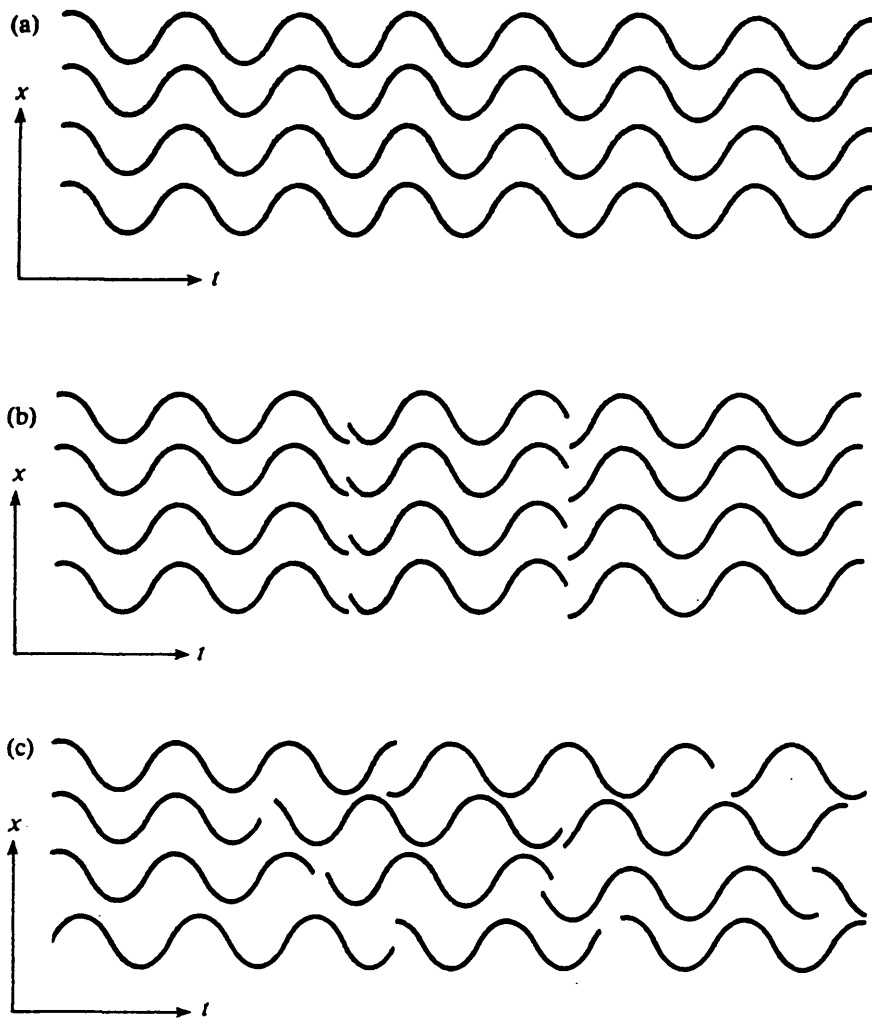


Figure 17. An illustration of coherence. (a) shows a perfectly coherent beam. All the constituent waves are in phase at all times. (b) shows a beam which is spatially coherent, but which exhibits only partial temporal coherence. This is because the waves simultaneously change their phases by an identical amount every few oscillations. (c) shows an almost completely incoherent beam where the phases of each wave change randomly at random times.

(Reproduced with permission from "Lasers Principles and Applications" by J.Wilson, Prentice Hall, 1987, p.103.)

the correlation between the light wave at two points at different times t and $t + t'$. It has an absolute value between 0 and 1. The value 0 represents complete incoherence and the value 1 complete coherence. Although these extreme values are never reached in practice, a gas laser operating in the TEM_{00} mode has a mutual coherence function approaching 1.

There are two useful quantities that are related to coherence, namely the coherence time and the coherence length. To understand these quantities it is necessary to consider a beam of radiation split into two equal parts. These components of the original beam travel different distances before they are recombined. This forms the basis of the Michelson interferometer which is used experimentally to measure coherence.

When the two beams are recombined they will interfere with each other. If the path lengths are such that the path difference is an integral multiple of the wavelength, the beams will recombine to produce a beam identical to the original. This is called constructive interference. If the path difference is an odd multiple of a half wavelength the two beams will cancel each other out. At each point in time and space along the beam direction the electric field components of the two beams are equal and opposite and sum to zero. This is called destructive interference. A path difference between these values produces an

intermediate resultant amplitude.

Consider the schematic of the Michelson interferometer given in figure 18. The original beam is split into two beams of equal irradiance by a beamsplitter B. These beams travel in different directions, one to mirror M_1 , the other to mirror M_2 where they are reflected back towards the beamsplitter. Since the beamsplitter is partially reflecting and partially transmitting it serves to recombine the beams forming once again a single beam. In travelling from the beamsplitter to the mirrors and back again, the distance travelled by the two beams can be adjusted by changing the length L_1 or L_2 .

If $L_1 = L_2$ the two waves travel the same distance and they exhibit complete coherence and produce an interference pattern consisting of a set of parallel sinusoidal fringes. If the two waves have equal amplitude the fringe visibility is unity. If the pathlength difference is increased, the coherence between the waves decreases and the fringe visibility decreases. The fringe visibility can be defined as the maximum fringe irradiance minus the minimum fringe irradiance divided by the maximum fringe irradiance plus the minimum fringe irradiance.

As the pathlength distance increases and the fringe visibility decreases a situation is reached where the fringes disappear completely. The pathlength difference then corresponds to the coherence length

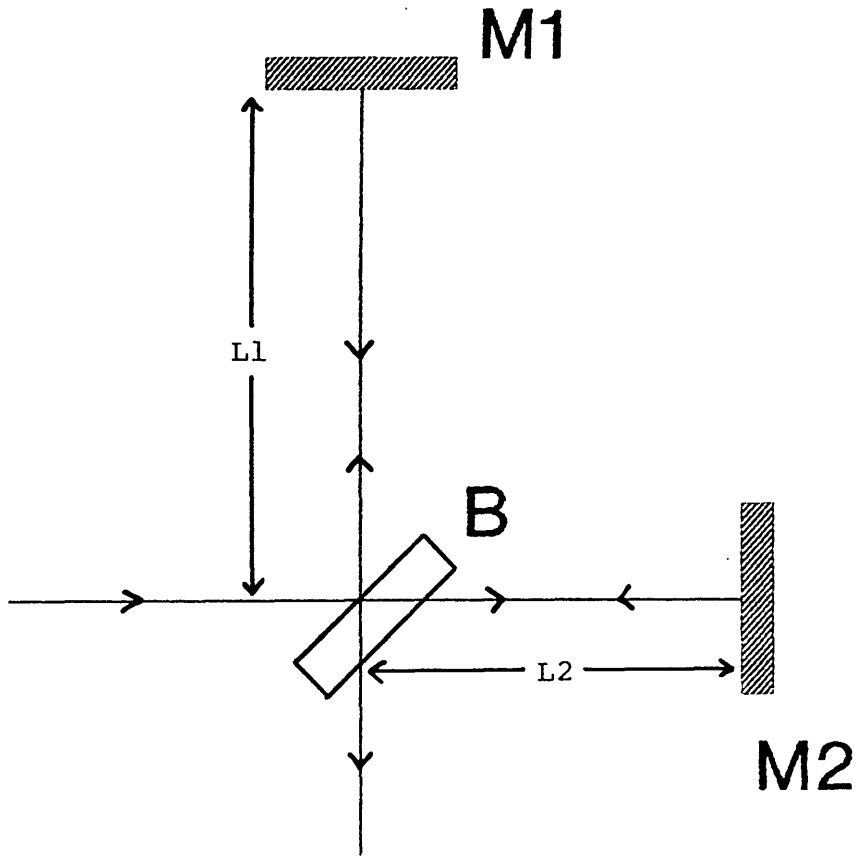


Figure 18. Michelson Interferometer showing mirrors M1 and M2 and beamsplitter B

of the radiation l_c . If the speed of the radiation in the medium is c , then the corresponding time delay known as the coherence time t_c of the source is given by;

$$t_c = \frac{l_c}{c} \quad (2.8)$$

The coherence length is also related to the degree of monochromaticity of the source;

$$l_c = \frac{c}{\Delta v} \quad (2.9)$$

where Δv is the linewidth of the source radiation. The coherence time is then related to the linewidth by;

$$t_c = \frac{1}{\Delta v} \quad (2.10)$$

Clearly, the presence of several modes can dramatically reduce the degree of coherence of a laser. A well stabilised laser emitting a single transverse mode (ie Δv is small) can have a coherence length upto 1000m. Coherence is important in any application where the beam is split into parts that travel different distances. These include the interferometric measurement of distance and holography.

2.2.6 Focusing

The 50 watt output of a laser does not seem impressive when compared to a 1000 watt tungsten filament lamp. But the laser can produce very high power densities when focused. The power densities achieved by focusing the 1000 watt lamp are significantly smaller due to its poor transverse coherence characteristics. Even the laser exhibits some divergence and it is this that limits the achievable diameter of a focused spot. It can be shown that the Gaussian beam from a laser operating in the TEM₀₀ mode can be focused to a spot of radius;

$$w_0 = \frac{\lambda \cdot f}{\pi w_1} \quad (2.11)$$

where f is the focal length of the focusing lens and w_1 is the radius of the beam incident on the lens as measured from the beam centre to the point where the beam irradiance is $1/e^2$ of that at the beam centre.

Equation (2.11) shows that the focused spot size is proportional to both wavelength and focal length of the focusing lens. Consequently, neodymium lasers are sometimes used in applications where a CO₂ laser might otherwise serve were it not for particularly stringent focusing requirements. Also, focusing lenses of relatively short focal length produce smaller focal spots and higher irradiances.

When a laser beam is focused there is an

associated depth of focus, where, in the region of the focused spot, the beam diameter remains small. This concept is important in material processing applications as it indicates how deep a focused beam will cut without refocusing. A useful definition for depth of focus for a Gaussian beam has the form;

$$d = \frac{2\lambda}{\pi} \sqrt{p^2 - 1} \left(\frac{f}{w_1} \right)^2 \quad (2.12)$$

In this equation, p is a tolerance factor. If within the distance d the spot size is to increase by no more than 10 percent (0.10) from its minimum value at focus, then $p = 1.10$. Expressed in terms of the minimum spot size w_0 , equation (2.12) becomes;

$$d = \frac{2\pi}{\lambda} \sqrt{p^2 - 1} w_0^2 \quad (2.13)$$

Note that a large depth of focus is not compatible with a small spot size.

2.2.7 Q-switching

Q-switching refers to changing the Q value of the cavity. The Q value is inversely proportional to the energy dissipated per cycle. In a high loss situation Q is small but when the losses are removed or reduced Q "switches" to a higher value.

Q-switching is a method by which very short but intense bursts of radiation are produced by a laser.

It involves introducing time dependent losses into the cavity. When a high loss is present the gain due to the population inversion can reach large values without laser action occurring. The high losses keep the gain below the threshold level while energy is being pumped into the excited state of the medium. When a large population inversion has been produced the cavity loss can be suddenly reduced and laser oscillations can begin. The threshold gain is now much less than the actual gain so a very rapid build up of laser oscillations occurs. All the energy is in fact dumped in a single giant pulse. This rapidly depopulates the upper lasing level such that the gain is reduced below threshold and laser action ceases. Q-switching dramatically increases the peak powers obtainable from lasers.

A single laser pulse from a laser such as a Nd:YAG can be shown to consist of many random "spikes" of about 1 microsecond duration and with a separation of about 1 microsecond also. These spikes are due to relaxation oscillations representing the competition between population of the upper laser level by the pumping source and depopulation of it by stimulated emission. The total length of the train of spikes is dependent upon the duration of the pumping source, generally about 1ms. The peak powers of these spikes are of the order of kilowatts. Q-switching produces a single spike whose power is in the megawatt range

with a duration of 10-100ns. However, the total energy emitted is less than that emitted in non-Q-switched operation due to the losses associated with the Q-switching mechanism.

Q-switching may simply be imagined as placing a shutter within the laser cavity thereby isolating the active medium from the cavity. Once the laser has been pumped and a high gain achieved the shutter is quickly opened, restoring the Q of the cavity. There are two main requirements for effective Q-switching;

- (i) the pumping rate must be faster than the spontaneous decay rate of the upper lasing level, otherwise it will not be possible to create a sufficiently large population inversion;
- (ii) the Q-switching mechanism must operate rapidly compared to the build up of laser oscillations, otherwise the latter will build up only gradually and a longer pulse will be obtained with lower peak power. Practically, the Q-switch should operate within a nanosecond or so.

The first method of Q-switching to be developed was the rotating mirror method where one of the cavity mirrors rotates at high angular velocities. Cavity losses will be high except for the brief moment during every rotation that the mirrors are parallel. Just before this moment is reached a trigger initiates the pumping mechanism thus allowing the population inversion to build without laser action occurring. As the mirrors

become parallel Q-switching occurs and a pulse of radiation emitted. This Q-switch is cheap, reliable and rugged but it is basically slow (approximately lms) which results in longer pulses of relatively low peak power.

A popular method of Q-switching a laser utilises an electro-optical Pockel's cell. This is used in conjunction with a polariser in the laser cavity. The Pockels cell contains an electro-optic crystal, which when a voltage is applied to it rotates plane polarised light through 90° . Consider light leaving the laser medium, it passes through a vertical polariser and becomes plane polarised. When a voltage is applied to the Pockels cell this plane polarised light becomes circularly polarised, is reflected at the cavity mirror and passes back through the Pockels cell such that the emergent radiation is horizontally polarised. This radiation can not now pass through the polariser and the laser cavity losses are high. When no voltage is applied to the crystal, vertically polarised light can pass through in both directions unaffected. To produce a Q-switched pulse, a voltage is applied to the Pockels cell whilst the population inversion builds up and then it is quickly switched off to allow rapid build up of laser oscillations. The applied voltages are of the order of kilowatts and the switching time is in the nanosecond range. The laser used in this study utilises this Q-switching technique.

When an ultra-sonic wave is passed through a medium, the strains it imposes produce periodic variations in refractive index within the medium. This creates a diffraction grating and forms the basis of acousto-optic Q-switching. When the ultra-sonic wave is applied the diffraction grating diffracts the laser radiation out of the cavity thus reducing the Q. If the ultra-sonic wave is momentarily stopped the cavity Q increases rapidly and a Q-switched pulse is emitted.

2.3 LASER APPLICATIONS

The laser in all its forms, is a very versatile tool and as such has been put to use in a wide variety of applications. Generally, a laser offers several advantages when considering a particular application and these are usually related to the unique properties of laser radiation. It is possible, however, for one of these properties to be disadvantageous to its use.

The major advantages are;

- (i) High monochromaticity
- (ii) High coherence
- (iii) Low divergence
- (iv) Can be focused to a small spot
- (v) Easy to direct beam over considerable distances
- (vi) Propagate through most gases
- (vii) Can be transmitted through transparent materials
- (viii) Easily computer controlled
- (ix) Not affected by electromagnetic fields
- (x) Wide range of power levels, mW to tens of kW
- (xi) Wide range of pulse energies
- (xii) Wide range of pulse repetition rates, pulse lengths and pulse shapes.

Not all these advantages are associated with all lasers. Diode lasers have relatively large angles of divergence, excimer lasers exhibit poor spatial coherence and some lasers have relatively large bandwidths. This does not negate the usefulness of

these lasers in a variety of applications.

High monochromaticity and coherence are not important in materials processing applications, except potentially in the polymer and semiconductor industries. The lack of coherence of excimer lasers is actually an advantage for photolithographic work in the semiconductor industry. There are few materials transparent to carbon dioxide or excimer laser radiation.

High spatial coherence produces a phenomenon called speckle, which gives laser radiation a characteristic grainy appearance. This interference effect can be problematical in some cases but speckle interferometry is a useful technique for determining small distortions of parts.

In low power applications such as holography and distance measurements, good coherence and monochromaticity are requirements along with high radiance and the potential for very good frequency stabilisation. The latter is very important for Doppler velocimetry and interferometric displacement measurements.

In high power applications, high radiance is of paramount importance as it is related to the capability of focusing the beam to a small spot thus creating very high irradiances.

There are several disadvantages associated with lasers when considering their use in a given application. When a lasers unique properties are required the disadvantages become incidental. The major

disadvantages are;

- (i) High capital cost
- (ii) Low efficiency
- (iii) High technology
- (iv) Safety
- (v) Operator training

These disadvantages are not always applicable.

A HeNe laser for example may be purchased for about one hundred pounds. Others may cost hundreds of thousands of pounds. The laser may only account for a small fraction of an overall system and if its use increases productivity the high capital cost may be justifiable.

Efficiencies vary from 0.1% for HeNe lasers to 10-15% for carbon dioxide and 10-20% for diode lasers. Poor efficiency is generally of little importance when a laser is required to perform a particular function that nothing else can and when total power consumption is low.

Lasers are usually regarded as high technology devices but much of the technology is fairly standard. The resonator and optics (internal and external) are generally the only unfamiliar parts of a laser or system that incorporates a laser.

Some form of training in laser safety is a prerequisite to the use of a laser. Not only does the beam itself present a hazard but other associated dangers arise from electrical equipment and the effects the laser has on materials eg flammable liquids.

2.3.1 Metrological Applications

Optical measurement of parameters such as distance, alignment, angle and flatness has been performed for many years. But the introduction of lasers, particularly visible gas lasers, has dramatically increased the scope of optical metrology and often greatly simplified its use. Lasers are now routinely used for a variety of metrological measurements including velocities of solid objects and fluid flows, rotation, geometrical and mechanical parameters, deformation, vibration, strain and surface roughness.

Perhaps the most obvious application of lasers such as the HeNe laser is alignment. The laser produces a visible line which may be used for positioning an object, surveying, guidance of equipment in construction or for aiming other lasers or optical equipment. Using a beam of light for alignment, often called optical tooling, has many advantages over mechanical alignment methods which are slow, cumbersome and often require more than one operator. Optical tooling may be used for alignment, angular alignment, definition of planes, leveling and fixing of right angles. Such measurements are of particular interest to surveyors and civil engineering projects such as pipeline construction and where the guidance of machinery is required.

Short to intermediate distances may be accurately measured using interferometric techniques, while for longer distances beam-modulation telemetry or

time-of-flight methods may be used. The classical method of measuring distance and small displacements is the Michelson interferometer. Variants of the basic instrument (figure 18) are used to measure surface flatness and to test optical components. In distance measurement, accuracies of a tenth of a wavelength are easily attainable.

Interferometers are also used for the measurement of surface topography and optical component testing. The Fizeau interferometer is the classical instrument used for measuring the variation between a test and reference surface. The test surface may be placed in contact with the reference surface such that any irregularities in the test surface produce air wedges between the two surfaces. These irregularities may be located and characterised by observation of any distortion of the interference fringe pattern. A derivation of the Michelson interferometer called the Twyman Green interferometer may also be used for testing optical components. It should be noted that whereas the Fizeau interferometer enables the optical quality of the surface of a component to be measured the Twyman Green interferometer tests the optical path through the component.

Beam-modulation telemetry is used to measure distances greater than 100m. This technique involves amplitude (or polarisation) modulation of a laser beam. The amplitude of a laser beam is modulated at a frequency

f and projected to the target whose distance is to be measured. The light reflected by the target is collected by a telescope and sent to a detector. The phase of the modulation of the reflected beam is different from that of the emitted beam because of the time taken for the light to travel to the target and back. The phase shift is simply related to the distance travelled. Amplitude modulation may be performed using simple mechanical choppers and polarisation modulation may be achieved by using an electro-optic Pockels cell (see section 2.2.7). Beam-modulation instruments have been developed with accuracies of better than 1 in 10^6 .

Pulse-echo techniques are used for the measurement of very large distances. Such methods involve timing the round-trip transit time for a very short pulse of light reflected from a distant target. The system consists of a pulsed laser, preferably Q-switched, a telescope to collect the reflected radiation, a photodetector and an accurate timer. A typical hand held military rangefinder incorporates a Nd:YAG laser which emits 15mJ pulses of energy which are 8ns long. Accuracies of plus or minus 5m in ranges of 5-10Km are readily achievable. Accuracy can be improved by mounting retroreflectors on the target. Retroreflectors left on the surface of the moon during Apollo space missions have enabled the lunar distance to be measured to an accuracy of about plus or minus 0.15m [106].

The technique, often called optical radar or lidar (light detection and ranging) is widely used and has been extended to atmospheric studies. By measuring the amount of backscattered light the presence of air turbulence can be detected and the amounts of various atmospheric pollutants can be measured.

As stated above, pulse-echo techniques provide information on the range of a target but the target velocity can also be determined from the Doppler frequency shift in the returned pulse. This is the basis of laser Doppler velocimetry [107]. The technique has the advantage of being non-invasive and although it was used before the development of lasers, the highly coherent output of lasers has made possible the development of almost ideal Doppler velocimeters. They require no calibration and produce a reading which is linear with velocity in liquids and gases. The technique has been used for measurements in wind tunnels, internal combustion engines, near flames, of the velocity of moving parts of machinery, propellers and the like. It has also been used for the measurement of blood flow. The dynamic range extends from micrometers per second to several times the speed of sound.

Doppler velocimetry is best suited to the determination of the velocity of relatively smooth surfaces. Rough surfaces, where irregularities are larger than the wavelength of the illuminating radiation, are best determined using the speckle pattern. The

speckle pattern produced by the target surface appears to move if the surface is moving and a simple relationship between the apparent velocity of the pattern and the actual velocity of the target surface allows determination of the latter. This provides a useful non-contact method of measuring the velocity of surfaces with a variety of textures and colours. It has been used in the velocity range from 0.1m/s to 10m/s.

2.3.2 Materials Processing Applications

Surface hardening was one of the first successful applications of high power lasers in industry. Surface hardening of ferrous materials involves heating to above a critical temperature followed by a rapid cooling (quenching). The laser beam is defocused or averaged out by scanning the beam in a zig-zig or helical fashion across the surface to be treated. Either the beam or the part is translated. The CO₂ laser is the most common in such applications and power densities of a few thousand watts per square centimetre usually suffice if the intent is to heat the surface without melting. Some metallic surfaces exhibit high reflectance at 10.6 micrometers, so coatings are generally used to help couple the beam power into the metal surface. The incident beam raises the surface temperature of the metal to some point generally below the melting point. Thermal conduction carries heat into the metal, causing the temperature to rise. At some depth below

the surface the maximum temperature reached will be the critical temperature for transformation hardening. If the part is large compared to the beam diameter, thermal conduction will result in sufficiently rapid cooling to provide self-quenching. Laser hardening improves wear resistance, impact strength and fatigue strength.

Laser surface melting can be achieved in two possible ways, slow melting and rapid melting. In the former a defocused beam is scanned across a surface at a speed which results in substantial melting. The purpose of this melting is to homogenise the microstructure. In rapid melting a focused beam is used and rapidly scanned across the surface. This produces a very thin and narrow melt layer. This treatment can produce a non-crystalline or glossy layer which is generally more resistant to corrosion.

Laser chemical vapour deposition (LCVD) is a process whereby the laser is used to heat a substrate so that a vapour can be deposited on it. In some cases the laser is also used to vaporise the material to be deposited. LCVD is used for several purposes, including improved wear and corrosion resistance. In the semiconductor industry it is used extensively for deposition of a variety of dopants. The major advantage of using the laser for heating the substrate is for the selective deposition of the material.

Cladding and alloying are similar processes.

In both cases an appropriate powder is laid down on the surface and is melted by the heat from the laser beam. In cladding, sufficient heat is put into the part to melt the powder and to produce a metallurgical band between the solidified material that is added and the base metal surface. In alloying, the base metal is melted to a substantial depth and the alloying material is mixed into the base metal to produce a new alloy. Such processes may improve wear resistance, corrosion resistance and impact strength but the most appropriate applications are usually when only selected areas require treatment.

Lasers have found widespread use in welding. Both continuous wave (cw) and pulsed lasers can be used. For situations where only a small spot weld is required a single pulse from a pulsed laser may be sufficient. If a continuous weld is required, the beam is moved across the workpiece. The cw laser produces a continuous weld, while the pulsed laser produces a train of spot welds, which may overlap or be separated, depending on the scanning speed. As the beam can be focused to very small spot sizes, laser welding and soldering of minute metal contacts such as those in electronic circuits is readily achievable.

Lasers are also used for cutting applications. Most materials can be readily cut using a CO₂ laser with the exception of those such as brass, copper and aluminium which have high reflectancies at 10.6

micrometers and also high thermal conductivities. Since the reflectancies are much lower at 1.06 micrometers Nd:YAG lasers can be used instead. Lasers may also be used for cutting materials such as paper, nylon and foam rubber. The related processes of drilling, scribing and marking may also be performed using lasers.

2.3.3 Miscellaneous Applications

A complete resumé of all laser applications would be beyond the scope of this thesis. In this section, a range of laser applications not mentioned earlier will be discussed. It should not be interpreted that inclusion in this section indicates a less significant application.

Lasers have been used to perform uranium enrichment for use in the nuclear power industry. The laser is used to preferentially ionise the U-235 isotope which may then be separated out using an electrostatic field.

A variety of applications exist in medicine, such as in surgery as a cutting tool, in ophthalmology and in dermatology. When cutting tissue, the laser may be positioned and used with high accuracy, used in relatively inaccessible regions, causes little damage to adjacent tissue and has a cauterising effect thus reducing bleeding. The beam may be directed by a fibre optic placed inside an endoscope. Detached retinas have been treated for many years using lasers but a

relatively new applicaion involves the treatment of heart disease. Blood vessels in and around the heart can become constricted due to the deposition of plaque. Laser radiation carried along an optic fibre placed inside the blood vessel can be used to vaporise the plaque so removing the constriction.

Very soon after the development of the laser, its potential military applications were being contemplated. They are currently used as rangefinders and in missile guidance systems. A recent development involves the use of a laser to induce temporary blindness in military personnel.

The applications of holography are many and varied and their range is increasing rapidly as the field continues to develop. Many of these applications require the combination of holography and other techniques. Some of the more important applications are particle size analysis, high-resolution imaging, holographic optical elements such as gratings, information storage and processing, displays and holographic interferometry as applied to the measurement and analysis of vibrations, stress and strain and small movements of a wide range of objects.

Optical communication systems rely on lasers. The high frequencies offered by lasers increase the amount of information that may be transmitted. Modulation of the laser creates a signal which may be transmitted along optical fibres over large distances. A fibre

based communication system consists of three main elements; the emitter which converts the original electrical signal into an optical one, the fibre itself and the detector which re-converts the optical signal back into an electrical one.

Lasers are now found in many households within compact disc players. The disc has a high storage density and retrieval of data does not require physical contact hence reducing wear. The data is stored as a spiral track of pits on the disk. To read the stored information an optical pick-up converts the variations in reflectance due to the pits and bands (areas between pits) into an electronic signal. A lens within the pick-up focuses a low power laser beam to a small spot on the track and also redirects the light reflected from the disk to a photodetector. The output of the photodetector varies according to the distribution of the pits and produces an electrical signal which enables the original audio signal to be regained.

Lasers are truly versatile instruments and although the range of applications discussed here has been necessarily brief it should be realised that there are many applications that have not been mentioned. New applications arise continuously as development is progressing very rapidly. Areas of intense research include laser fusion, military applications such as the Strategic Defence Initiative (SDI) often referred to as "Star Wars" which forms part of American defence

policy and research into achieving laser action at higher frequencies such as the X-ray region of the electromagnetic spectrum.

2.3.4 Lasers in Analytical Spectroscopy

Lasers have become an integral part of modern analytical spectroscopy. Their unique properties have been applied to a variety of spectroscopic techniques which will be discussed here. The field is extensive and rapidly expanding, consequently the methods discussed have been selected to indicate the diversity of laser techniques and applications and are by no means exhaustive.

Laser excited atomic fluorescence spectrometry (LEAFS) originated analytically when Winefordner and Vickers [108] described their first experiments using a conventional atomic absorption atomiser, a flame operating at atmospheric pressure. At this stage a laser was not utilised but it soon became apparent that atomic fluorescence was a source intensity starved method. The excitation provided by sources such as hollow cathode lamps was completely inadequate for obtaining good signals. Not only was source intensity a problem but atomiser noise for flames and electrothermal atomisers in the spectral region above 300nm was also of concern. Best results would therefore be obtained by pulsing the excitation source (thus achieving high peak intensities) and gating the detector so that the

noise is only measured for short periods of time. The pulsed, tunable dye laser [109,110] soon became the preferred source. It has the advantages of being tunable over a wide wavelength range, high intensity, high degree of coherence and a range of pulsing frequencies. Laser excitation provides better detection limits due to the high intensity and greater selectivity due to the source resolution. A variety of atomisers have been used for LEAFS such as graphite cups [111], electrothermal atomisers [112-114] and plasmas and flames [115]. The technique is extremely sensitive providing elemental limits of detection to 10^{-4} microgrammes per litre [116], has a wide linear range, high analytical selectivity and is relatively simple. A wide range of analytical applications includes nuclear fuel reprocessing [117], determination of rare earth elements [118], group three elements [114], plant samples glasses and alloys [113] and diagnostic studies of the Zeeman effect [119] and of flames and plasmas [115]. The latter often involves fluorescence dip spectroscopy which utilises the decrease of the fluorescent signal caused by the laser induced depletion of the atomic population of the fluorescent energy level.

Photoacoustic spectroscopy involves the absorption of a pulsed laser beam by a medium which consequently produces an acoustic wave. This can be detected by a sensitive microphone in the gas phase or a piezoelectric device in the solid phase. The technique is very

sensitive and absorbances as low as 10^{-7} have been detected.

The interaction of a laser with a sample is an efficient way of generating gas-phase ions, whilst mass spectrometry is the most sensitive and selective way to measure ions. Consequently, it is only natural that lasers should be investigated and used in ionisation techniques for analytical mass spectrometry [120]. Laser mass spectrometry is commercially available under the following acronyms, LAMMA, laser microprobe mass analyser and LIMA, laser ionisation mass analyser. The technique is applicable to the elemental analysis of solids [121]. The laser effectively vaporises localised areas of the sample producing significant proportions of positive atomic ions which are amenable to detection by mass spectrometry. Lasers are attractive elemental ion sources; the power density incident upon the sample is easily controlled; microsampling of discrete areas is possible; spatial and depth profiling is feasible; the beam does not add charge to the sample so insulators and conductors may be determined. Gaseous species may be determined by using the laser to photoionise species. The radiance of the laser is sufficient to produce multiphoton ionisation and there is evidence that it may be used to selectively ionise a particular analyte if the source wavelength and laser power density are selected appropriately. LAMMA has been used for structural analysis of organics [122]

and also to obtain information about spectroscopic properties of a wide variety of species [123,124].

Practical Raman spectroscopy was made possible with the advent of lasers. The higher powers available mean that coherent and stimulated Raman processes can be investigated (CARS and SRS). In conventional spontaneous Raman, which has conventionally used a visible laser source (Ar or Kr ion laser), the problem of fluorescent samples has limited some analytical applications of the technique. The use of a continuous wave Nd:YAG laser at 1064nm eliminated many of these difficulties as far fewer samples fluoresce in the infra-red. Rubbers and other polymeric materials are now being studied.

Laser enhanced ionisation (LEI) spectroscopy in flames is a specialised area of optogalvanic spectroscopy. The optogalvanic effect may be defined as the perturbation of the electrical properties of a plasma in response to the absorption of light via discrete optical transitions in atomic or molecular constituents of the plasma. The use of tunable dye lasers has widened the applicability of the technique to a greater variety of transitions and plasmas than with conventional light sources [125,126]. The medium in which the optogalvanic effect occurs, a plasma or flame, supports some degree of ionisation in the absence of a perturbing laser, either by electrical or chemical means. The laser indirectly alters the degree of

ionisation in the plasma by perturbing atomic energy state distributions, thereby shifting the kinetic balance of the plasma. Although either pulsed or continuous wave lasers may be employed, the latter would typically be amplitude modulated so that synchronous detection may be used to distinguish laser enhanced ionisation from the continuous thermal ionisation background of the flame. Laser enhanced ionisation is then detected as changes in a current passed through the flame by the application of a high voltage across electrodes, one of which may be the burner head. The technique has been used for a variety of elements and samples [127-130] including multielement determination of waters [131]. Sub-nanogramme per millilitre detection limits are routine [132] which will undoubtedly be improved upon.

Tunable lasers, with their narrowband output, have enabled new applications of atomic absorption measurements that are difficult, if not impossible, with traditional sources like hollow cathode lamps. Modern tunable dye lasers as sources for atomic absorption spectroscopy offer several advantages over other sources; narrow linewidths; continuous tuning over selected wavelengths; high intensity; collimation and excellent focusing properties; short pulse duration. A laser may be tuned to the center of a sample cell absorption line where the absorption signal is strongest. Atomic and ionic absorption wavelengths not produced by ordinary

emission sources may also be produced. The laser linewidth can be much narrower than the narrowest line from hollow cathode lamps which eliminates finite spectral bandwidths as a cause of non-linearity in analytical curves especially at high absorbances. The high intensity of the laser beam minimises the influence of shot noise allowing greater precision in the measurement of transient signals such as produced by electrothermal vaporisation, laser ablation and sparks. The high irradiance also promotes a large fraction of an atomic population to the excited state allowing atomic absorption measurements to be made from the excited state. This provides additional analytical wavelengths which may be used to eliminate spectral interferences. The technique is at the early stages of development but a range of applications is envisaged. The range of wavelengths made available by the laser facilitates measurements of atomic, ionic and molecular species in excited states and ground states. This may enable a total analysis of an element in all of the forms in which it exists in the sample cell. Another unique application involves placing the sample inside the laser cavity to obtain an enhanced absorption signal thus offering the promise of very low detection limits.

Lasers have found widespread application as atomisers. The high radiance of the beam is used to produce an atomic vapor from a solid or liquid sample. The free atoms in the vapor may then be detected by

means of their absorption spectra or, if suitably excited, their emission spectra. Ionised species may be subjected to mass spectrometric analysis as described earlier. Vaporisation, atomisation and excitation are often performed by the same source, although potential advantages may be realised by separating these processes and optimising them individually. In the case of electrical excitation sources all three processes are performed by an electrical arc or spark. A laser facilitates in situ microanalysis of a sample surface with very high spatial resolution. Conducting and non-conducting samples are amenable to laser atomisation and the atomisation and excitation processes may be separated. Analytical spectra from an atomic vapor produced by laser atomisation may be generated in a variety of ways. The vapor cloud has a considerable proportion of ground state neutral atoms, therefore atomic absorption methods may be used to identify these atoms. Such methods were first proposed by Mossotti [133]. The atomic absorption may be directly observed by passing the source radiation directly through the laser produced vapor cloud. However, the vapor cloud may be subjected to additional heating in a flame or furnace prior to the absorption measurement. In the case of flame methods, the sample is remote from the flame and the vapor cloud produced by the lasers interaction with the sample is transported in a gas stream to it [134]. Optical emission spectra may also

be obtained from the vapor cloud. Using a Q-switched laser produces a plume above the sample surface which is hot enough to radiate in the optical region of the spectrum. Emission from the plume may be measured directly or an additional excitation source may be used. The most common additional source is spark cross excitation, where electrodes are positioned such that the plume is between them. The charged particles of the plume initiate the discharge and the emission is recorded. As with the atomic absorption measurements, the vapor cloud may be transported to a remote excitation source to generate emission spectra. A wealth of information on this and related techniques is available in a book edited by Omenetto [135]. Table 5 summarises a range of laser types, their characteristics and applications.

In this work, the laser is used to remove material from a sample for excitation by a remote source. The term "laser ablation" is used to describe the process of material removal by an incident laser beam. The term "laser vaporisation" has been used but this implies that all the material removed is in the vapor phase. The material actually consists of atoms, ions, molecules and clusters of particles in a range of sizes [136], so the former term will be used in this report. A Nd:YAG laser is used to ablate material from samples under investigation and this material is transported in a gaseous stream to an Inductively Coupled Plasma

(ICP). The ICP generates emission spectra of the sample material which provides information on its elemental composition.

This research project considered the configuration of an ICP and a laser to produce an analytical system suitable for laser ablation ICP studies. The design of a novel laser ablation chamber was also undertaken. This resulted in a sample chamber which incorporated an electrothermal heating capability, a facility not considered by other research groups.

Aims of this research included the investigation and optimisation of a variety of parameters associated with the ablation process. Electrothermal heating was to be used to consider laser ablation of molten samples and to make small metallurgical turnings more amenable to laser ablation studies.

To investigate different sample types was a further requirement of this work, and preferably samples not considered by other workers. Consequently, the applicability of laser ablation ICP to paints and polymers was considered. A further novel aspect of this work was the ablation of aqueous solutions as a means of calibration and analysis.

Having discussed ICP and lasers, we may now consider the equipment used in this study and the methodology employed to fulfil the above objectives of this project.

<u>TYPE</u>	<u>NAME</u>	<u>WAVELENGTH</u>	<u>OUTPUT</u>	<u>MEDIUM</u>	<u>EFFICIENCY</u>	<u>APPLICATIONS</u>
Semiconductor	GaAlAs	750-905nm	CW <40mW Pulsed <5mJ	Solid	1-20%	Communications, Recording
	PbNaCl	3-30um	CW <100mW	Solid	30%	Communications
Excimer	ArF	193nm	Pulsed <500mJ	Gas	1%	Spectroscopy
	KrF	248nm	Pulsed <1J	Gas	2%	Spectroscopy
Dye	Flash lamp pumped	340-940nm	CW or Pulsed	Liquid	1%	Photochemistry, Light shows
			<50J			
Solid State	Ruby Nd:YAG	694.3nm 1064nm	Pulsed <100J	Crystal	0.5%	Holography
			CW <600W	Crystal	3%	Holography, Medicine
			Pulsed <200J			
Chemical	HF	2.6-3um	CW <150W	Gas	1%	Research, Military
			Pulsed <600mJ			

Table 5. Brief Summary of Laser Types and their Applications

CHAPTER THREE

EXPERIMENTAL INSTRUMENTATION

3.0 THE LASER

The laser system used was a Quanta-Ray DCR-11, pulsed Nd:YAG laser supplied in the U.K. by Spectra-Physics. It is a Class IV high power laser and as such is potentially very hazardous. The lasing wavelength of 1064nm is invisible and passes easily through the cornea of the eye. This, coupled with the high output power could result in instantaneous and permanent damage to the retina. Precautions to prevent accidental exposure to the beam, and to diffuse and specular reflections, must be taken as severe eye or skin damage are potential hazards.

Neodymium-doped yttrium aluminium garnet (Nd:YAG) is the most widely studied and best understood of all solid state laser media. Its transition scheme is depicted in figure 19. Level E_3 represents the pump bands, E_2 the ${}^4F_{3/2}$ level at 11502cm^{-1} , E_1 the ${}^4I_{11/2}$ level at 2111cm^{-1} and E_0 the ${}^4I_{9/2}$ level which is the ground state of triply ionised neodymium. The active medium, triply ionised neodymium, is pumped by a flash lamp whose output matches principle absorption bands in the red and near infrared. The excited ions quickly drop to the E_2 level, the upper level of the lasing transition, where they remain for a relatively long time, about 230 microseconds. The most probable lasing transition is to the ${}^4I_{11/2}$ level emitting a photon at 1064nm. From here the ions relax quickly to the ground state and consequently its population remains low.

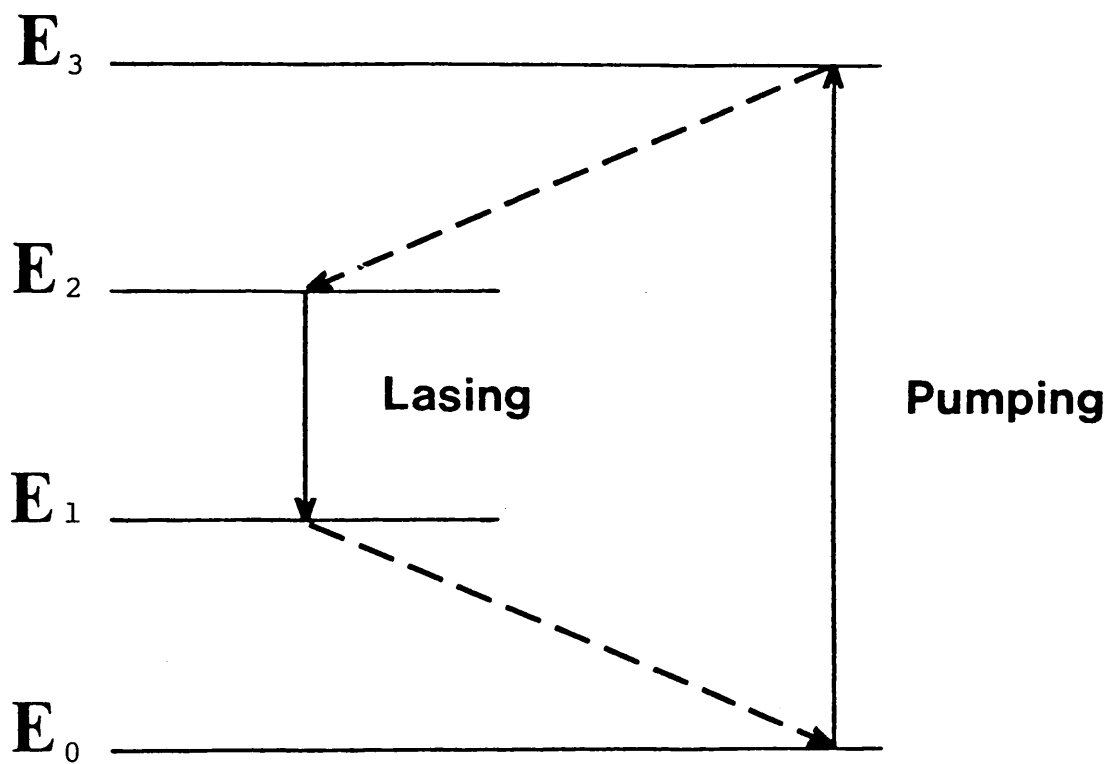


Figure 19. Nd:YAG Transition Scheme

It is therefore relatively easy to create a population inversion between level E_2 and E_1 .

There are competing transitions from the same upper state, most notably at 1319nm, 1338nm and 946nm, but they all have lower gain and higher threshold than the 1064nm transition. In normal operation, these factors and wavelength selective optics limit oscillation to 1064nm.

A laser made up of just the active medium and the resonator will emit a pulse of laser light each time the flash lamp fires. However, the pulse duration will be long, about the same as the flash lamp, and its peak power will be low. A Q-switch is used to shorten the pulse and raise its peak power.

The fact that the upper lasing energy level has a relatively long lifetime means a large population inversion can be created. If oscillation can be prevented while the inversion builds and if the stored energy can be released quickly, the laser will emit a short pulse of high intensity radiation. The DCR-11 utilises an electro-optic Q-switch comprising a polariser, a quarter wave plate and a Pockels Cell (see section 2.2.7).

During Q-switched operation the flash lamp excites the Nd ions for approximately 200 microseconds to build up a large population inversion. At the point of maximum population inversion, a fast high voltage pulse applied to the Pockels cell changes the Q-switch

from high to low loss. The resultant Q-switched pulse width is about 9ns and the peak optical power is tens of megawatts.

The laser also provides a long pulse mode of operation. Voltage is applied to the Pockels Cell as soon as the flash lamp fires and the Q-switch is held open for the duration of the flash. This produces a train of pulses about 200 microseconds long with a separation between individual pulses of 2 to 4 microseconds. This mode of operation allows safer experimental alignment and is useful in situations where total pulse energy, not its distribution in time, is important. The total pulse energy, in both modes of operation, was measured as the laser was commissioned. In long pulse mode it was found to be 415mJ while in Q-switched mode it was 375mJ.

The resonant cavity is defined by two mirrors providing optical feedback to the active medium. Both mirrors are coated to reflect the wavelength of interest while transmitting all others. One of the mirrors, the output coupler, transmits a fraction of the radiation incident upon it and this becomes the output beam of the laser. The resonator configuration used in the DCR-11 is of the unstable type (see section 2.1.3). Unstable resonators can have large beam diameters. Consequently, they can efficiently extract energy from active media whose cross-sectional area is large, such as Nd:YAG laser rods.

The output coupler of the DCR-11 is a small high reflector mounted on the centre of a transparent substrate which lies on the optic axis of the resonator. Radiation leaves the resonator by diffracting around this spot which gives the "diffraction coupled resonator" (DCR) its name. This produces an output beam of annular cross-section.

To generate a uniformly distributed beam, the Nd:YAG rod must be uniformly illuminated. This is achieved by placing the laser rod at one focus of an elliptical reflecting chamber and the flash lamp at the other focus. It is also essential that the laser rod be cooled to maintain stability of the output beam. An enclosed water cooling system is employed.

The laser oscillates within a narrow range of frequencies around the transition frequency. The width of this frequency distribution (the linewidth) and its amplitude depend on the active medium, its temperature and the magnitude of the population inversion. A frequency selecting element called an etalon is used in the DCR-11 to reduce the linewidth. Further line narrowing is achieved electronically by optimising the operating conditions of the Q-switch. The quarter wave plate in the Q-switch is rotated to allow long "prelase" oscillations to occur while the Q-switch is closed. This state favours the mode with the lowest loss, both because it has the highest net gain and because the etalon suppresses the other modes. The

Q-switch opens at the point of maximum population inversion and the resultant linewidth is about 100MHz, with a coherence length of 3m.

The stability of the oscillating frequency is partly dependent on the design of the resonator structure. The resonant frequency can be changed by small changes in cavity length which may be caused by temperature changes and mechanical shifts. Changes in the cavity length due to changes in temperature may be expressed as;

$$\Delta L = a L \Delta T$$

where L is the cavity length, a is the thermal expansion coefficient of the resonator structure and ΔT is the temperature change. To eliminate frequency drift either a or ΔT must be zero. The material used for the resonator structure should have a low thermal expansion coefficient and the ability to distribute heat evenly, producing a constant temperature along the structure. Graphite composite is used in the DCR-11, which has a negative thermal expansion coefficient. The negative expansion of the graphite rods offsets the positive expansion of metallic parts, so the net change remains near zero over a wide temperature range.

The general specification of the DCR-11 is given in table 6 below.

Wavelength (nm)	1064
Pulse Width (ns)	8-9
Pulse Energy (mJ)	415
Pulse Energy Stability	+/-4%
Repetition Rate	10Hz optimum, 1-14Hz range
Beam Diameter (mm)	6.4
Linewidth	<1.0cm
Linear Polarisation	>98%
Divergence	<0.5mrad

Table 6. Specification of DCR-11. Pulse width and energy are given for Q-switched operation.

All the laser functions are controlled from a remote control panel. The flash lamp energy may be varied between 30-70J which in turn varies the output energy of the beam. The repetition rate may be varied between 1-15Hz but 10Hz is specified as optimal. The laser may be fired in the Q-switched or long pulse mode and may be fired repetitively or on a single shot basis.

The laser is mounted on a custom built optical bench. The bench is of a rigid construction fabricated from stainless steel. It has been designed to limit access to the laser head from all sides thus reducing

the possibilities of inadvertent exposure to the beam. The optics are also mounted on the bench, inside an enclosure, situated such that it rests against the laser head. Consequently, the beam may be completely enclosed and the laser operated in the Class 1 mode. Both the optical bench and the enclosure were built in the workshops at Sheffield City Polytechnic. A schematic of this configuration is given in figure 20.

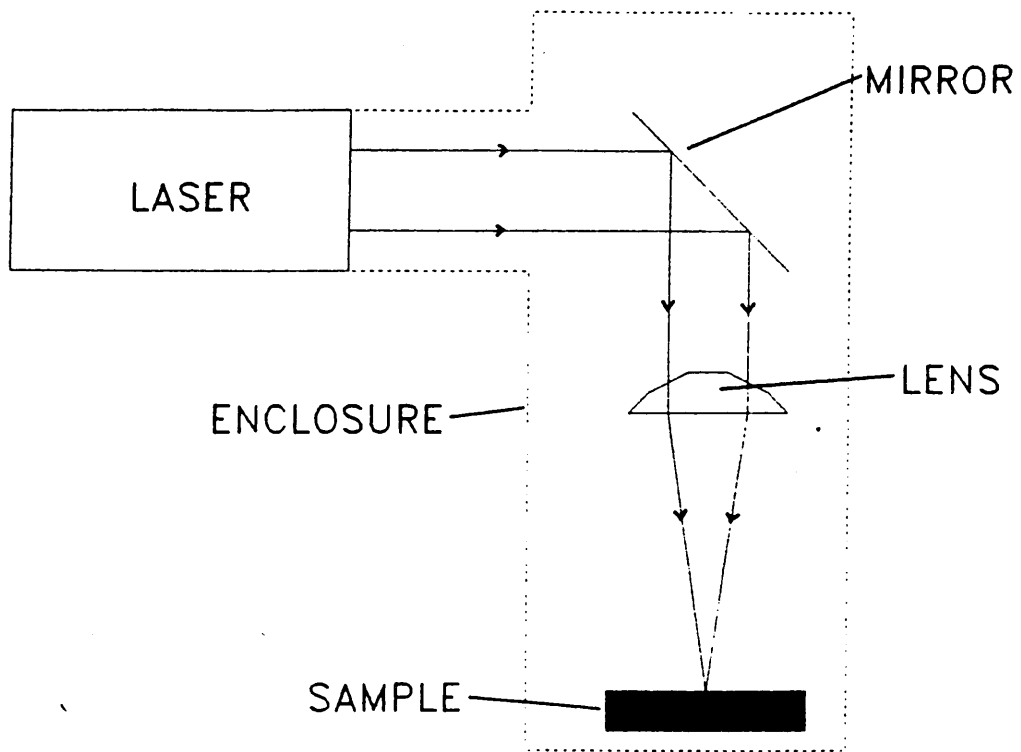


Figure 20. Schematic of Laser Configuration. Samples may be ablated directly or placed into the ablation chamber beneath the focusing lens.

3.1 OPTICS

A beam steering unit (product code LBS-1) supplied by Photon Control of Cambridge, U.K., is used to mount the optics. This unit was designed to hold two mirrors such that their reflecting surfaces are held at 90° to each other. Using mirrors in this way folds the laser beam back on itself after an adjustable vertical displacement. The beam steering unit is mounted firmly onto the optical bench and was modified to hold one mirror and one lens.

The laser is mounted horizontally on the optic bench such that the emergent beam runs parallel to the bench surface. The beam is incident upon a mirror held at 45° to the axis of the beam, reflecting it through 90° towards the surface of the optical bench. The beam then falls upon the convex surface of a plano-convex lens which focuses the beam. Both optics are fixed, consequently the process of focusing the beam onto a sample surface is performed by moving the sample relative to the lens.

The optics are supplied by the Newport Corporation of Harpenden, U.K.. The mirror (product code 10QM20HM-15), a high power laser mirror is made from high purity fused silica and coated with a hard refractory multi-layer. The coating provides high reflectivity at 1064nm for an incident angle of 45° . The lens (product code SPX022AR.33) is also made from high purity silica. A coating on the lens reduces surface losses to less

than 0.2%. It is positioned such that the beam is incident upon the convex surface of the lens thus reducing the possibility of reflections passing back into the laser cavity. Both optics have a diameter of 25.4mm.

The laser beam is focused through a silica window and into the laser ablation chamber which houses the sample under investigation.

Early experiments resulted in damage to the focusing lens. An internal void was formed in the body of the lens due to laser radiation coming to a focus within it [128, Chapter 6]. It was discovered that a proportion of the beam was reflecting off the surface of the silica window and propagating back to the lens. This was due to the fact that the beam was normal to the window, and was simply remedied by tilting the window so that the reflections passed harmlessly by the lens.

3.2 DURR-JOBIN YVON 38-48 ICP

A Durr-Jobin Yvon 38-48 plasma torch and generator was used for the initial development work in this project. The generator operates at a frequency of 56MHz. The radio frequency (rf) wave is created by a triode oscillator circuit whose anode wires are tuned to 1/4 wave. The central frequency, ν , of the oscillator is determined by the length l , of the anode wires according to the relationship;

$$\nu = c/4l$$

where c is the velocity of light. The ICP is operated at a forward power of 1.4kW.

The ICP torch is of modular design which has the advantages of low maintenance cost, flexibility of adaptation and easy replacement of parts (figure 21). The torch is composed of three concentric tubes (A,B,C) and three teflon supports (D,E,F). The tubes are sealed with o-rings and the supports are interconnected by threaded joints.

The outer tube is made of silica glass and has a diameter of 28mm. The intermediate tube is also of silica but the central injector tube is made of alumina and has an internal diameter of 3mm. The central injector is available in several dimensions to adapt the torch to various applications. An injector of 2mm internal diameter is intended for use with ultrasonic

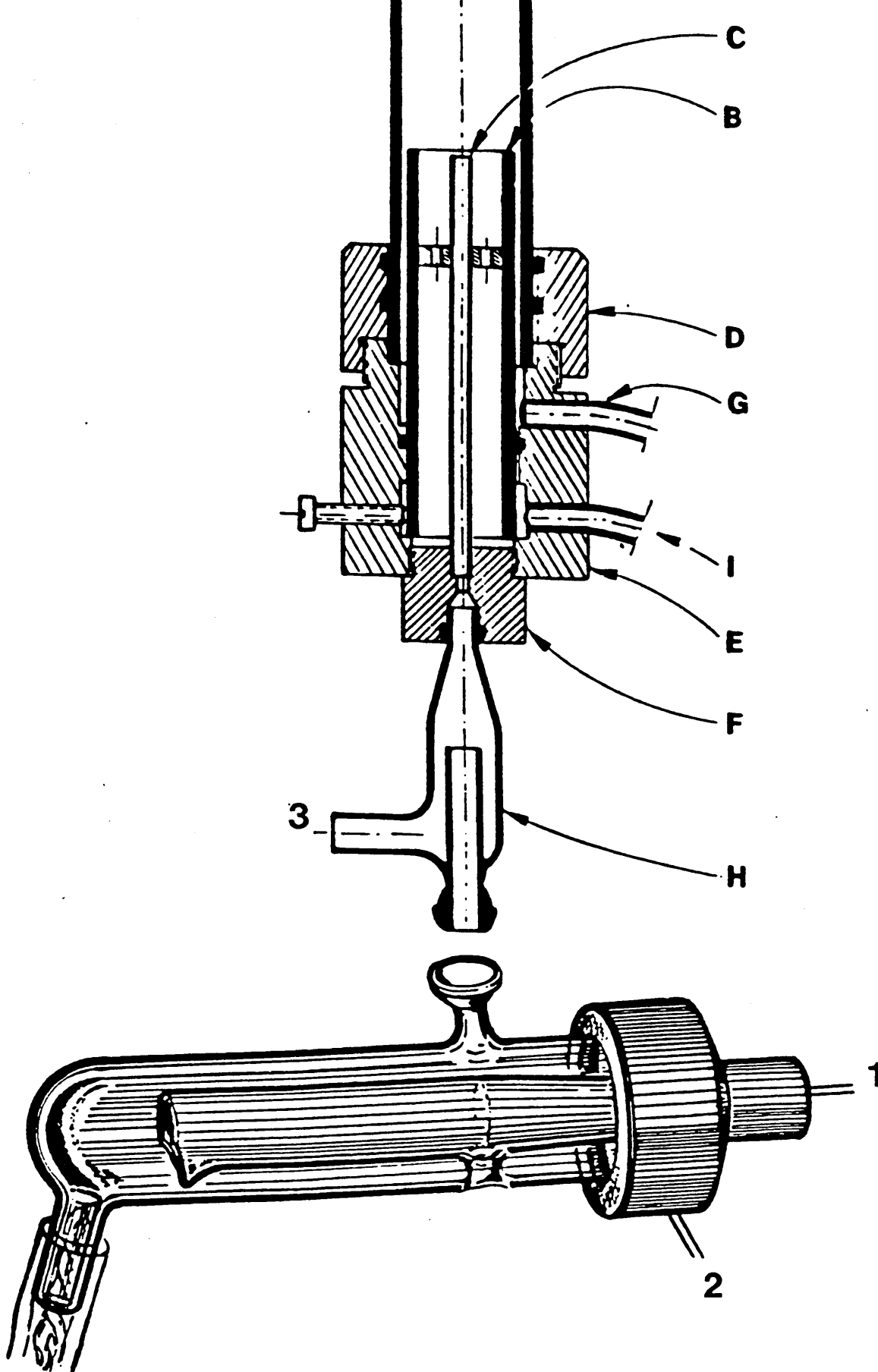


Figure 21. Jobin Yvon ICP Torch & Spray Chamber
 (see text for further details)

nebulisation. The concentricity of the tubes relative to each other is adjusted with centering screws and spacers.

Operation of the plasma is controlled via three panels on the instrument. The upper control panel is used to initiate and control the rf power, the central panel houses the plasma torch, spray chamber and nebuliser and the third lower panel is the fluid metering panel which is used to set the gas and cooling water flow rates (figure 22).

The fluid metering panel consists of several rotameters. There are four argon circuits in the instrument which branch off a common argon input through four gas regulating valves and flowmeters. A fifth flowmeter is used for cooling water fed through the induction coil at a flow rate of approximately 0.3L/min. Coolant argon gas is introduced tangentially at the upper gas connection (G), see figure 21. A flow rate of 16 L/min is used. During solution nebulisation, nebuliser argon gas, at a flow rate of 0.7 L/min, is introduced to the nebuliser at point 1 and the sample solution is drawn up through point 2. An intermediate plasma gas flow may be introduced at the lower gas connection (I) but this is not normally used. The fourth argon gas flow is unique to Jobin-Yvon instrumentation. The coating gas, as it is described, is introduced to the sheathing gas unit (H) at point 3. Its function is to carry a nebulised

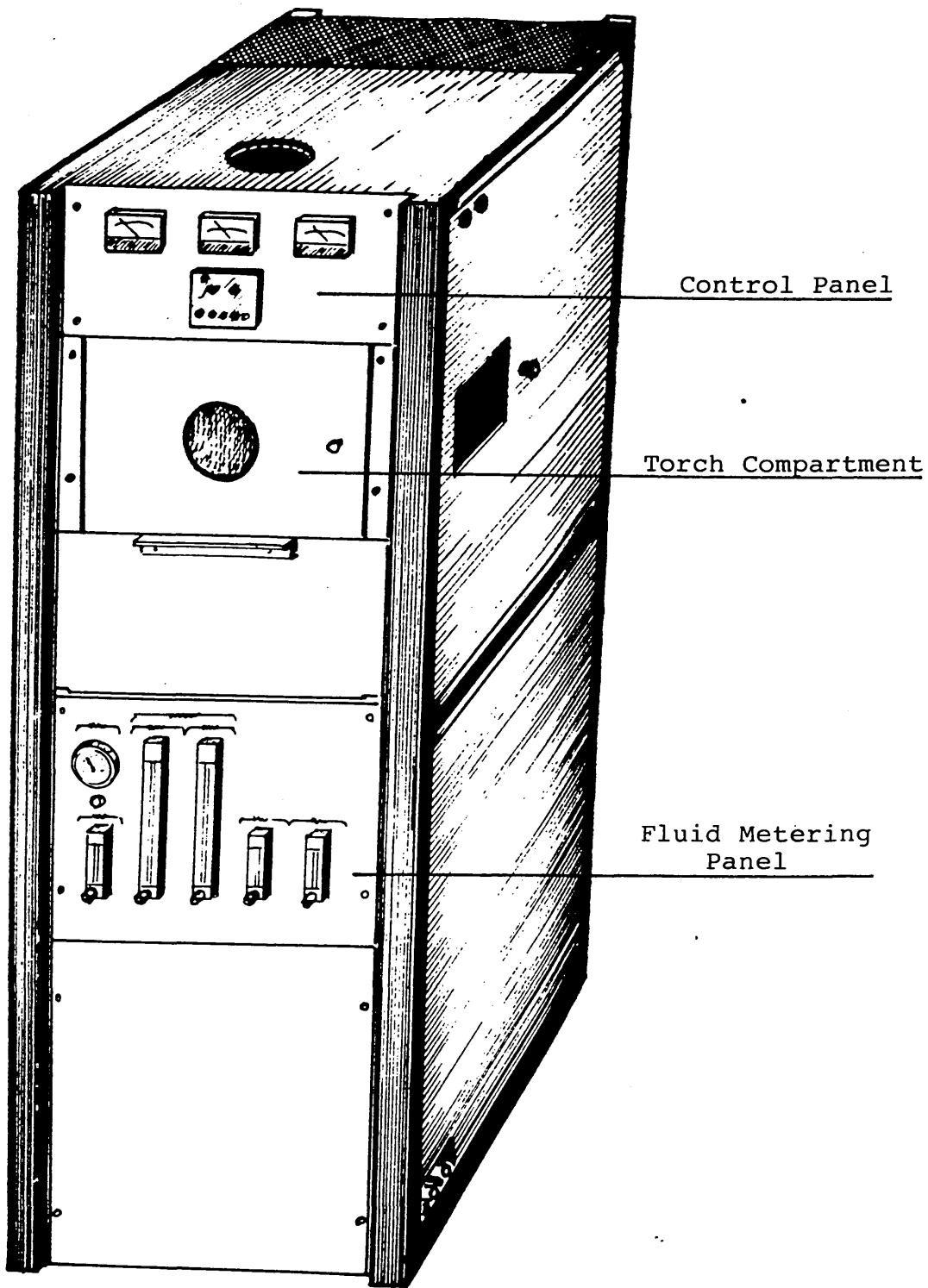


Figure 22. Front Panel of Jobin Yvon 38-48

sample up into the torch in a uniform stream, thereby avoiding turbulence and plasma instability. During this study, solutions nebulisation was only used for wavelength profiling to isolate an analytical line of interest, and for this purpose the coating gas was not used. In summary, for wavelength profiling a coolant gas flow of 16 L/min and a nebuliser gas flow of 0.7 L/min is used.

For solid sample introduction by laser ablation the coolant gas remains unchanged, and the nebuliser gas is turned off. The coating gas supply mentioned above is now used as the sample carrier gas. This gas supply has a flow rate of 0.7 L/min and passes through the laser ablation chamber and on to the sheathing gas unit via PVC tubing (0.8m long, 5mm inside diameter). The solid sample aerosol is introduced at point 3 and passes on to the ICP. This configuration allows rapid modification from conventional solutions nebulisation to solid sample introduction. In summary, for solid sample introduction, a coolant gas flow of 16 L/min and a sample carrier gas flow of 0.7 L/min is used.

The central panel of the instrument is the torch compartment. This houses the torch, spray chamber and nebuliser. Access to the torch compartment is via a door on the front panel. The ICP may be viewed through a UV filter positioned in the door as direct viewing may result in serious damage

to the eyes. To prevent such direct viewing an interlock is used on the door to switch off the rf power when the door is open. Above the torch compartment is an 11cm diameter chimney hole which is used to evacuate heat and harmful vapours from the compartment. It is connected to the laboratory extraction system. The induction coil which surrounds the torch is water cooled and has five turns. This large coil results in an elevated transit time of the gas and particles in the rf field. During solutions nebulisation a capillary tube draws the sample solution into the nebuliser. This is a consequence of the reduction of pressure at the nebuliser due to the Venturi effect. Sample transport to the nebuliser may be assisted by the use of a peristaltic pump. This will avoid changes in sample uptake rate due to changes in sample viscosity for example. The sample solution is nebulised by a cross-flow nebuliser into a Scott, double pass spray chamber. Any condensation runs off to the drain while the nebulised sample is carried in the argon stream to the ICP. Solutions nebulisation is a very inefficient process with only about 1-3% efficiency. Any improvements in this would readily produce improvements in detection limits and consequently much attention has been directed towards research in this field [137].

The upper panel of the instrument consists of the high voltage voltmeter, the anode ammeter, the grid milliammeter and the control panel. The latter

facilitates control of the rf power. The instrument on/off switch initiates mains power thus turning on the cooling fan and starting the triode valve warm up period. A black push button instantaneously triggers the rf power whilst a similar red button switches it off. A series of four toggle switches may be used to adjust the rf power level, a fifth acts as a safety switch and may be used to turn the rf power off. A yellow pilot light indicates the ready state of the generator.

To operate the instrument the following procedures are adopted;

- (i) the mains power is switched on at the control panel,
- (ii) the cooling water is turned on and the flowmeter on the fluid metering panel adjusted to assure a water flow of about 0.3 L/min.,
- (iii) three minutes after the mains supply is initiated the yellow pilot light illuminates, if all safeguards are closed. A 60 second timer assures the progressive powering of the triode, thus avoiding cold overloads. A second timer of 120 seconds, prevents starting the generator before the triode is hot. Thus the three minute delay,
- (iv) the coolant gas, plasma gas and carrier gas are all turned on to purge the system of air. After a minute or so the carrier gas is turned

- off; the plasma is always lit with this gas flow cut,
- (v) the ignition wire is placed axially into the centre of the load coil by turning the knurled wheel on the door to the torch compartment,
 - (vi) with the four toggle switches controlling the rf power in the lower position, the black push-button is pressed to initiate the rf power,
 - (vii) the plates of the tuning condenser of the triode are slowly brought together using the plexiglass screwdriver on the right side of the generator,
 - (viii) once the plates are tuned the ignition wire will be inductively heated producing thermionic emission which in turn leads to the instantaneous formation of a plasma,
 - (ix) the ignition wire should be quickly removed from the coil to avoid melting,
 - (x) the carrier gas flow is slowly introduced as the plasma gas is reduced until finally the plasma is operated with a coolant gas flow of 16 L/min and a carrier gas flow of 0.7 L/min. Deionised water should be nebulised during a 10 minute warm up period after which the plasma is ready for use.

A Jobin-Yvon HR1000 high resolution monochromator is used to isolate small regions of the spectrum of

wavelengths emitted by the plasma. These emissions are detected by a photomultiplier tube and recorded by means of an integrator and chart recorder.

The monochromator is a Czerny-Turner type with a focal length of 1m and slits on the Fastie circle. A holographic grating(1200Lines/mm)is supplied as standard which favours the instrument with a very high luminosity. The slits are curved to eliminate any decrease in resolution when their height is increased. In addition, they are mounted independently and in this study an axial entrance slit and side exit slit were used.

The main components of the HR.1000 are;

- (i) the cast base which supports the grating drive assembly, the controls and the slit support unit,
- (ii) the slit support unit which houses the entrance and exit slits. Slit height, variable from 0 to 50mm, is controlled by a knob above the slit, where one division on the drum represents 1mm. Slit width, variable from 0 to 3mm is similarly controlled and one division represents 0.01mm,
- (iii)the control panel which features the mains switch, wavelength display counter and the grating drive controls. The wavelength can be increased or decreased by means of push buttons at a variety of speeds allowing precise wavelength positioning. Base speeds are 0.06,

0.12 and 0.3nm/min and coefficients of x10, x25 and x100 may be applied to achieve increasing scanning speeds to a maximum of 750nm/min.

The monochromator was aligned relative to the ICP torch and also calibrated using a HeNe laser emitting at 632.8nm and a mercury vapour lamp using the 253.65nm and 546.07nm emission lines.

A schematic of the Jobin-Yvon system is given in figure 23.

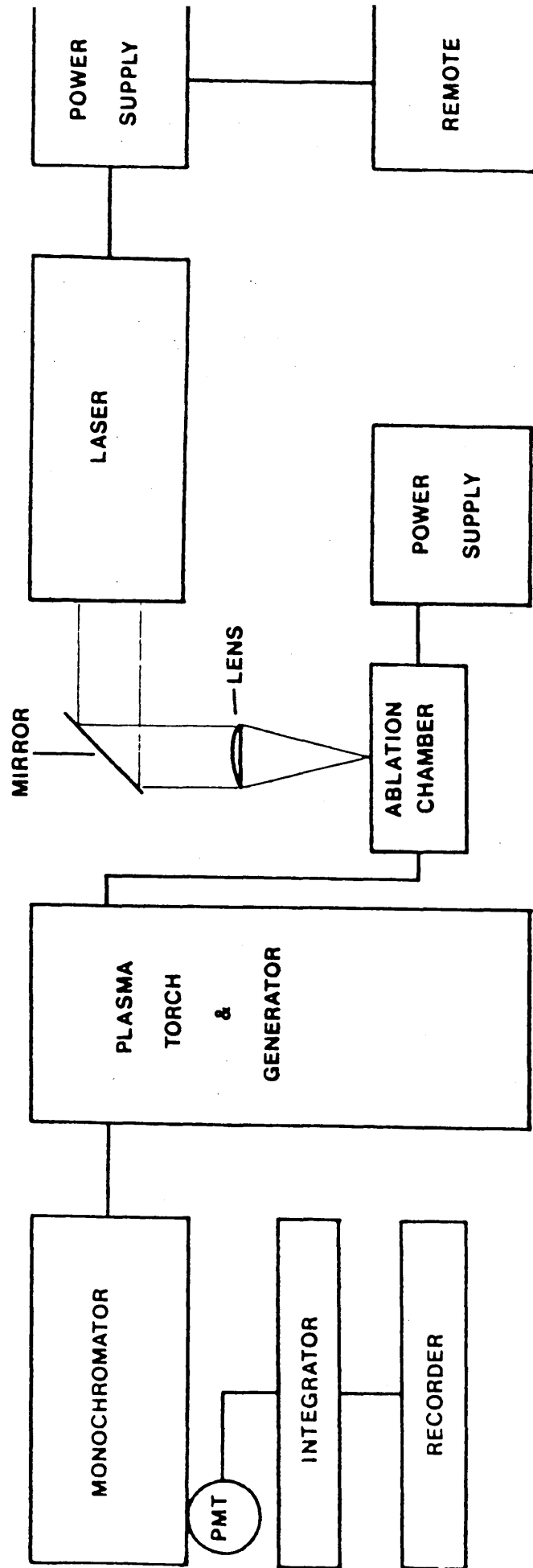


Figure 23. Schematic of Jobin Yvon System

3.3 JARRELL-ASH ICAP 9000

The ICAP 9000 consists of a 0.75m direct reading spectrometer, an r.f. generator, an inductively coupled plasma source and the Apple II+ data acquisition system. The instruments technical specifications are given in table 7.

The spectrometer, to the left side of the instrument, is a rugged, heat treated, cast iron, A-frame base to which the entrance slit, grating and focal curve are mounted. To the right of the instrument is the plasma source assembly. The plasma source consists of a plasma torch surrounded by a water cooled induction coil. A 2.5kW crystal controlled r.f. generator operating at 27.12MHz provides energy to the torch and creates an oscillating magnetic field, which sustains the plasma. Radiation emitted from the plasma is directed through the entrance slit, diffracted by the grating, refocused on the exit slits and projected onto the photomultiplier tubes (PMT's). The PMT's convert light energy to electrical signals which are digitised and processed by the computer.

The instrument is fitted with a fixed cross-flow nebuliser where the gas needle and the sample aspirator needle are set at right angles to each other. The high velocity of argon gas passing across the sample aspirator needle causes a reduction in pressure due to the Venturi effect, thus drawing the sample out. The argon collides with the sample and nebulises it.

For this work, the spray chamber/plasma torch interface was modified using the sheathing gas unit described earlier (see section 3.2). This facilitated conventional solutions nebulisation and sample introduction by laser ablation without making any adjustments to the instrumental configuration.

The diffraction grating (1510 Lines/mm) is made from an aluminised replica of an interferometrically ruled master grating. The grating mount is a rigid, cast iron stand upon which the grating holder is mounted. The grating holder is an Invar plate to which the grating is permanently bonded. A metal baffle plate shields the concave grating from stray light.

The entrance slit is mounted on the A frame. Its height is defined by the aperture plate. Behind the entrance slit is an enclosed refractor plate, which is rotated during profiling by turning the micrometer knob at the entrance slit. This procedure displaces the entrance slit laterally and therefore displaces the spectrum of radiation within the spectrometer. The entrance slit is used to maintain optimum optical alignment between the spectrum and the fixed array of exit slits.

The focal curve is a semi-circular machined curve that is bolted to the A frame. It holds the exit slits, refractor plates, photomultiplier tubes and channel cards for the spectral lines being analysed. The focal curve is 580mm in length and has been predrilled

OPTICS: 0.75m Rowland Circle,
Paschen-Runge mount.
1510 Lines/mm ruled grating
at 500nm.

LINEAR DISPERSION: 0.92 nm/mm first order
0.46 nm/mm second order
0.31 nm/mm third order

RESOLUTION: 0.045 nm first order
0.023 nm second order
0.015 nm third order

WAVELENGTH RANGE: 190-800 nm (air spectrometer)
170-800 nm (vacuum
spectrometer)

VARIABLE WAVELENGTH CHANNEL: 0.5 Ebert. 190-900 nm.

BACKGROUND CORRECTION: 63 available steps on
a computer controlled
scanning refractor plate
covering a 0.5nm range
(1st order).

SOURCE: 2.5kW R.F. generator
operating at 27.12 MHz
with automatic power control
and automatic tuning.

NEBULISER: Cross-flow pneumatic.

TORCH: Quartz

Table 7 : Technical Specifications of ICAP 9000.

for as many as 120 different slit holders and PMT's. The holes are drilled under computer control to an accuracy of 40 microns.

The exit slits select the individual lines and the PMT's directly behind the slits convert light energy into electrical energy. The electrical energy so produced is proportional to the intensity of the incident radiation. The exit slits are accurately positioned and secured on the focal curve. The wavelength is indicated in front of each slit position. Baffles are strategically placed above and below the exit slits and around the PMT's to reduce the effects of stray light.

A fibre optic fatigue lamp is situated in front of the grating and directed towards the exit slits. It supplies energy to the PMT's and constantly generates a small current (the "dark" current) whenever the instrument is not measuring an exposure of sample generated energy. This process is called fatiguing and enhances the PMT's response.

A spectrum shifter moves the spectral lines across the exit slit to produce a spectral scan of intensity against wavelength. It is used to measure background signals or perform spectral investigations. It consists of a motor driven refractor plate, placed behind the entrance slit refractor plate.

The R.F. generator is the power source for the ICP. It provides upto 2500 W of R.F. power to

energise the argon gas in the plasma torch. The generator is housed inside the spectrometer cabinet. All controls and indicators are located on the R.F. generator panel in the centre of the spectrometer.

The instrument is equipped with an N+1 channel, a 0.5m Ebert scanning monochromator that is mounted below the plasma chamber of the spectrometer. The N+1 channel allows the addition of one analytical channel of variable wavelength. This permits analysis of an element not provided for in the polychromator and is useful when there are interfering elements or a change in analytical requirements.

There are three main control panels on the instrument; the gas flow control panel, the controller panel and the R.F. generator panel. The gas flow control panel (figure 24) is located on the right front panel of the ICAP 9000. It houses three flow-meters that measure the coolant, plasma and sample carrier gas flow, along with their associated toggle switches and needle valve control knobs. The ignitor button provides a spark from a tesla coil to initiate the plasma. Two indicator lights illuminate when power is on and water is flowing through the induction coil. If the water pressure is too low then a failsafe device cuts the power thus preventing ignition of the plasma.

The controller panel is located on the left side of the instruments front panel. This panel features a profile meter and its gain control, a jack-plug socket

Flow Meters

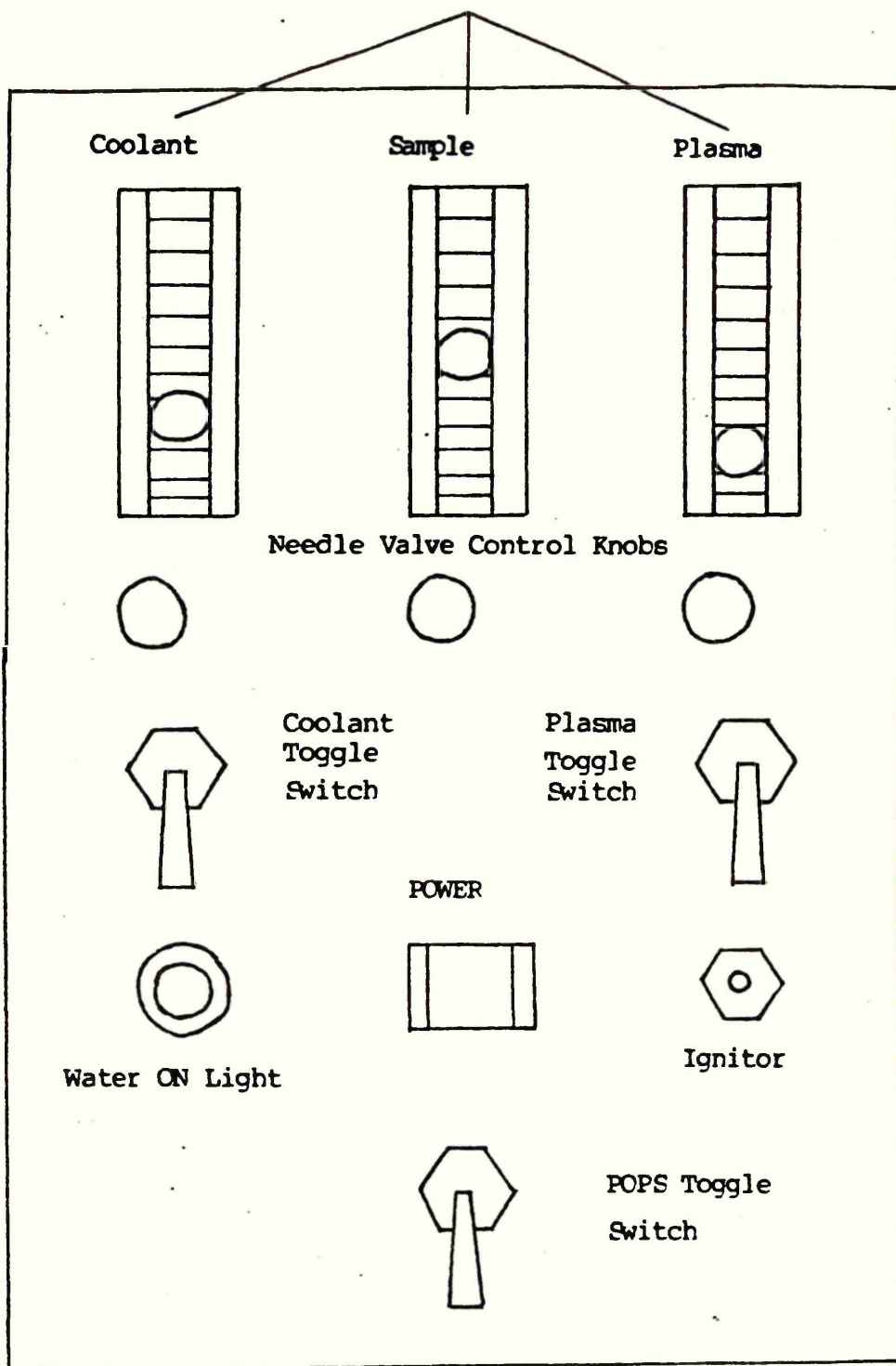


Figure 24. Jarrel Ash Gas Control Panel

for an external recorder and a control for the dynode voltage sensitivity of the N+1 channel. The profile meter measures the intensity of radiation passing through an exit slit when the spectrometer is in the profile mode. A series of light emitting diode lights on this panel indicate the status of the spectrometer. These lights are characterised as follows;

- (i) SB - standby mode, awaiting further input,
- (ii) FAT - fatigue lamp,
- (iii) EXP - indicates that an exposure is being measured,
- (iv) S2 - indicates a pre-exposure period.

The central panel of the spectrometer is the R.F. generator panel (figure 25). It is equipped with safety features that automatically shut down the system in case of malfunction or possible danger to the operator. A reflected power alarm sounds when the reflected power exceeds an unacceptable level. If this situation is not rectified within 30s then the system shuts down. The line and control circuit breakers allow the generator to be turned completely on or off. The R.F. on and off buttons and the power control knob are used for start-up and shut-down of the ICP.

The spectrometer is equipped with 30 fixed channels, each corresponding to a different element and each identified by a physical channel number recognised by the software. The elements, channels

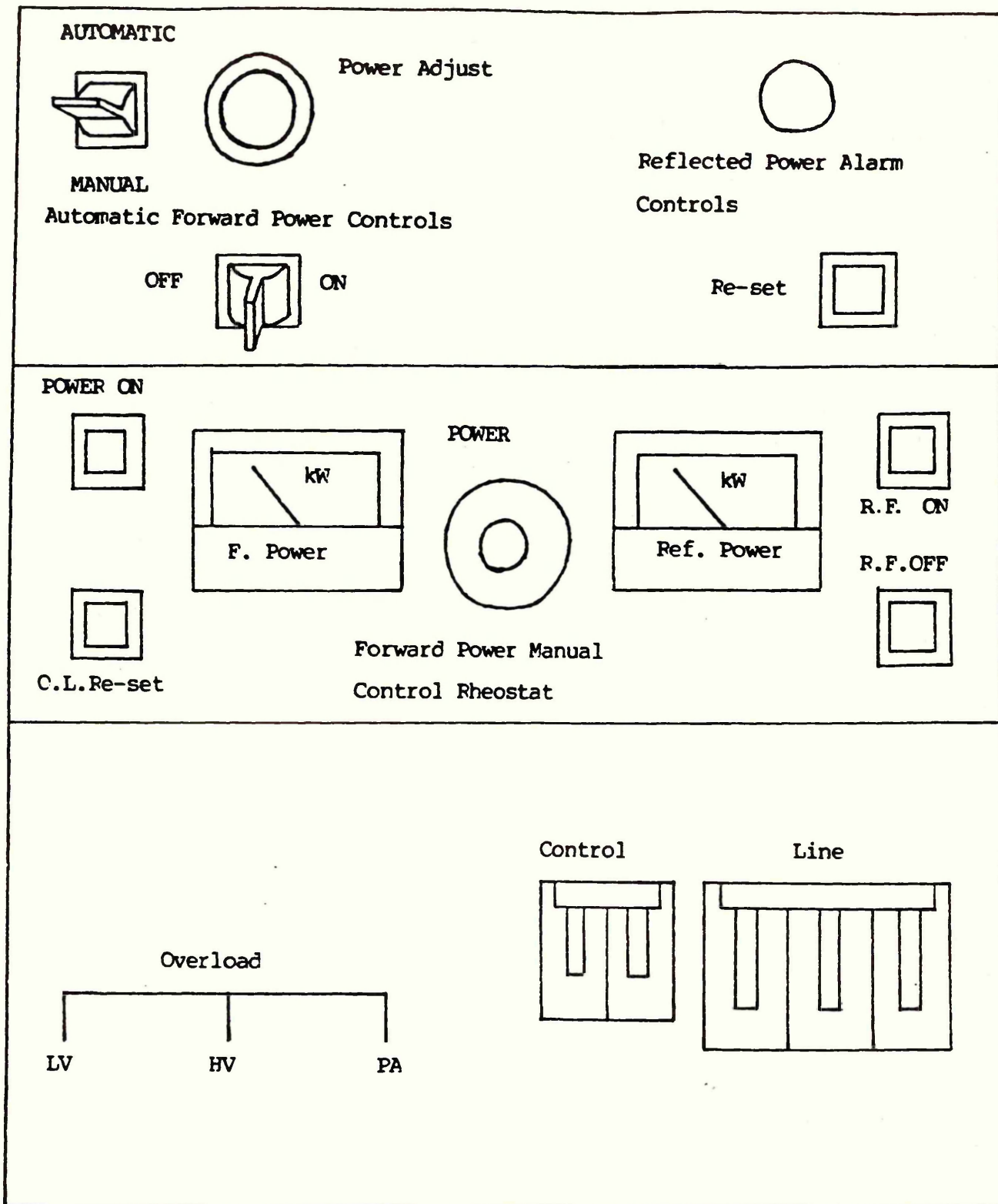


Figure 25. Jarrel Ash r.f. Generator Panel

and analytical wavelengths are given in table 8.

As described earlier in section 3.2, analysis by laser ablation requires four argon gas supplies. As the ICAP 9000 has only three, a remote cylinder of analytical grade argon gas was used as the solid sample carrier gas. The gas flow was controlled by a rotameter which produced the flow rates shown graphically in figure 26. The solid sample carrier gas was directed by PVC tubing through the laser ablation chamber and on to the sheathing gas unit mounted directly below the ICP torch, as in the Jobin-Yvon system.

The data acquisition system consists of the Apple II+ computer, keyboard, monitor, dual 5¼" floppy disk drives and a compact dot matrix printer. There are five system disks in the ICAP 9000 software package, the analytical, report, diagnostics, help and calibration disks. In this work the analytical and report disks were used almost exclusively and shall be considered in more detail. The menus unique to these two disks are;

(i) Analytical disk:

THIS IS THE ANALYTICAL DISK

PLEASE SELECT OPTION FROM LIST:-

1.(SAT) SAMPLE ANALYSIS TASK
2.(ACT) CONTROL TABLE EDITOR
3.(CAL) CALIBRATION
4.TIME STUDY
5.EXIT

<u>ELEMENT</u>	<u>CHANNEL NO.</u>	<u>WAVELENGTH</u>
Ag	19	328.07
Al	14	308.22
As	11	193.70
B	9	249.70
Ba	6	493.40
Ca	35	317.93
Cd	23	228.80
Co	45	228.62
Cr	42	267.72
Cu	34	324.75
Fe	8	259.94
Ge	16	209.42
Hg	4	194.22
K	25	766.49
Li	21	670.78
Mg	10	279.08
Mn	44	257.76
Mo	38	202.03
Na	12	588.99
Nb	17	319.50
Ni	28	231.60
Pb	32	220.35
Se	46	196.03
Si	41	288.16
Sn	48	189.99
Ti	2	334.94
V	40	292.40
W	36	207.91
Zn	5	213.86
Zr	30	339.20
N+l	26	Variable

Table 8. Available Spectrometer Channels

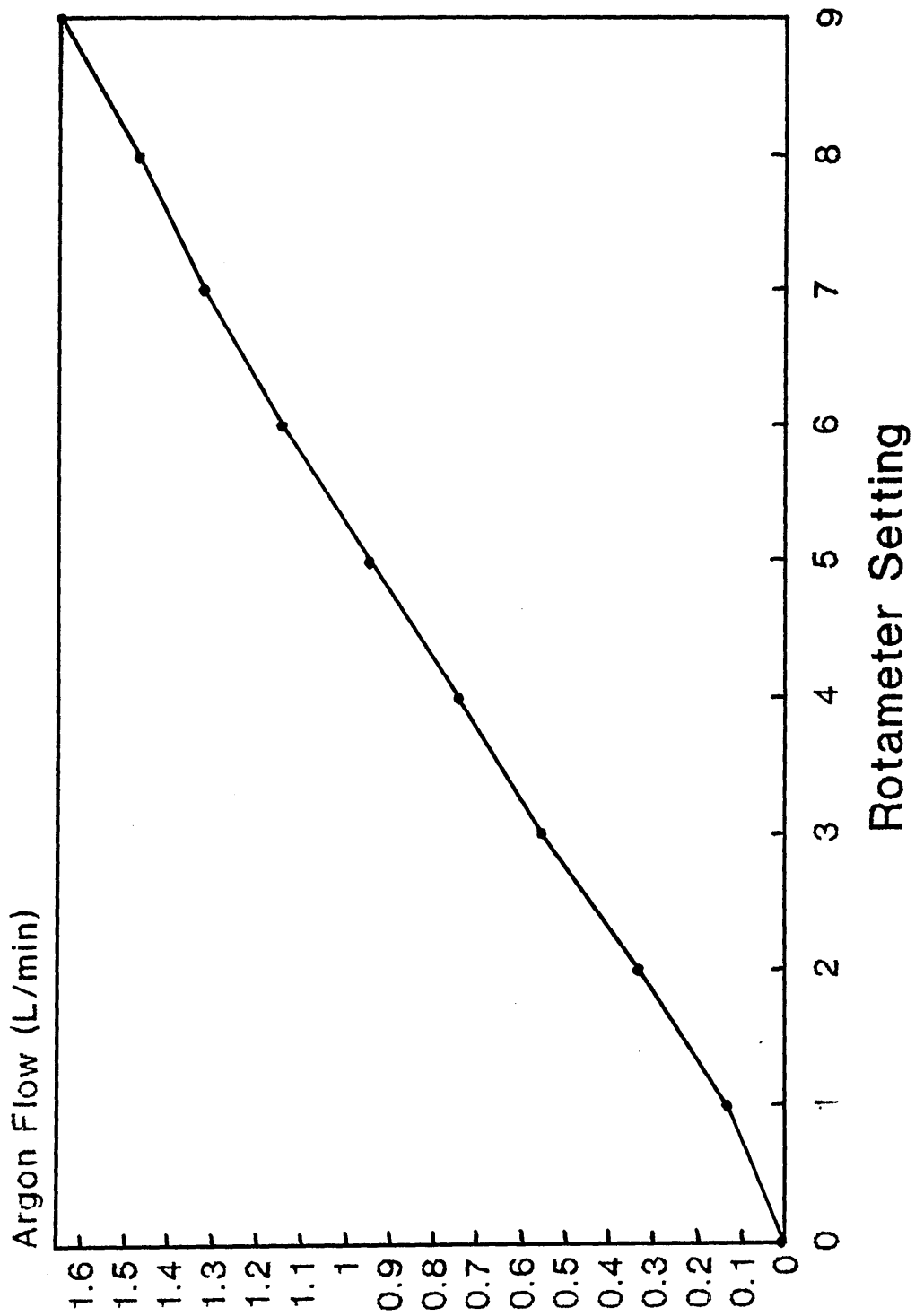


Figure 26. Calibration of the Rotameter used to control Carrier Gas Flow Rate.

(ii) Report disk:

REPORT DISK HAS THE FOLLOWING OPTIONS:

1. COPY DISK
2. COPY FILE
3. COPY PROGRAM
4. DATA DISK INIT
5. GRAPHICS ROUTINE
6. REPORT WRITER
7. EXIT

ENTER SELECTION ...

The first stage of an analysis is the preparation of an analytical control table (ACT) by selecting option 2 on the analytical disk. An ACT is a table that contains all the parameters necessary to analyse a sample for a specific set of elements. The control table editor allows the user to create, edit, print or delete an ACT.

When creating an ACT the user must input a name for the ACT, the number of analytical channels, the source, any flush time required, the internal standards, the exposure times to be used and the names of the calibration standards. The element array must then be defined by inputting element names, physical channel numbers, wavelengths and details about the standards for the element being defined eg. high and low concentrations. Once all the data for all the elements of interest has been input, the ACT may be

used, printed or edited if there is a change in the analytical requirements.

The ACT may be used to analyse a sample by selecting option 1, sample analysis task, on the analytical disk. The user is firstly asked if reprofiling is required. The spectrometer should be profiled at the beginning of an analysis and at approximately 1 hour intervals thereafter during the analysis. Profiling was usually performed using a 2ppm copper solution and examining the emission intensity on channel 34 as a function of micrometer position. Once the maximum intensity had been established the sample analysis could begin.

The user continues by calibrating the instrument using the synthetic standards defined in the ACT. This complete, the prompt "ENTER NEW COMMAND SEQUENCE?" is displayed. The commands used at this point are those that manipulate SAT itself and those that control the acquisition and storage of results in main memory. The SAT commands most frequently used are listed below;

- (i) AA - changes the ACT and restandardises
- (ii) EX - exits SAT
- (iii) G1-G10 - performs 1 to 10 exposures
- (iv) MO - permits a change of output format
- (v) PF - profiling command
- (vi) WS - activates wavelength scanning routine
- (vii) <ABC> - stores a comment on the disk to be

used as an ACT sorting message

- (viii) PA - prints an average of all exposures
- (ix) PE - prints individual exposures
- (x) PS - prints the standard deviation
- (xi) PT - prints output of 95% confidence limit
and standard deviation
- (xii) ESC key - aborts the current exposure.

If the user wished to take 4 exposures of sample x and wanted the individual exposures, their average and standard deviation printed, the command sequence would be; <SAMPLE X>G4PEPAPS. Pressing the RETURN key at this point would execute the command sequence.

Another widely used area of the software during this work is option 4 on the analytical disk, time study. A time study measures the intensity as a function of time, for all the elements defined in the ACT used. The user must define the ACT and the total exposure to be used, aspirate the sample and press return to initiate the time study.

The report disk was most frequently used for graphical representations of data, option 5 in the menu. The graphics routine program obtains intensities or concentrations from a scan file, be it a time study or wavelength scan. There are four types of plot available, a line without points, a line with points, scatter and a histogram. The plots may be scaled linearly or logarithmically and upto five elements may be overlaid

on the same plot.

Finally, to initiate a plasma for analysis the following procedure should be adopted;

- (i) turn on the water pump and fume extraction system,
- (ii) turn on the coolant gas (18 L/min), sample carrier gas (0.4 L/min) and plasma gas (1L/min) and nebulise deionised water. This process will purge the system of air. Under these conditions some of the nebulised aerosol will pass down the PVC tubing towards the laser ablation chamber. This is prevented by creating a back pressure by passing a small flow of solid sample carrier gas through the laser ablation chamber to the ICP,
- (iii) ensure that the forward power manual control rheostat is turned fully anticlockwise and the automatic forward power control switch is in the lower "manual" position,
- (iv) lift the control circuit breaker to turn on the generator, the power on and r.f. off buttons will illuminate,
- (v) turn off the sample carrier gas and the solid sample carrier gas,
- (vi) press the r.f. on button and slowly increase the forward power using the manual control rheostat. When a forward power of 0.5kW is reached press the ignition button while further

- increasing the forward power,
- (vii) as the plasma lights lift the automatic forward power control switch to the upper "automatic" position and turn the forward power manual control rheostat fully clockwise,
 - (viii) slowly introduce sample carrier gas, nebulising deionised water, remembering to use a small flow of solid sample carrier gas, as the plasma gas is slowly reduced to zero. At this point the bottom of the plasma should be 2-3mm above the intermediate tube of the torch,
 - (ix) the spectrometer may now be profiled and used for the analysis of samples.

A schematic diagram of the analytical system based on the Jarrell-Ash ICAP 9000 is given in figure 27.

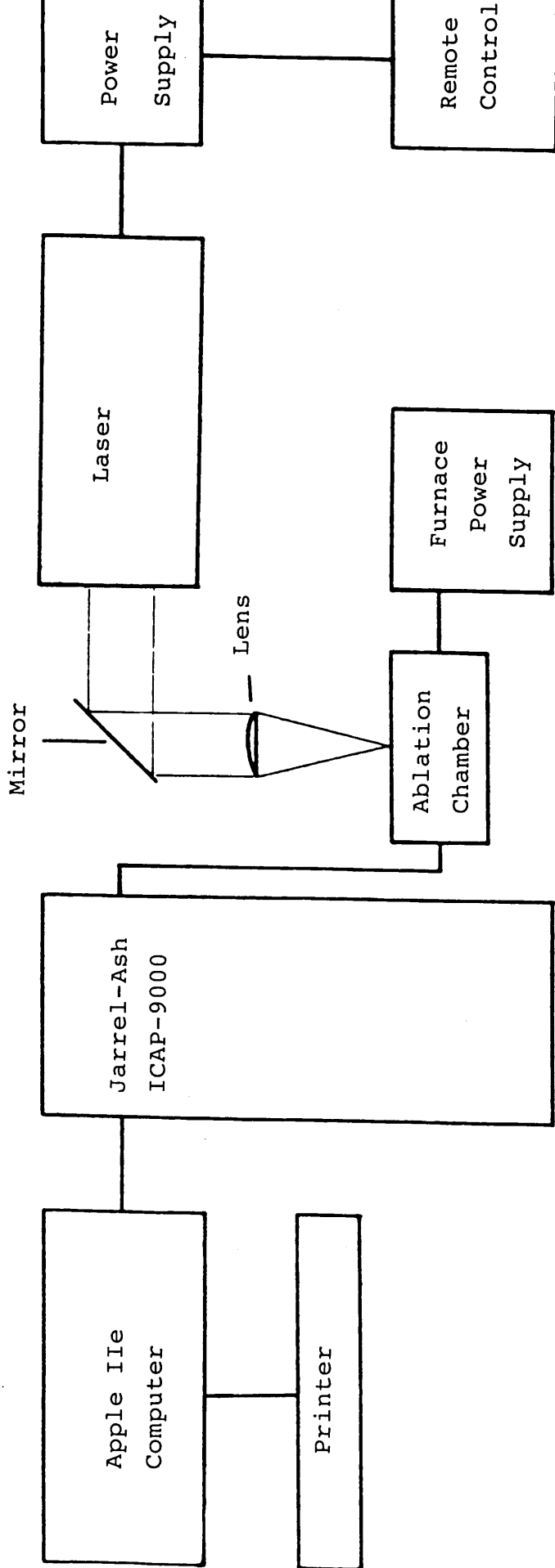


Figure 27. Schematic of Jarrel-Ash System.

3.4 LASER ABLATION CHAMBER

Several designs of sample chamber for laser ablation have been reported by other workers in this field. A simple glass dome was adopted by Thompson [87] which was designed to hold irregularly shaped samples such as geological materials. Carr [86] reported a chamber designed for rods and discs. Other designs allow the sample to be rotated thus presenting a fresh sample surface to the laser after each shot. This is thought to provide more representative sampling.

The laser ablation chamber used in this work represents a novel concept combining an ablation chamber with an electrothermal graphite furnace. This design facilitates the use of a wide range of certified reference materials which are supplied as turnings. Positioning a single turning under a laser beam would be very difficult, but if electrothermal melting is used several turnings may be fused prior to ablation, thus presenting a larger more representative sample to the laser. Solutions may also be examined either directly or dried prior to ablation of the residue. Furthermore, the system allows measurements by electrothermal vaporisation of both solid and liquid samples for comparison.

The ablation chamber is in two sections constructed from stainless steel (figure 28). The upper section is detachable from the main body by screw thread to allow sample changing. This section houses a 1cm diameter quartz window through which the laser

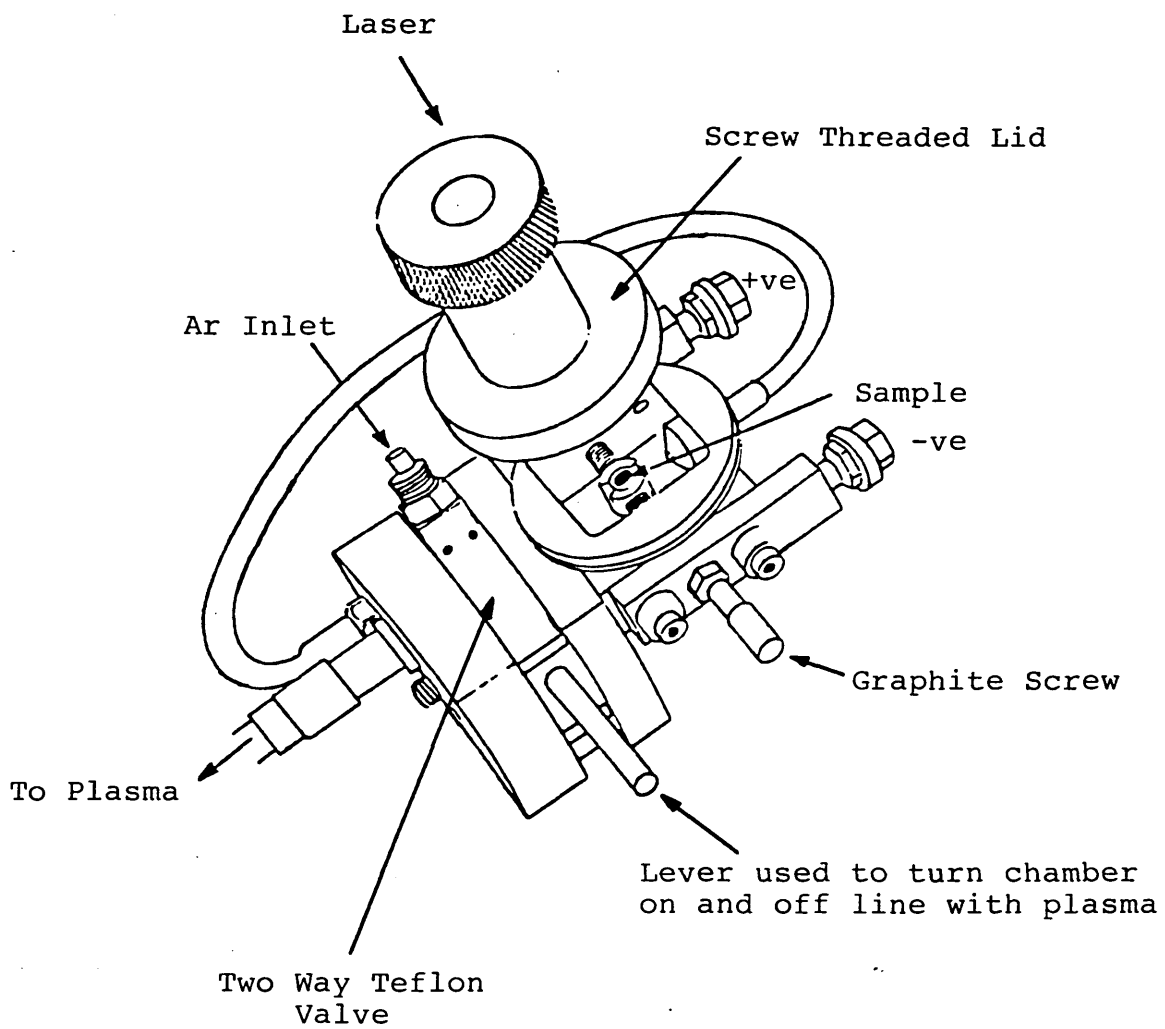


Figure 28. Laser Ablation Chamber

radiation passes. This window is slightly tilted such that the laser is not incident normally to the window, thus minimising the possibility of back reflections which could seriously damage the laser. The window may be removed for cleaning or replacement.

The lower section accommodates the graphite furnace. The furnace consists of a graphite crucible held centrally in the ablation chamber by two graphite screws. The screws pass through brass pins and the side walls of the chamber. They are in close contact with the pins but the pins themselves are completely isolated from the chamber by Macor. This arrangement ensures that the chamber does not become "live" during electrothermal heating of the furnace.

The material to be examined is placed into a graphite sample cup which in turn is placed into the graphite crucible. The sample cup fits closely into the crucible ensuring good electrical contact. When a voltage is placed across the brass pins the furnace is resistively heated, allowing electrothermal pretreatment of the sample. The components of the furnace and their dimensions are shown in figure 29. All graphite materials were supplied by Spectrochem Supplies Ltd..

The solid sample carrier gas inlet and outlet are situated on a two-way teflon valve. The valve can direct the carrier gas directly to the ICP or through the ablation chamber and then on to the ICP. The former

SAMPLE CUP



GRAPHITE CRUCIBLE

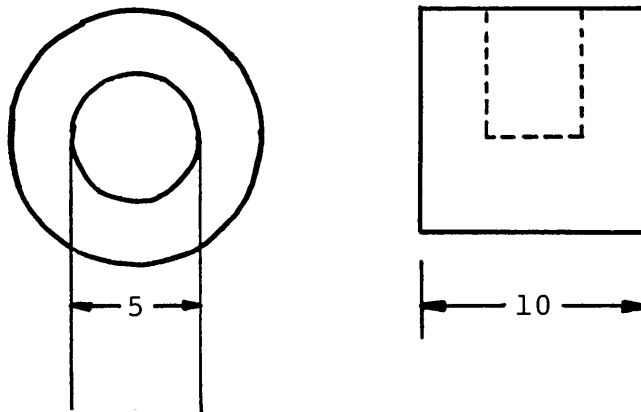


Figure 29. Graphite Furnace Components.

(All dimensions in mm)

situation is required during sample changing and prevents the entrainment of air. The latter situation is used during laser ablation or electrothermal vaporisation. The sample is carried from the ablation chamber, in a stream of argon gas, via Tygon tubing (0.8m long, 5mm internal diameter) to the sheathing gas unit and the ICP. Similar tubing is used to connect the ablation chamber to the argon gas supply.

The laser ablation chamber is fixed to a laboratory jack whose vertical movement permits focusing of the laser beam onto the sample surface.

3.5 PERKIN-ELMER HGA-2100

The Perkin-Elmer HGA-2100 is a graphite furnace and power supply unit normally used for electrothermal atomisation atomic absorption spectrometry (ETA-AAS). This technique improves detection limits for many elements by factors of upto 1000 times when compared to flame atomic absorption spectrometry. This improvement is due to increased residence times and superior sample introduction efficiencies.

The power supply passes a current through the graphite furnace which as a consequence becomes resistively heated. The magnitude of the current (and hence the temperature of the furnace), and the period for which it is applied are variable. A sample in the furnace may be dried at a temperature around 120°C for perhaps 20s, then charred at 600°C to remove any organic matrix and finally atomised at temperatures upto 2600°C for a maximum of 30s. The resultant atomic absorption signals are naturally transient in nature.

In this work only the power supply unit was used. The high tension cables were adapted to fit a graphite furnace housed inside the laser ablation chamber designed and constructed specifically for this work (see section 2.5). This adaptation removed any temperature/voltage feedback control that the unit had with its original furnace and consequently rendered several of its features inoperative.

With the power supply connected to the laser

ablation chamber, the drying temperature and its duration were the only functional parameters. The temperature meter, rather than indicating the temperature of the furnace, showed the fraction of total available power being used. Since the power supply was to be used to dry sample solutions and to melt metallurgical ones, this lack of operational features was not disadvantageous to this work.

The unit was operated by setting a heating temperature, in arbitrary units, on the drying temperature control and a heating time on the drying time control. This setting is continuously variable up to 120s. Having set these conditions, the program push button activates the heating cycle. This button is lit during the cycle and for approximately 30s afterwards. Another heating cycle cannot be initiated until this light is extinguished.

The front panel of the HGA-2100 power supply is shown in figure 30.

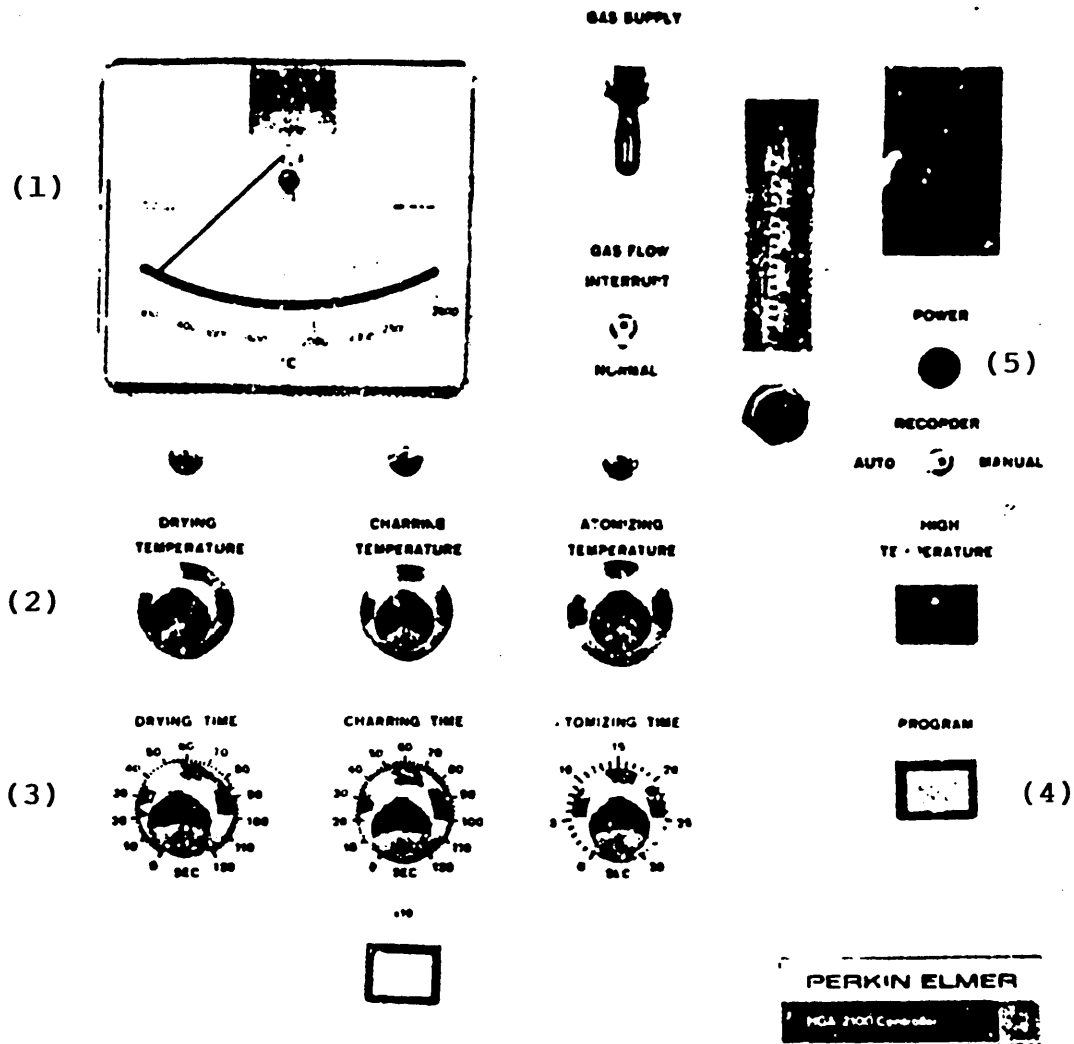


Figure 30. Front Panel of Perkin Elmer HGA-2100 Furnace Power Supply Showing Temperature Meter (1), Temperature Control (2), Time Control (3), Program Button to initiate heating sequence (4) and Mains Power On/Off Button (5).

3.6 LASER SAFETY

The laser used in this work is a Class IV laser product. Class IV lasers operate in the wavelength range 200nm to 1mm and their output power exceeds 500mW. Direct viewing of the beam and viewing specular and diffuse reflections is very hazardous and likely to result in permanent damage to vision. In addition, there is also a risk of skin burns from the direct beam and from first order specular reflections.

The beam from such lasers is also capable of igniting flammable material so care must be taken to minimise the risk of fire.

The laser itself is equipped with safety features to reduce potential hazards. The power supply and laser head are fitted with interlocks that prevent laser action when their covers are removed. The power supply is activated by a key which limits its operation to qualified personnel only and the laser is operated via a remote control panel which removes the operator from the laser area.

Other safety features incorporated during this work include; the enclosure of the beam and the optics is a specially built "black box"; wearing of safety goggles at all times; designation of the laboratory as a laser area and restricting access to qualified personnel only; increasing the ambient light levels in the laboratory thus reducing pupil size; ensuring that the laser is not at eye level for any person standing

or sitting in the laboratory and blacking out of the laboratory windows.

Lasers should always be treated with respect since they can, when carelessly used, be very dangerous.

CHAPTER FOUR

STUDIES WITH METALLURGICAL SAMPLES

4.0 INTRODUCTION

Atomic spectroscopy has been used for many years for the analysis of metallurgical materials. Major components may require determination in quality control laboratories to ensure that products are manufactured to specification. Trace elements can seriously affect physical and mechanical properties of metals and in areas such as the aerospace industry the determination of such elements is very important. Techniques such as atomic absorption and ICP spectroscopy are widely used for such analyses.

These methods of analysis are similar in that there is a general requirement that samples are in solution. Hence metals require digestion, usually with nitric acid or aqua regia. Such sample preparation lengthens total analysis times and deteriorates the absolute detection limits attainable. Hence the interest in laser ablation ICP as a means of achieving rapid and direct analysis.

The following work utilises both the Jobin Yvon and Jarrel Ash ICP systems using the operating condition described in chapter three.

A variety of metallurgical samples have been examined to determine the feasibility of laser ablation ICP studies using the instrumental configuration described. This work involved a novel ablation chamber which facilitated ablation of molten samples and fusing turnings prior to ablation. Several laser operating parameters were examined and optimised.

4.1 PRELIMINARY STUDIES

The early work on metallurgical samples was conducted on the Durr Jobin-Yvon ICP system described in section 3.2. The objectives were simply to ensure that the instrumental configuration was suitable for the detection of signals generated by laser ablation and to investigate the ability of the laser to ablate different sample types.

4.1.1 Laser Sampling

The concept of using laser ablation as a remote sampling device for ICP spectrometry relies on its ability to remove material from a sample. This was investigated on three sample types namely, glassy carbon, aluminium and copper, by measuring weight loss as a function of ablation period.

4.1.1.1 Experimental

Samples of glassy carbon, aluminium and copper were used for this investigation. The latter two were high purity X-Ray Fluorescence standards. All the samples were disc shaped, having a diameter of 25mm and a thickness of 5mm.

The sample under examination was mounted on a revolving platform (4 r.p.m.) and positioned under the focused laser beam. The laser was directed as described in section 3.1 and focused onto the surface of the sample.

The sample was weighed, placed onto the revolving platform and ablated for a set period of time. The sample was re-weighed and the loss in weight noted. This procedure was performed in triplicate for each determination. Ablation periods of 5s, 10s, and 15s were used operating the laser in the long pulsed and Q-switched mode. At all times the laser was operated at maximum lamp energy and 10Hz.

4.1.1.2 Observations

Visual examination of the test pieces during laser ablation revealed two very different situations;

- (i) During laser ablation in the long pulse mode many sparks of molten material could be seen being ejected from the sample. The degree of sparking was noticeably lower in the case of copper, while that from aluminium was so intense that the lower surface of the focusing lens became coated with aluminium.
- (ii) Laser ablation in the Q-switched mode did not produce sparks of material. At the point of interaction, a small, luminous, laser induced plasma was produced which stood approximately 5mm high.

Examination of the test pieces after laser ablation using an optical microscope (50x magnification) revealed the following;

- (i) The interaction of long pulsed laser radiation

with the samples of glassy carbon and aluminium produced localised melting and drilling resulting in a crater. The crater was elliptical and approximately 0.5mm across the major axis.

The copper sample showed no evidence of melting or drilling, but the point of interaction was much brighter than its surroundings indicating that the surface oxide layer had been penetrated.

- (ii) There was no evidence to suggest that the Q-switched laser radiation had interacted with the glassy carbon and aluminium samples. The effects on the copper sample were similar to those observed using the long pulsed mode of operation. Furthermore, a pale blue circular band was observed surrounding the point of interaction. This suggests the presence of an area of differing oxidation state produced by localised heating.

4.1.1.3 Results

The weight loss of sample as a function of ablation period is tabulated below for glassy carbon, aluminium and copper in tables 9, 10 and 11 respectively. Data for the long pulse mode of operation alone, is given. Any weight loss produced in the Q-switch mode was immeasurable using a 5 figure balance ie. less than 10 ug. All data are presented graphically in figures 31,32 and 33.

Table 9. Weight Loss for Glassy Carbon due to Laser Ablation.

ABLATION PERIOD(s)	WEIGHT LOSS (mg)			MEAN (mg)	RSD %
	1	2	3		
5	0.55	0.62	0.65	0.61	6.9
10	0.98	1.00	1.14	1.04	6.8
15	1.51	1.65	1.48	1.55	4.8

Table 10. Weight Loss for Aluminium due to Laser Ablation.

ABLATION PERIOD(s)	WEIGHT LOSS (mg)			MEAN (mg)	RSD %
	1	2	3		
5	3.08	3.10	3.51	3.23	6.1
10	6.39	6.91	6.77	6.69	3.3
15	8.89	9.30	8.96	9.05	2.0

Table 11. Weight Loss for Copper due to Laser Ablation.

ABLATION PERIOD(s)	WEIGHT LOSS (mg)			MEAN (mg)	RSD %
	1	2	3		
5	0.00	0.00	0.00	0.00	--
10	0.11	0.17	0.11	0.13	22
15	0.17	0.24	0.19	0.20	15

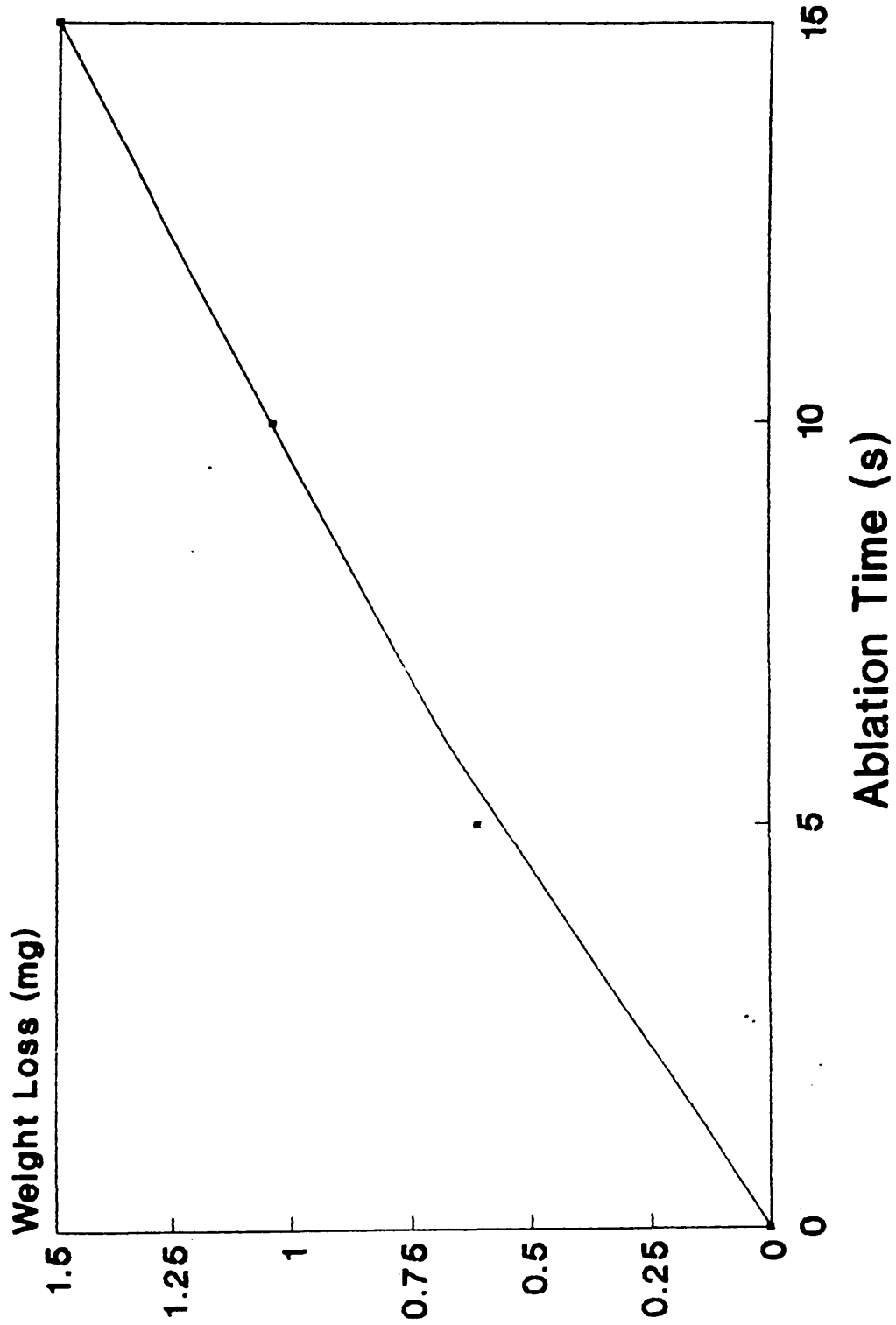


Figure 31. Weight Loss as a Function of Ablation Period for Glassy Carbon.

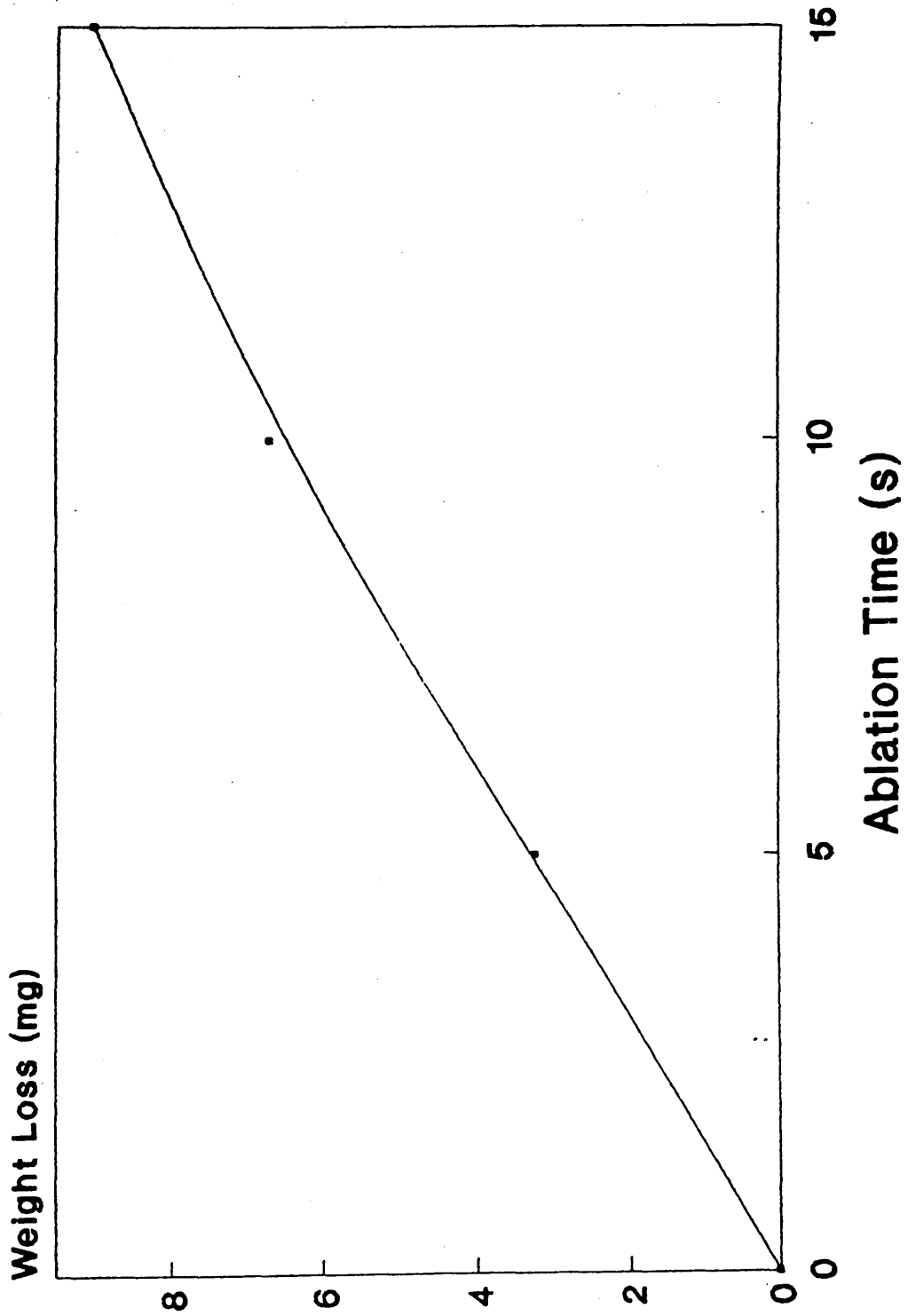


Figure 32. Weight Loss as a Function of Ablation Period for Aluminium.

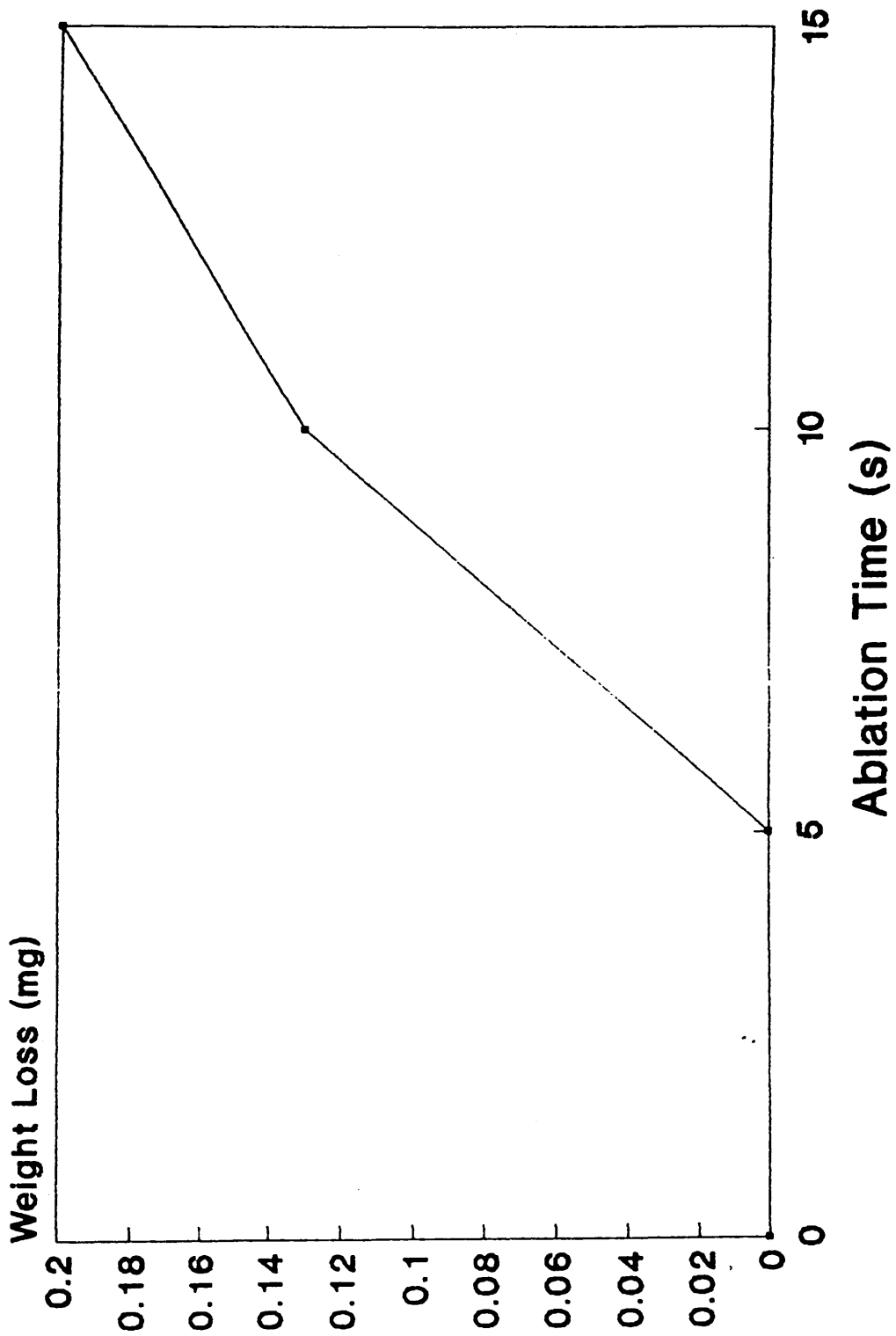


Figure 33. Weight Loss as a Function of Ablation Period for Copper.

4.1.1.4 Discussion

The observed effects of laser radiation on the samples are clearly dependent upon the radiant flux, or power output of the laser, and the irradiance upon the sample surface. These quantities are defined as follows;

$$\text{Radiant Flux} = \frac{\text{Pulse Energy}}{\text{Pulse Length}}$$

$$\text{Irradiance} = \frac{\text{Radiant Flux}}{\text{Area}}$$

Irradiance is dependent upon the area of interaction of the laser beam with the sample. This, in turn, is governed by the focusing criteria applied to the beam.

The laser can be focused to a spot of radius r given by;

$$r = \frac{\lambda}{\pi} \times \frac{F}{R}$$

where λ is the laser wavelength, F is the focal length of the focusing lens and R is the radius of the beam incident on the lens.

The laser output is specified by the manufacturer as having a diameter of 6.4mm. As the beam divergence is very low ($<0.5\text{mrad}$) and only propagates a distance of approximately 20cm before it is incident upon the focusing lens, the value of R may be taken as 3.2mm. The laser wavelength is 1064nm and the focal length

of the lens is 100mm. Hence;

$$r = \frac{1064 \times 10^{-9}}{\pi} \times \frac{100 \times 10^{-3}}{3.2 \times 10^{-3}}$$

$$r = 10.6 \mu\text{m}$$

Assuming a circular spot, this radius corresponds to a spot area of $3.53 \times 10^{-6} \text{ cm}^2$.

Having established the area of the spot produced on the sample when the beam is focused onto it, the maximum irradiance may be calculated from the above equations. The pulse energies have been measured as 415mJ in long pulsed operation and 345mJ in Q-switched operation. The pulse lengths specified by the manufacturer are about 200 μ s in long pulsed operation and 9ns in Q-switched mode.

Using the above data, the following may be calculated;

	<u>Q-switched mode</u>	<u>Long pulsed mode</u>
Radiant Flux =	$\frac{0.345}{9 \times 10^{-9}}$	$\frac{0.415}{200 \times 10^{-6}}$
=	$3.83 \times 10^7 \text{ W}$	2075 W
Irradiance =	$\frac{3.83 \times 10^7}{3.53 \times 10^{-6}}$	$\frac{2075}{3.53 \times 10^{-6}}$
=	$1.08 \times 10^{13} \text{ W.cm}^{-2}$	$5.88 \times 10^8 \text{ W.cm}^{-2}$

The above irradiances are only obtained when

the laser is focused. Defocusing the beam increases the spot size and decreases the irradiance. Furthermore, at focus, a spot size of radius $10.6\mu\text{m}$ is produced but the observed craters are significantly larger than this. This is due to the conduction of heat through the sample and the eruption of material from the heated area.

Examination of the craters produced by laser ablation revealed that they were elliptical. Consequently, the beam focused onto the sample surface must also be elliptical. This is due to an effect called "Coma" which is a lens aberration that appears when light is brought to a focus at points off the optical axis [130].

The above experiments have shown that long pulsed operation results in melting of the sample in the focal area and the ejection of relatively large masses of sample. In Q-switched operation no evidence of melting is observed and the loss of mass is less than $10\mu\text{g}$.

The interaction of laser radiation with matter is a complicated phenomenon dependent upon many parameters of the laser pulse and the surface material. A simple model has been presented by Klocke [131]. Part of the incident laser radiation is absorbed to a depth of some microns, raising the temperature to the boiling point and vaporisation begins. The energy of the electrons of the surface elements is raised and this

high energy is transferred by electron impact. The material undergoes a change of state and material erupts at a high velocity producing a crater. Vaporisation of the front surface occurs, thus removing energy from the region nearest the surface. Maximum temperatures therefore, lie just below the surface. If the temperature below the surface is sufficiently high to cause vaporisation, the pressure below the surface is increased and the material is removed explosively.

The extent to which the above processes occur is dependent upon parameters such as irradiance and pulse length. At irradiances of approximately 10^7 W.cm^{-2} and pulse widths of $< 200\mu\text{s}$ some vaporisation occurs but only about 0.1% of the ablated matter is in the vapour state [132]. Many particles are ejected from the crater [133], a process attributed to a flushing mechanism where molten material is pushed out towards the crater walls and then from the surface by a high vapour pressure in the laser induced plume [134]. Van Deijck et al. [135] has summarised literature values and concluded that at low irradiances (10^7 W.cm^{-2}), most of the material is removed as molten droplets.

At irradiances greater than about 10^9 W.cm^{-2} and pulse widths $< 100\mu\text{s}$, vaporisation is the dominant process, with only minor expulsion of molten material from the surface. No particles are observed from surfaces irradiated with these high-power pulses [133]. At such irradiance, solid material is quickly vaporised,

so only a small fraction of the material in the focal area is molten at one time. The vaporised material also forms the luminous plume which absorbs some of the incoming radiation. This view is also supported by Van Deijck [135].

The experimental results and observations given earlier fit very well into these regimes. Operation in the long pulse mode produces irradiances and pulse lengths which are conducive to the production of melting and subsequently the removal of relatively large masses of sample. The effects observed in the copper sample are due to differences in reflectivity and a higher thermal conductivity. The latter allows the heat generated at the focal area to be conducted away relatively quickly ensuring that the temperatures attained are insufficient to cause the same degree of melting observed in aluminium. Operation in the Q-switched mode produces predominantly vaporisation. The pulse durations are too short and the irradiances too high to produce effective melting, although some melting does occur.

In summary, it has been shown that long pulsed operation of the laser removes significantly larger masses of the test pieces than Q-switched operation. However, when using laser ablation as a sampling device for a remote excitation source such as an ICP, it is imperative that the ablated material may be transported in a flowing stream of argon. Since the ablated material

produced by long pulsed operation may not be amenable to such transport, further work in conjunction with the ICP was required.

4.1.2 Preparation for Laser Ablation Studies

The plasma of the Jobin-Yvon 38-48 was initiated and the instrument prepared for use as described in section 3.2. Deionised water was aspirated into the plasma during a 10 minute stabilisation period.

The deionised water was then replaced by a 5mg/L solution of the element of interest. The monochromator was driven to an appropriate wavelength and the emission line profiled until the wavelength corresponding to the peak maximum was located. Line profiling involved the energy meter on the integrator. Deionised water was then re-introduced to ensure that the emission intensity returned to zero, thus confirming that the emission line profiled was characteristic of the element of interest.

The nebuliser gas flow was gradually reduced as the carrier gas flow was increased until the latter replaced the former (see Figure 21). Under these conditions the plasma was running "dry". The carrier gas reached the plasma only after it had passed through the laser ablation chamber.

Laser ablation of a sample held within the laser ablation chamber produced material, which under the correct conditions, could be transported to the

ICP. If this material included sufficient of the element of interest, then a signal would be recorded on the chart recorder.

The verification of the optimum operating conditions became the subject of further investigation.

4.1.3 Feasibility Studies

Initially, there was a requirement to ensure that the configuration of the analytical system was suitable for the proposed investigation. These feasibility studies were carried out using a replica of the ablation chamber described by Ishizuka and Uwamino [84]. The only modification was a screw-threaded base to the chamber, rather than simply standing the chamber on the sample. For this work the stainless steel base was used as the sample, by focusing the laser beam onto the base.

4.1.3.1 Iron in Stainless Steel

The instrument was prepared as described in section 3.2. A 5mg/L iron solution was used to locate the emission line at 238.204nm, and the instrument prepared for laser ablation work by turning off the nebuliser gas and replacing it with the carrier gas. A flow of 0.7 L/min was used.

The laser was operated in the long pulse mode at a frequency of 10Hz. Single laser shots were fired at the ablation chamber base, at lamp energies of 40J,

50J, 60J and 70J (maximum energy). The chamber was moved slightly after each shot to ensure that a new and untested area of the sample was presented to the laser for each shot. The signals so produced are given in figure 34.

4.1.3.2 Chromium in Stainless Steel

The above experiment was repeated at the chromium line at 267.716nm using single laser shots at lamp energies of 30J, 40J, 50J, 60J and 70J. All other experimental conditions were the same.

The peak shapes produced were very similar to those for iron (figure 34). However, the observed trend was quite different as can be seen from the peak height data given below (see figure 35).

Lamp Energy (J)	30	40	50	60	70
Peak Height (mm)	20	68	179	110	15

The reproducibility of these signals was briefly examined by firing 3 laser shots at a lamp energy of 50J, again in the long pulse mode. The reproducibility expressed as % RSD (relative standard deviation) was 37%.

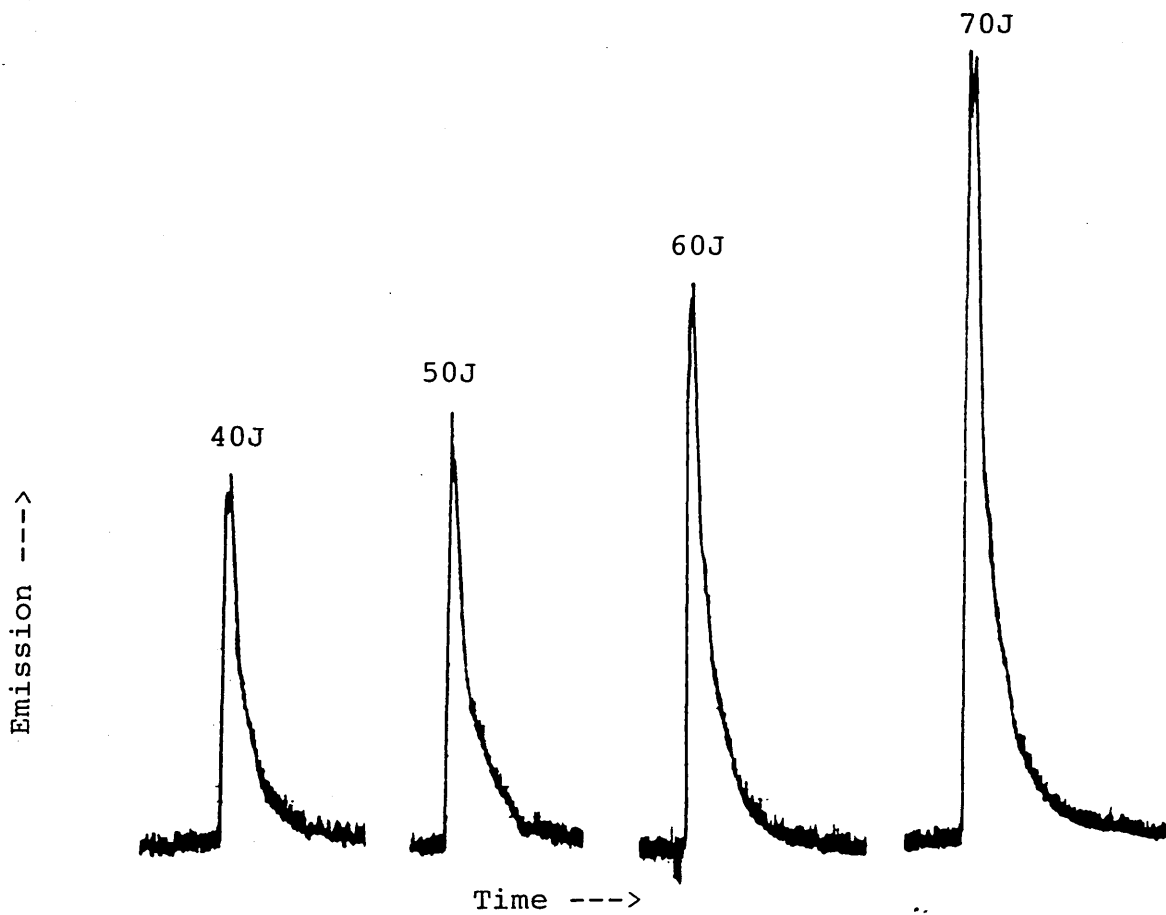


Figure 34. Iron in Stainless Steel at Various Laser Lamp Energies.

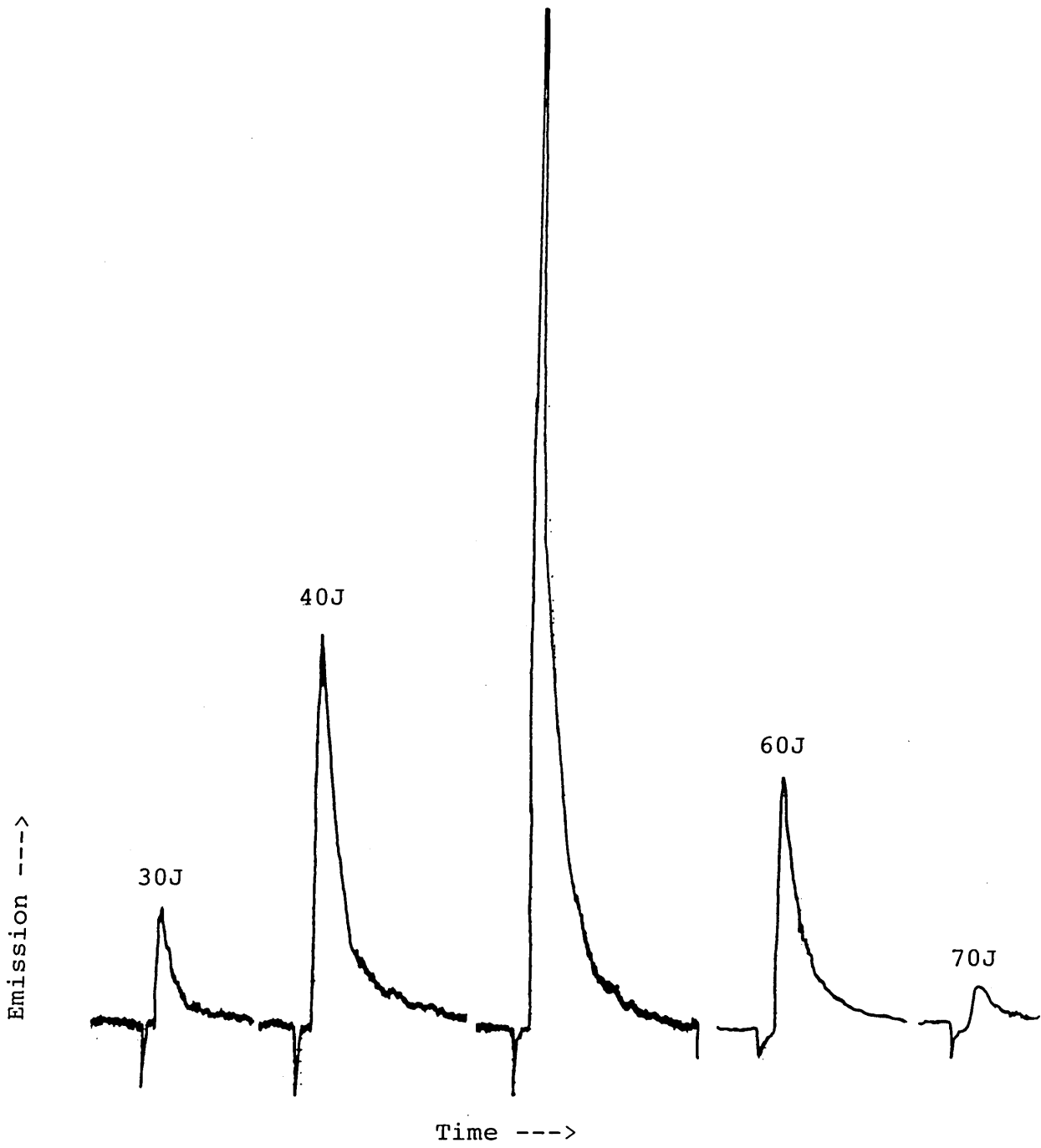


Figure 35. Chromium in Stainless Steel at Various Laser Lamp Energies. Chart Recorder Voltage 0.2V Except Signals at 60J and 70J, 0.5V.

4.1.3.3 Lens Damage

After the above work it was noticed that the focusing lens had become damaged. The quartz window to the ablation chamber was at 90° to the incident laser beam. Some of this radiation was being reflected and focused onto the lens. This situation was corrected by tilting the window such that any reflected radiation was absorbed by the lens holder, and not the lens. This is shown in figure 36.

4.1.3.4 Discussion

The feasibility studies described above clearly demonstrated that the analytical system as configured, was suitable for the work underway.

The magnitude of the emission signal was dependent upon the laser output energy as controlled by the flash lamp energy. The maximum intensity for iron was obtained at 70J lamp energy, whilst for chromium 50J produced the largest signal. Operation at energies greater than 50J produces more melting and the removal of material as molten globules. In this situation it is likely that chromium becomes entrained in this molten material, the vast majority of which is sputtered onto the walls of the chamber, and thus is prevented from reaching the ICP. This effect is less pronounced for iron.

Reproducibility has been shown to be poor. This is due to a combination of sample heterogeneity on a microsampling scale and the irregular and poor

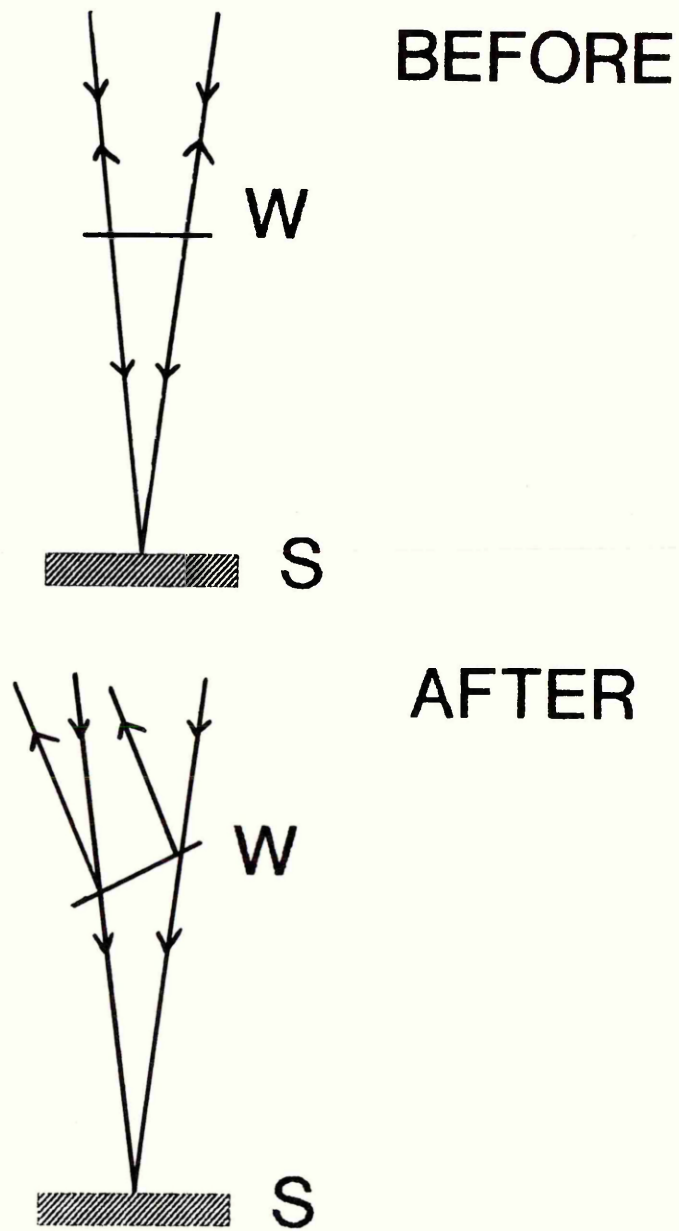


Figure 36. Diagram Showing the Change in Orientation of the Ablation Chamber Window (W) to Avoid Lens Damage. The Laser is Focused onto the Surface of the Sample (S)

condition of the sample surface which was pitted with many craters.

As stated earlier, in chapter 2, lasers have a poor efficiency in terms of conversion of input energy to laser power. With an input energy of 70J the laser in this study has an output energy of 345mJ Q-switched and 415mJ long pulsed. This equates to efficiencies of 0.5% and 0.6% respectively. If the efficiency is assumed to remain constant at all lamp energies above the threshold, then the following output energies can be achieved:

Lamp Energy (J)	Output Energy (mJ)	
	Q-switched	Long Pulsed
30	147	177
40	196	236
50	245	295
60	294	354
70	345	415

4.2 EXPERIMENTAL (JOBIN-YVON 38-48)

It has been shown in the previous section that the instrumental configuration described was suitable for the work underway. Analytes of interest were removed from the solid sample by laser ablation and transported to the ICP resulting in an emission signal. The following work considers the optimisation of several of the operating conditions.

4.2.1 Materials

Argon: High purity grade (British Oxygen Co. Ltd.).

Silicon: 1000mg/L silicon solution (BDH Ltd.).

Manganese: 1000mg/L manganese as manganous nitrate
(BDH Ltd.).

High Purity Iron: CRM 088-1 (Bureau of Analysed Samples
Ltd.).

Aluminium Alloy: BCS 216/2 (Bureau of Analysed Samples
Ltd.).

Graphite: High purity grade (Spectrochem Supplies Ltd.).

All graphite components were fabricated in the workshops at Sheffield City Polytechnic.

4.2.2 Apparatus

The Durr Jobin-Yvon 38-48 ICP system was used in conjunction with the laser, its optics, the Perkin Elmer HGA-2100 power supply and the laser ablation

chamber all described in chapter three.

4.2.3 Spectrometer Resolution

A simple experiment was conducted to determine the resolution of the HR.1000 monochromator. The ICP was initiated and prepared for conventional solutions nebulisation. Coolant and nebuliser gas flows of 16L/min and 0.7L/min respectively were used. A forward power of 1.4kW was set and the system was allowed to stabilise for a period of 5 minutes while nebulising deionised water.

The entrance and exit slits on the monochromator were set as follows;

Entrance Slit:	Width	15 μ m
	Height	30mm
Exit Slit:	Width	50 μ m
	Height	40mm

A 10mg/L boron solution (prepared by dilution of a 1000mg/L standard solution from BDH Ltd.) was nebulised into the ICP and a wavelength scan was performed from 249.60nm to 249.81nm, scanning at 0.3nm/min. The resultant chart recorder trace is given in figure 37.

The resolving power required to resolve the two boron lines at 249.678nm and 249.773nm is given by the ratio of the mean wavelength to the separation

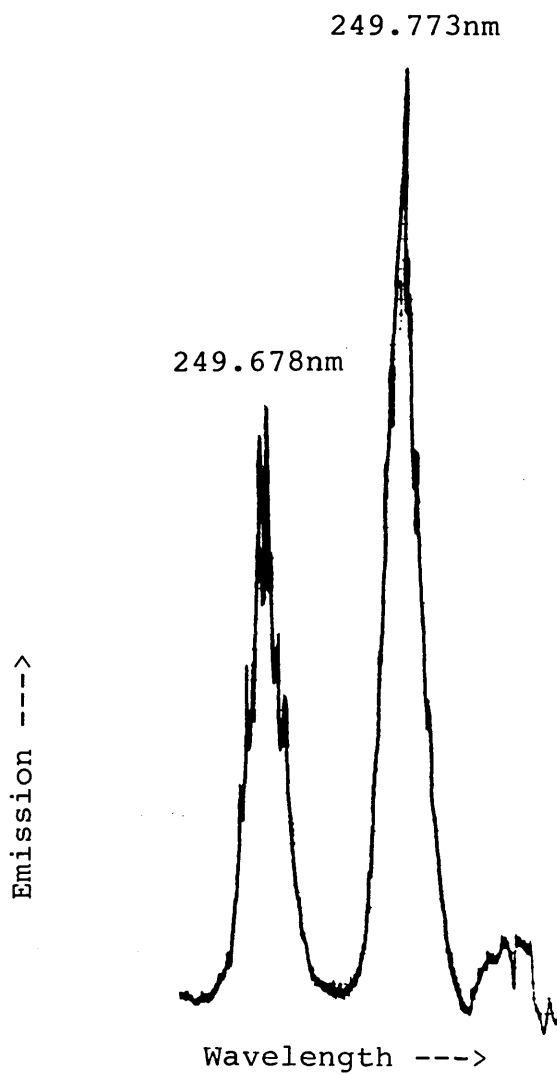


Figure 37. Monochromator Resolution as Shown by the Boron .
Doublet at 249.7nm.

of the two lines,

$$\text{Resolving Power} = \frac{\lambda}{\Delta\lambda}$$

In this case a resolving power of approximately 3000 is required. From the chart recording it can be seen that this is easily attained. Modern spectrometers based on Echelle gratings have resolving powers in excess of 100,000.

The practical resolving power is usually defined as the bandwidth at half intensity. The measured bandwidth at half intensity ie. 4mm must be converted to nm. The peak maxima are separated by 19mm on the recording which is equivalent to 0.095nm (249.773 - 249.678 = 0.095nm). Therefore, 4mm corresponds to a bandwidth of 0.02nm which in turn corresponds to the practical resolution of the spectrometer.

As the two peaks are so clearly resolved, it is likely that the resolution of the spectrometer is somewhat better than 0.02nm.

4.2.4 Electrothermal Melting

The most appropriate samples for this investigation were metallurgical certified reference materials. A relatively small number of these are produced as discs for use as X-ray Fluorescence Spectroscopy standards, but the majority are produced

as finely divided powders or turnings. Standard discs have been used in laser ablation studies [84,86-89] as powders and turnings are less amenable to laser ablation. In this work, the electrothermal melting capability allows metallurgical powders or turnings to be fused, thus creating a larger sample, prior to laser ablation. The melting capability, in principle, therefore extends the range of sample types that may be examined.

Two solid metallurgical samples were examined, a high purity iron (CRM 088-1) and an aluminium alloy (BCS 216/2). The former is a finely divided powder while the latter comprises coarse turnings, each weighing 1-6mg. Samples were placed into graphite sample cups which in turn were placed into graphite crucibles held in the ablation chamber (see figure 29). The samples were subjected to a heating regime sufficient to produce melting, followed by laser ablation of the cooled melt.

Experiments were performed to establish the minimum degree of heating required to melt the samples. This minimised loss of analyte due to electrothermal vaporisation. A power setting of 1.25 was found to be sufficient. On initiation of the heating sequence, the temperature of the furnace increased over a period of 10s and then stabilised. This temperature was then maintained for a further 20s to allow complete melting. The heating sequence was therefore 30s long. The temperature reached was approximately 1500°C as this

is the melting point of iron.

There were occasions when the heating sequence produced large amounts of smoke. New carbon cups and crucibles, when heated, caused significant deposits of carbon on the inside surfaces of the ablation chamber and the transport tubing to the plasma. The melting of BCS 216/2, which has a high magnesium content, compounded this effect. It was found that allowing this deposition of matrix constituents to go unchecked reduced the ICP emission signals for the analyte of interest. The deposits produced an active surface capable of adsorbing analyte from the sample gas stream. To minimise this effect, new graphite cups and crucibles were electro-thermally cleaned prior to use and the chamber and tubing were regularly cleaned.

When CRM 088-1 was subjected to the heating sequence described earlier, it melted, producing a flat meniscus across the top of the sample cup on cooling. BCS 216/2 on the other hand, produced a sphere which positioned itself centrally in the cup. Cooled melts of CRM 088-1 have been examined using scanning electron microscopy. This investigation showed that the melting of the sample on a microscopic scale was not reproducible. The surfaces examined exhibited three differing conditions which were of identical elemental composition. Some areas of the sample surface showed very clear dendritic structure signifying complete melting. Other areas showed slight dendritic structure while the third area

showed no dendritic structure at all, signifying partial melting. Very dark areas were also observed, particularly around the circumference of the sample surface. This was thought to be graphite which had migrated from the cup onto the sample during melting. These surface irregularities are shown in photographs 1 and 2.

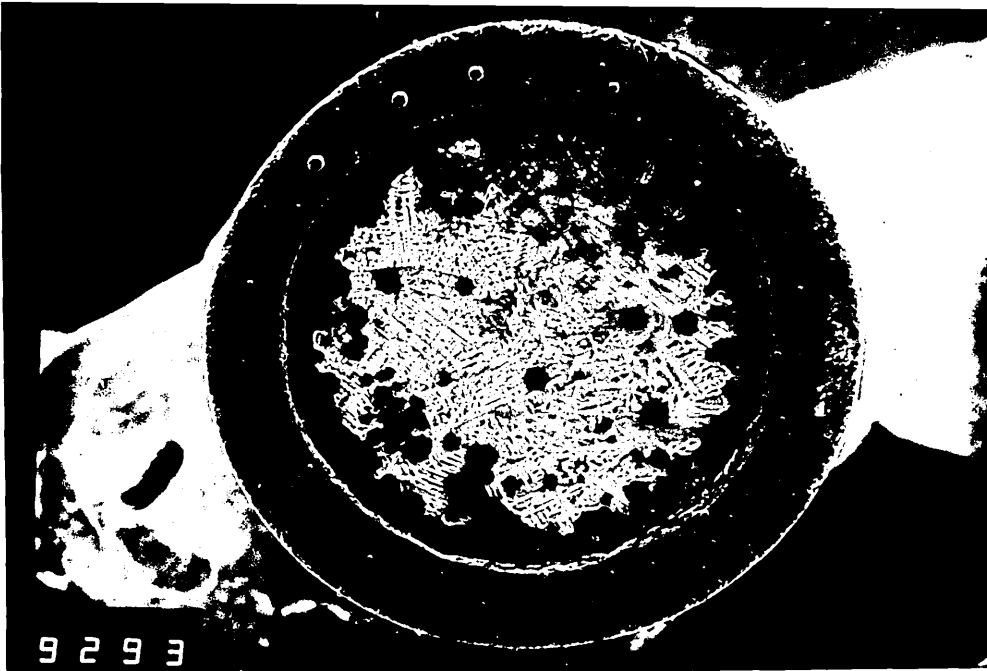
These differences in surface structure which occurred on a single sample were due to the fact that different areas of the sample were at different stages of melting when the heating sequence came to an end. This could have implications on the reproducibility of the emission signals generated by laser ablation.

The laser may ablate any one or any combination of the areas described above and it is known that sample surface irregularities can lead to irreproducible measurements.

Two elements, namely silicon and manganese, have been investigated in each of the samples. It was found that both elements in both samples produced signals due to electrothermal volatilisation during the sample melting sequence. This effect was minimised at a power setting of 1.25 which was just sufficient to melt the samples.

4.2.5 The Effects of Laser Focusing

The effects of focusing the laser beam have been investigated by monitoring the resultant changes in emission signals for silicon and manganese in CRM



Photograph 1. Sample of CRM 088-1 Showing the Non-Uniform Nature of the Sample After Melting.
(25x Magnification)



Photograph 2. Dendritic Structure Signifies Complete Melting and Other Areas Show Only Partial Melting. The Black Areas May be Due to Migration of Graphite onto the Sample Surface. (220x Magnification)

088-1 and BCS 216/2. This allows comparison of results for two elements in two matrices. The analyte concentrations and the wavelengths used are given below:

	<u>Wavelength(nm)</u>	<u>CRM 088-1 (mg/kg)</u>	<u>BCS 216/2 (%m/m)</u>
Si	251.611	24	0.71
Mn	257.610	207	0.71

Focusing was achieved by moving the sample relative to the focusing lens. The ablation chamber was mounted on a laboratory jack which provided vertical movements of the sample. Due to the physical constraints of the equipment, the focusing distance ie the lens to sample distance, could only be varied between 87mm and 102mm when using a 100mm focal length lens.

A new graphite cup was placed into the graphite crucible of the ablation chamber and cleaned by subjecting it to the normal heating sequence. This was done "on-line" with the plasma, using the two-way teflon valve of the ablation chamber. The cup was then filled with sample which was melted "on-line", briefly allowed to cool and then subjected to laser ablation. The emission signal was recorded using a chart recorder. The above procedure was performed in triplicate for each focusing distance used. The focusing distance was varied from 87mm to 102mm in multiples of 3mm.

The ICP operating conditions are given in chapter three. The laser was operated in the long pulse mode

at maximum lamp energy (70J) and at a frequency of 10 Hz. The laser was fired repetitively for a period of 1s producing a train of 10 pulses each about 200 μ s long. It had been established earlier that single shots were insufficient to produce an emission signal.

4.2.5.1 Results

The peak heights of the emission signals were recorded and the data is tabulated below.

Table 12. Silicon in CRM 088-1

Focusing Distance(mm)	Peak Height			Mean (mm)
	1	2	3	
87	7	8	6	7
90	26	36	51	38
93	77	63	58	66
96	70	78	54	67
99	38	44	40	41
102	47	55	44	49

Table 13. Silicon in BCS 216/2

Focusing Distance(mm)	Peak Height			Mean (mm)
	1	2	3	
87	18	29	18	22
90	66	46	90	67
93	150	120	109	126
96	71	41	58	57
99	33	33	28	31
102	105	70	85	87

Table 14. Manganese in CRM 088-1

Focusing Distance(mm)	Peak Height			Mean (mm)
	1	2	3	
87	143	117	134	131
90	215	175	175	188
93	295	390	285	323
96	220	150	235	202
99	110	119	145	125
102	161	150	145	152

Table 15. Manganese in BCS 216/2

Focusing Distance(mm)	Peak Height			Mean (mm)
	1	2	3	
87	25	15	15	18
90	15	38	95	49
93	380	433	355	389
96	93	75	85	84
99	28	43	40	37
102	68	40	28	45

The above data are shown graphically in figures 38-41 respectively.

4.2.5.2 Discussion

Examination of the plots of average peak height against focusing distance reveals that the trends are essentially the same for both elements in both samples. The most intense signals and hence the greatest analytical sensitivities are produced at a focusing distance of 93mm. This is 7mm removed from the focal length of the lens ($f=100\text{mm}$).

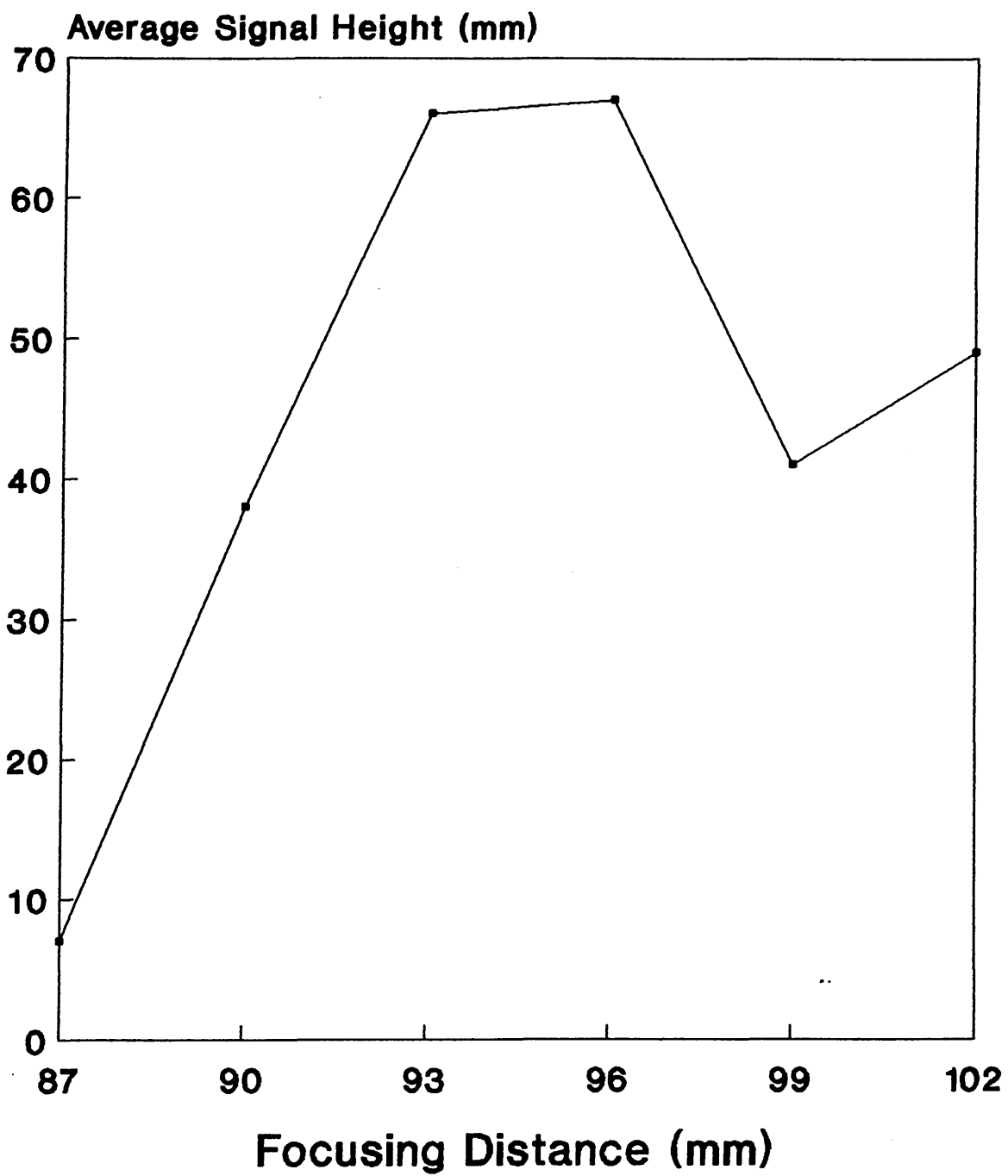


Figure 38. Effect of Focusing on Si in CRM 088-1.

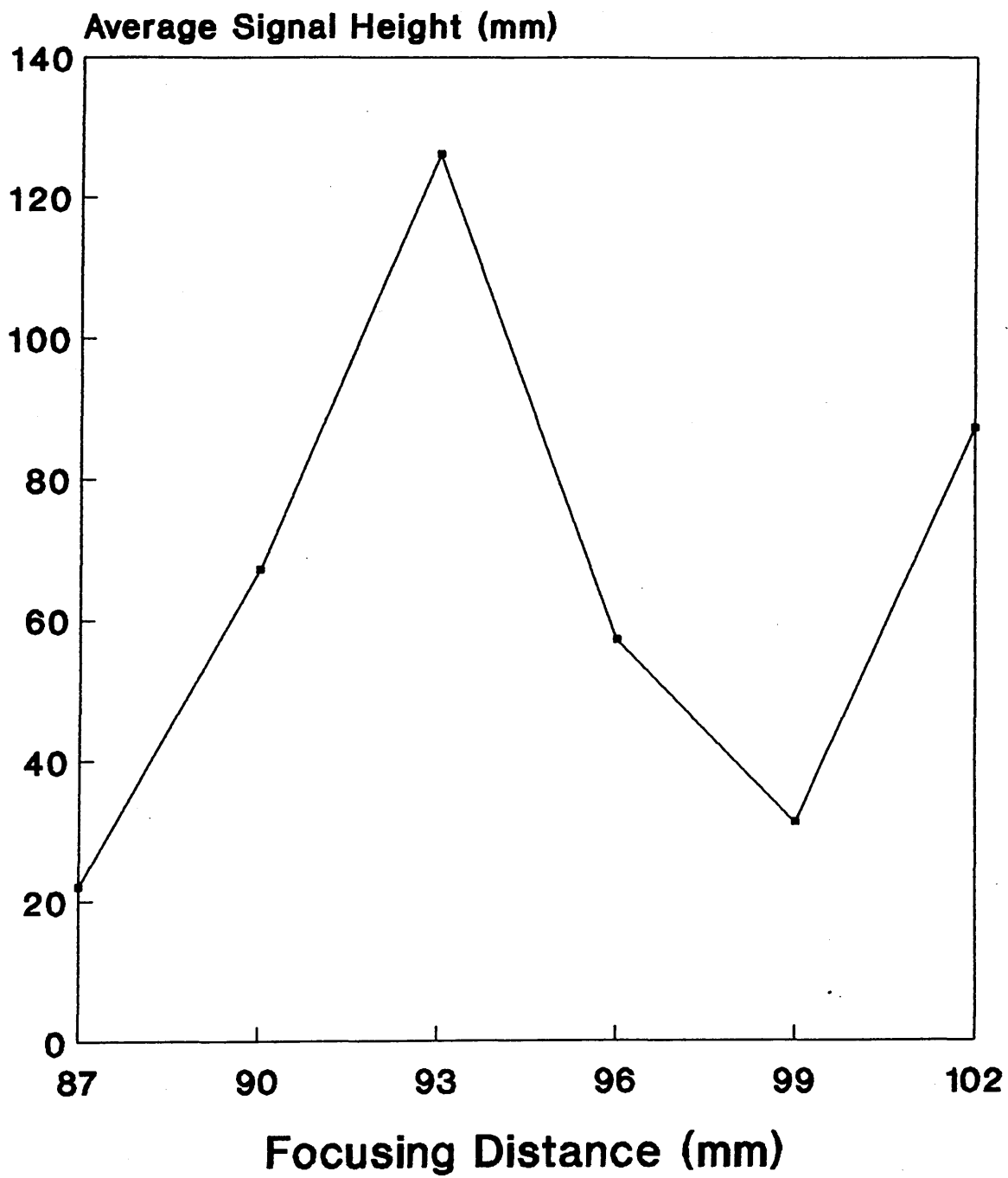


Figure 39. Effect of Focusing on Si in BCS 216/2.

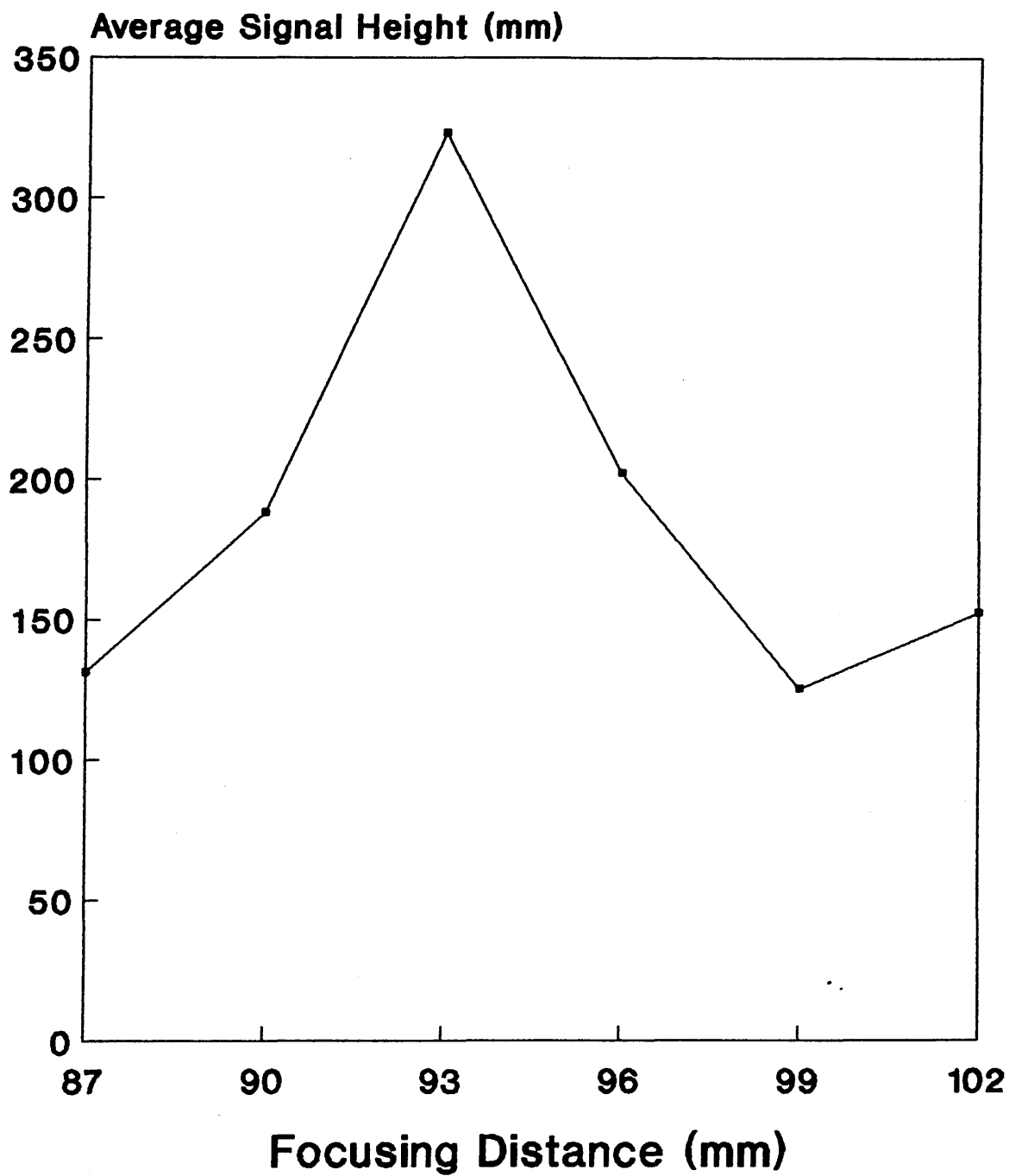


Figure 40. Effect of Focusing on Mn in CRM 088-1.

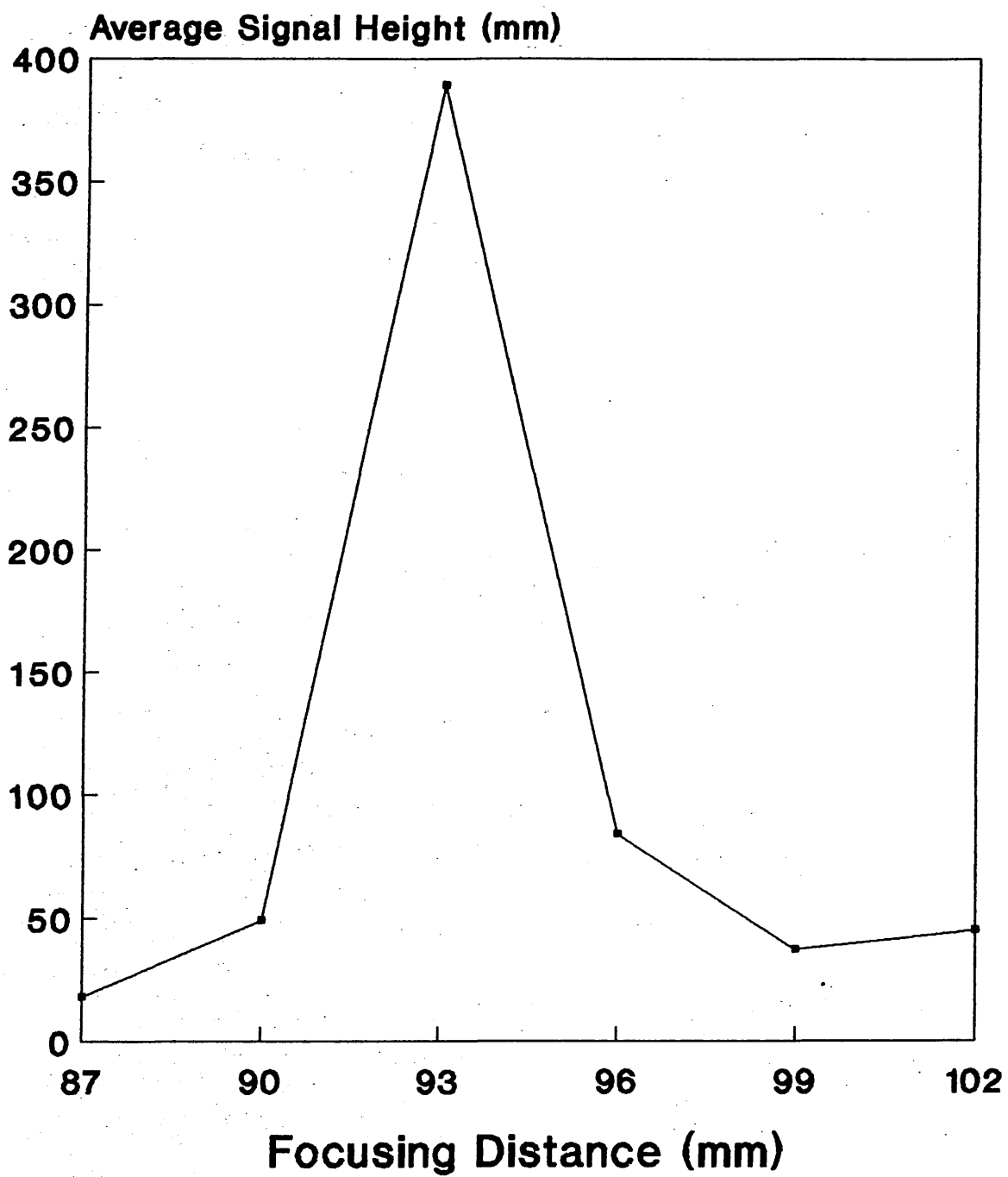


Figure 41. Effect of Focusing on Mn in BCS 216/2.

The results also show that there is a tendency for the peak heights to increase at a focusing distance of 102mm. Had the experiment continued to larger focusing distances, it is thought likely that the resultant plots of the data would show two maxima separated by a valley corresponding to the focal length of the lens.

The experimental data may be subdivided into three differing situations where;

- i) the sample is placed at the focal point,
- ii) the sample is 7mm away from the focal point,
- iii) the sample is more than 7mm away from focus.

When the beam is focused onto the sample surface, melting is the predominant process. The laser bores relatively deeply into the sample ejecting molten particles. Very little of the ablated material is amenable to transport in the argon stream, resulting in relatively small emission signals from the ICP. When the sample is moved to a position 7mm from the focal point, vaporisation becomes more significant. A high degree of melting still occurs, but at the lower energy density more of the ablated material is taken up by the argon stream and transported to the ICP. At positions greater than 7mm away from focus the energy densities become lower still and the degree of ablation decreases. The amount of material removed from the sample becomes progressively lower as does the ICP emission signal.

The precision associated with the triplicate measurements was in the range 4-68 %RSD. When compared to conventional solutions nebulisation techniques, the precision of laser ablation is relatively poor. Contributory factors include sample surface condition, sample heterogeneity and the reproducibility of the 1s long ablation period. This 1s was controlled manually by throwing a switch and timing the event on a stop-watch.

4.2.6 The Effect of Ablation Period

Having established the optimum focusing distance, experiments considering the effects of ablation period were considered. It had been shown earlier that a single long pulsed shot did not yield a signal, whereas a 1s ablation period produced significant signals. The effects of increasing this period still further were of interest.

As before, the emission signals for silicon and manganese in CRM 088-1 and BCS 216/2 were monitored. The samples were positioned at a focusing distance of 93mm and laser ablation periods of 1s, 2s, 3s, 4s, 5s, 10s and 20s were used. The ablation period was controlled manually by throwing the repetitive firing switch and by using a stop-watch.

The ICP and laser operating conditions were the same as for the focusing experiment and the same sample pretreatment procedures were adopted. The only variable was the ablation period.

4.2.6.1 Results

As with the focusing experiments, the results for both elements in both matrices were essentially the same. Here, the results for silicon in CRM 088-1 will be considered.

The emission peak heights for the signals were recorded and used to determine the mean peak height. The peak widths were similarly determined, being measured as the full width at half the peak maximum. These data are tabulated below in tables 16 and 17 respectively.

Table 16. Silicon in CRM 088-1 Peak Heights.

Ablation Period(s)	Peak Height (mm)			Mean (mm)
	1	2	3	
1	57	65	63	62
2	49	60	56	55
3	53	47	52	51
4	34	51	47	44
5	37	42	35	38
10	35	35	37	36
20	20	22	33	25

Table 17. Silicon in CRM 088-1 Peak Widths.

Ablation Period(s)	Peak Width (s)			Mean (s)
	1	2	3	
1	3	3	3	3
2	3	3	3	3
3	4	4	4	4
4	5	5	5	5
5	6	6	6	6
10	11	11	11	11
20	21	22	21	21

The above data is shown graphically in figure 42 and typical emission signals are given in figure 43.

4.2.6.2 Discussion

The results clearly show that increasing the ablation period produces a decrease in signal intensity and hence analytical sensitivity. The optimum ablation period is 1s. As expected, peak width increases proportionally with ablation period.

Examination of the analytical signals (figure 43) reveals that memory effects are negligible. The signal returns to baseline very quickly once the laser is switched off. More interesting is the progressive decrease in intensity with time. The effect is most easily seen in the 10s and 20s signals. This is due to the erosion of the sample surface. As the ablation process progresses so the concentration of analyte in the area of laser interaction decreases.

Clearly, as the ablation period increases, the amount of material reaching the ICP decreases. It is believed that during the first 1s of the ablation period the emission signal increases to a maximum, but fractions of a second later other processes begin to suppress the analytical signal. The longer ablation periods may cause the sample temperature to be elevated long enough to produce a greater degree of melting. This results in the ejection of relatively large molten

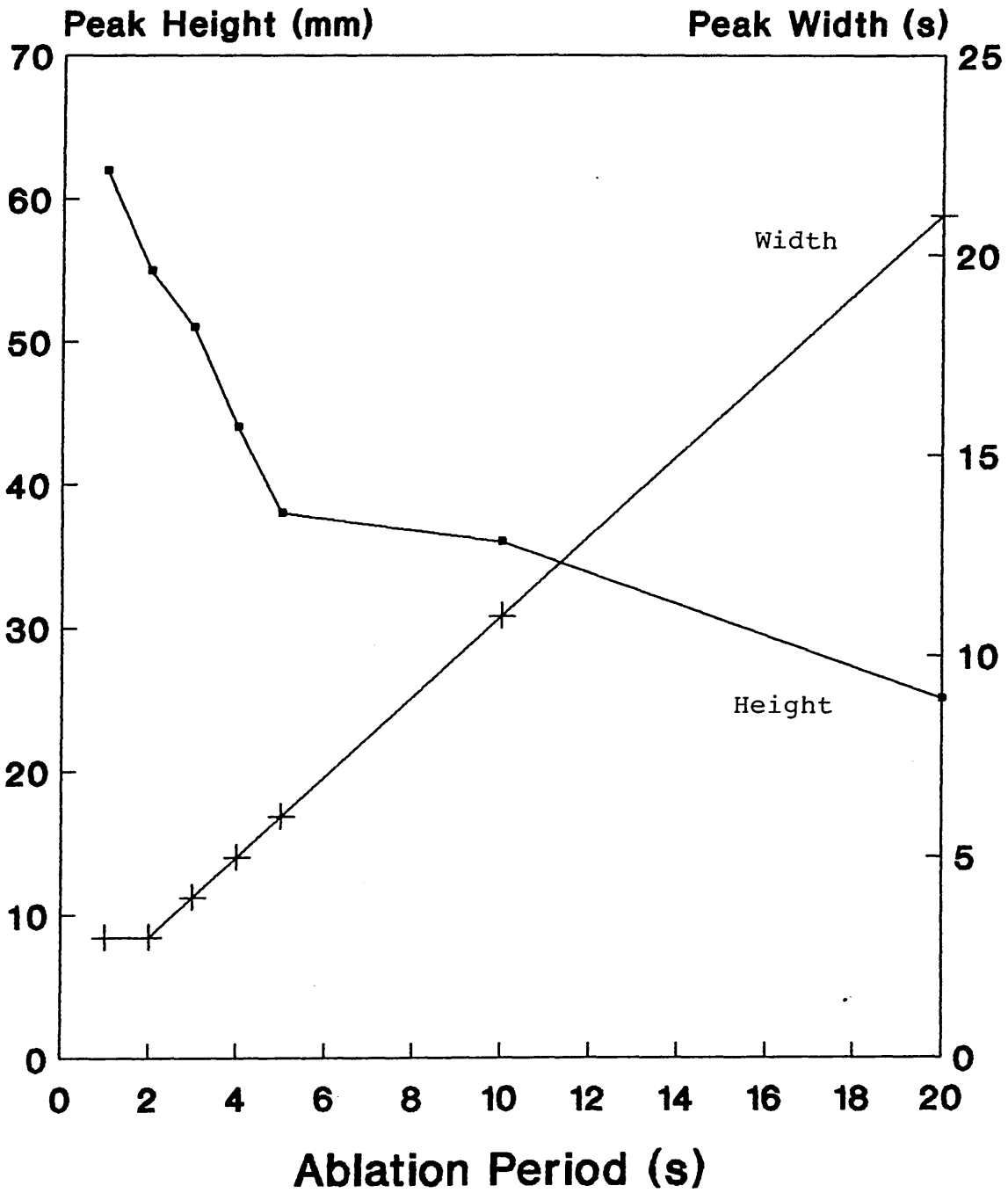


Figure 42. Effect of Ablation Period on Peak Height and Peak Width for Silicon in CRM 088-1.

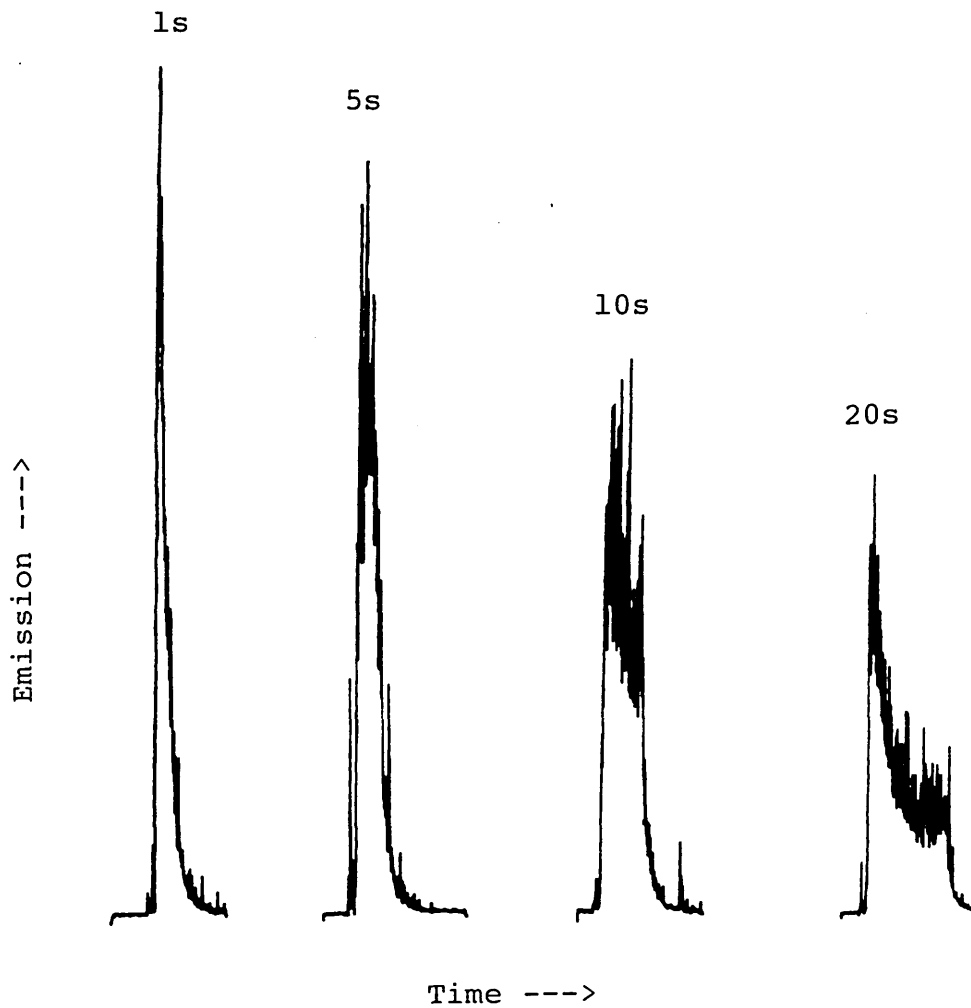


Figure 43. Typical Signals for Si in CRM 088-1 at Various Ablation Periods.

droplets which are not transported to the ICP.

Alternatively, some unknown laser interaction may occur with the material leaving the sample surface, particularly the laser induced plasma, that may cause this effect.

4.2.7 The Effect of Laser Operating Mode

As described in chapter 3, the laser may be operated in one of two modes, the long pulsed or the Q-switched mode. By monitoring the emission signals for silicon and manganese in CRM 088-1 and BCS 216/2, the effect of laser operating mode was investigated. As before, the observed trends were identical for both elements in both matrices. The signals for silicon in CRM 088-1 will be considered here.

The ICP operating conditions were as above. The laser was operated at maximum lamp energy and 10Hz. The operating mode and the ablation period were varied. A focusing distance of 93mm was used.

4.2.7.1 Results

As stated earlier, it was found that a single laser shot in the long pulsed mode was insufficient to produce an analytical signal. Indeed it was necessary to ablate for a period of 1s to produce a measurable emission signal from the ICP. In contrast, a single Q-switched shot was sufficient to produce a relatively large signal (see figure 44).

A single Q-switched shot produced a signal

SI IN CRM 088-1

Q-switched, 1 Shot.

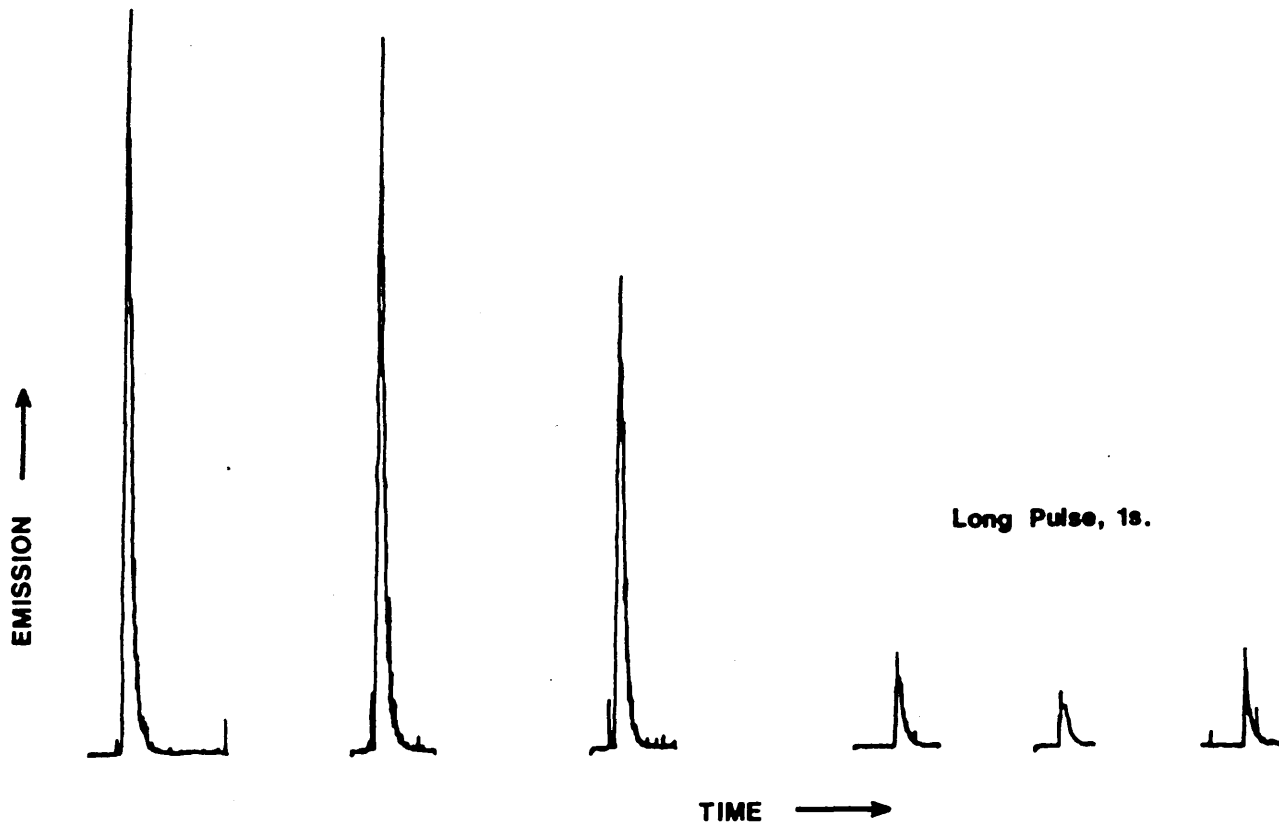


Figure 44. Comparison of Mode of Laser Operation.

10-fold larger than that produced by a 1s long period of ablation in the long pulsed mode. If the relative periods of laser-sample interaction are also considered, the improvement offered by Q-switched operation is highly significant. The intense Q-switched signals result from a pulse of radiation about 9ns long, whereas the long pulse signals result from repetitive laser firing for a period of 1s at 10Hz.

4.2.7.2 Discussion

The results indicate that the sample material ablated by Q-switched laser action is more amenable to transport in a gaseous stream than that produced by long pulsed laser action.

The dominant process during ablation in the long pulsed mode is melting. Relatively large masses of sample are ejected from the area of laser-sample interaction but very little of this material is transported to the ICP. Deep craters in the sample are produced but this results in relatively small emission signals.

During ablation in the Q-switched mode, vaporisation is the dominant process. Relatively small amounts are removed from the sample, but the ablated material is effectively transported to the ICP. In terms of laser sampling efficiency, where efficiency is defined as the proportion of ablated material which reaches the plasma, Q-switched operation is superior.

Relatively shallow craters are produced by Q-switched laser shots, which produce relatively large emission signals. The ablated material, rather than existing as molten globules, exists as atoms, ions, radicals, molecules and clusters of these particles [128].

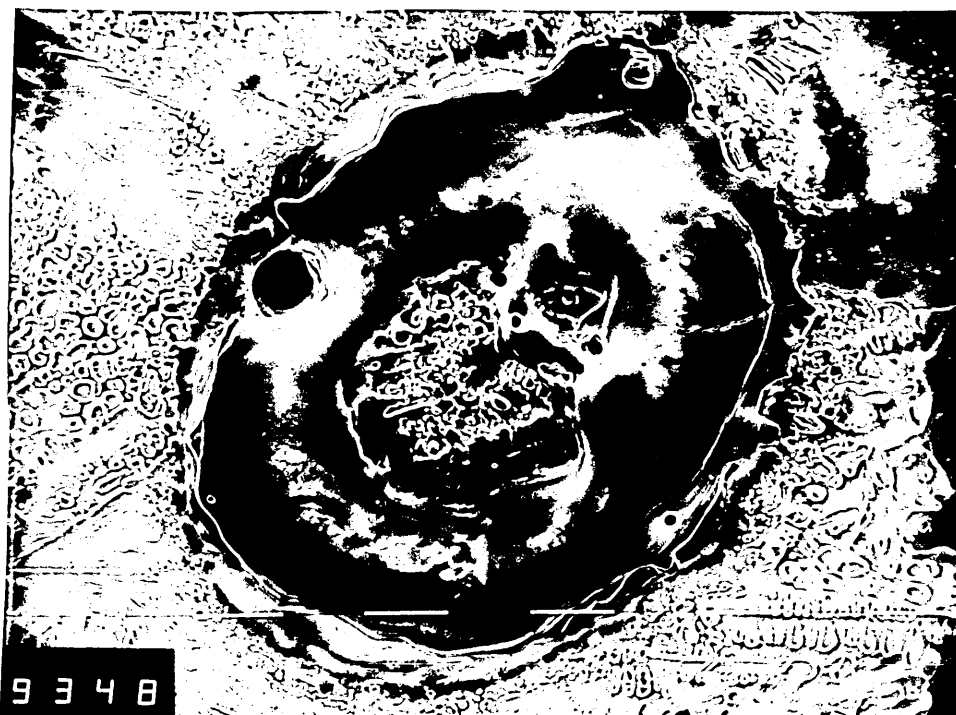
The relative effects of long pulsed and Q-switched laser radiation on the sample surface are shown in photographs 3 and 4 respectively. Clearly, long pulsed operation produces a good deal of melting. "Splashes" of molten material are seen radiating from the crater which is an elliptical shape. The major axis of this crater is 675 microns long while the minor axis is 520 microns long. Q-switched operation produced a crater of similar dimensions but there is less evidence of melting due to the brevity of the laser pulse. The crater also shows the toroidal output of the laser as the material in the centre of the crater shows no signs of laser interaction.

4.2.8 Conclusions

The work carried out on the Jobin-Yvon 38-48 system demonstrated clearly the feasibility of using laser ablation as a remote sampling device for the ICP. The magnitude of the emission signals and hence analytical sensitivity are very dependent upon laser focusing, the period of ablation and the operating mode.



Photograph 3. Crater Produced by a Single Long Pulsed Laser Shot at 70J Lamp Energy.



Photograph 4. Crater Produced by a Single Q-Switched Laser Shot at 70J Lamp Energy.

When it had been established that Q-switched operation offered significant improvements in signal magnitude, the focusing and ablation period experiments were repeated in the Q-switched mode. Although the emission signals were more intense, the results were exactly the same as in the long pulse mode, thus confirming the trends discussed earlier.

4.3 EXPERIMENTAL (JARRELL ASH ICAP-9000)

The work performed on the Jobin Yvon 38-48 system was limited by the monochromator. This restricted the studies to the measurement of only one element at any given time. By transferring the laser ablation system to the Jarrell Ash ICAP 9000 this limitation was removed. The latter instrument, having a 31 channel polychromator, provided the facility to measure anything upto 31 elements simultaneously.

This system was used to investigate the effects of contamination of graphite components, of electrothermal melting of samples, the relative merits of Q-switched and long pulsed laser operation and the depth profiling capability of the laser ablation technique.

4.3.1 Materials

Argon: High purity grade (British Oxygen Co.)

Nickel based alloy: BAS 346 (Bureau of Analysed Samples)

Graphite: High purity grade (Spectrochem Supplies)

The certified reference concentrations of elements in BAS 346 are given in table 18.

All graphite components were fabricated in the workshops at Sheffield City Polytechnic.

Element Concentration(µg/g) Melting pt°C Boiling pt°C

Co	150,000	1495	2870
Cr	100,000	1857	2672
Al	55,000	660	2467
Ti	50,000	1660	3287
Mo	30,000	2617	4612
V	10,000	1890	3380
C	1,500	3550	4827
Mg	147	649	1090
Sn	91	232	2270
As	50	817	613(sublimes)
Sb	47	630	1750
Ag	35	962	2212
Zn	29	420	907
Pb	21	328	1740
Te	12	450	990
Bi	10	271	1560
Sc	9	217	685
Ca	(37)	839	1484

Table 18. Certified Reference Values for BAS 346 with Melting and Boiling Point Data taken from The Handbook of Chemistry and Physics published by the Chemical and Rubber Company.
(The value for Calcium is not certified)

4.3.2 Apparatus

The Jarrell Ash ICAP 9000 ICP system was used in conjunction with the laser, its optics, the Perkin Elmer HGA 2100 power supply and the laser ablation chamber all described in chapter 3.

4.3.3 Electrothermal Pretreatment

As explained earlier, the electrothermal melting facility allowed the examination of a range of materials not normally suitable for laser ablation studies. Certified reference materials supplied as powders and chips may be fused prior to laser ablation, presenting a larger sample on which to focus the laser.

BAS 346, a nickel-based alloy, is supplied as chips graded 1700-250 microns (10-60 mesh). Several chips were placed into a graphite sample cup using forceps. The cup was then placed into the graphite crucible inside the ablation chamber. Once the chamber lid had been replaced, the chamber was turned back on-line such that the carrier gas passed through the chamber and on to the ICP.

The sample was fused using a power setting of 1.75, a total heating time of 30s and a 20s ramp. On initiation of the melting sequence, the temperature increased over a period of 20s and then remained stable for a further 10s. This heating regime was sufficient to completely melt BAS 346.

A potential problem with this electrothermal pretreatment was the possibility of loss of analyte, particularly the more volatile elements. This was examined by utilising the Time Study facility on the spectrometer software.

A Time Study was prepared consisting of sixty 1s integrations ie total measurement time 60s. A sample was placed into the ablation chamber and the chamber switched on-line. The Time Study was initiated coincidentally with the heating sequence allowing data to be acquired throughout the entire sample melting

process.

4.3.3.1 Results

The Time Studies for twelve of the elements certified in BAS 346 are given in figures 45-47. The y-axis is emission intensity in counts and the x-axis is time in seconds. These emission-time responses were all obtained simultaneously using the instrumental operating parameters specified in chapter three.

The elements monitored may be sub-divided into three categories;

- i) High boiling points - Mo,V,Ti,Co.
- ii) Moderate boiling points - Cr,Al,Pb,Ca
- iii) Low boiling points - Mg,Zn,Se,As

which are discussed in more detail below.

4.3.3.2 Discussion

A.Molybdenum, Vanadium, Titanium, Cobalt(Figure 45)

The time studies for molybdenum and vanadium are very similar. They show a slight, but insignificant, increase in intensity approximately 20s into the heating sequence. The maximum intensity is approximately equivalent to two times the standard deviation of the background noise. When it is considered that BAS 346 is 3% molybdenum and 1% vanadium it is clear that these elements are not volatilised during sample melting.

Titanium and cobalt are somewhat different in that significant signals are produced. Two peaks are observed in the response for titanium, although it is believed that the second and largest is due to electrical noise associated with the furnace power supply. This effect is also evident in the traces for magnesium, lead and zinc. The first peak is believed to be due to the volatilisation of relatively small levels of titanium.

Volatilisation of cobalt appears to be more significant. But again, an emission intensity of 348

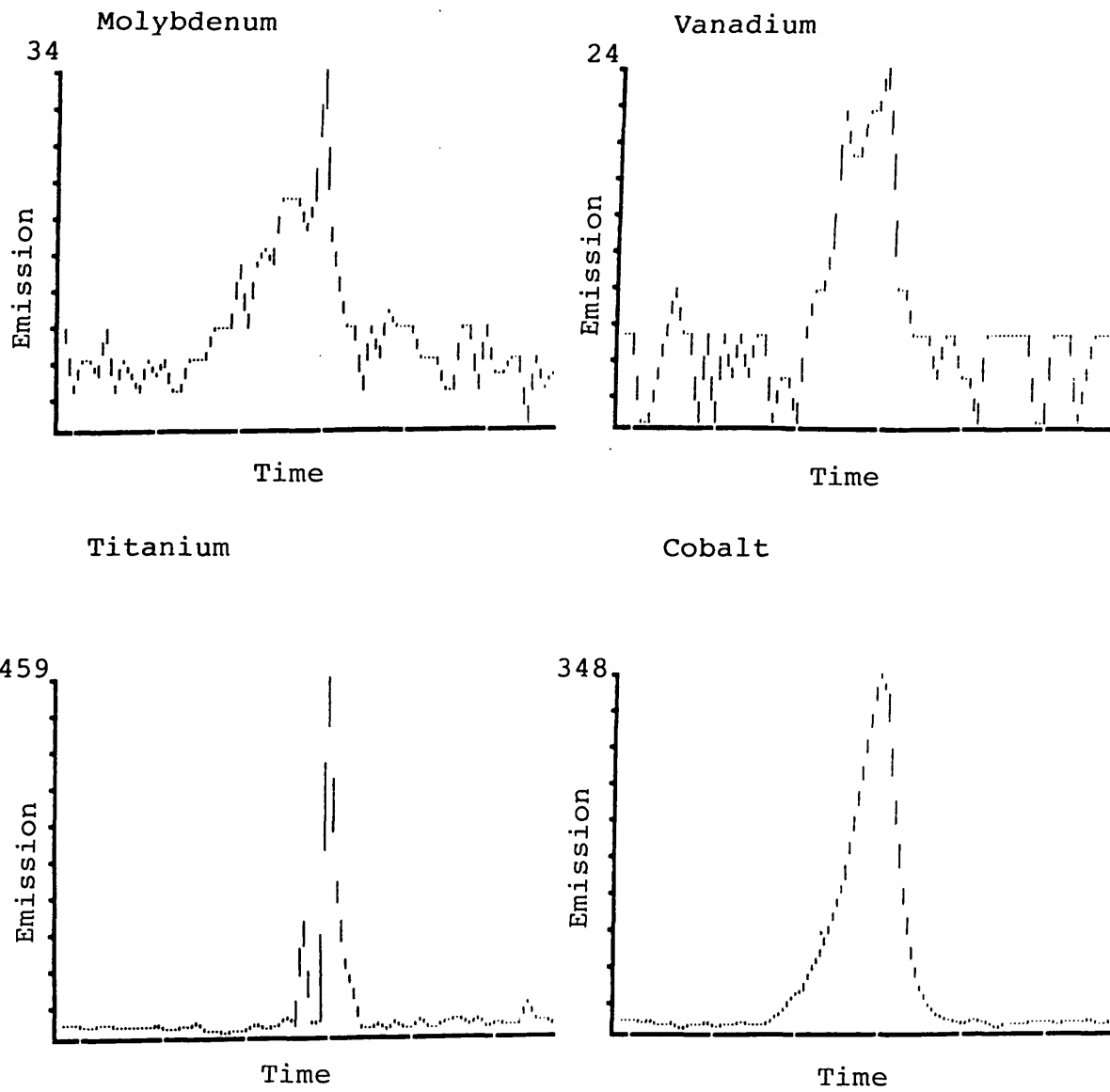


Figure 45. Emission Time Profiles During Melting of BAS 346. Maximum Emission Intensities are given on the Y-axis, the Time Axis is 60s long.

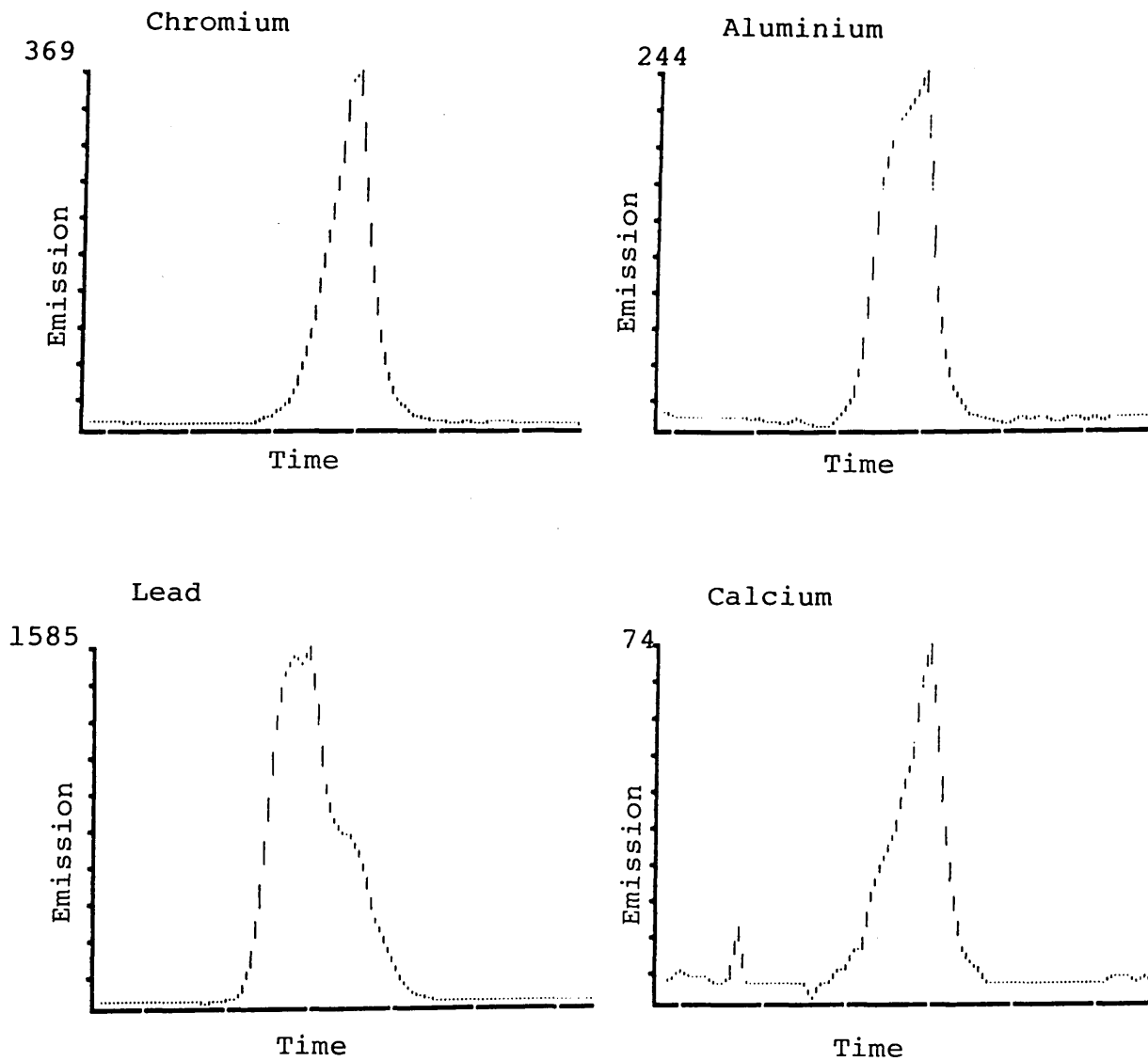


Figure 46. Emission Time Profiles During Melting of BAS 346. Maximum Emission Intensities are given on the Y-axis and the Time Axis is 60s long.

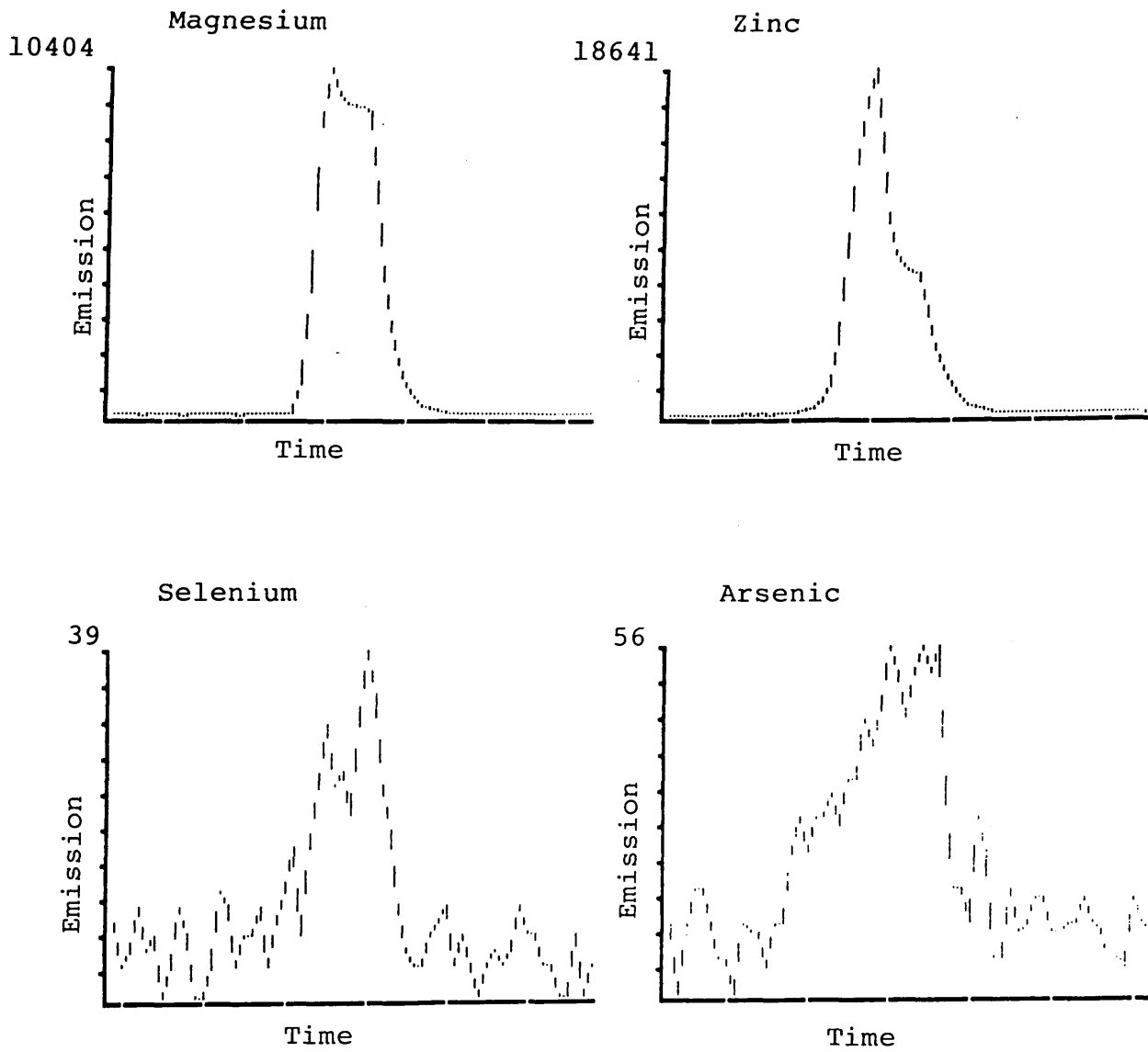


Figure 47. Emission Time Profiles During Melting of BAS 346. Maximum Emission Intensities are given on the Y-axis and the Time Axis is 60s long.

counts from a sample containing 15% cobalt is negligible. Another possibility is that the peak may be due to a spectral interference.

B. Chromium, Aluminium, Lead, Calcium(Figure 46)

All of these elements have similar traces. The signal maxima are significantly higher than the background level and they all begin to appear after a lag time of approximately 20s.

The volatilisation of chromium and aluminium is insignificant considering that the sample is 10% chromium and 5.5% aluminium. The losses of calcium and lead however are significant as they are present at the 37µg/g and 21µg/g levels.

C. Magnesium, Zinc, Selenium, Arsenic(Figure 47)

All of these elements are relatively volatile. The results suggest that significant volatilisation losses occur for all four elements.

Clearly, electrothermal melting has implications for the determination of volatile elements by laser ablation and would need to be avoided. But for refractory elements where no volatilisation losses occur, electrothermal melting provides a sample mass amenable to laser ablation avoiding the necessity for a microscope to ensure that the laser is correctly focused onto a sample piece.

4.3.4 Melting and Ablation Time Studies

The significance of pre-volatilisation losses in laser ablation was further investigated by performing time studies for both melting and laser ablation of the same samples. This involved the creation of time study programs using ninety 1s integrations, resulting in a time study of 90s duration.

Several chips of BAS 346 were placed into a sample cup which in turn was positioned in the graphite crucible inside the ablation chamber. The chamber

was turned on-line in preparation for the time study.

The heating sequence was initiated coincidentally with the time study and the laser was fired after 60s had elapsed. Under these conditions any signal produced during the melting process would appear alongside any signal produced by laser ablation in the same time study. The heating sequence described above was used.

This experiment was conducted on two samples. The first being melted and ablated by a single shot in the long pulse mode, the second being melted and ablated by a single shot in the Q-switched mode. The other laser operating conditions were as previously described.

4.3.4.1 Results

As with the previous section the time studies have been sub-divided into three categories dependent on the relative volatilities of the elements of interest.

Figures 48-50 show the time studies produced after long pulsed laser operation and figures 51-53 after Q-switched laser operation. The data shows the significance of losses during the melting process and allows comparison of laser operating modes.

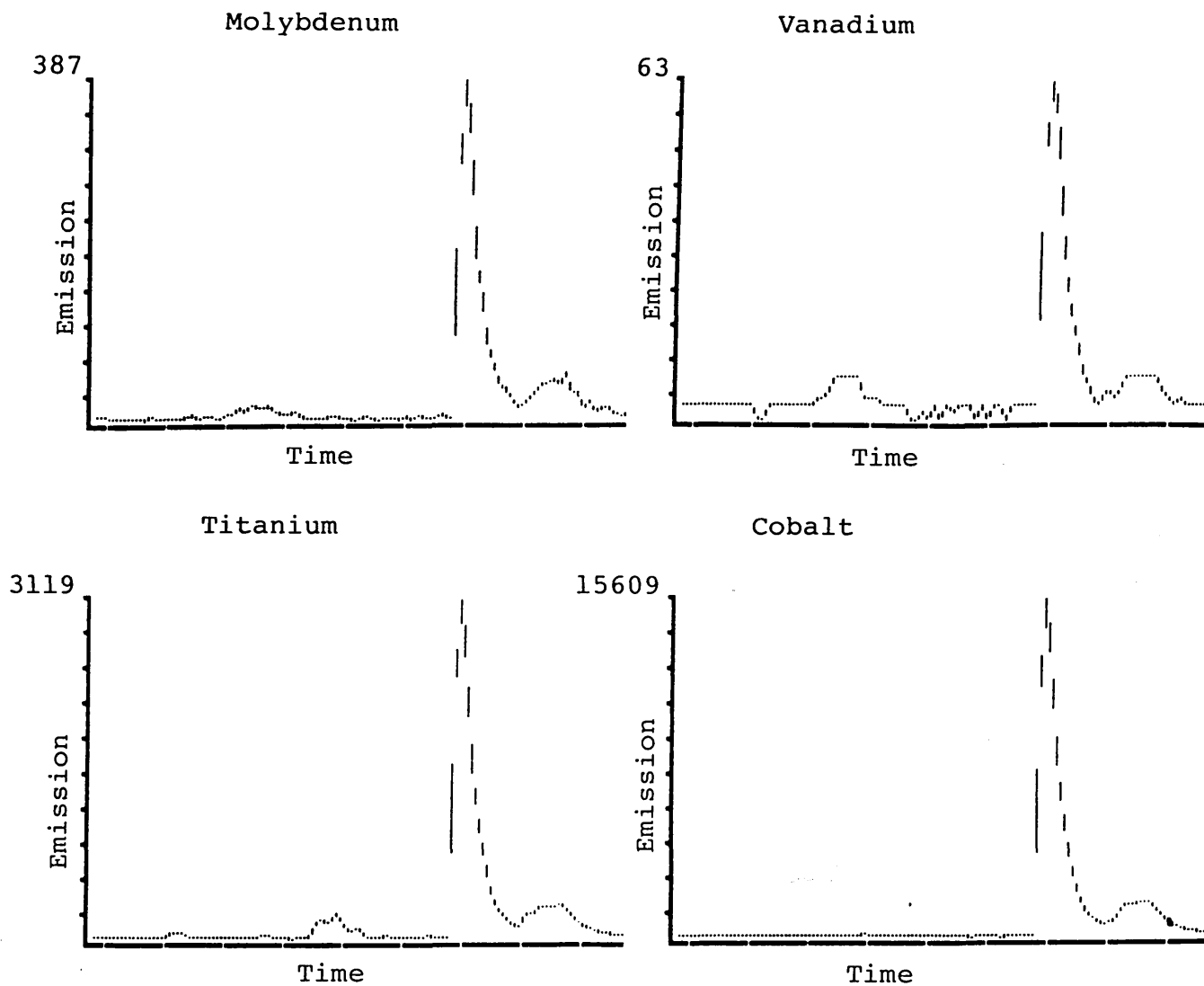


Figure 48. Emission Time Profiles During Melting and Laser Ablation of BAS 346 using a Single Long Pulsed Shot. The Time Axis is 90s Long and Maximum Emission Intensities are given on the Y-axis.

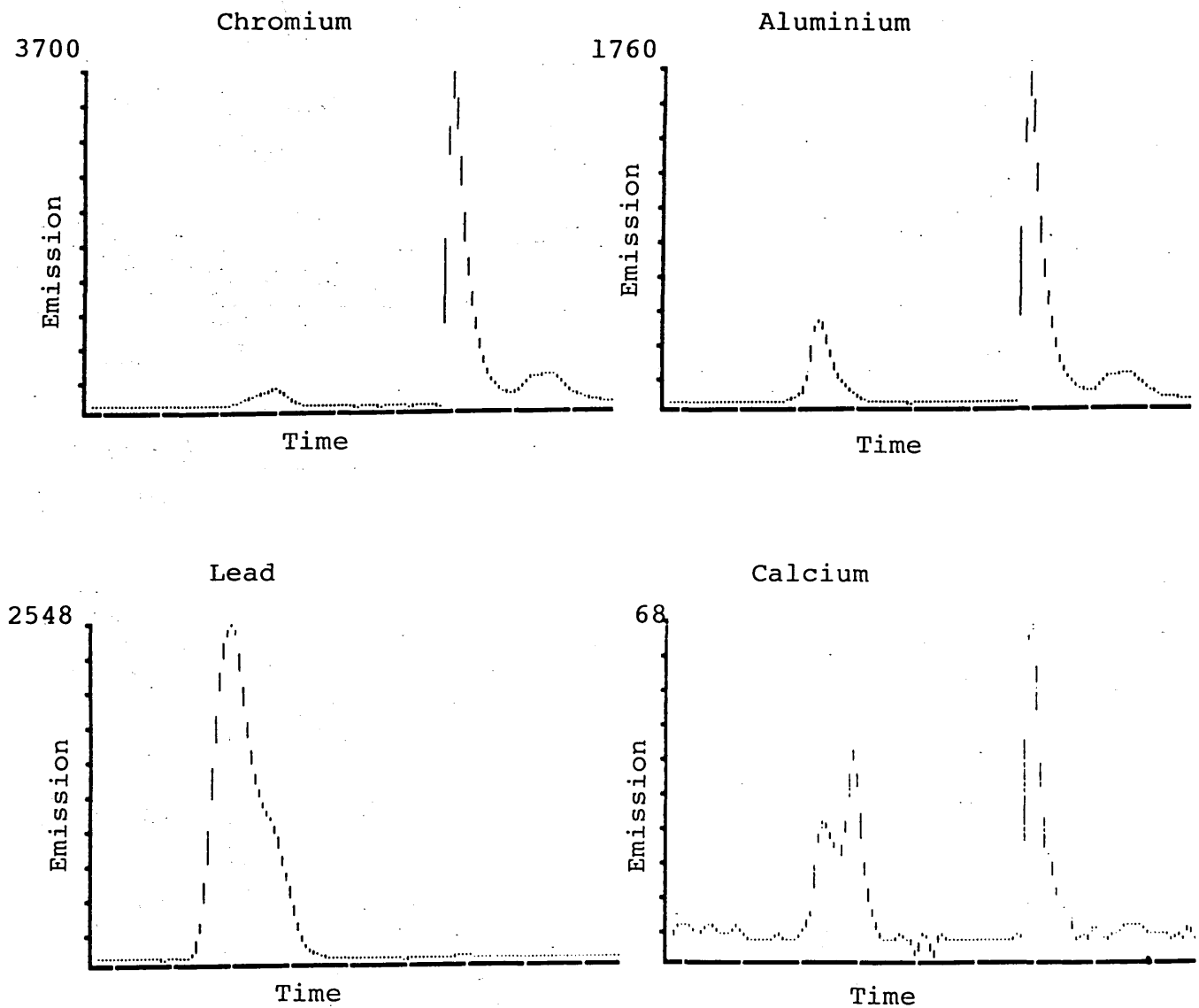


Figure 49. Emission Time Profiles During Melting and Laser Ablation of BAS 346 using a Single Long Pulsed Shot. The Time Axis is 90s Long and Maximum Emission Intensities are given on the Y-axis.

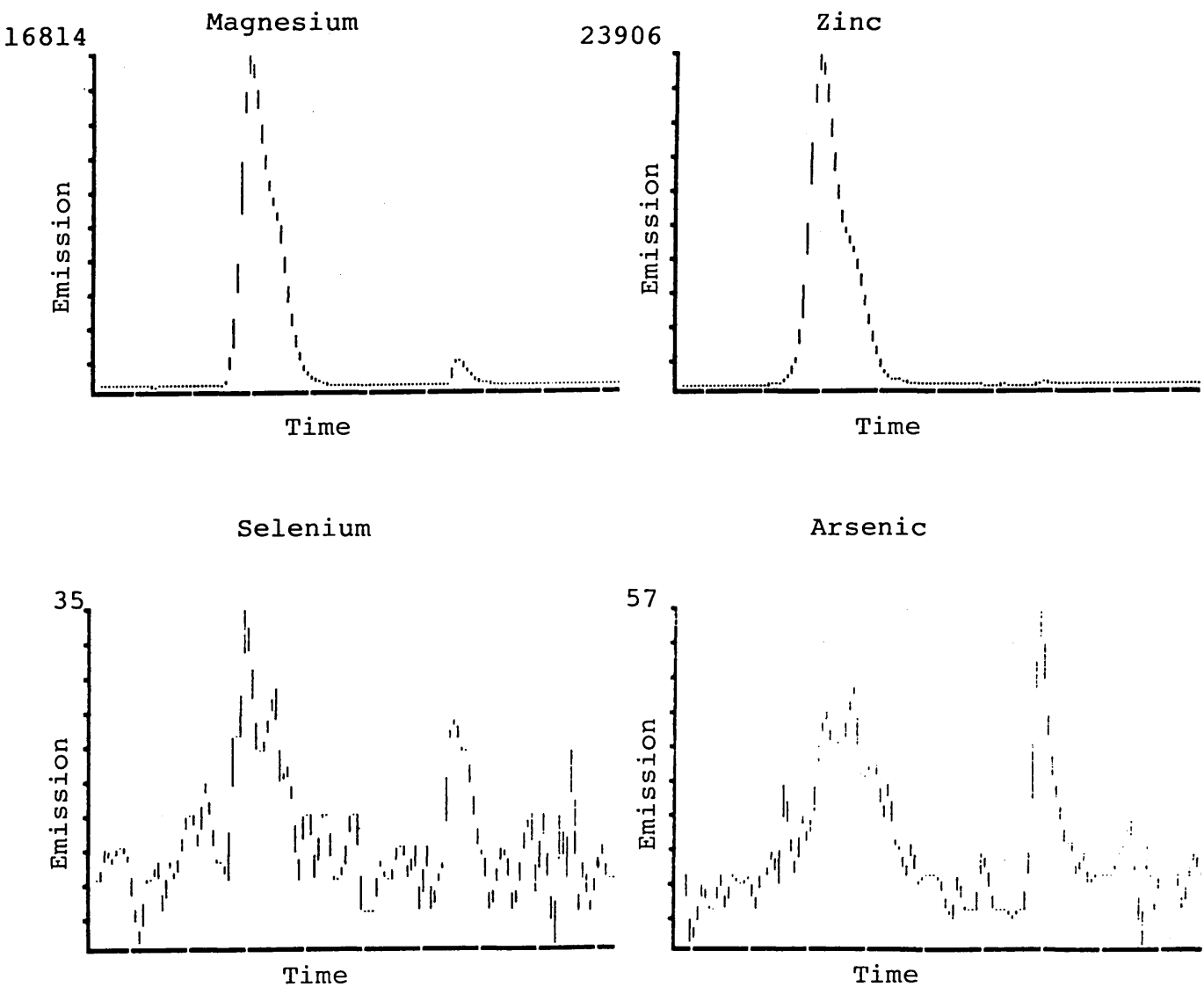


Figure 50. Emission Time Profiles During Melting and Laser Ablation of BAS 346 using a Single Long Pulsed Shot. The Time Axis is 90s Long and Maximum Emission Intensities are given on the Y-axis.

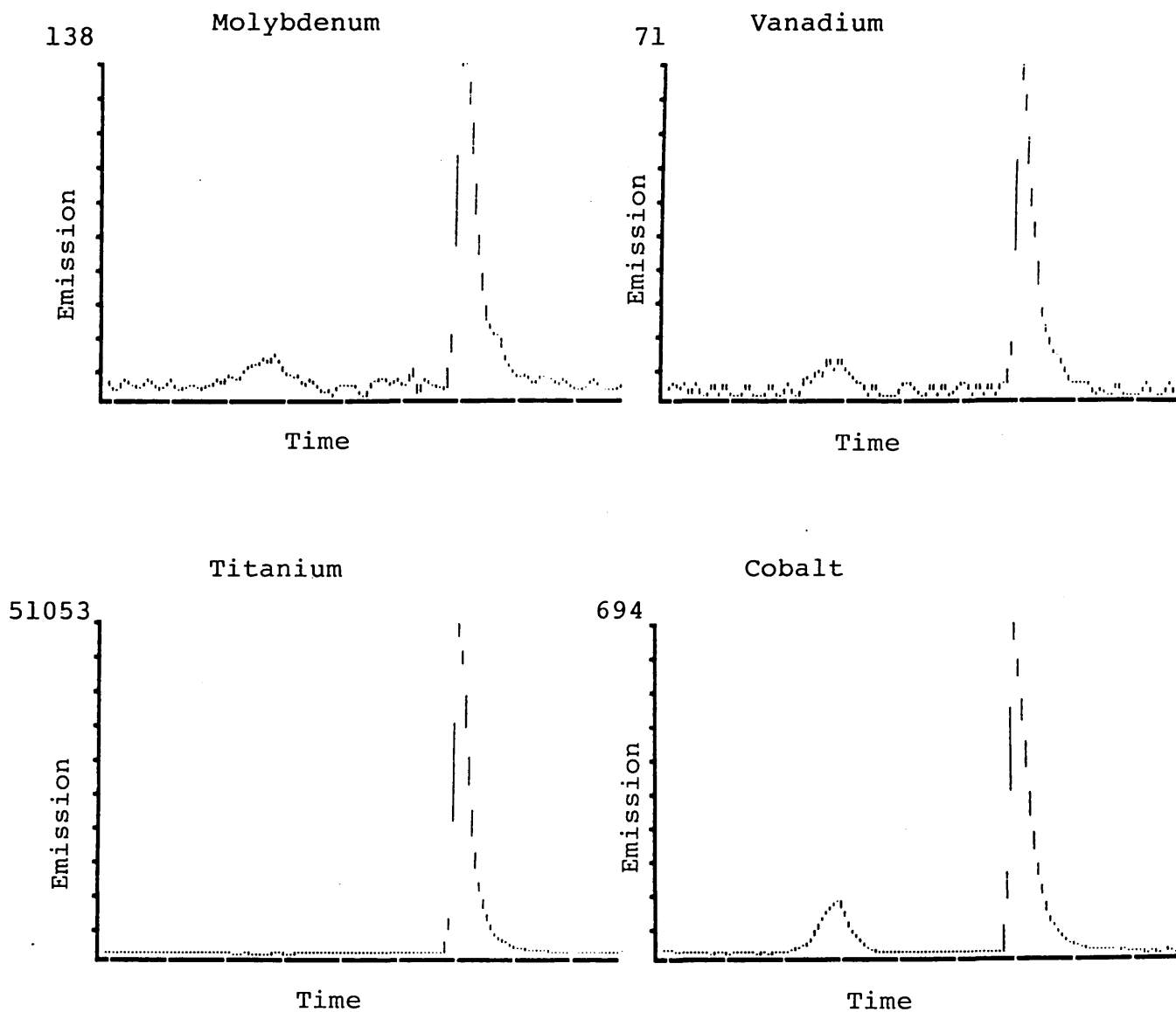


Figure 51. Emission Time Profiles During Melting and Laser Ablation of BAS 346 using a Single Q-Switched Shot. The Time Axis is 90s Long and Maximum Emission Intensities are given on the Y-axis.

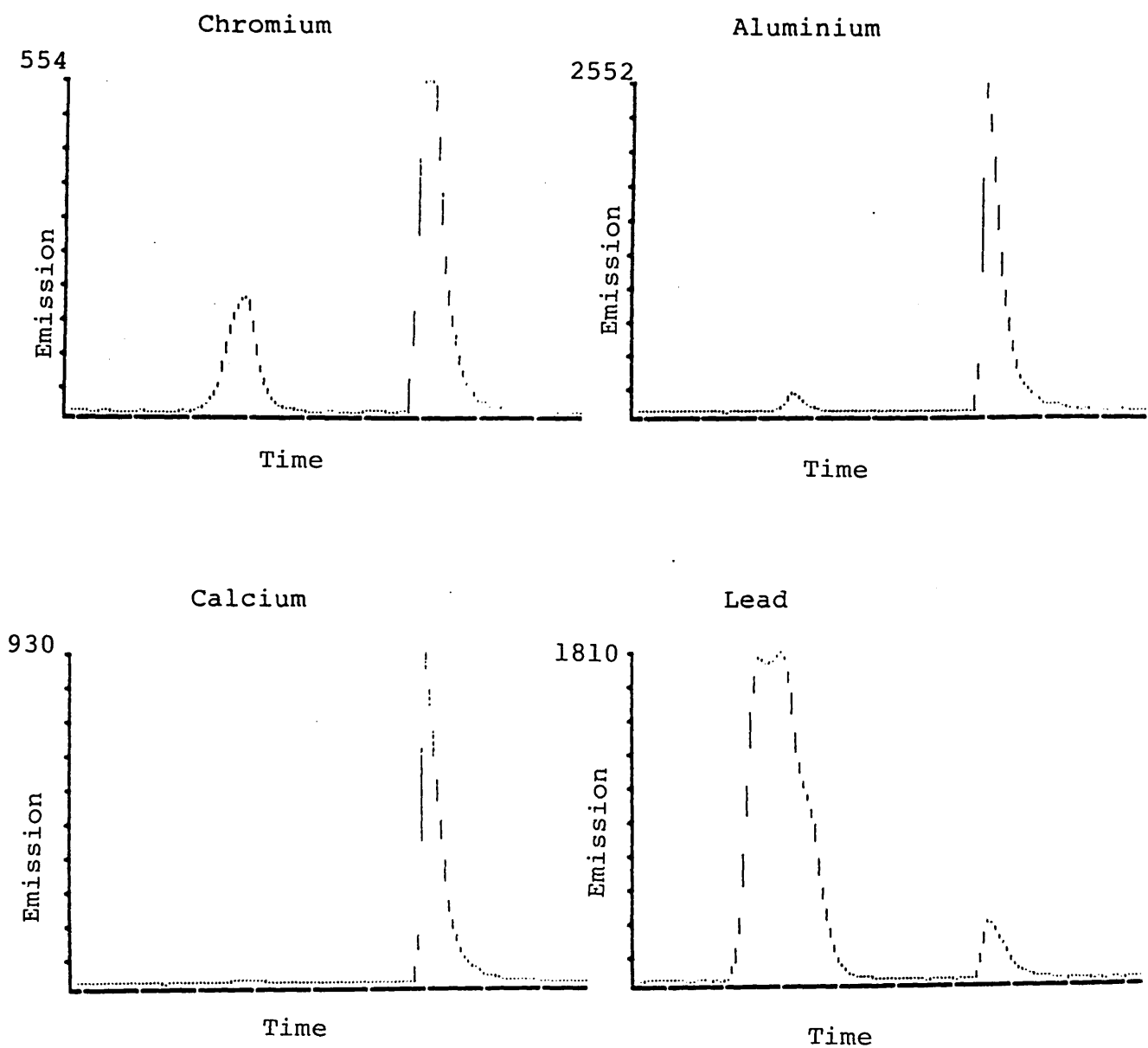


Figure 52. Emission Time Profiles During Melting and Laser Ablation of BAS 346 using a Single Q-Switched Shot. The Time Axis is 90s Long and Maximum Emission Intensities are given on the Y-axis.

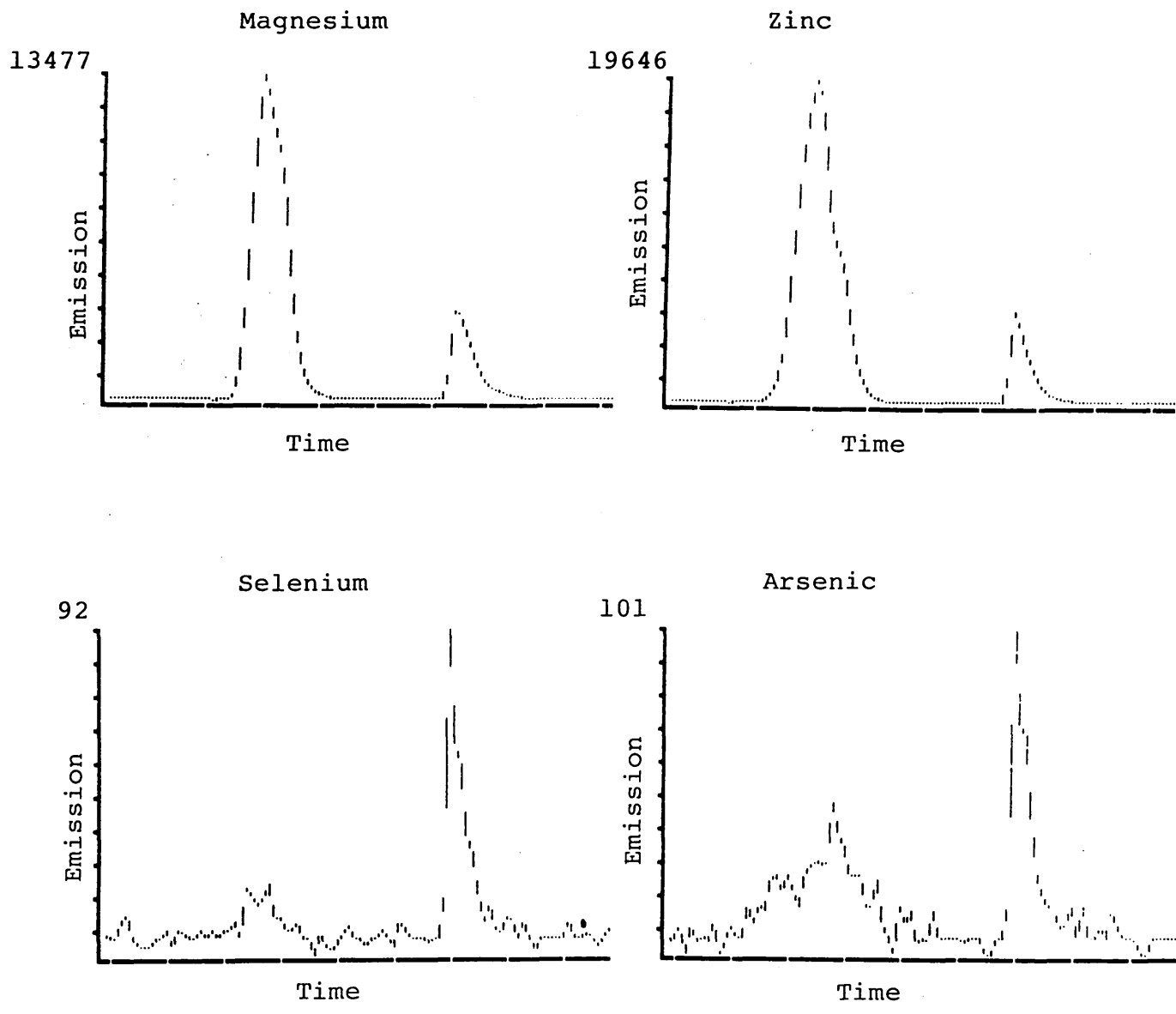


Figure 53. Emission Time Profiles During Melting and Laser Ablation of BAS 346 using a Single Q-Switched Shot. The Time Axis is 90s Long and Maximum Emission Intensities are given on the Y-axis.

The maximum emission intensities produced by laser ablation are given below in table 19.

Element	Emission Intensity (Counts)	
	Long Pulsed	Q-switched
Mo	387	138
V	63	71
Ti	3119	51053
Co	15609	694
Cr	3700	554
Al	1760	2552
Pb	-	360
Ca	68	930
Mg	1678	4035
Zn	-	6085
Se	-	92
As	57	101

Table 19. Maximum Emission Intensity Data for both Modes of Laser Operation.

4.3.4.2 Discussion

The x-axis of the time studies is the time axis and runs from 0 to 90s. Any signal produced during the melting sequence would be expected at approximately 25s while that produced by laser ablation would be expected at about 60s. The time studies may now be considered in more detail.

A. Molybdenum, Vanadium, Titanium, Cobalt.

The results for these elements confirm that analyte losses during the melting sequence are relatively small. Furthermore, they suggest that for refractory elements such as those listed, laser ablation is more likely to produce useful analytical signals than electrothermal vaporisation for the ICP in the existing instrumental configuration.

It is apparent that best analytical sensitivity by laser ablation for each element is dependent upon the mode of laser operation. Molybdenum and cobalt show improved sensitivity by long pulsed operation, Q-switched operation is preferred for titanium while the emission signals for vanadium are similar in both modes of operation.

From these results it may be speculated that the preferred mode of laser operation is a function of analyte distribution within the sample. Molybdenum and cobalt are thought to predominate in the bulk of the sample below the surface. Titanium, however, is thought to accumulate on the surface during melting and vanadium appears to be distributed evenly. As long pulsed operation bores relatively deeply into the sample, it is preferred for molybdenum and cobalt. Q-switched operation vaporises only the surface of the sample and is consequently the mode of choice for titanium.

The melting sequence is thought to affect the distribution of elements within the sample. A process similar to fractional distillation may occur, resulting in more volatile elements migrating to the sample surface. Volatile elements present in high concentrations are likely to undergo this process to a lesser degree and will still be present in the bulk of the sample at high concentrations. Consequently, in this case, the long pulsed mode of operation may be more appropriate.

B. Chromium, Aluminium, Lead, Calcium.

Analyte losses during the melting sequence were significant, particularly for lead.

Long pulsed operation is preferred for chromium. It is a relatively predominant element in the sample (10%) and ablation of the sample bulk produces more intense emission than ablation of the sample surface as achieved by Q-switched operation.

Melting losses of aluminium are comparable

to chromium, but this element appears to concentrate at the sample surface resulting in larger emission signals after ablation in the Q-switched mode.

Melting losses of lead are so severe that measurement by laser ablation is inappropriate. Thus, signals produced by laser ablation are very small.

Calcium is a little unusual in that some of the element is lost during melting and the remainder appears to accumulate on the sample surface. Hence Q-switched laser operation produces intense emission signals.

C. Magnesium, Zinc, Selenium, Arsenic

Melting losses for this group of elements are most significant. Consequently, measurement by laser ablation is considered inappropriate.

This study revealed one other interesting characteristic. The emission signals produced by long pulsed laser operation consist of an initial sharp peak followed by a second, broader peak approximately one tenth of the earlier peaks intensity. Such double peaks are frequently encountered in various atomic spectroscopic techniques and usually signify the existence of two analyte species.

4.3.5 The Effect of Ablation Period

The significance of the ablation period was studied by monitoring the emission time profiles of several of the more refractory elements in BAS 346.

Several turnings of BAS 346 were placed into a sample cup and subjected to the melting sequence. Once the sample had cooled, the time study was initiated and 5s later the laser was fired. A time study of 60s duration was employed, using sixty 1s integrations. Consequently, the time studies show only the signals produced by laser ablation.

Ablation periods of 1 shot, 5s and 10s were used in both long pulsed and Q-switched mode resulting

in a total of six time studies. Each was performed on a new sample of BAS 346.

4.3.5.1 Results

The time studies for molybdenum, vanadium, titanium, cobalt, chromium, aluminium and calcium are shown in figures 54-60. Each element may now be considered in more detail.

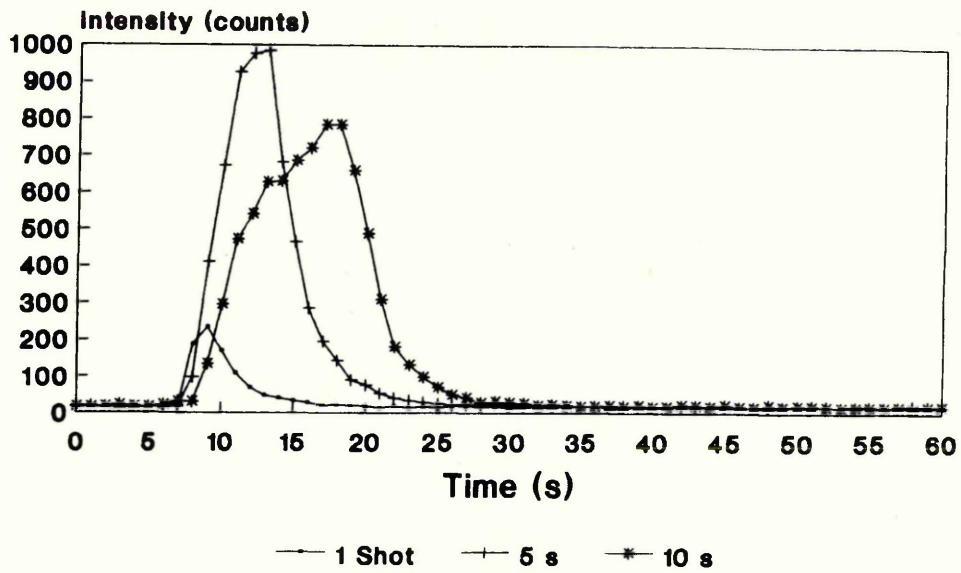
4.3.5.2 Discussion

A. Molybdenum

In the long pulsed mode of laser operation the greatest emission signal intensity is achieved using a single laser shot. Increasing the ablation period produces more melting at the point of interaction of the laser with the sample. As explained earlier, this results in the ejection of more, relatively large molten particles which do not reach the ICP and hence do not contribute to an emission signal. Indeed, an ablation period of 10s suppresses the emission signal completely.

In Q-switched mode, a single shot produces a signal of intensity similar to that produced by a single long pulsed shot. Increasing the ablation period to 5s increases the analytical sensitivity by a factor of four. An ablation period of 10s produces an emission signal of somewhat lower peak height. This is thought to be due to some interaction of the laser with the laser induced plume and/or the material being vaporised from the sample surface, which reduces the amount of analyte reaching the ICP. This explanation is supported by the rise time of the three signals. Increasing the ablation period produces a longer rise time (ie the leading edge of the peak has a lower gradient) which implies that the interaction of the laser with the plume in some way hinders or restricts the transport of the analyte to the ICP.

MOLYBDENUM Q-Switched Operation



MOLYBDENUM Long Pulsed Operation

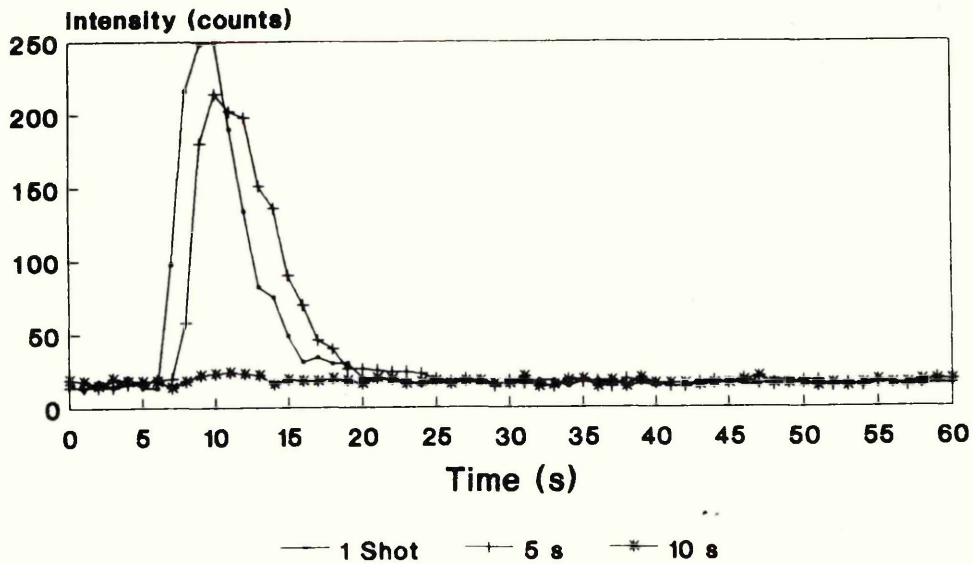
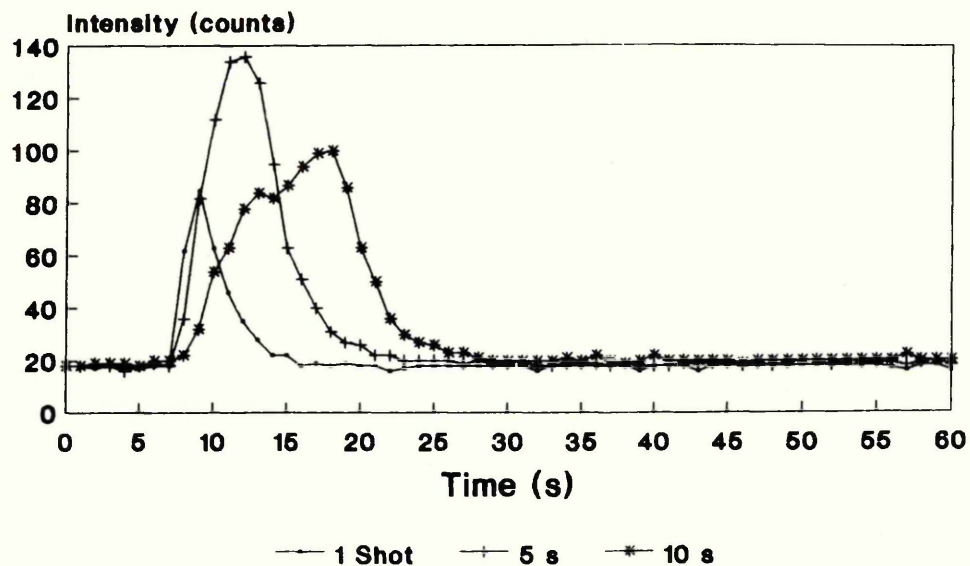


Figure 54. Effect of Ablation Period on Emission Intensity for Molybdenum in BAS 346.

VANADIUM

Q-Switched Operation



VANADIUM

Long Pulsed Operation

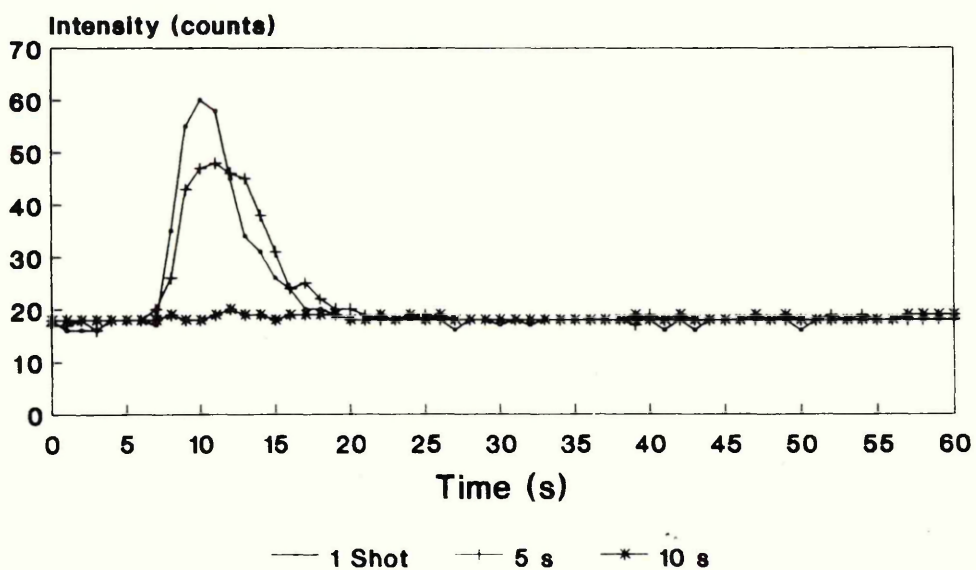
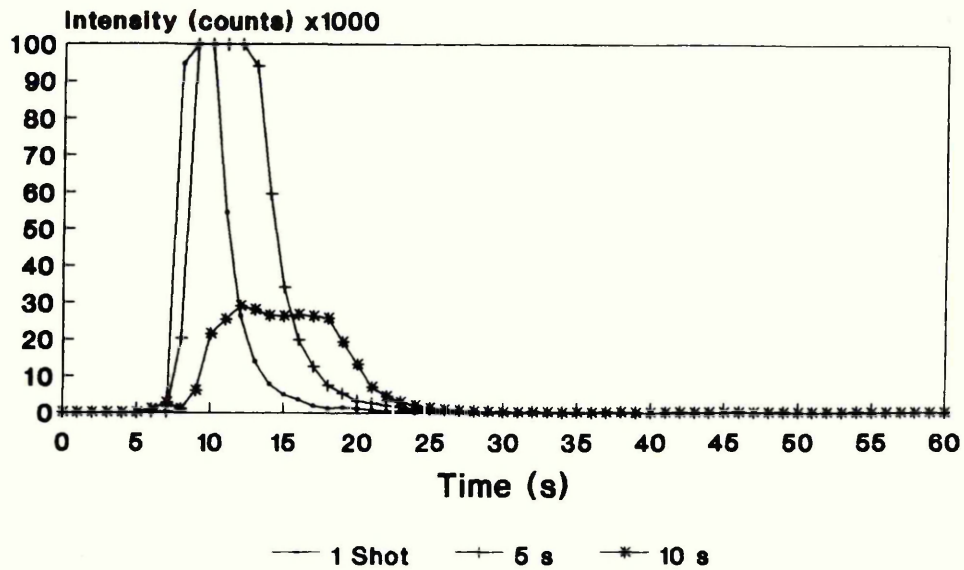


Figure 55. Effect of Ablation Period on Emission Intensity for Vanadium in BAS 346.

TITANIUM

Q-Switched Operation



TITANIUM

Long Pulsed Operation

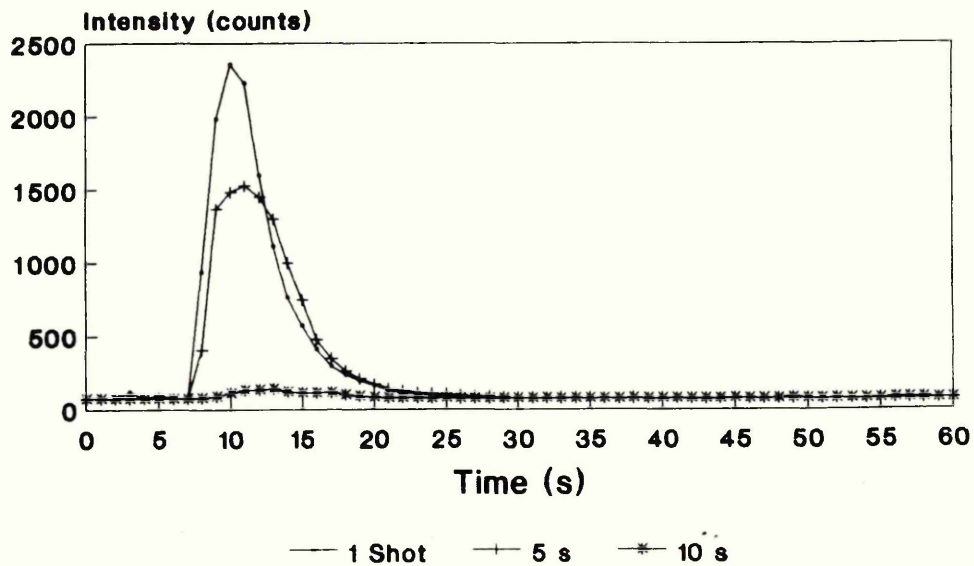
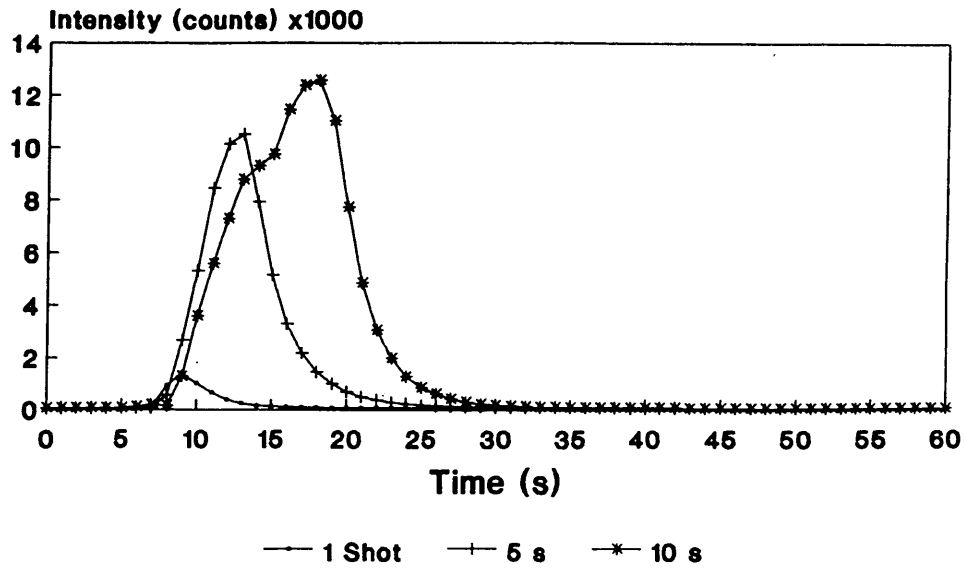


Figure 56. Effect of Ablation Period on Emission Intensity for Titanium in BAS 346.

COBALT

Q-Switched Operation



COBALT

Long Pulsed Operation

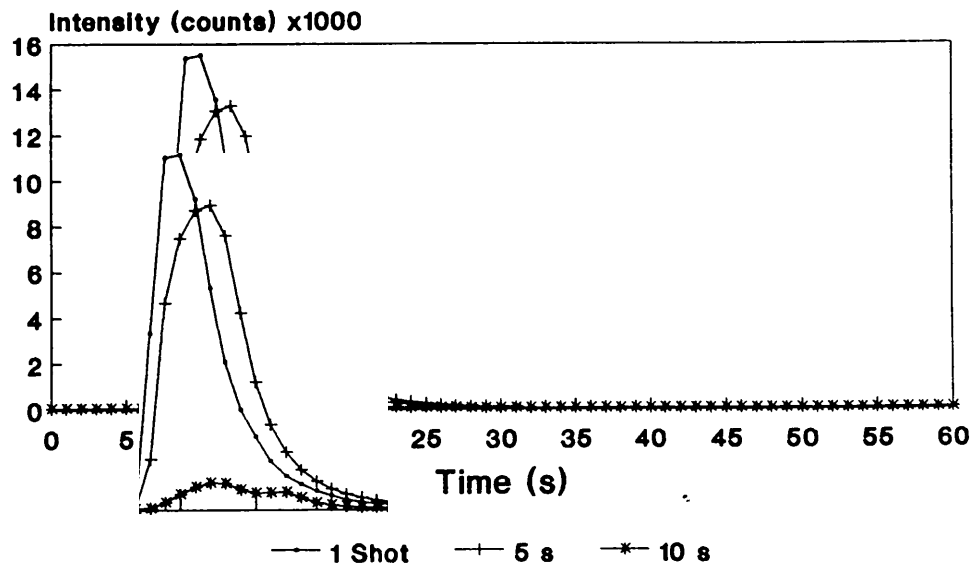
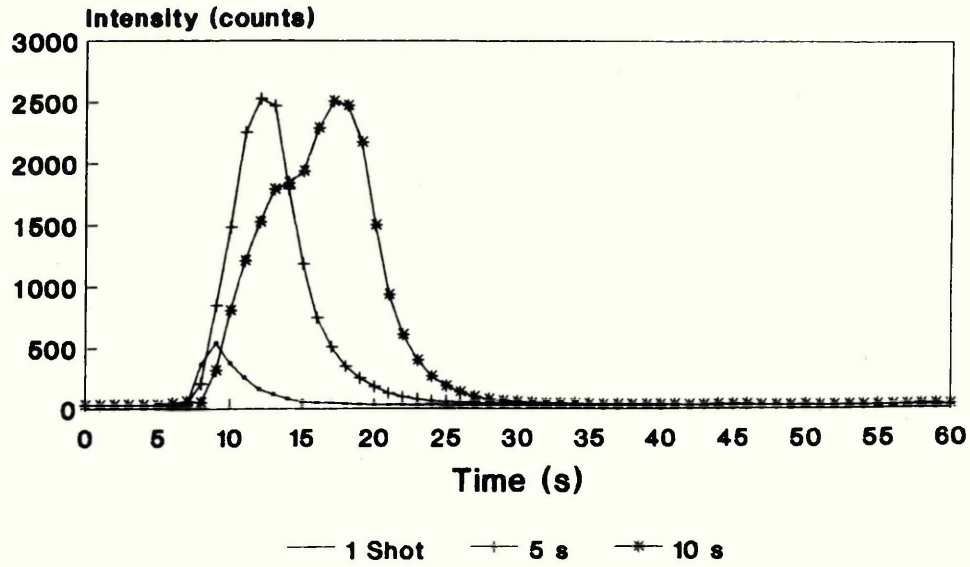


Figure 57. Effect of Ablation Period on Emission Intensity for Cobalt in BAS 346.

CHROMIUM

Q-Switched Operation



CHROMIUM

Long Pulsed Operation

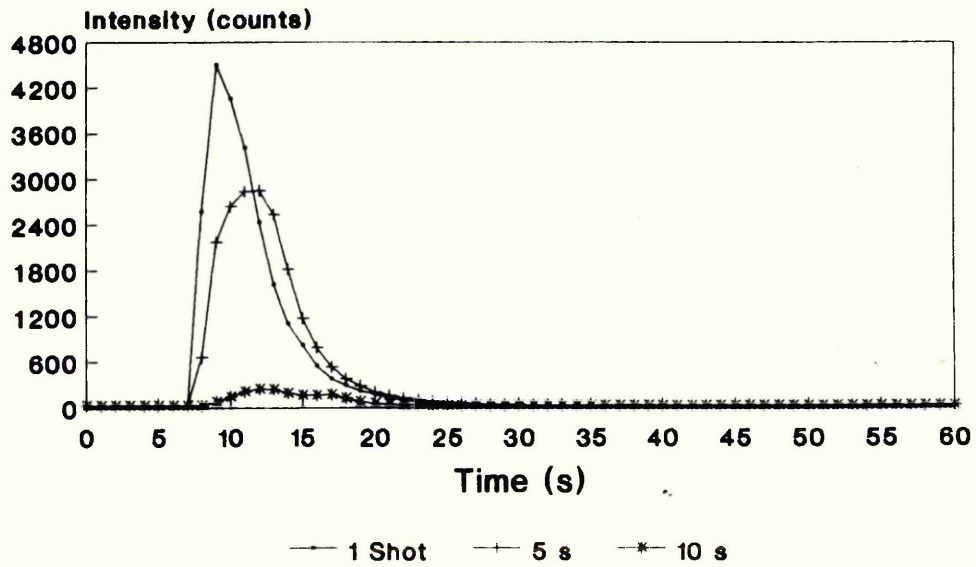
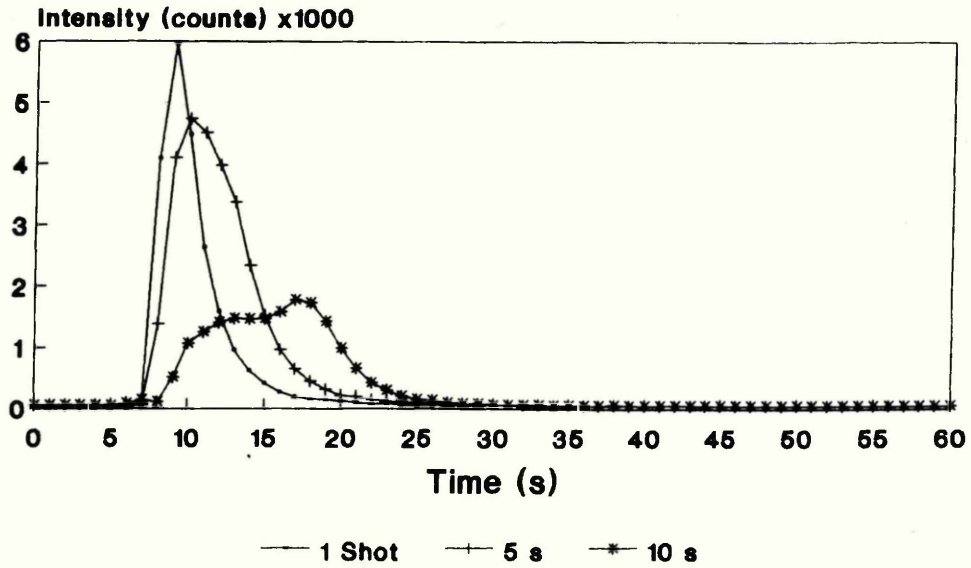


Figure 58. Effect of Ablation Period on Emission Intensity for Chromium in BAS 346.

ALUMINIUM

Q-Switched Operation



ALUMINIUM

Long Pulsed Operation

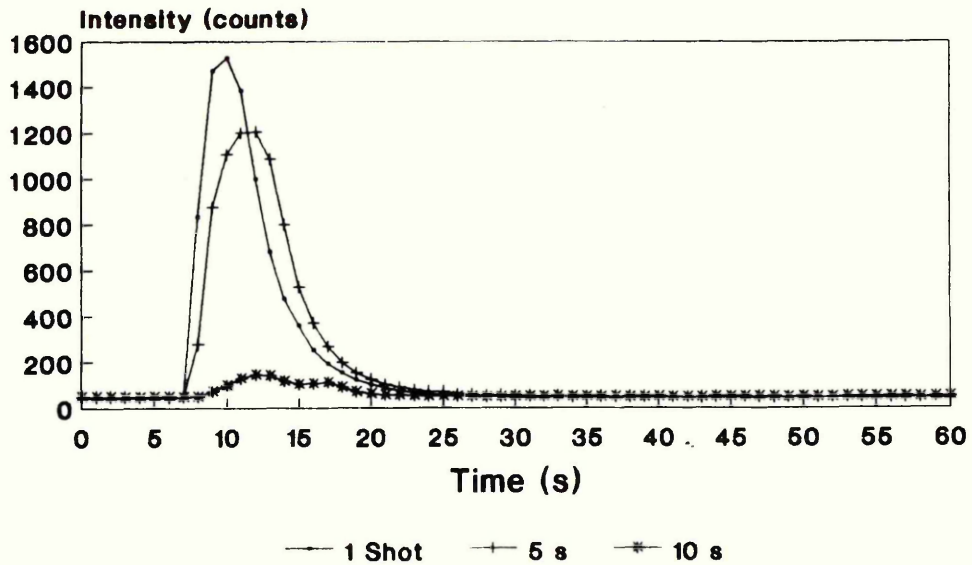
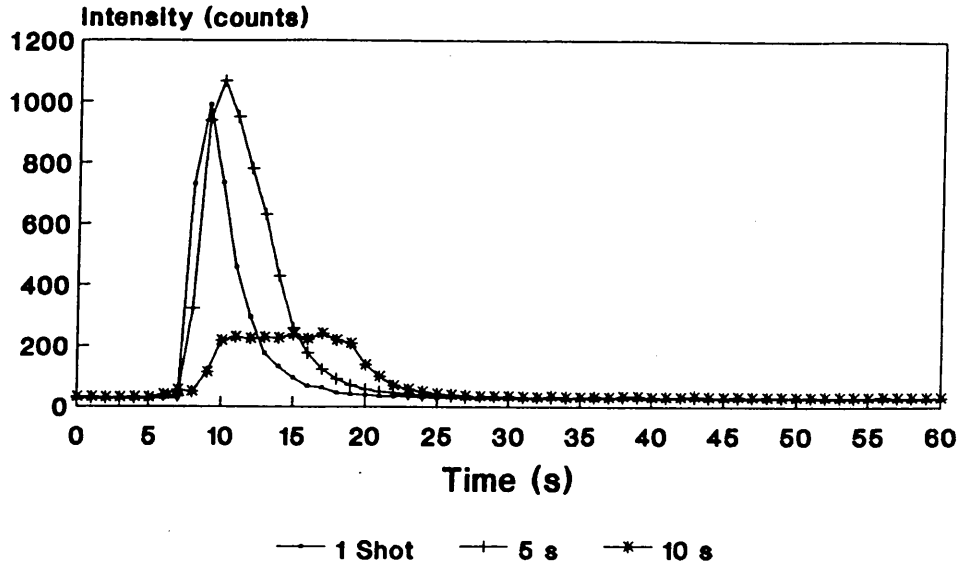


Figure 59. Effect of Ablation Period on Emission Intensity for Aluminium in BAS 346.

CALCIUM

Q-Switched Operation



CALCIUM

Long Pulsed Operation

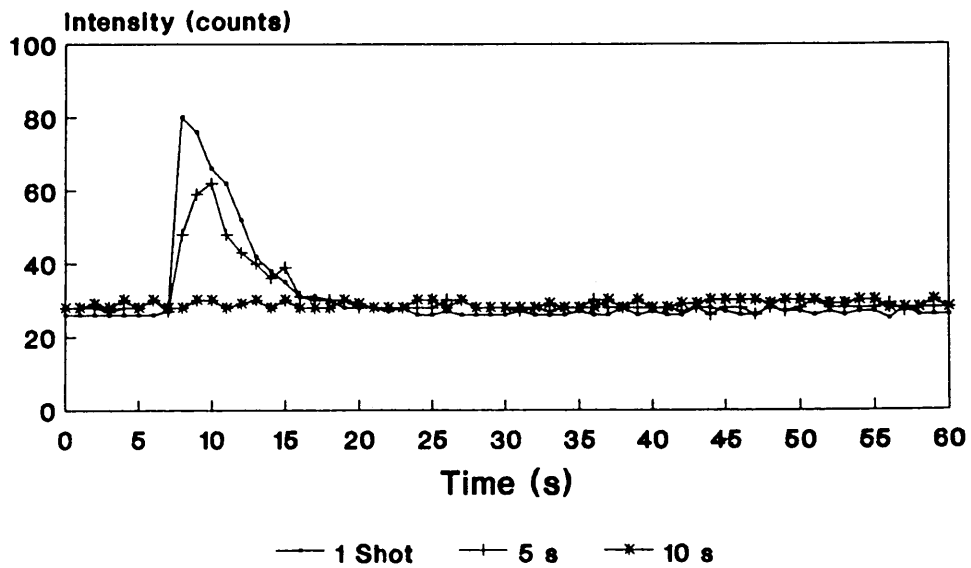


Figure 60. Effect of Ablation Period on Emission Intensity for Calcium in BAS 346.

B. Vanadium

Vanadium behaves very similarly to molybdenum. Emission signal intensities decrease with increasing ablation period in the long pulsed mode. In Q-switched mode, a 5s ablation period produces maximum sensitivity.

C. Titanium

As with the previous two elements, increasing ablation period in the long pulsed mode decreases emission intensity. A 10s ablation period suppresses the signal completely.

Similarly, maximum emission intensity is achieved using a 5s period of Q-switched laser radiation. Titanium was found to be so sensitive that a single Q-switched shot and 5s repetitive Q-switched firing are sufficient to overload the detection system. This is believed to be a consequence of this element undergoing a type of fractional distillation which results in it accumulating on the sample surface.

D. Cobalt

The observed trend in the long pulsed mode of operation is as previously reported. A 10s period of ablation does produce a peak which was not the case with the previous elements. This is thought to be a consequence of the relatively high concentration of cobalt (15%).

In Q-switched operation 5s and 10s periods produce emission peaks of similar intensity. The interaction of laser with the laser induced plume appears to be less significant in this case which is also believed to be a consequence of a relatively high analyte concentration.

E. Chromium

The results for chromium are very similar to those for cobalt, again as a consequence of relatively high analyte concentration (10%).

F. Aluminium

In the long pulsed mode of operation, aluminium demonstrates the same trend as the elements discussed above. In Q-switched mode the trend is slightly different. A single Q-switched shot produces the most intense emission signal and increasing the ablation period decreases the emission intensity.

This result suggests that aluminium is less susceptible to the restriction to analyte transport which occurs as a consequence of the lasers interaction with the laser induced plume above the sample surface.

The most intense emission signals are achieved in Q-switched mode of operation reflecting the likelihood of aluminium preconcentrating at the sample surface.

G. Calcium

As with all the elements examined, in the long pulsed mode, increasing ablation period decreases emission intensity. Also, the signals produced in the long pulse mode are relatively small for calcium.

Maximum sensitivity is achieved in Q-switched mode. The signals produced by a single shot and a 5s ablation period were very similar in intensity. This reflects the relatively high concentration of calcium at the sample surface.

For maximum analytical sensitivities molybdenum, vanadium, titanium and calcium require a 5s ablation period in the Q-switched mode; cobalt and chromium require a single long pulsed shot and aluminium a single Q-switched shot.

This study revealed several important observations and trends which are original and have not been reported in the literature. It was found that the analytical sensitivity of this technique is dependent on the analyte, its concentration and volatility, mode of laser operation and duration of laser operation along with many other processes which occur as a consequence of the interaction

of laser radiation with matter, but are little understood.

4.3.6 Analyte Erosion

Experiments in this section were performed on one sample.

A sample cup was loaded with BAS 346, placed in the ablation chamber and subjected to the melting sequence. Once the sample had cooled a series of 10 laser shots were fired and the emission signal maxima were noted. This experiment was performed on one sample in long pulsed mode while monitoring emission intensity from cobalt and chromium. A second sample was used for the Q-switched mode, monitoring emission intensity from calcium and aluminium. The elements were selected as most appropriate for each mode of laser operation. All laser shots were single shots fired at maximum lamp energy.

4.3.6.1 Results

The results are shown graphically in figures 61 (Long Pulsed operation) and 62 (Q-switched operation).

4.3.6.2 Discussion

The results for both modes of laser operation and the four elements examined are essentially the same.

Ablating the same point over and over again produces emission signals which become progressively smaller. Clearly, with each laser shot the concentration of analyte remaining decreases at the point of laser interaction which results in a subsequently smaller signal.

This is one of the limiting factors of such microsampling techniques as laser and spark ablation. It may be somewhat alleviated by scanning the laser across the sample to ablate a different area of the

sample with each laser shot. Such a facility was not available on the equipment described.

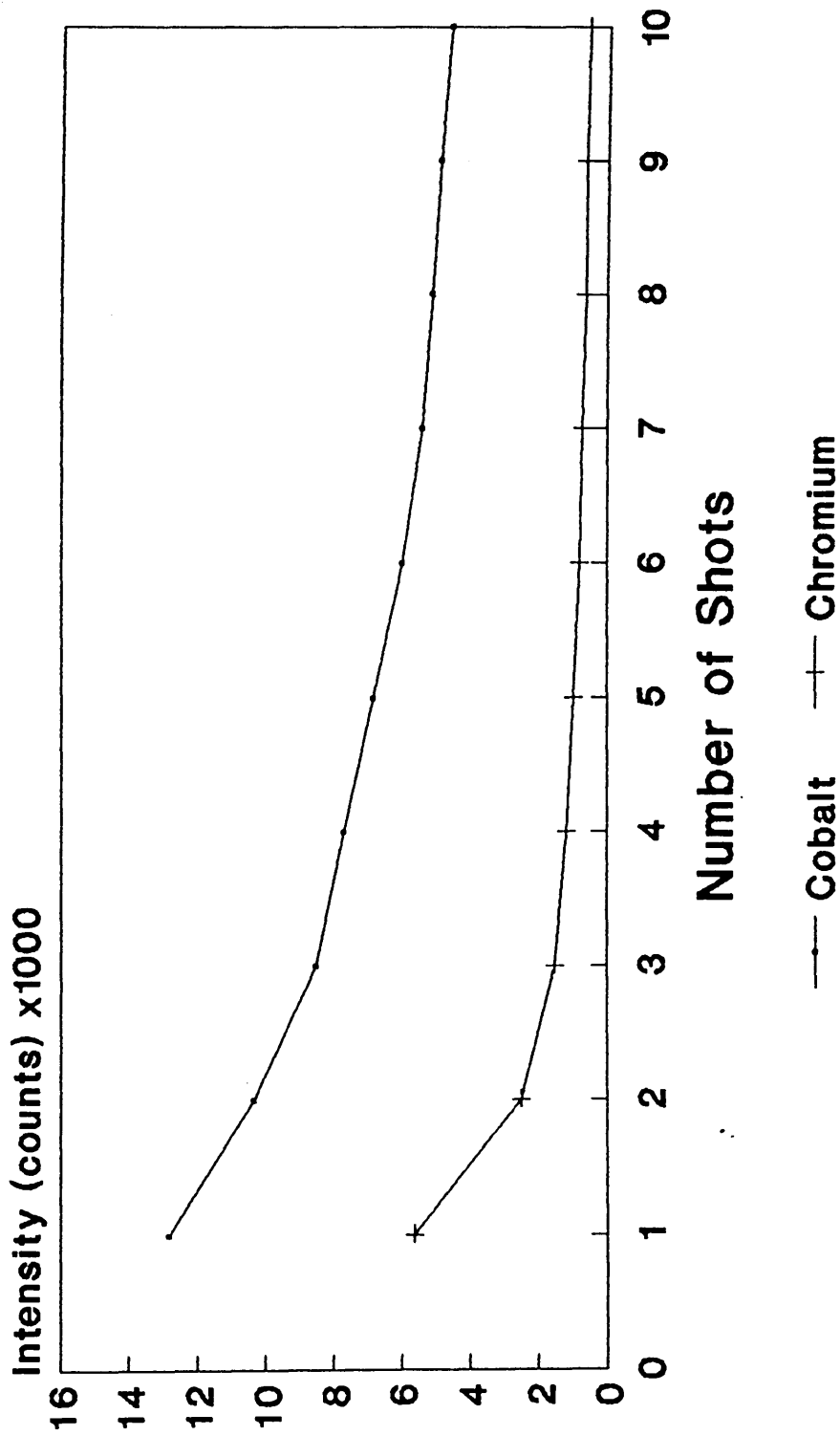


Figure 61. Reduction in Analyte Emission Intensity as a Consequence of Repeated Laser Shots at One Sample. Data for Cobalt and Chromium in BAS 346 is Shown for Long Pulsed Laser Operation.

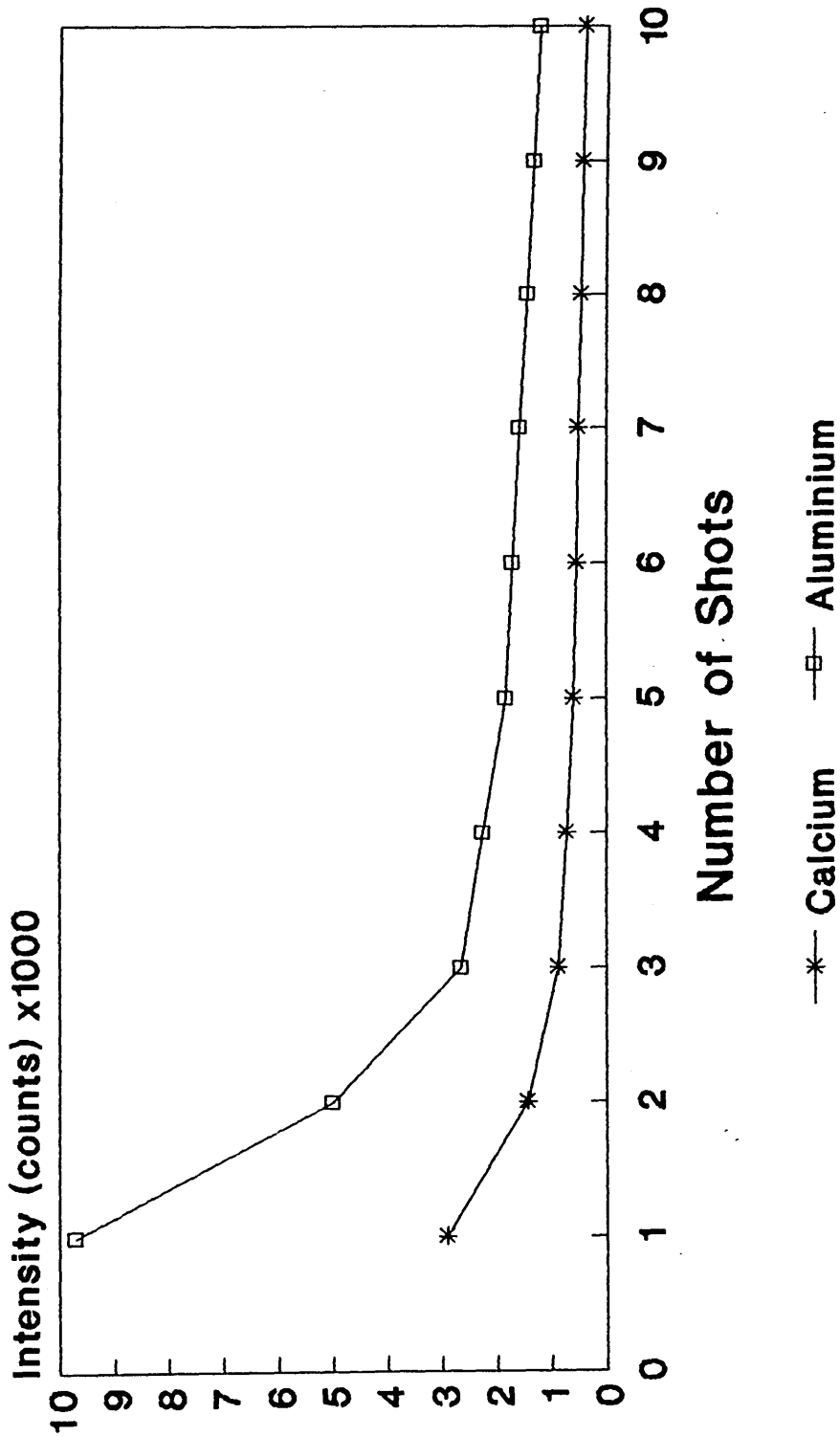


Figure 62. Reduction in Analyte Emission Intensity as a Consequence of Repeated Laser Shots at One Sample. Data for Calcium and Aluminium in BAS 346 is Shown for Q-Switched Laser Operation.

4.4 CONCLUDING REMARKS

It has been demonstrated that the instrumental configuration developed is suitable for laser ablation studies. The significance of laser operating conditions, particularly focusing, ablation period and mode of operation are now understood. The best analytical sensitivity for a given analyte is dependent upon all the above and the effects of the electrothermal melting stage.

Electrothermal melting makes the determination of volatile elements inappropriate but it is well suited to the measurement of refractory elements whose losses during melting are minimal.

As with other microsampling methods precision is relatively poor when compared with solutions nebulisation. This is due to heterogeneity of samples and may be improved by slewing the laser across the sample surface. This problem was clearly demonstrated during the analyte erosion experiments.

Due to insufficient time, the electrothermal melting capabilities of the ablation chamber were not fully evaluated. The ablation of molten samples is of interest and may be applicable to the steels industry. Laser ablation ICP may be a technique suitable for on-line monitoring of molten steels. This area requires further work.

CHAPTER FIVE

STUDIES WITH POLYMERIC SAMPLES

5.0 INTRODUCTION

The analysis of paints and polymers by ICP spectrometry presents a significant problem due to the sample preparation procedures that are required. For metallurgical samples, wet digestion with nitric acid or aqua regia will usually suffice. Sample preparation of paints and polymers can take more than 24 hours as it usually involves lengthy dry ashing procedures followed by wet ashing of the inorganic residue [136, 137]. Consequently, the ability to analyse such materials directly offers a much quicker and greatly simplified method of analysis. Hence, the interest in laser ablation ICP as a possible way of achieving rapid and direct analysis of such materials.

The following work utilises the simultaneous multi-element capability of the Jarrell Ash ICAP 9000 spectrometer using operating conditions as described earlier.

The most appropriate way to present paint samples to the laser has been examined, along with key laser operating parameters. Precision data for analysis of liquid and dried paint has been obtained and qualitative studies on a range of paints performed.

Polymeric samples were briefly examined and an interesting application arose from this work. Part of this work has been published elsewhere [138] and represented the first publication to consider laser ablation ICP studies on paints and polymer materials.

A term previously unused in this thesis will be introduced in this chapter. "Sputtering" has been used in this work, and by other workers in the field of laser ablation, to describe the controlled process of material removal from a sample surface due to laser action. The ablation of liquids is to be considered in chapters five and six where, under certain operating conditions, large volumes of sample were displaced from sample cups and collided with the walls of the ablation chamber. This relatively uncontrolled process will be described as "spattering".

5.1 PREPARATION OF PAINT SAMPLES

Two methods of sample preparation were investigated. The first utilised the electrothermal heating facility of the laser ablation chamber to produce dry, thin films of paint. The second method involved direct ablation of the liquid paint samples.

5.1.1 Electrothermal Drying

The experimental procedures adopted to produce emission signals were identical to those used for measurements with metallurgical samples. The ICP was initiated and the spectrometer profiled. The nebuliser gas was turned off and the carrier gas turned on ready for laser ablation measurements.

A 20 microlitre aliquot of an oil based, brilliant white, liquid gloss paint was pipetted into a graphite sample cup. The cup was placed into the graphite crucible inside the laser ablation chamber and the lid of the chamber replaced. The ablation chamber was switched on-line to the ICP and a heating sequence just sufficient to dry the paint sample was initiated. On the Perkin Elmer HGA - 2100, a power setting of zero, a time of 90s and a ramp of 10s were used. Hence the temperature was increased from ambient to that corresponding to a power setting of zero over a period of 10s and then maintained for a further 80s. The maximum temperature achieved was thought to be approximately 100°C as the heating sequence was sufficient to dry a 20 microlitre

aliquot of deionised water. Once this sequence had ended, the sample was ready for laser ablation measurements.

The first parameter investigated was that of laser operating mode. Samples were prepared as described above and then ablated using either long pulsed or Q-switched laser shots at 10Hz and maximum lamp energy.

Time studies were used to monitor emission during the sample drying phase and during laser ablation. These studies showed that volatile elements such as arsenic, selenium and mercury were all lost during the sample drying phase. Furthermore, emission signals produced by laser ablation in the Q-switched mode demonstrated far greater intensity than those produced by long pulsed mode. Consequently, as with the metallurgical studies, Q-switched laser shots offered improved sensitivity when compared with long pulsed shots. However, repetitive firing on one sample revealed a progressive decline in signal intensity with each laser shot. This analyte erosion, as observed with metallurgical samples, indicated that repetitive firings at one sample would exhibit poor precision.

The differences between dried and wet paint samples were then investigated.

5.1.2 Direct Measurement

As with electrothermal drying, a 20 microlitre aliquot of paint was placed into a graphite sample

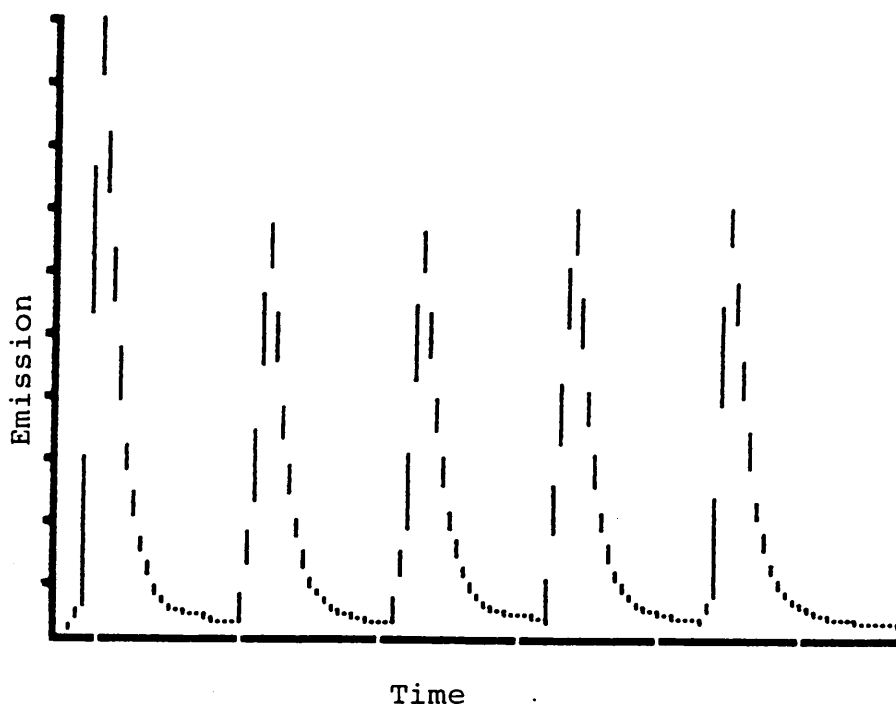
cup. This was then positioned inside the graphite crucible held within the laser ablation chamber. However, once the chamber lid was replaced and the chamber turned on-line with the ICP, the sample was ready for laser ablation measurements.

Again, a time study of 120s duration was used. To investigate the signals produced from wet paint, five Q-switched laser shots (10Hz, 70J) were fired at 22s intervals, thus producing five peaks in a single time study. Q-switched shots were used because the previous experiments suggested improved sensitivity when using the Q-switched mode.

Several of the elements examined showed good reproducibility between the five peaks produced. This experiment was extended to dried paint samples using electrothermal drying followed by five consecutive Q-switched laser shots. The results of this experiment were significantly different from those obtained when ablating wet paint.

Figures 63-65 show the time studies for aluminium, cobalt and zirconium respectively in both wet and dry paint samples. These results show clearly that wet paint samples offer significant improvements in reproducibility compared to dried paint samples.

3570



1871

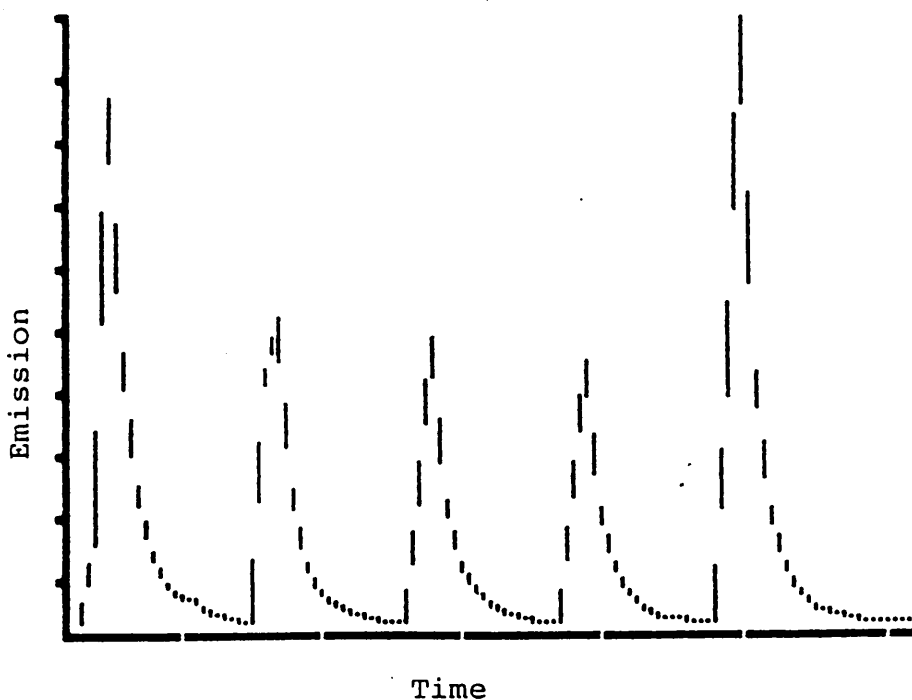


Figure 63. Effect of Replicate Laser Shots on Emission Time Profiles for Aluminium in Paint. Precision using Peak Height was 17.3% RSD for Wet Paint (upper diagram) and 34.8% RSD for Dry Paint (lower diagram). The Time Axis is 120s Long and Maximum Emission Intensities are given on the Y-axis.

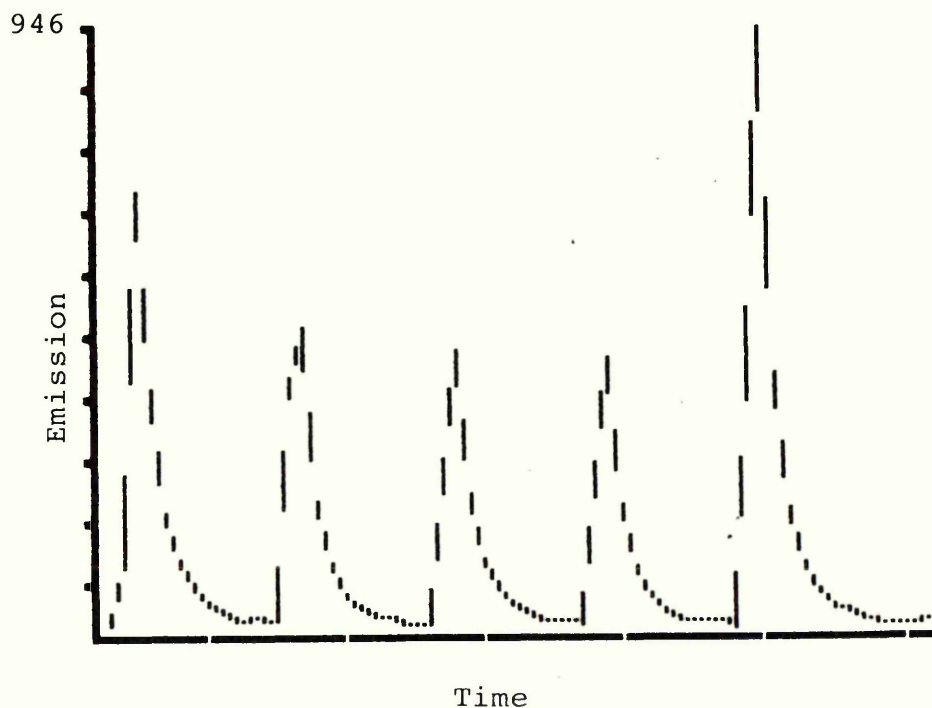
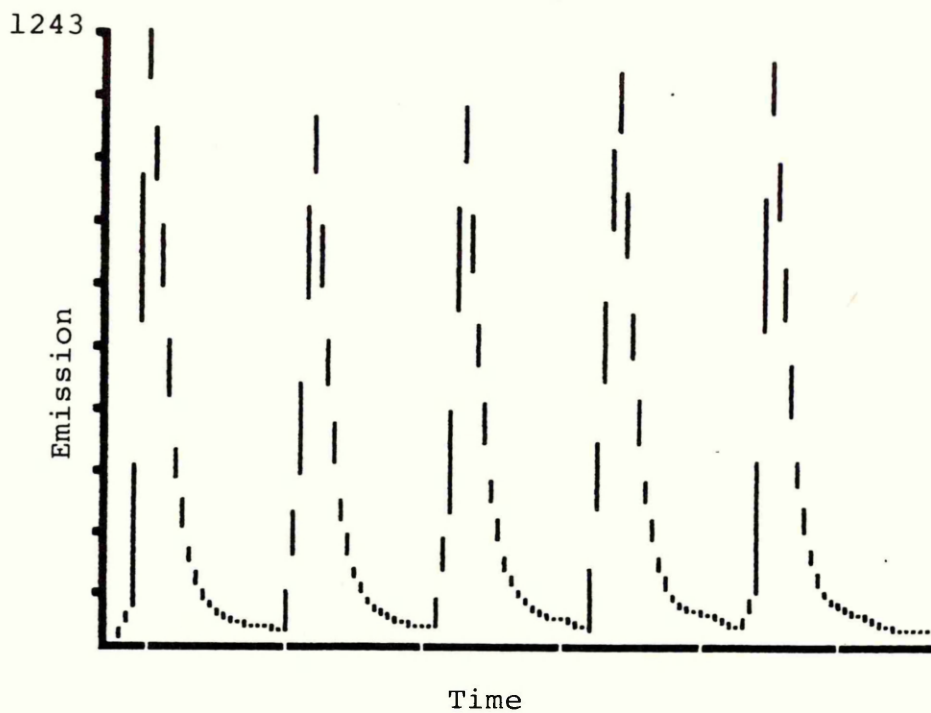
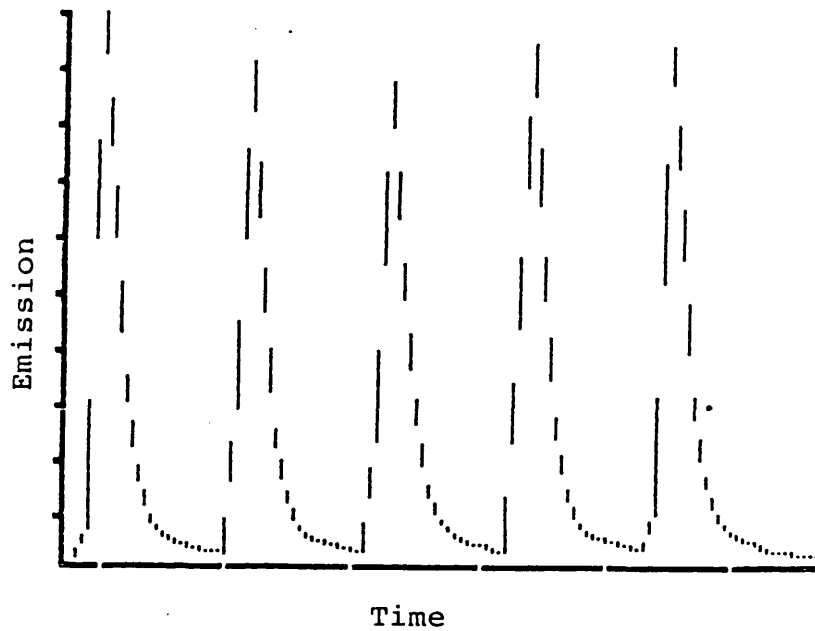


Figure 64. Effect of Replicate Laser Shots on Emission Time Profiles for Cobalt in Paint. Precision using Peak Height was 5.4% RSD for Wet Paint (upper diagram) and 33.5% RSD for Dry Paint (lower diagram). The Time Axis is 120s Long and Maximum Emission Intensities are given on the Y-axis.

1446



1135

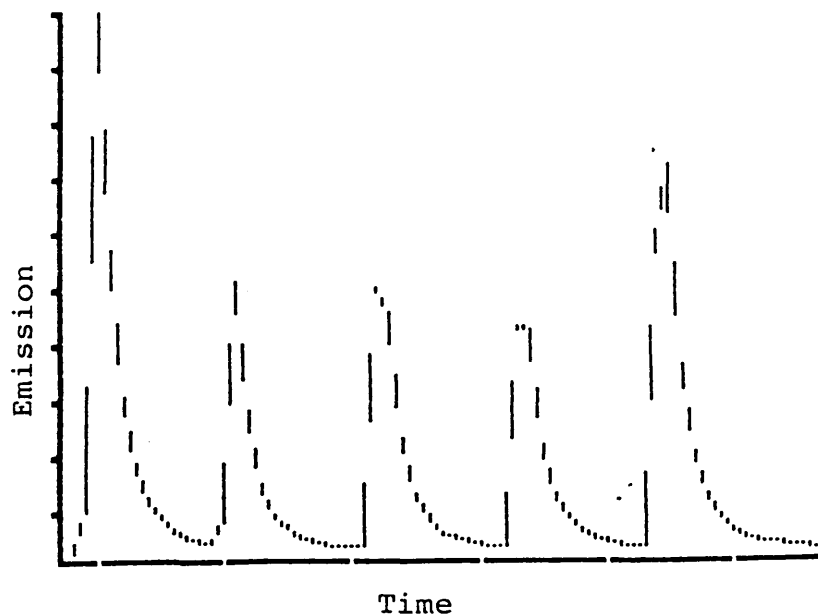


Figure 65. Effect of Replicate Laser Shots on Emission Time Profiles for Zirconium in Paint. Precision using Peak Height was 4% RSD for Wet Paint (upper diagram) and 33% RSD for Dry Paint (lower diagram). The Time Axis is 120s Long and Maximum Emission Intensities are given on the Y-axis.

5.1.3 Conclusions

The above experiments showed that Q-switched ablation of dried paint samples offered greater sensitivity than long pulsed ablation. Using wet paint samples reduces the analysis time since a heating sequence is not required, and improves the precision of repeat measurements. This improvement is due to a replenishment of the area of laser/sample interaction as a consequence of the fluidity of the sample. In the case of a dried paint film, the sample is eroded or modified with consecutive laser shots as this replenishment process does not occur.

Wet paint also provided greater homogeneity than dried films of paint. This in conjunction with the fluid nature and viscosity of wet paint resulted in the observed improvement in precision.

Closer examination of the time studies for dried paint showed that all three elements demonstrated very similar trends. This suggested that internal standardisation may improve precision.

The precision (%RSD) for aluminium and cobalt was determined using zirconium as internal standard. The Al/Zr and Co/Zr ratios were calculated for the five peaks and the resultant values used to determine the %RSD. In both cases the precision was improved from 35% to 17% RSD for aluminium and from 33% to 21% RSD for cobalt. Zirconium was selected as the internal standard because it was found to offer the most

significant improvement in precision. This implies that the three elements considered have similar transport and ablation characteristics under the experimental conditions described.

At this point it was decided to make all further measurements on wet paint due to the improved precision. But it still remained to be seen if Q-switched operation was more sensitive than long pulsed operation for wet paint samples. Consequently, time studies of 3 long pulsed and 3 Q-switched laser shots at wet paint were run. These were overlaid and are presented in figures 66-68 for aluminium, cobalt and zirconium respectively. It can be clearly seen that Q-switched operation produces emission signals of greater intensity by a factor of approximately two.

Although the above discussion considers only aluminium, cobalt and zirconium, these experiments provided useful qualitative data on many elements; signals equivalent to or slightly greater than the plasma background were measured for As, B, Mo, Se and Hg; emission signals for Al, Ba, Ca, Cd, Co, Cu, Fe, K, Mg, Mn, Na, Ni, Pb, Si, V, Zn and Zr were found to be significant and easily measureable; Ti was somewhat exceptional in that the emission signal was so intense that the detector became saturated. This result was expected since titanium dioxide is a white pigment used in the manufacture of brilliant white paint at relatively high percentage levels. It provides the

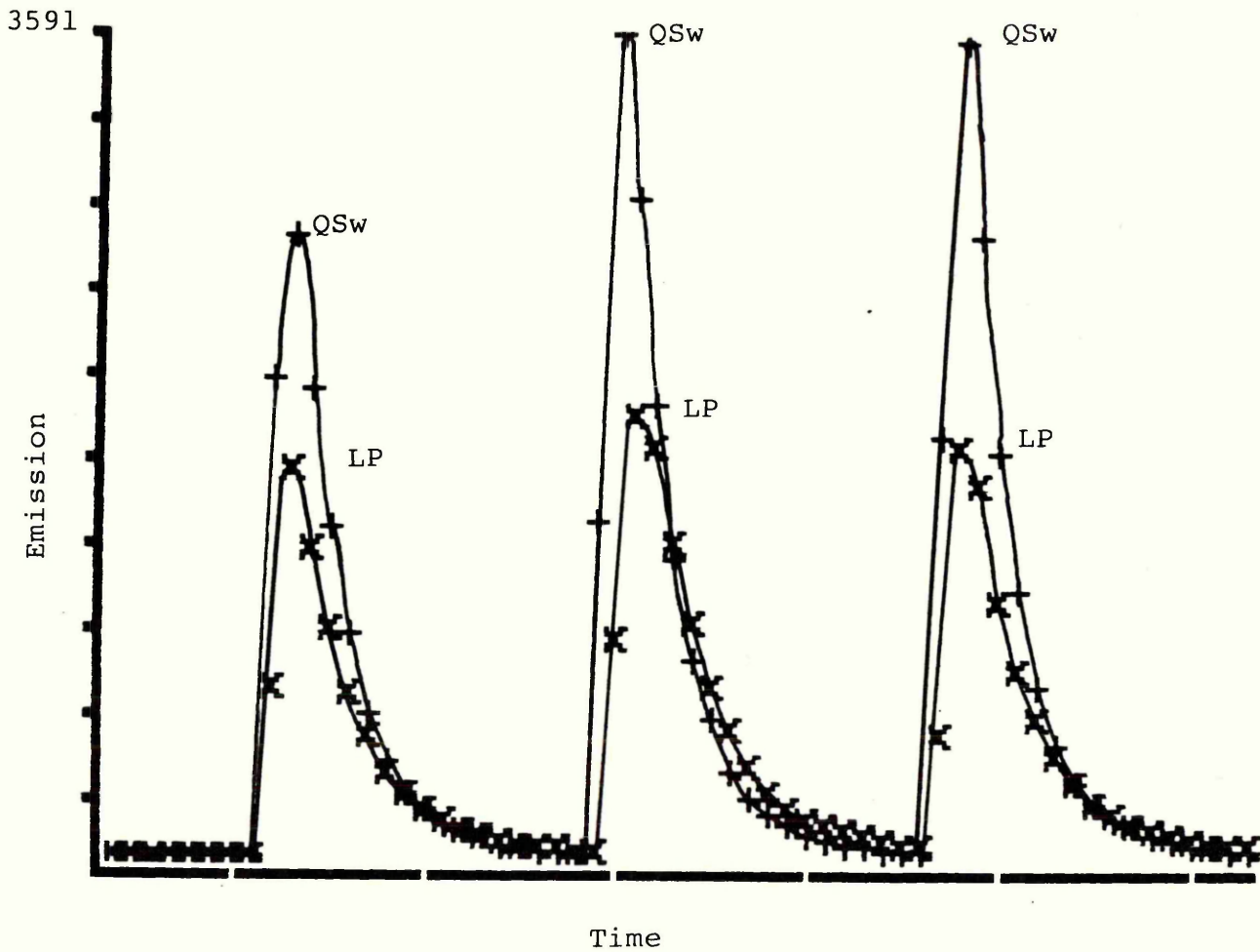


Figure 66. Emission Time Profiles for Aluminium During Laser Ablation of Wet Paint. The Diagram Shows Three Consecutive Peaks due to Single Q-Switched (QSw) and Long Pulsed (LP) Laser Shots. The Time Axis is 60s Long and the Maximum Emission Intensity is given on the Y-axis.

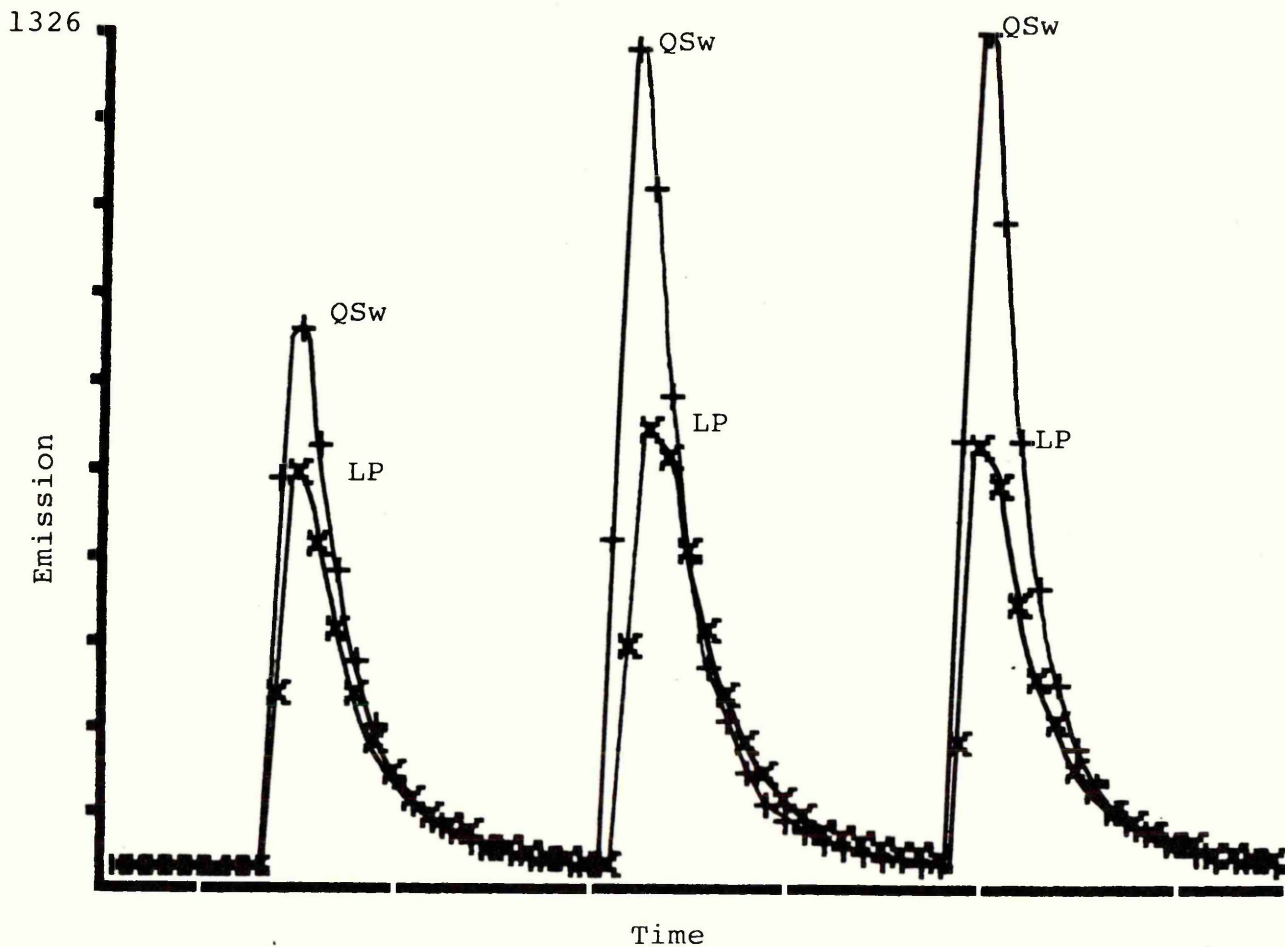


Figure 67. Emission Time Profiles for Cobalt During Laser Ablation of Wet Paint. The Diagram Shows Three Consecutive Peaks due to Single Q-Switched (QSw) and Long Pulsed (LP) Laser Shots. The Time Axis is 60s Long and the Maximum Emission Intensity is given on the Y-axis.

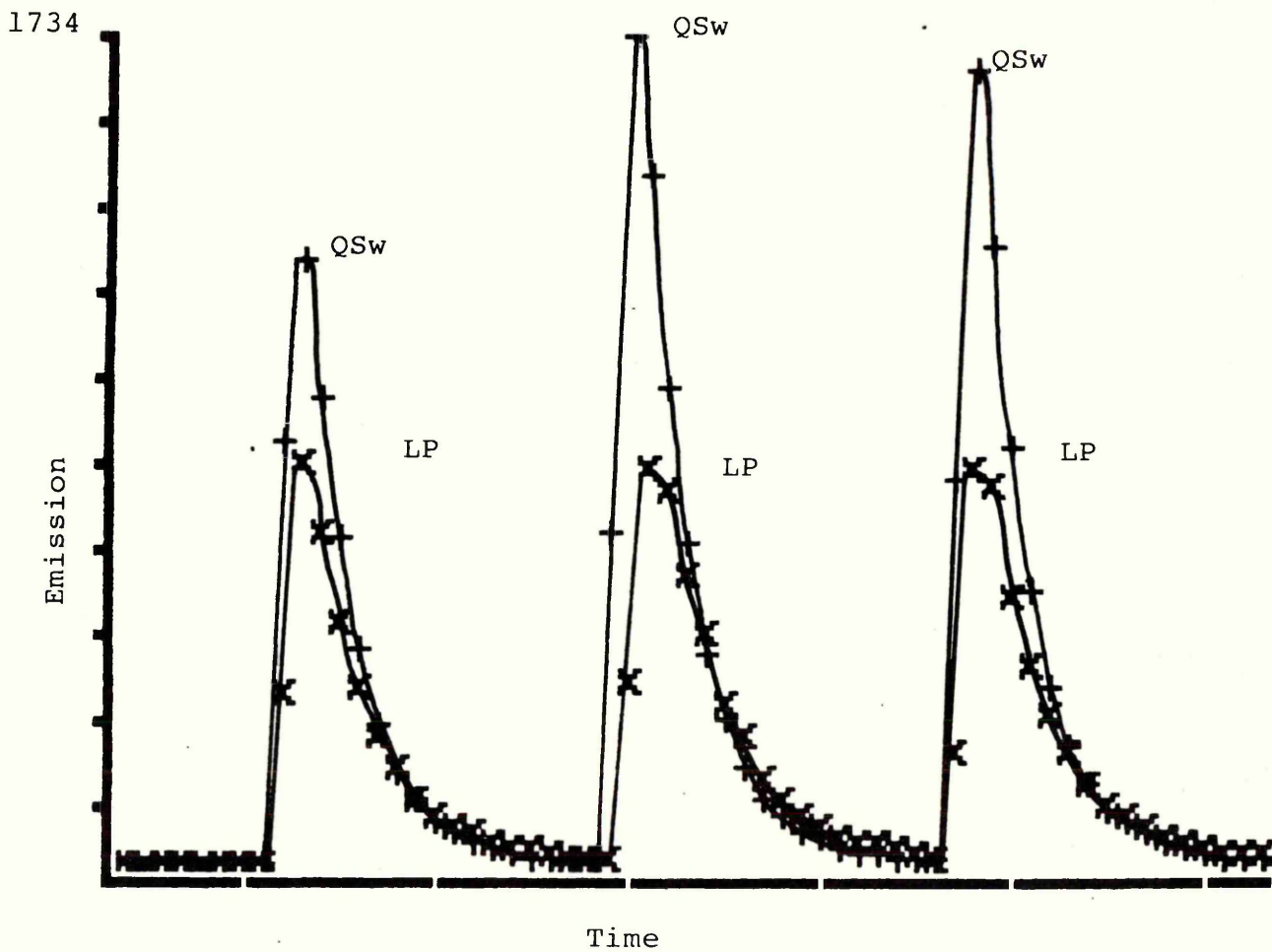


Figure 68. Emission Time Profiles for Zirconium During Laser Ablation of Wet Paint. The Diagram Shows Three Consecutive Peaks due to Single Q-Switched (QSw) and Long Pulsed (LP) Laser Shots. The Time Axis is 60s Long and the Maximum Emission Intensity is given on the Y-axis.

5.2 EXPERIMENTAL (PAINTS)

Having established the most appropriate way to introduce paint samples to the analytical system, further studies were undertaken using the Jarrell Ash ICAP 9000. These utilised the simultaneous multi-element capability of the system to investigate several operating conditions. Such work allowed the comparison of operating conditions for two distinct types of material, namely metals and polymers.

5.2.1 Materials

Argon: High purity grade (British Oxygen Co Ltd)

Graphite: High purity grade (Spectrochem Supplies Ltd)

Paints: A variety of oil based gloss paints obtained from High Street stores.

All graphite components were fabricated in the workshops at Sheffield City Polytechnic.

5.2.2 Apparatus

The Jarrell Ash ICAP 9000 ICP system was used in conjunction with the laser, its optics and the laser ablation chamber as described in chapter three.

5.2.3 The Effect of Laser Focusing

It has already been shown in chapter four that laser focusing changes the irradiance upon the sample

surface which in turn affects the ablation process. The significance of laser focusing for paint samples was investigated.

The plasma operating conditions are given in chapter three. The laser was used at maximum lamp energy (70J) and 10Hz. The only experimental variables were the focusing distance (lens to sample distance) which was varied from 85mm to 103mm and the laser operating mode.

Data were accumulated using the time study option of the controlling software. Each time study was 90s long.

A graphite sample cup was filled with paint such that the meniscus was level with the top of the cup. The cup was placed into the graphite crucible inside the laser ablation chamber which was then turned on-line with the ICP.

The focusing distance was set by adjusting the height of the laboratory jack onto which the ablation chamber was mounted. The time study was initiated and after a 5s delay, a single Q-switched shot was fired at the sample. After a further 40s a single long pulsed shot was fired at the same sample.

After the 90s time study, the sample was replaced by a fresh one and the focusing distance adjusted. The above experiment was repeated over the range of focusing distances thus allowing the effect of focusing distance to be established for both laser modes.

5.2.3.1 Results

Examination of the time studies for the elements present in measureable amounts (see section 5.1.3) revealed two transient peaks. The first, which appeared at approximately 5s was due to the Q-switched laser shot and the second at 45s, due to the long pulsed shot.

The maximum emission intensities (ie. peak heights in counts) were measured for both laser modes as a function of focusing distance. It was found that a general trend existed which described all the elements examined. Typical examples were aluminium, cobalt, titanium and zirconium. The data for these elements are given in table 20, and shown graphically in figures 69-72 respectively.

To further illustrate the results of this experiment, the complete time studies for aluminium and zirconium are given in figure 73. These are typical of all the detectable elements in the wet paint sample used and further shows that the elements appear in the same time window. There is no evidence of selective volatilisation as would be observed in graphite furnace atomic absorption spectroscopy. This implies that temperatures at the laser/sample area are in excess of those achieved in commercial graphite furnaces. Consequently, integration is a relatively simple matter as one integration period is suitable for all elements of interest.

Focusing Distance (mm)	Peak Height (counts)							
	Aluminium		Cobalt		Titanium		Zirconium	
	Q-Sw	L.P.	Q-Sw	L.P.	Q-Sw	L.P.	Q-Sw	L.P.
85	2580	330	957	176	99999	26955	1174	156
88	2804	1420	1031	640	99999	99999	1238	778
91	3466	1306	1274	574	99999	99999	1586	730
94	2238	2055	846	884	99999	99999	966	1092
97	888	583	368	270	74046	52334	368	232
100	936	370	414	194	81056	31060	390	182
103	1280	318	504	168	99999	25056	519	154

Table 20. Peak Height Data as a Function of Focusing Distance for Q-Switched (QSw) and Long Pulsed (LP) Laser Operation. All Peak Heights are the Result of Single Laser Shots. The Maximum Peak Height Measurable by the Spectrometer is 99999 Counts.

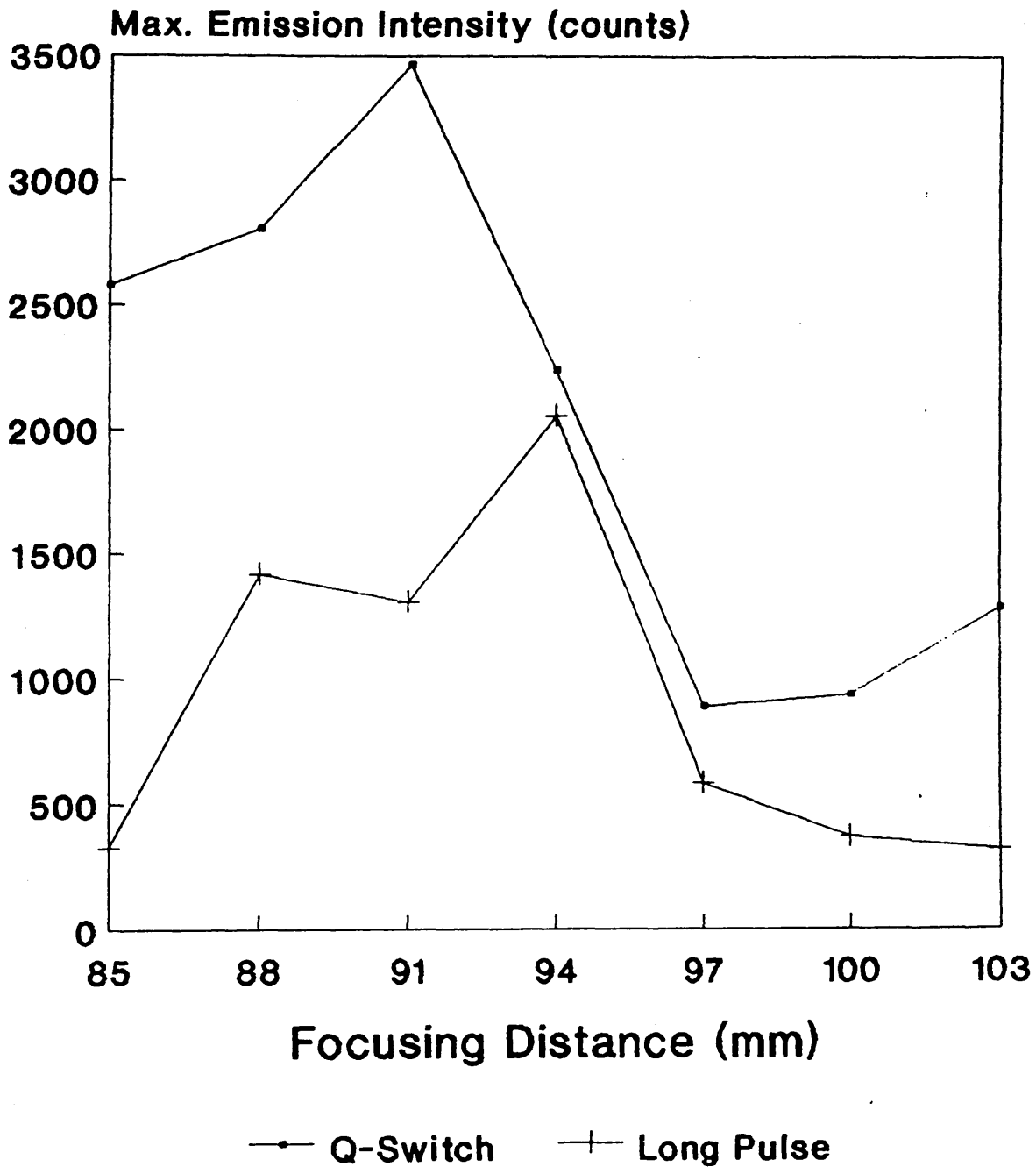


Figure 69. Effect of Laser Focusing on Emission Intensity for Aluminium in Paint.

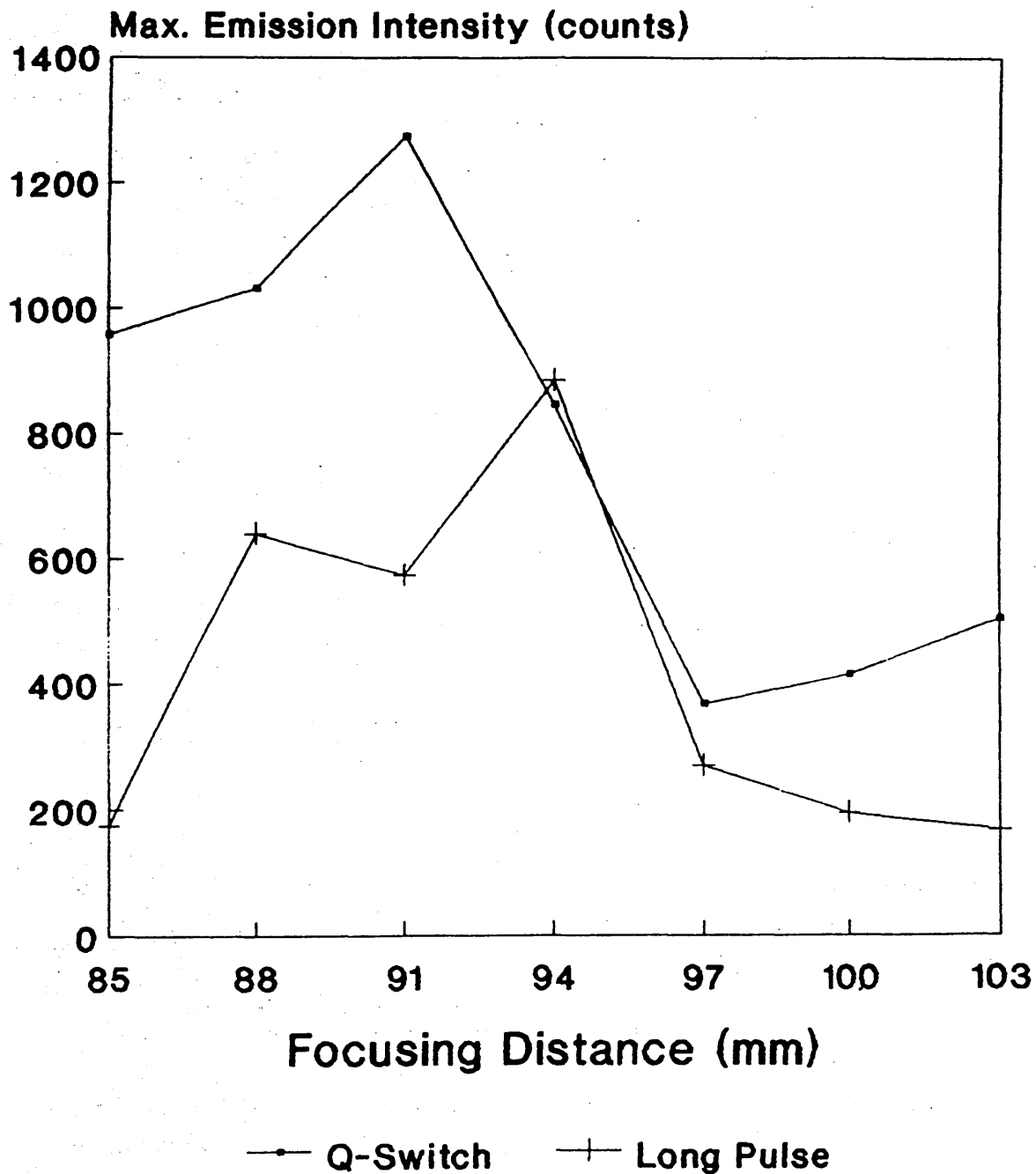


Figure 70. Effect of Laser Focusing on Emission Intensity for Cobalt in Paint.

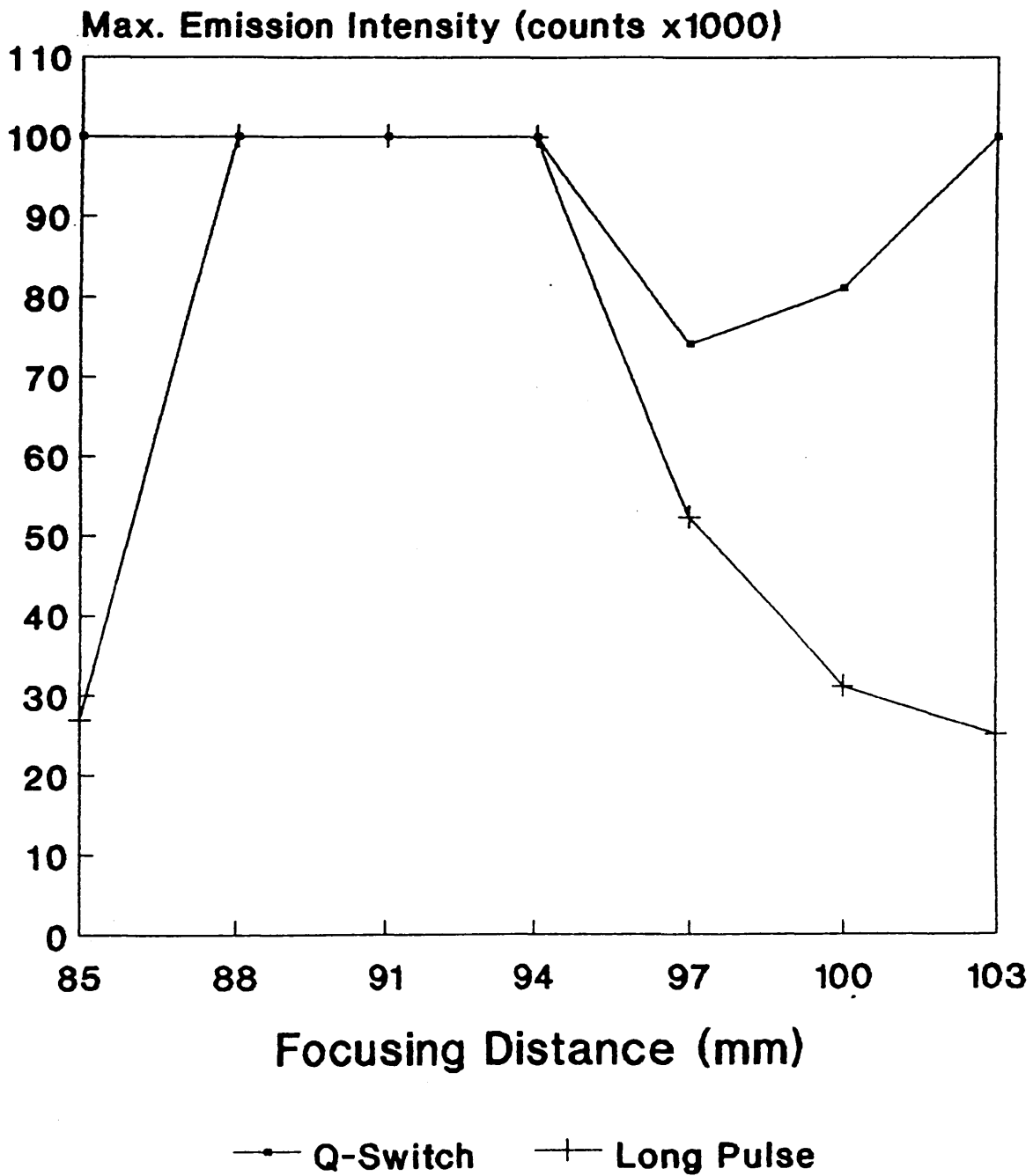


Figure 71. Effect of Laser Focusing on Emission Intensity for Titanium in Paint.

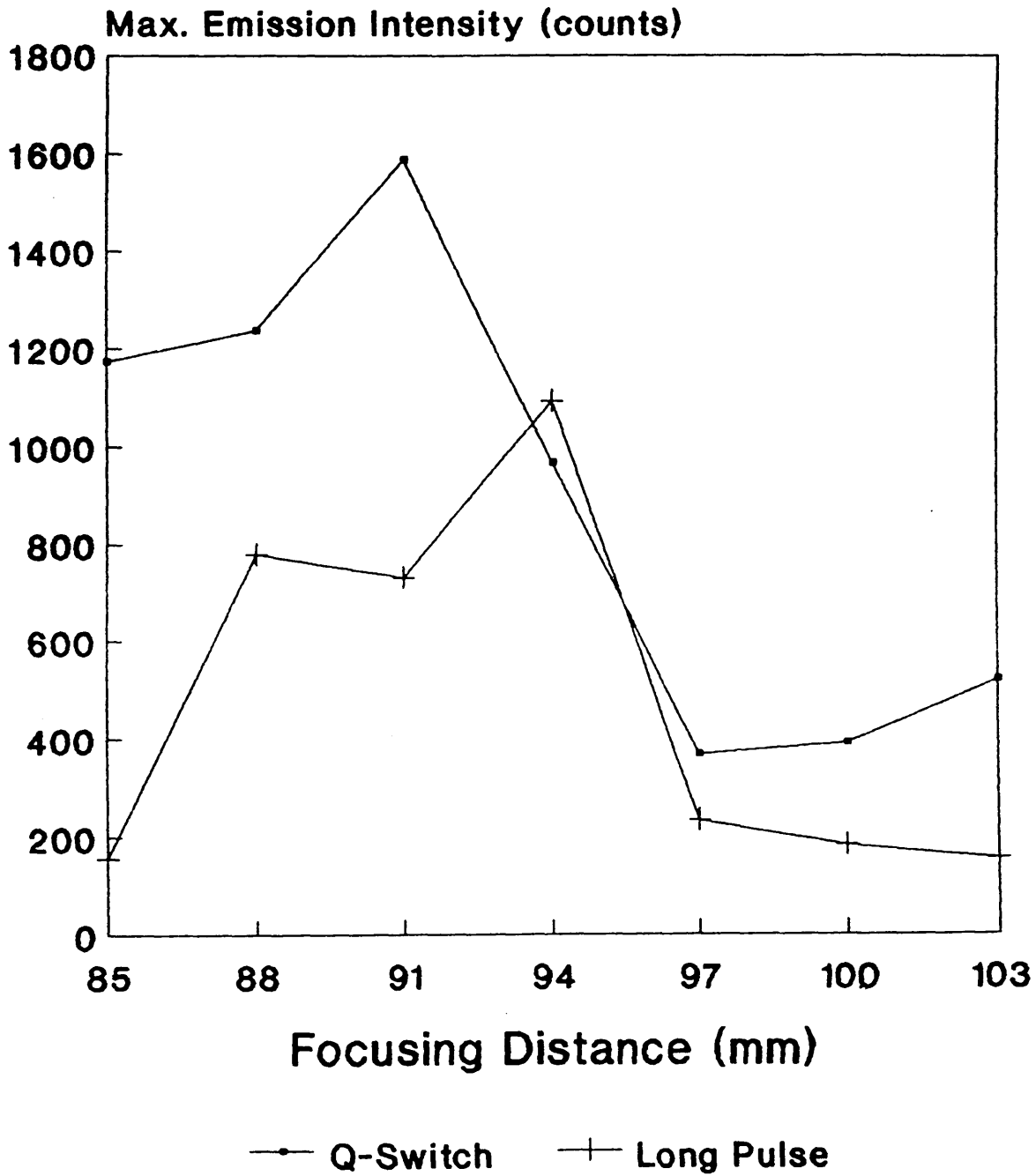


Figure 72. Effect of Laser Focusing on Emission Intensity for Zirconium in Paint.

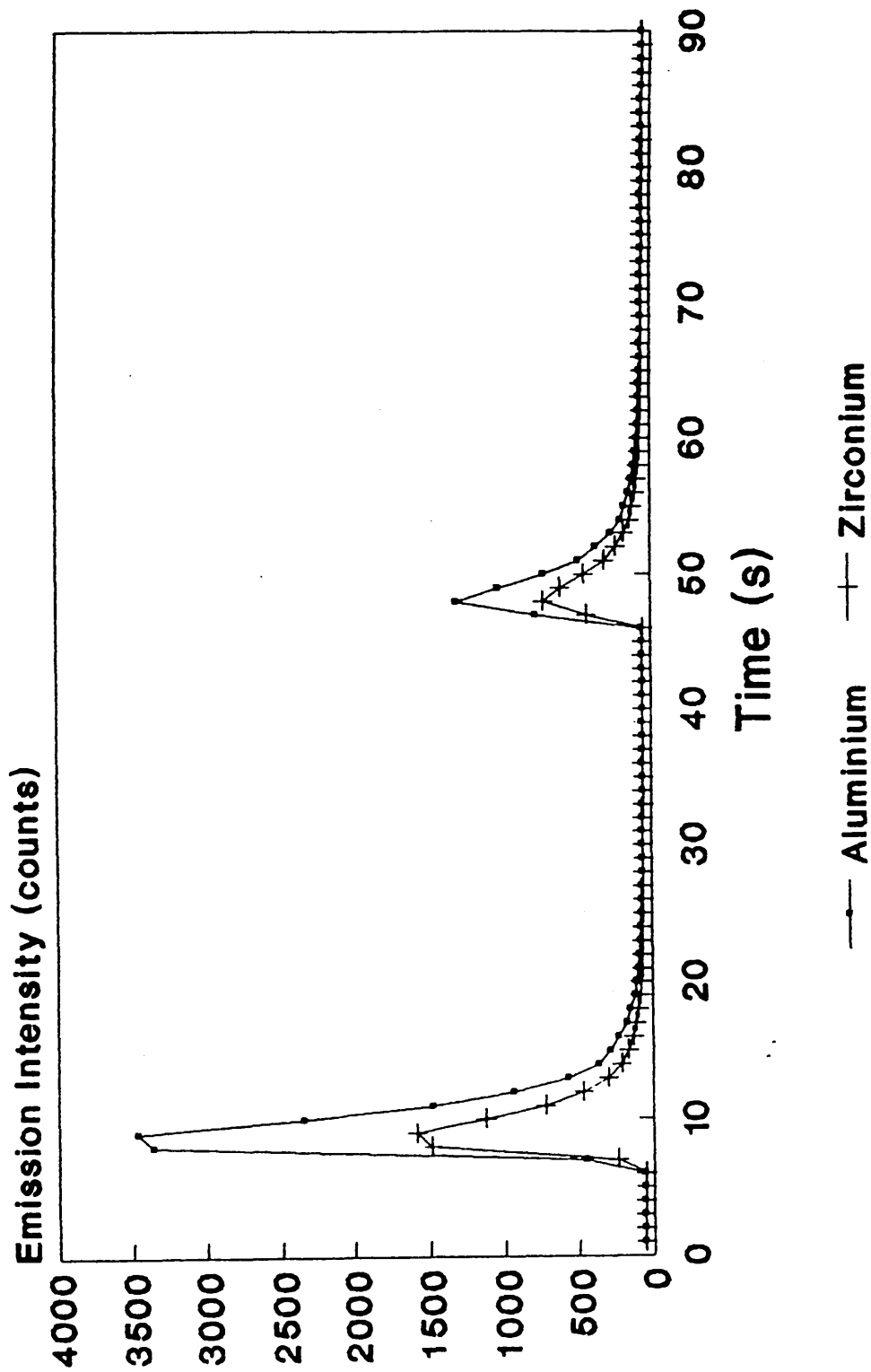


Figure 73. Emission Time Profiles for Aluminium and Zirconium in Paint.

5.2.3.2 Discussion

The results show that for Q-switched operation, the optimum focusing distance is 91mm. Defocusing the laser in this way reduces the irradiance on the sample surface. This appears to reduce the degree of sample spattering and creates a situation where the ablated material is in a form more appropriate for transport to the plasma.

The results for long pulsed operation are somewhat different. The optimum focusing distance appears to be 94mm. This unexpected result may be explained in one of two ways. Either, the observed trend is accurate in which case the optimum focusing distance is dependent on laser operating mode or, the trend is inaccurate due to an erroneously low measurement at a focusing distance of 91mm.

If the latter is true then a single focusing distance would be appropriate for both modes of operation. If the former is true then slight focusing adjustments would be required depending on the laser mode to be used.

A Q-switched shot consists of a single pulse of radiation. When incident upon a sample it produces a laser induced plume and ablates material from the surface over a period of approximately 9ns. A long pulsed shot, however, consists of a train of pulses about 200 microseconds long. In this case, the first pulse produces a laser induced plume and begins the

ablation process. Later pulses in the train then interact with the plume and the sample surface. This interaction of later pulses with the plume distinguishes the long pulsed shot from the Q-switched shot. This effect may be responsible for the slight difference in the observed optimum focusing distance. Validation of this hypothesis would require further experimentation.

The range of focusing distances used was necessarily small due to the physical constraints of the equipment. However, had this range been extended, the results suggest that two emission maxima may have been observed at 91mm and 109mm with a minima at the focal point of 100mm. This conclusion is drawn from the fact that focusing distances greater than 100mm show an upturn in emission intensity. This further suggests that moving the sample away from the focal point allows the production of ablated material which is more suitable for transport to the ICP.

Further examination of the results reveals that Q-switched operation is generally more sensitive than long pulsed operation by virtue of the greater emission intensities.

The optimum focusing distance for paints is 91mm and that for metallurgical samples was 93mm. Within the limits of experimental error these values are believed to be the same. Consequently, such a focusing distance is optimal for the experimental configuration used and should be independent of sample

type.

5.2.4 The Effect of Ablation Period

To this point all experiments had been performed using single laser shots. Consequently, the significance of increasing the ablation period to increase the amount of material ablated was studied.

All experimental conditions were as previously described but a focusing distance of 91mm was used throughout.

As with the previous experiment the time study facility was used to acquire data. On this occasion a time study of 120s duration was used since broader peaks may be anticipated when ablating for longer periods. The laser was operated at maximum lamp energy and 10Hz. When firing the laser for anything more than a single shot, a switch on the remote control was put into repetitive firing mode for as long as required, then put back to single shot firing which turns the laser off. When in the single shot mode, the "fire" button needs to be pressed to produce a single laser shot.

Wet paint samples were placed into the laser ablation chamber as described earlier and the chamber switched on-line with the ICP. The time study was initiated and after 5s the laser was fired in the Q-switched mode. After a further 55s the laser was fired in the long pulsed mode. Four time studies were recorded using a single shot, 2s, 5s and 10s repetitive

firing. For example, the second time study comprised 2s repetitive Q-switched firing and 2s repetitive long pulsed firing. A fresh sample was used for each time study.

It was found that the 2s, long pulsed firing experiment produced sufficient spattering to completely coat the window to the ablation chamber with paint. Consequently, the long pulsed experiments were not continued beyond that point.

5.2.4.1 Results

The time studies that recorded the single shot and 2s ablation periods both exhibit two peaks. The first appears at approximately 8s and corresponds to Q-switched ablation, the second appears at about 62s due to long pulsed ablation. For the 5s and 10s ablation period time studies only a single Q-switched peak appears as discussed above.

It was again observed that peaks due to long pulsed ablation were of significantly lower emission intensity than Q-switched peaks. Consequently, long pulsed ablation will not be considered further.

As with previous experiments, the observed trends were similar for all the detectable elements. Typical examples are aluminium, cobalt and zirconium whose emission-time profiles are given in figures 74-76 respectively.

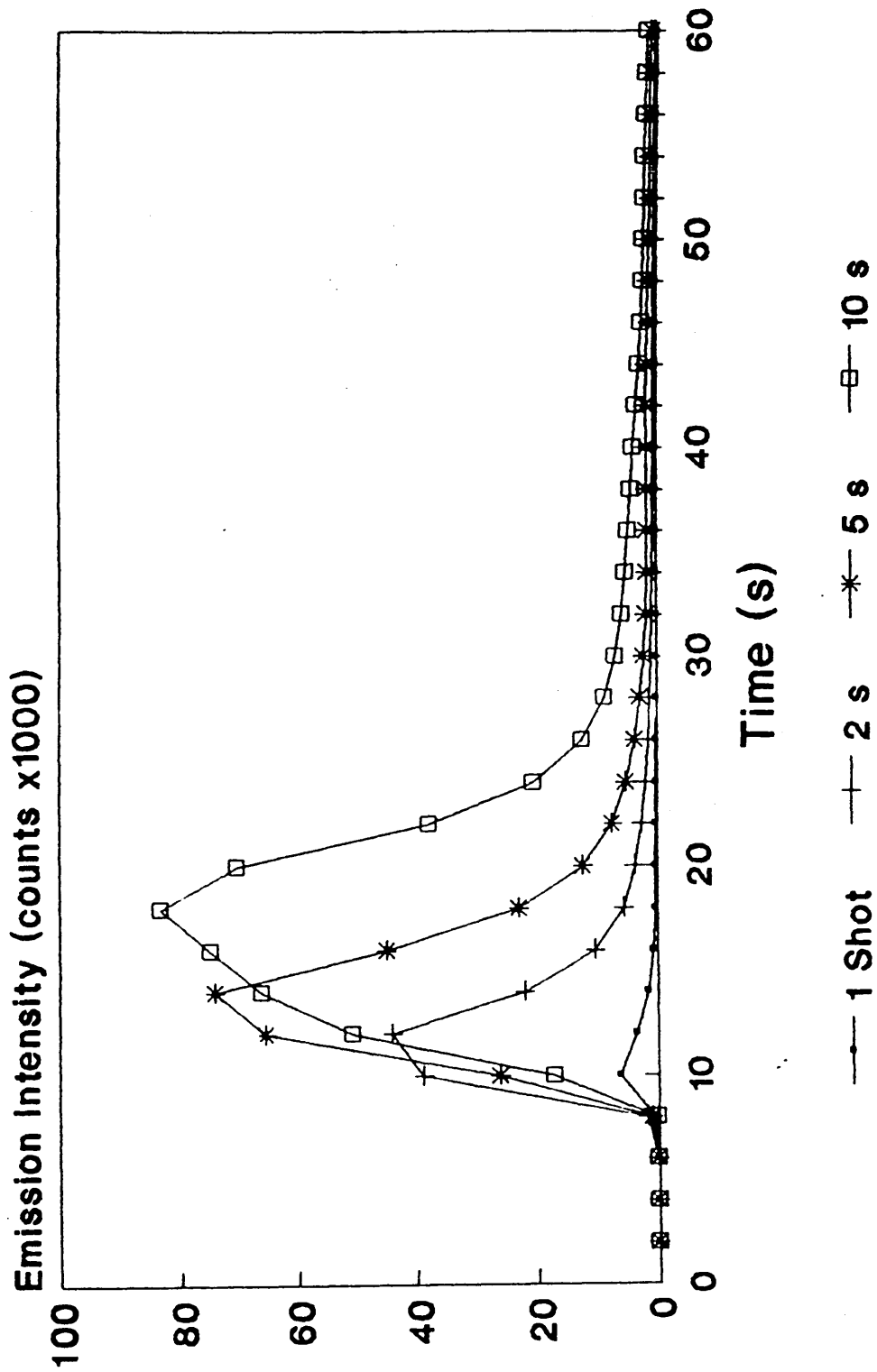


Figure 74. Emission Time Profiles for Aluminum in Paint Showing the Effect of Ablation Period.

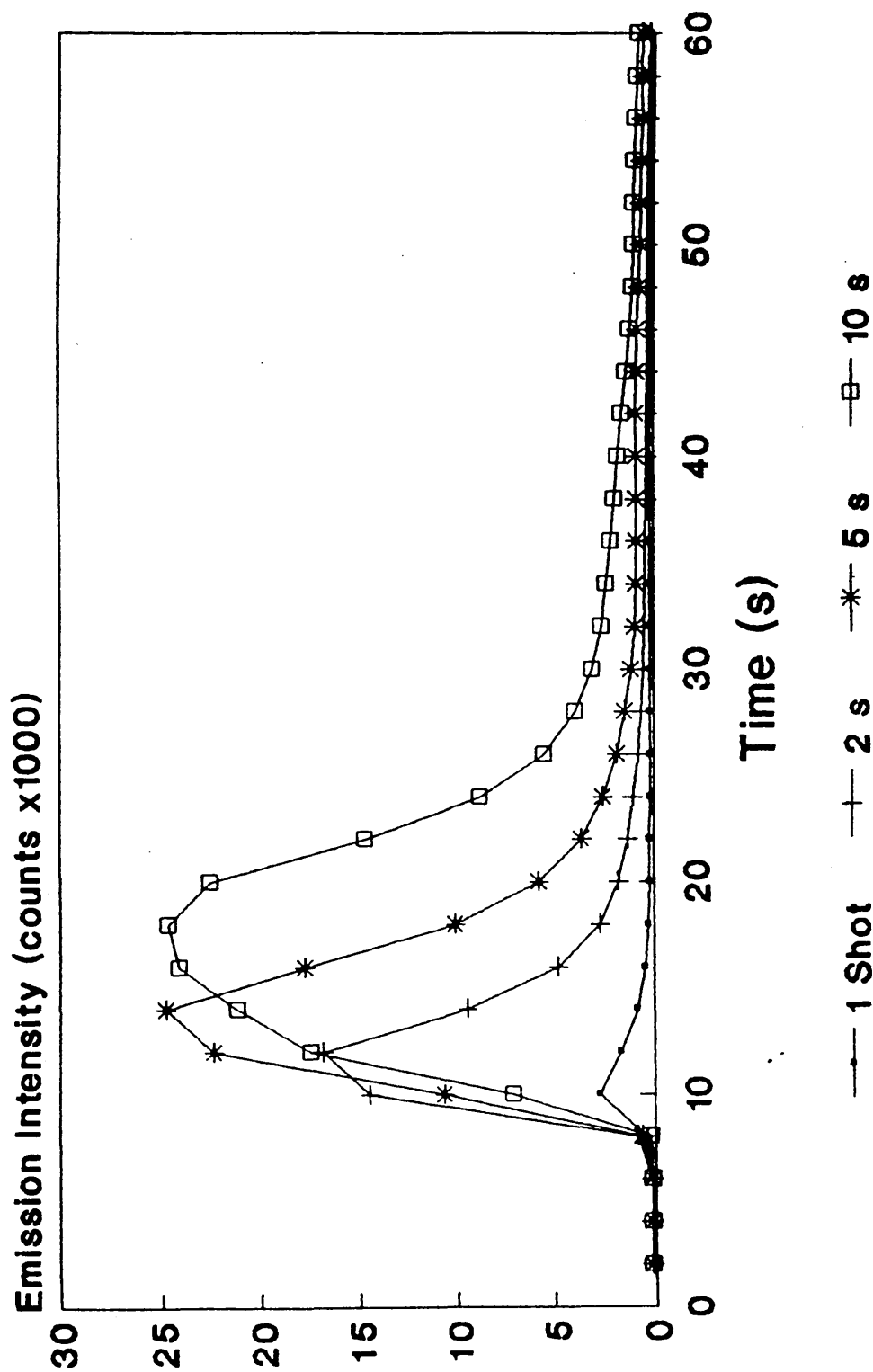


Figure 75. Emission Time Profiles for Cobalt in Paint Showing the Effect of Ablation Period.

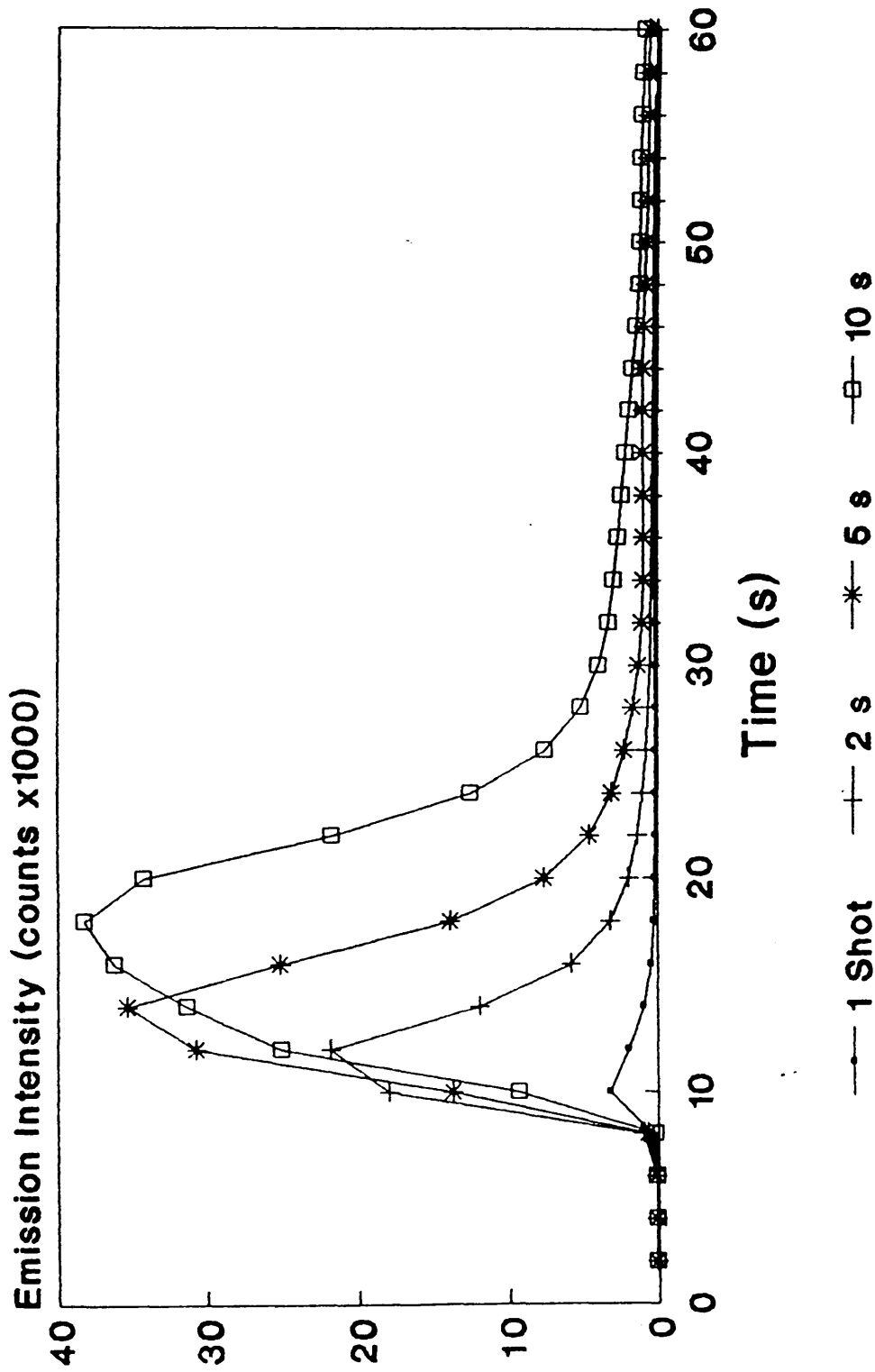


Figure 76. Emission Time Profiles for Zirconium in Paint Showing the Effect of Ablation Period.

A further representation of the results is given in figure 77. Here, the maximum emission intensity is plotted as a function of ablation period. For single shot laser pulses the ablation period is plotted as zero although to be accurate it should be 9ns.

5.2.4.2 Discussion

The results show that the leading edge of the emission peak appears at approximately 8s. Hence, there is a 3s lag ie the time it takes for ablated material to reach the plasma. Increasing the ablation period increases peak heights, peak areas and the widths at half maxima. As would be expected, long ablation periods ablate more material and more material reaches the plasma.

Examination of figure 77 shows that although peak heights increase with increasing ablation period, the relationship is not linear. In fact, there is a suggestion that ablation periods of greater than 10s may produce steady state emission.

Clearly, increasing ablation period increases sensitivity, but only upto a point. As peak heights begin to level off, greater sensitivity may be achieved by utilising peak area rather than peak height measurements. The ability to produce steady state signals is an attractive possibility as it would allow several integrations to be made and may provide improved analytical precision.

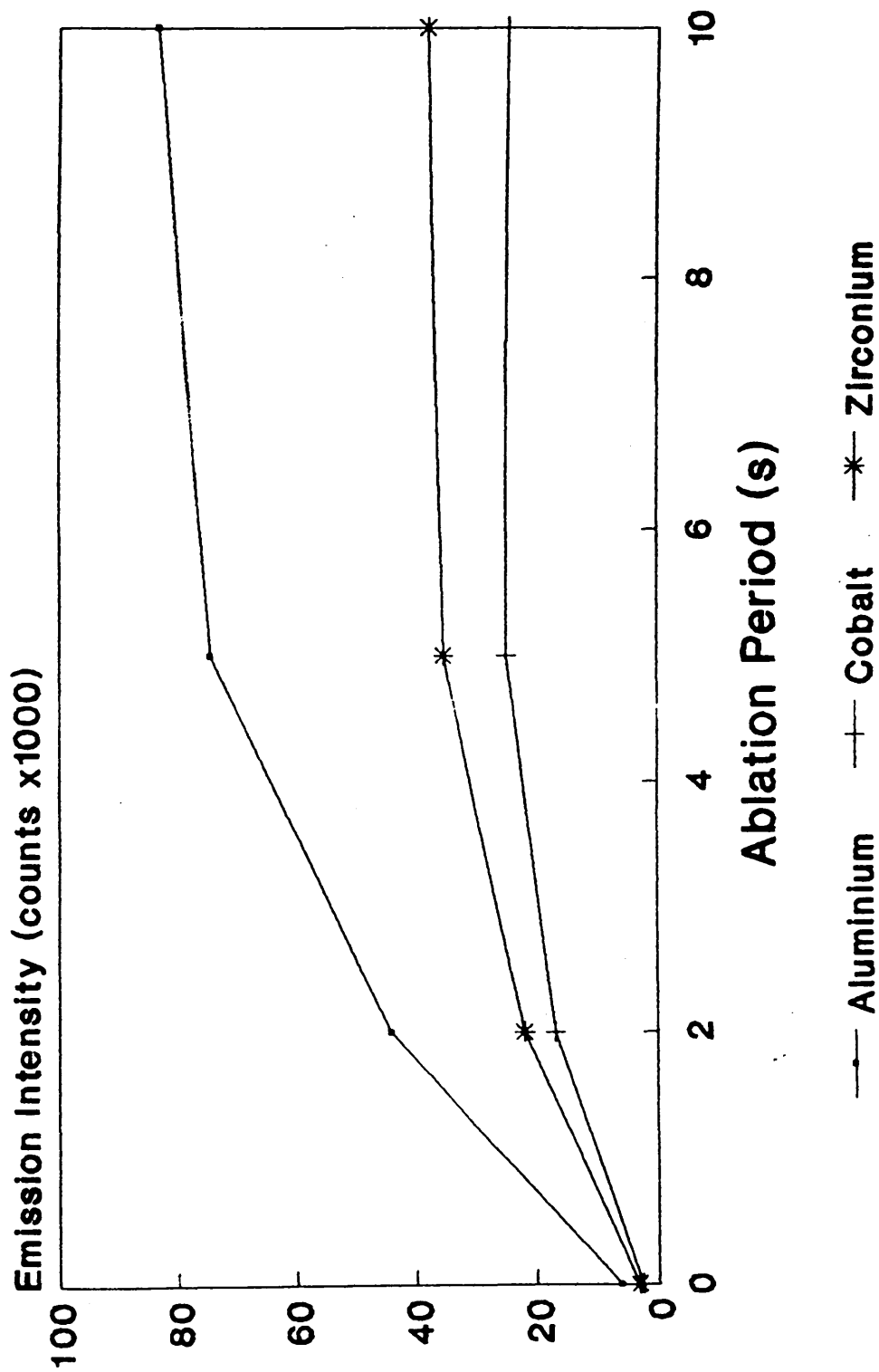


Figure 77. Emission Intensity as a Function of Ablation Period.

Data is given for Al, Co and Zr in Wet Paint.

The non-linear relationship between maximum peak heights and ablation period may be due to an interaction of the laser with the laser induced plume. Longer ablation periods will result in this interaction playing a progressively greater role in the ablation process. It may be that such an interaction decreases the efficiency of material removal or increases the degree of sample spattering leaving smaller masses to be transported to the plasma. Alternatively, this relationship may be due to sample erosion. Using consecutive single shots on wet paint does not demonstrate erosion but repetitive firing at a frequency of 10Hz over periods of 2s, 5s and 10s may be sufficient for such a process to occur. If this is the case then further increases in ablation period would not result in a steady state signal but a progressive decrease in emission intensity as the sample is eroded.

This study has shown a clear relationship between sensitivity and ablation period. Furthermore, it demonstrates that single shot ablation is appropriate for elements at relatively high concentrations but increased ablation periods would be beneficial when the determination of elements at low concentration is required.

5.2.5 The Effect of Laser Lamp Energy

The active medium of the laser is the Nd:YAG rod is optically pumped by a xenon flash tube. The

energy output of this lamp is variable from 30J (the threshold condition ie just sufficient for laser action) to 70J. The output of the flash lamp is responsible for creating a population inversion in the active medium. The greater the output energy, the greater the population inversion and hence the greater the output energy of the laser. Consequently, the laser lamp energy has a direct bearing on the irradiance and hence on the ablation process.

All experimental conditions were as previously described. A time study of 60s duration was used to acquire data. Once a sample had been placed into the ablation chamber and the chamber switched on-line, the time study was initiated and after 5s a single Q-switched shot was fired. Five time studies were recorded using a fresh sample for each one, at 30, 40, 50, 60 and 70J lamp energy.

5.2.5.1 Results

Again, all the detectable elements exhibited identical trends. The resultant emission peaks for 30, 50 and 70J lamp energy for aluminium, cobalt and zirconium are given in figure 78.

The maximum peak intensities for the above elements at each lamp energy were recorded and are given in table 21. This data is also shown graphically in figure 79.

Energy (J)	Peak Height (Counts)		
	Al	Co	Zr
30	92	86	112
40	723	305	470
50	1650	750	850
60	2058	1046	1253
70	2944	1344	1667

Table 21. Peak Height Data as a Function of Lamp Energy

5.2.5.2 Discussion

As expected, there is a direct relationship between emission intensity and laser lamp energy. The most intense peaks and hence the greatest sensitivity is achieved at maximum lamp energy of 70J. The relationship is in fact linear (see figure 79).

Decreasing the lamp energy from the maximum value decreases the irradiance upon the sample surface. Consequently, less material is ablated and transported to the plasma. There may also be differences in sample spattering. This results in emission peaks of lower intensity, lower area and smaller full width at half maximum.

5.2.6 The Effect of Carrier Gas Flow

When a sample is ablated inside the laser ablation chamber, the ablated material is taken up by a flowing argon gas stream and transported to the plasma.

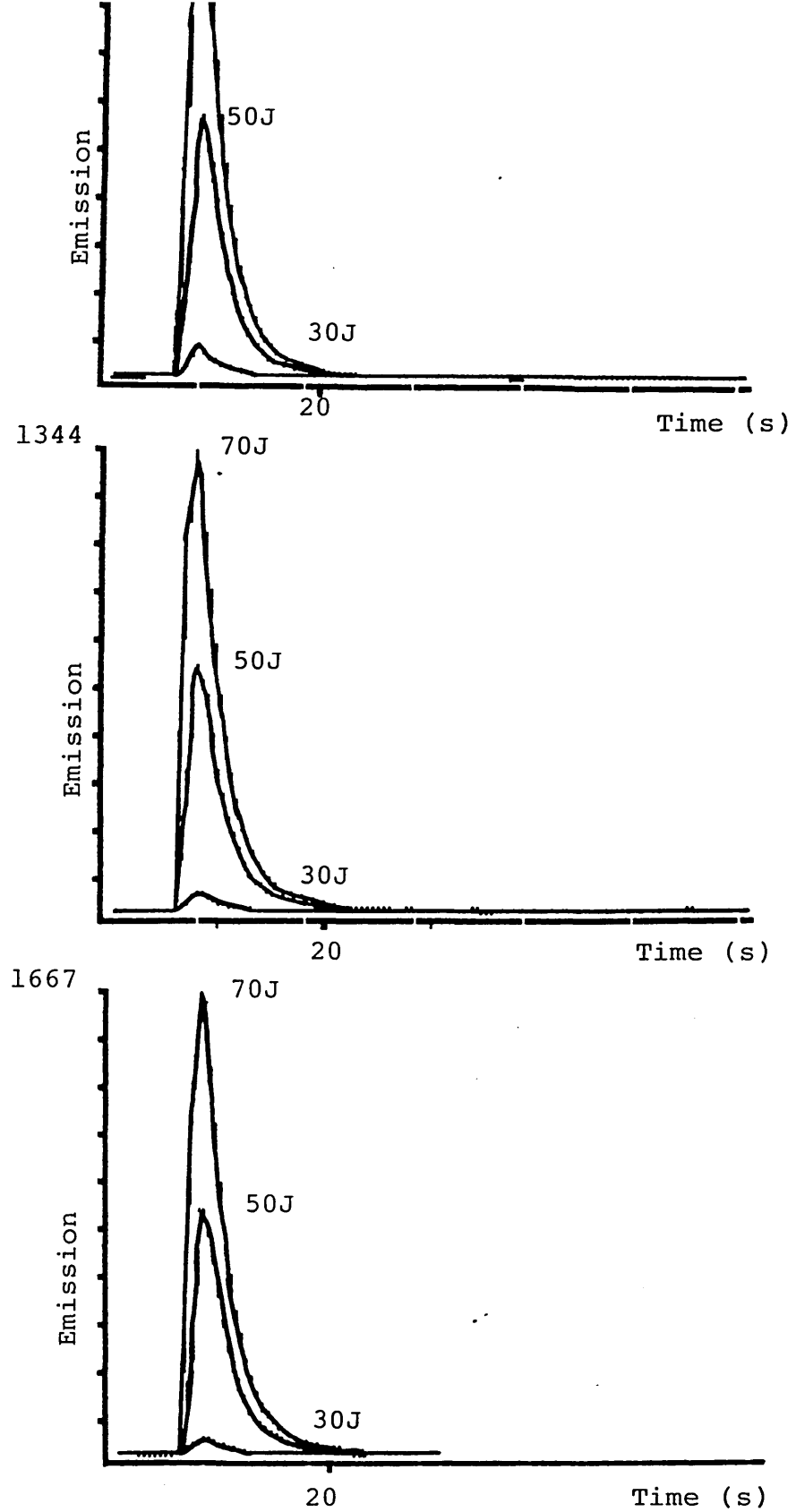


Figure 78. Emission Time Profiles Showing the Effect of Lamp Energy on Peak Shape for Aluminium (upper), Cobalt (middle) and Zirconium (lower) in Paint. All Peaks are the Result of Single Q-Switched Laser Shots. Maximum Emission Intensities are given on the Y-axis.

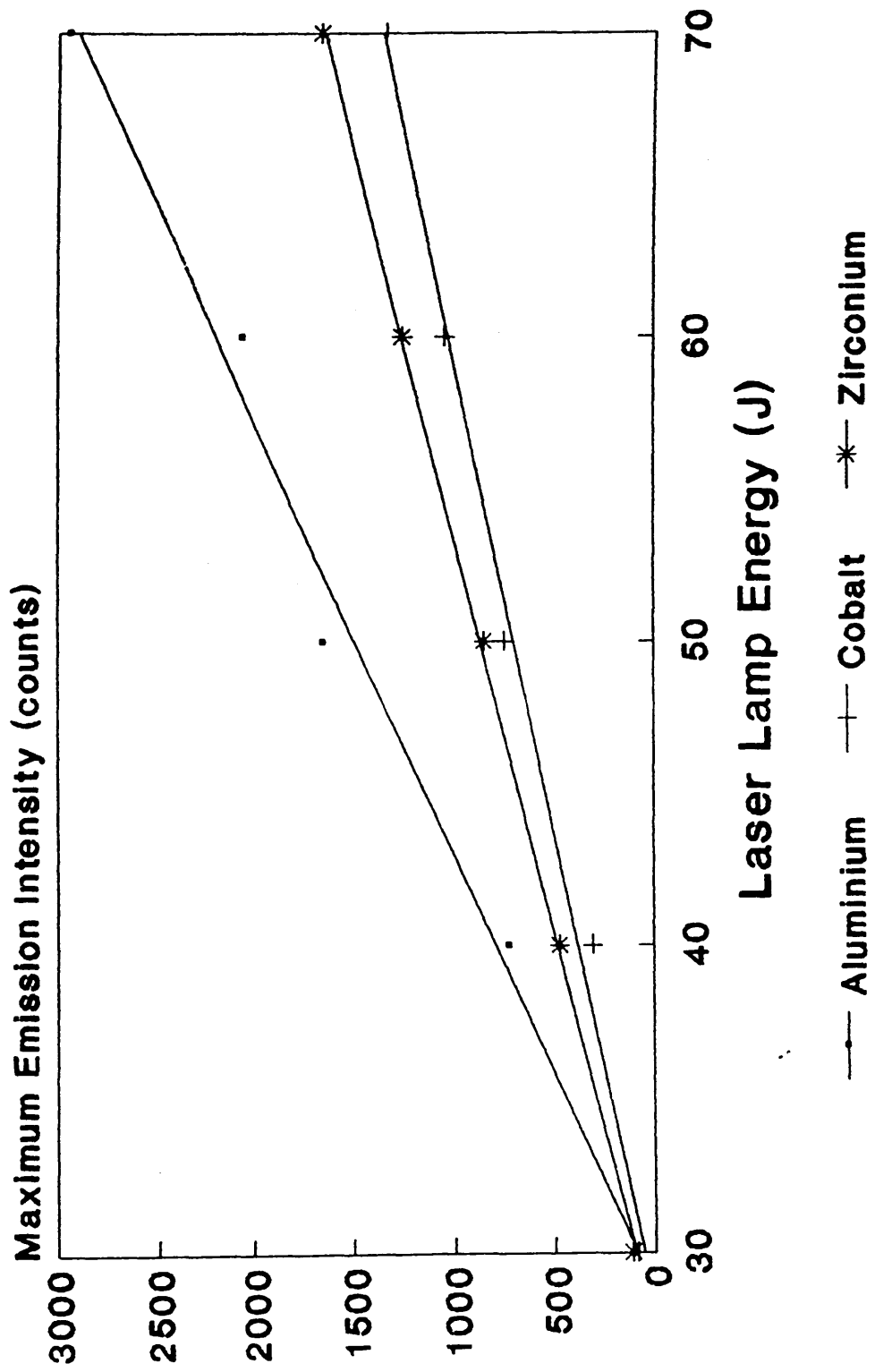


Figure 79. Emission Intensity as a Function of Laser Lamp Energy.

This gas supply is divorced from the main argon supply for the ICP. It passes through a rotameter and into the inlet of the laser ablation chamber (see figure 28). When the chamber is off line the carrier gas passes through the chamber and exhausts to the atmosphere. This expels air from the system. When the chamber is on line, the argon passes through the chamber and onto the plasma. It enters the sheathing gas unit and passes up through the central injector tube of the ICP torch (see figure 21).

Clearly, this gas flow is likely to have a bearing on parameters such as sample transport efficiency, residence time of sample in the plasma and the analytical characteristics of the plasma itself.

The gas flow rate is controlled by the rotameter whose calibration graph is given in figure 26.

All experimental conditions were as described earlier. Data were accumulated using a 60s long time study and the laser was fired 5s into this study. Seven time studies were recorded corresponding to rotameter settings of 2, 3, 4, 5, 6, 7 and 8. These rotameter settings correspond to gas flow rates of 0.33, 0.55, 0.74, 0.94, 1.14, 1.32 and 1.47 L/min argon.

Single Q-switched laser shots were used at 70J lamp energy, and a fresh sample was used for each time study.

5.2.6.1 Results

As with previous experiments the overall trends were virtually identical for all the detectable elements. Figure 80 shows the time studies for aluminium at gas flow rates of 0.33, 0.94 and 1.47 L/min. The other time studies have been omitted for clarity.

At each gas flow rate, the maximum peak heights were recorded for the elements aluminium, cobalt and zirconium. This data is given below in table 22.

Rotameter Setting	Gas Flow L/min	Peak Height (Counts)		
		Al	Co	Zr
2	0.33	2238	1100	1384
3	0.55	3489	1502	1923
4	0.74	4158	1485	2044
5	0.94	4116	1296	1632
6	1.14	4320	1216	1602
7	1.32	2958	768	960
8	1.47	2493	640	688

Table 22. Peak Height Data as a Function of Carrier Gas Flow Rate.

The above data is presented graphically in figure 81.

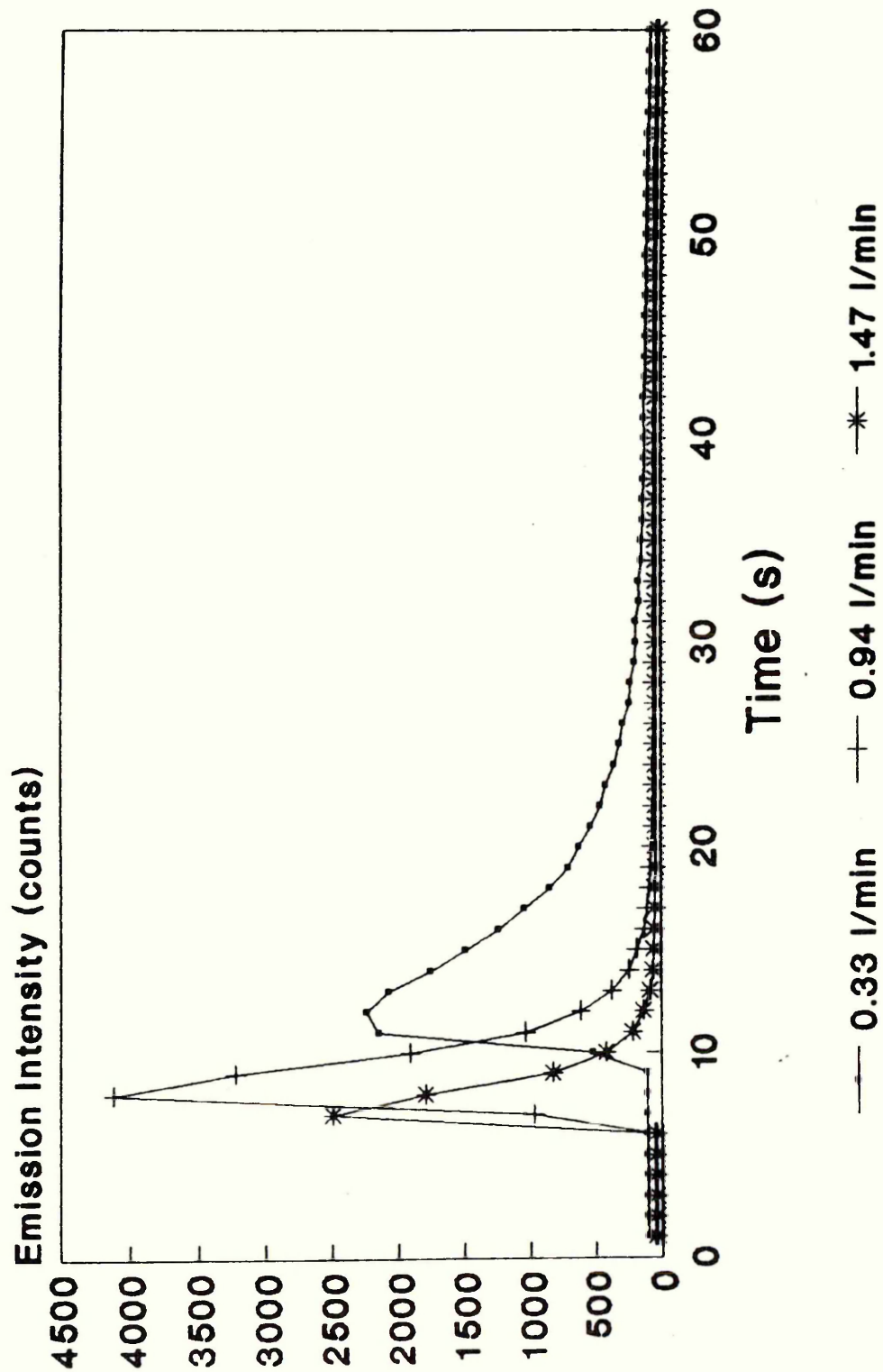


Figure 80. Effect of Carrier Gas Flow Rate on Emission Peak Profiles for Aluminium in Paint.

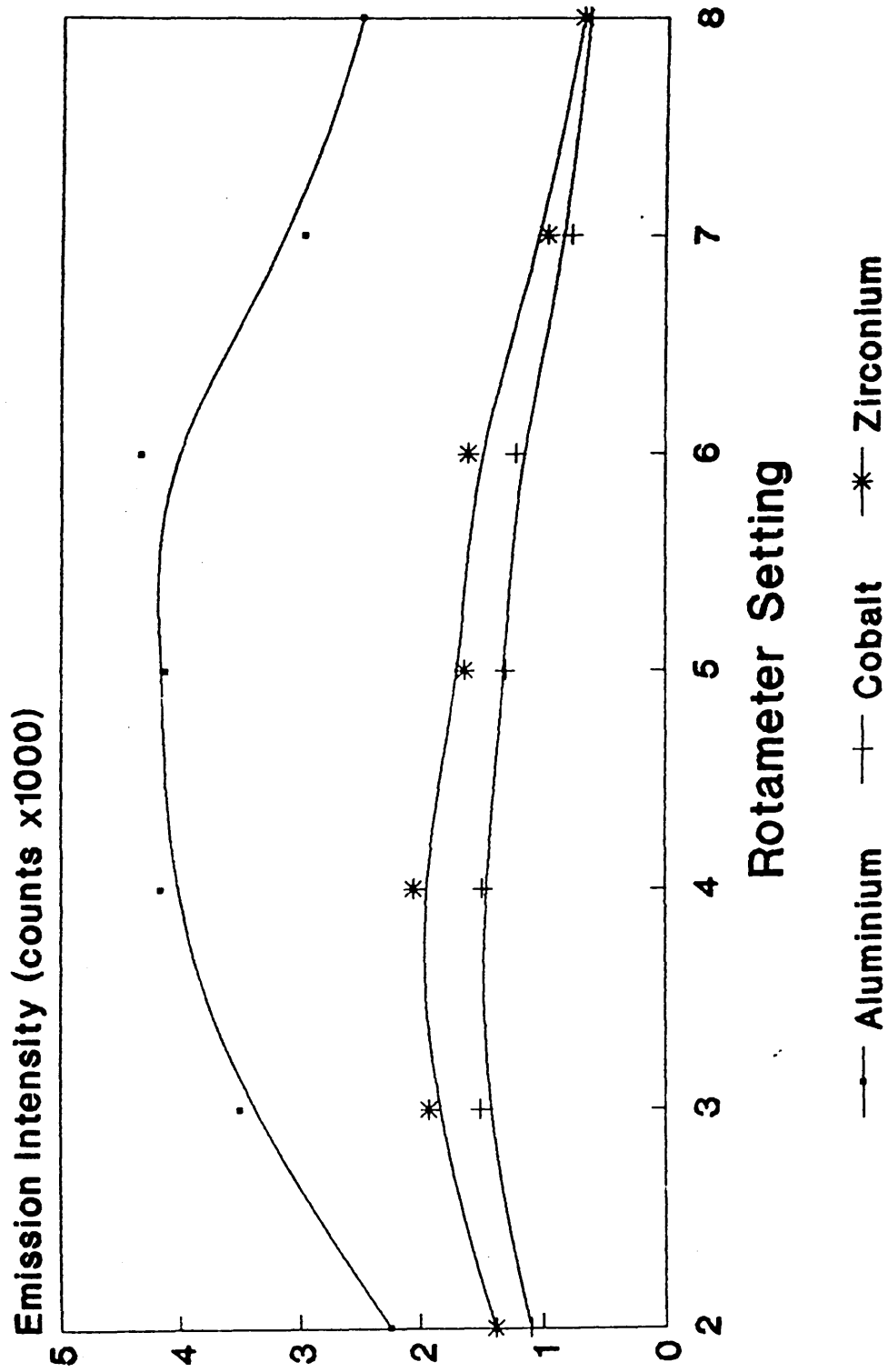


Figure 81. Peak Height as a Function of Carrier Gas Flow Rate.

See Text for Further Details.

5.2.6.2 Discussion

The carrier gas flow rate has a significant effect on analyte emission-time profiles. At relatively low gas flows, peak heights are generally low and the peak is broad. The slow moving transport gas allows greater diffusion of analyte resulting in a relatively long "slug" of analyte in the interconnecting tubing. It naturally takes longer for this slug to reach the plasma hence lag times are longer.

An intermediate gas flow produces much sharper peaks with a reduced lag time. In this case the slug is relatively small as diffusion effects are reduced. Peak heights are larger resulting in improved sensitivity.

At high gas flow rates the peaks are sharper still due to minimal diffusion effects. Lag times are no shorter than for intermediate gas flows implying that the sample cannot reach the plasma any quicker. However, peak heights are somewhat reduced. This is believed to be due to decreased residence times in the plasma itself.

When the ablated material reaches the plasma it must undergo dissociation and excitation processes prior to emitting radiation at wavelengths characteristic of the elements present. This relies on the material being subjected to plasma temperatures for a sufficiently long period of time. Increasing the carrier gas flow will force the sample material to pass through the plasma increasingly quickly, ie shorter residence time

resulting in fewer of the analyte species emitting radiation and hence lower peak heights.

Examination of figure 81 reveals that the optimum gas flow rate corresponds to a rotameter setting of 4, a flow of 0.74 L/min. As would be expected the trends for all three elements resemble an inverse parabola.

5.2.7 Precision Studies

Precision was mentioned earlier when comparing wet and dry paint samples. That study showed that wet paint offered an improvement in precision by virtue of its fluidity.

A further study was undertaken to determine intra-sample and inter-sample precision using normal analytical integrations rather than time studies.

In the first instance, intra-sample precision was determined. A single sample of wet paint was ablated five times. Single Q-switched laser shots were used at 70J lamp energy. A focusing distance of 91mm and a carrier gas flow of 0.74 L/min were used. All other experimental conditions were as described earlier.

The sample was placed inside the laser ablation chamber in the usual way. The chamber was turned on line with the plasma ready for ablation measurements to be made. A 20s integration time was used. This was sufficient to integrate the whole peak profile and allow a few seconds for the lag time. When the integration time was initiated the exposure light

illuminated on the spectrometer. As this light was observed the laser was fired. Five of these integrated measurements were taken from the same sample.

The inter-sample precision was studied by repeating the above experiment but rather than using the same sample, several aliquots of the same paint were used. In this case six aliquots were used and six integrations measured.

5.2.7.1 Results

The integrated intensities for the above experiments are shown below in table 23 for aluminium, cobalt and zirconium.

No.	INTENSITY (Counts)					
	INTRA SAMPLE			INTER SAMPLE		
	Al	Co	Zr	Al	Co	Zr
1	9828	4845	5328	10183	5044	5523
2	9505	5258	5801	8608	4526	4920
3	9481	5306	5865	10107	4826	5382
4	9337	5219	5628	8461	4311	4686
5	9626	5343	5824	10128	4584	4977
6	--	--	--	9911	5102	5684
S.D.	164	180	198	736	284	357
%RSD	1.7	3.5	3.5	7.7	6.0	6.9

Table 23. Emission Data Showing Intra and Inter Sample Precision.

5.2.7.2. Discussion

The precision of the intra-sample measurements is remarkably good. Although poorer than solution nebulisation, when compared with other solid sampling techniques the results are encouraging (see section 1.2.6). Furthermore, the precision quoted above represents some of the best values published for laser ablation ICP work.

Precision for paint samples is far superior to that observed for metallurgical samples. This is believed to be due to a combination of the fluidity of the paint and greater homogeneity.

An attempt to improve the precision still further was made by using an internal standard. This resulted in a deterioration of precision. For example, that for cobalt when ratioed to aluminium was 4.7% RSD. Hence internal standardisation was not appropriate for the elements investigated in wet paint.

Inter-sample precision is slightly worse and reflects some heterogeneity from sample to sample. Although the sample was mixed prior to aliquots being taken, this was not unexpected due to the settling out nature of paint. More thorough mixing is likely to be beneficial to inter-sample precision.

5.2.8 Comparative Studies

The qualitative capabilities of the system were put to use to compare three different types of

paint. Namely, oil based, liquid gloss paints in white, green and orange.

Compounds are added to paint as colouring agents or as extenders to add bulk for example. It should be possible to distinguish between these compounds using the analytical system described.

The following experiments were performed using the experimental conditions described earlier. A 90s long time study was used to accumulate data and a single Q-switched laser shot was used at 70J lamp energy.

A sample of white paint was examined first by firing the laser 5s into the time study. A second time study was used for the green paint and in this case the laser was fired 35s into the study. Finally, the orange paint was examined using a third time study and firing the laser 65s into the study. This staggering of laser shots allows all three studies to be overlaid thus distinguishing between the three samples.

5.2.8.1 Results

The time studies for barium, lead, titanium and zirconium are given in figure 82. The three peaks that may be observed are due to laser ablation of the white, green and orange paint reading from left to right.

5.2.8.2 Discussion

The results are a clear indication of the

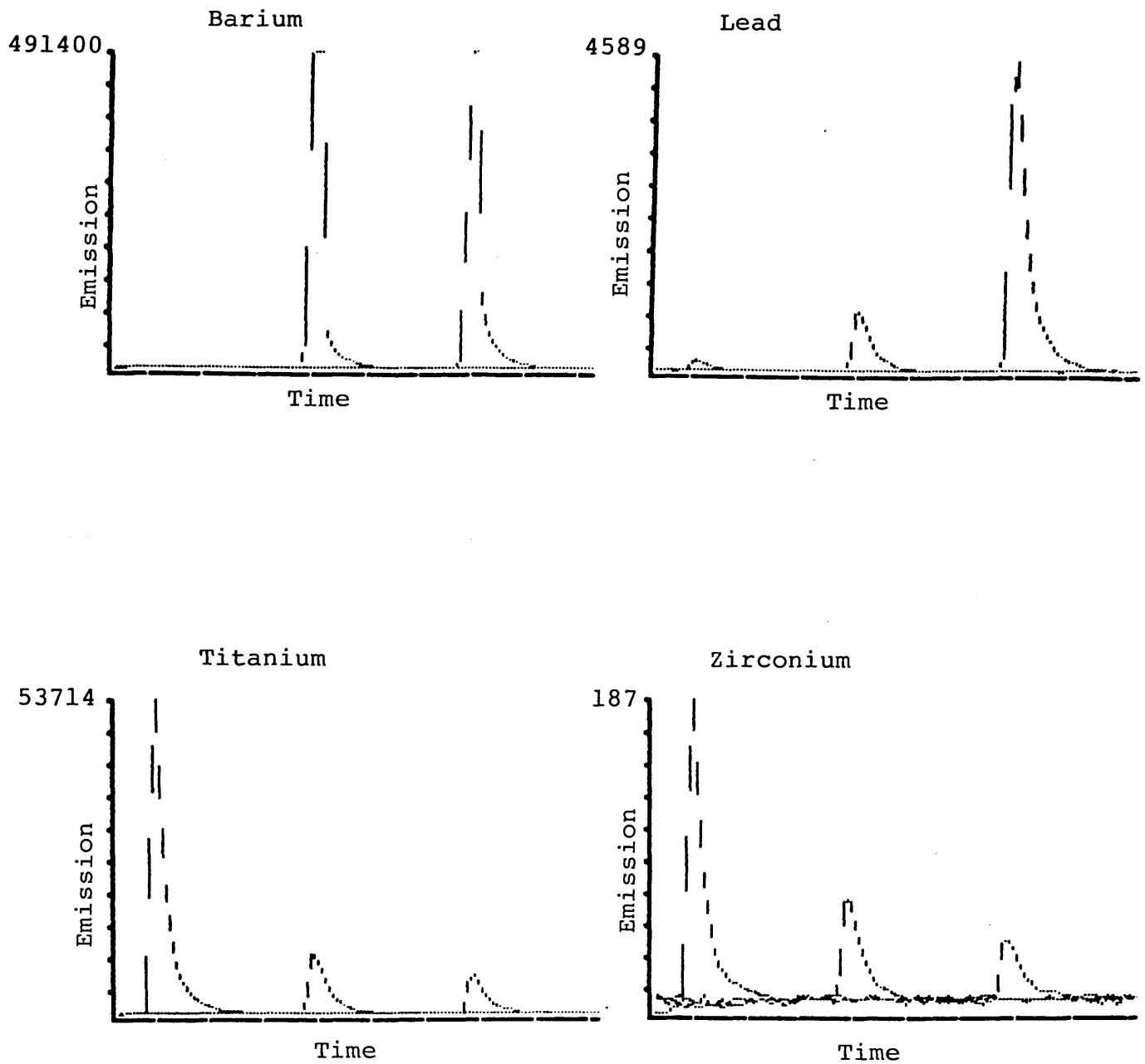


Figure 82. Emission Time Profiles During Laser Ablation of Paint Samples. The Emission Peaks are the Result of Single Q-Switched Laser Shots at White (left peak), Green (central peak) and Orange (right peak) Paint. The Time Axis is 90s Long and Maximum Emission Intensities are given on the Y-axis.

capabilities of the laser ablation ICP technique.

It is possible to make direct comparisons from one sample to another.

Titanium, for example, is added to paints as titanium dioxide. It is very widely used in paint manufacture as a whitening agent.

The results for titanium in figure 82 show a significantly greater concentration in the white paint than in the coloured paints. Titanium has clearly been detected in the green and orange paints where it may have been used to add bulk to the paint or, more likely, to help produce the required shade of green and orange.

Barium is used in paint manufacture as barium sulphate. This compound is used as an extender. These are materials which, when mixed with oil or varnish are almost transparent ie. they have little or no opacity and unless they are very dirty have little effect on the colour of the paint. They are incorporated into paints for specific reasons, eg. to cheapen the material, to increase body, or to harden the film. Barium sulphate is used to increase the gravity of the paint and it can produce a slight reinforcing effect on the paint film.

The results show levels of barium in the green and orange paints sufficient to saturate the detector. However, there appears to be little or no barium in the white paint examined. The absence of barium in

the white paint may be due to the presence of very high levels of titanium dioxide which itself may act to increase the body of the paint.

The qualitative and semi-quantitative capabilities of the above study are clear. The ability to differentiate between different colours of paint and to establish the presence or absence of particular elements has been demonstrated.

5.2.9 Concluding Remarks

This study of paint samples has revealed several important results.

To achieve the highest degree of precision, wet paint samples should be used. The fluidity of the sample results in the replenishment of the ablated area after each laser shot. Relative standard deviations of the order of 2% were found for many elements without the use of internal standardisation. This represents some of the most precise measurements reported for laser ablation ICP studies (see table 4).

The most appropriate focusing distance was established. Focusing has significant effects on the irradiance at the sample surface and hence ablation processes. A focusing distance of 91mm was found to be optimal. This value was very similar to that for metallurgical samples (93mm), and when considering experimental errors it is believed to be the same.

The period of laser ablation was found to have

a profound effect on emission intensities. A single Q-switched shot was sufficient for elements of high concentration but longer periods of Q-switched ablation were more appropriate for trace elements. Furthermore, longer ablation periods tended towards the production of steady state signals. If this were feasible, then the potential for integrating the signal several times, as with solutions nebulisation, may offer a further improvement in precision.

The flash lamp energy of the laser was found to be directly related to the emission intensity of all the elements examined. The lamp energy affects the laser output energy and hence the irradiance at the sample surface. It was found that the maximum lamp energy of 70J should be used to achieve greatest sensitivity. However, the ability to reduce lamp energy is likely to be useful when measuring elements of high concentration. Reducing lamp energy reduces sensitivity and would avoid saturation of the detector for elements such as titanium.

The carrier gas flow was optimised at 0.7 litres per minute of argon.

Laser ablation ICP provides a rapid and simple method to produce qualitative and semi-quantitative measurements on paint samples. Quantitative analysis by ICP would require a lengthy and labour intensive sample preparation technique to digest samples of paint. With laser ablation and a simultaneous ICP spectrometer

data on 34 elements may be obtained in approximately two minutes.

Quantitative analysis by laser ablation should also be feasible. A detailed study of calibration for laser ablation has been performed by Thompson [141]. He considered analysis of reference steels by laser ablation following conventional aqueous calibration. He concluded that matrix effects limit the use of aqueous calibration for the analysis of solids. However, this may be overcome by the use of a set of empirical matrix coefficients to correct for these effects.

Due to insufficient time, direct quantitative analysis of paints was not considered in this work. However, the possibility of performing quantitative analysis by ablating aqueous standards and digests of paints and polymers is to be considered in chapter six.

5.3 EXPERIMENTAL (POLYMERS)

Like paints, polymers such as polyvinylchloride (PVC) and rubbers, are relatively difficult to digest for atomic spectroscopic studies [137]. Sample preparation can take over 24 hours. Direct analysis by laser ablation offers much shorter times for the determination of trace elements and avoidance of other problems associated with sample digestion such as decreased absolute detection limits.

The presence of trace elements in polymeric materials can cause significant changes in the properties of such materials. Inorganic compounds are used as fillers and additives to control parameters such as elasticity, strength and durability. Hence the interest in the determination of elemental species in polymeric composite materials more commonly known as plastics.

5.3.1 Materials

Argon : High purity grade (British Oxygen Co.)

Graphite: High purity grade (Spectrochem Supplies Ltd.)

Polymers: Polyvinylchloride, a synthetic rubber and Polypropylene.

All graphite components were fabricated in the workshops at Sheffield City Polytechnic.

5.3.2 Apparatus

The Jarrell Ash ICAP 9000 ICP system was used in conjunction with the laser, its optics and the laser ablation chamber as described in chapter three.

5.3.3 The Effect of Laser Mode

The effects of laser operating mode and ablation period were studied by running two time studies. In the first a single Q-switched shot was fired 5s into the study followed by 5s repetitive Q-switched firing after a further 55s. In the second time study, the same ablation periods were used at the same points in time but the laser was operated in the long pulse mode. The time studies were 120s long.

The sample examined was a piece of polypropylene which was placed on the floor of the laser ablation chamber. The focusing distance used was 91mm which was achieved by raising the laboratory jack slightly. All other conditions were as optimised and discussed earlier.

5.3.3.1 Results

The time studies for aluminium, iron, nickel and titanium are given in figure 83. The peaks to the left are produced by the single shot, the ones to the right by 5s repetitive firing at 10Hz. The diagrams show both studies overlaid.

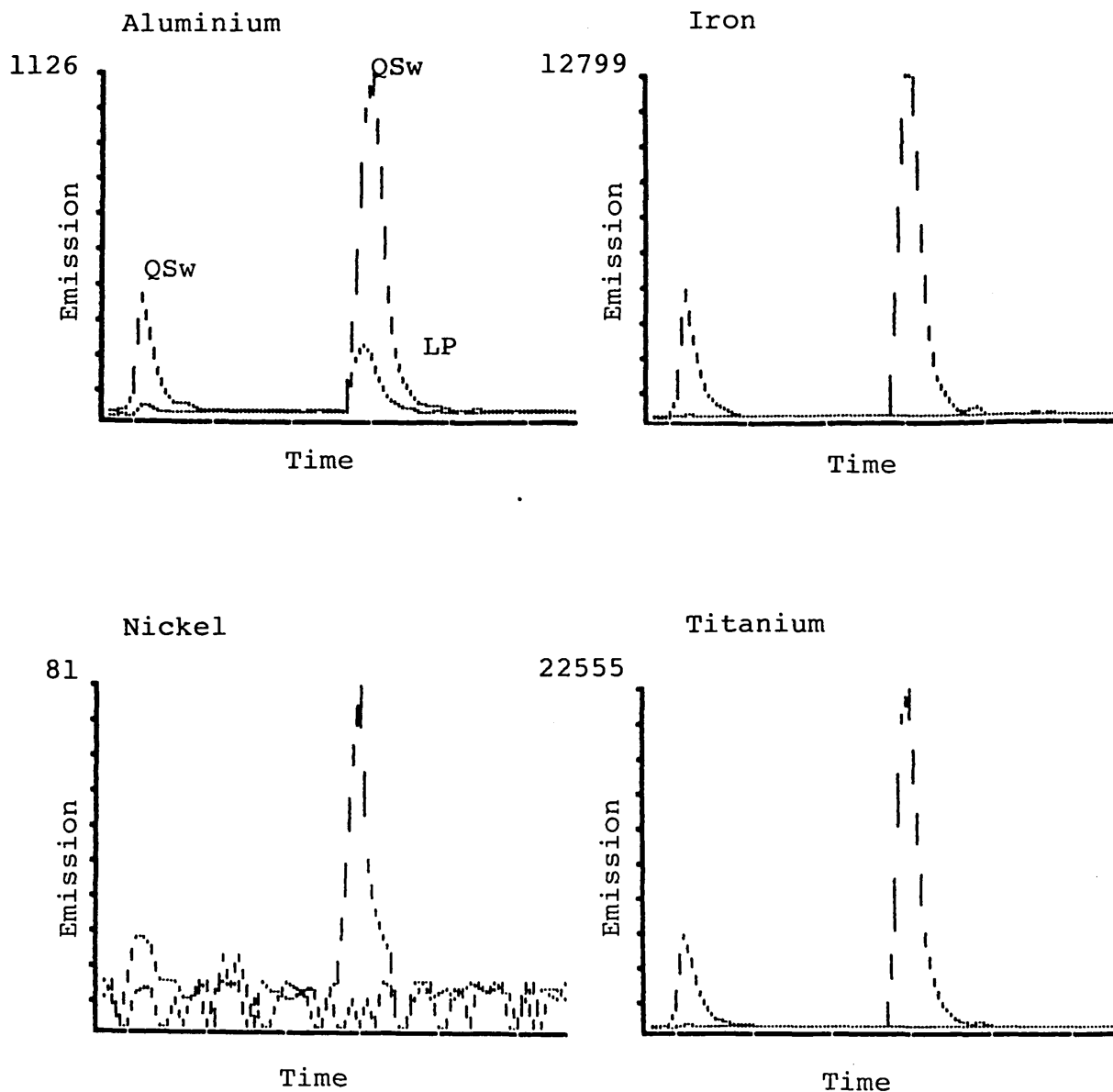


Figure 83. Emission Time Profiles for Four Elements in Polypropylene. Peaks to the Left are due to Single Laser Shots, those to the Right are due to 5s Repetitive Ablation. Time Studies for both Modes of Laser Operation are Overlaid but only Aluminium Generated Detectable Signals using Long Pulsed Mode. The Time Axis is 120s Long and Maximum Emission Intensities are given on the Y-axis.

Typical craters produced by single shots in both modes are shown in photographs 5 and 6.

5.3.3.2 Discussion

The results agree with all previous experiments in that they show Q-switched operation to produce emission signals of greatest intensity. In fact, aluminium and magnesium were the only elements to show a signal for long pulsed operation.

As expected, emission signals of even greater intensity are observed when using a 5s repetitive ablation period rather than a single shot. It was suggested earlier (see section 5.2.4) that increased ablation periods may be useful for analytes present at trace levels. This has been confirmed by the time studies for nickel. A single Q-switched shot produced a signal which is barely detectable when considering the level of noise present. Increasing the ablation period to 5s produces a signal which is approximately 5 times greater than the background noise level thus confirming the presence of nickel.

Examination of the craters revealed interesting though not unexpected differences. The crater produced by a single long pulsed shot (photograph 5) exhibits extensive melting and boring. The crater is relatively deep and a good deal of molten material has been ejected and lies around the crater on the otherwise undisturbed surface of the sample. The crater dimensions were



Photograph 5. Crater in Polypropylene Produced by a Single Long Pulsed Laser Shot. (60x Magnification)



Photograph 6. Crater in Polypropylene Produced by a Single Q-Switched Laser Shot. (100x Magnification)

found to be 530 microns along the major axis and 440 microns along the minor axis. The Q-switched shot (photograph 6) exhibits a relatively shallow crater and relatively little melting although the inner surfaces have been smoothed by slight melting. The area of interaction appears to have experienced a rapid (ie 9ns) shock wave which has broken off and displaced a "plug" of material which lies alongside the crater. This crater was found to have similar dimensions to that for long pulsed operation, 540 microns along the major axis and 465 microns along the minor axis.

The craters produced in polyethylene are somewhat smaller than those observed in metallurgical samples. This is thought to be due to the poorer thermal conductivity of polymers preventing heat being conducted into areas surrounding the point of interaction. The converse is true for metals and material is ejected from larger areas thus producing larger craters.

As with metallurgical samples and paint samples, the emission intensity data suggests that the material ablated in the Q-switched mode is more amenable to transportation in an argon stream to the ICP.

Twenty three elements were examined in the time studies. Detectable amounts of the following were observed; Al, Ba, Ca, Co, Cr, Cu, Fe, K, Mg, Mo, Mn, Na, Ni, Pb, Si, Zn and Zr although all were at levels just above background noise except for Al, Fe, Si, Ti and Zn.

5.3.4 Precision Study

The precision of replicate measurements was determined by firing six Q-switched shots at different areas of the polypropylene sample. The emission signal of each shot was integrated for 19s to include the whole of the peak profile. All other experimental conditions are given above.

5.3.4.1 Results

The integrated intensities for the elements that produce a significant emission signal under the experimental condition used are tabulated below. These values are total signal minus background intensity.

Element	Integrated Intensities (Counts)						%RSD
	1	2	3	4	5	6	
Al	5427	4761	4423	4297	5861	4340	12.2
Fe	54174	63685	41314	46192	46156	32266	20.8
Si	22291	19463	17052	20263	27118	18702	15.5
Ti	11096	9327	9775	8507	11247	8312	11.8
Zn	9278	8419	8264	9648	10324	8240	8.7

Table 24. Precision Data for Polypropylene.

5.3.4.2. Discussion

The precision is significantly inferior to that found for samples of wet paint. The most likely explanation of this is relatively poor sample homogeneity

on a microsampling scale. This is often encountered when ablating solid samples but this work has shown it to be less of a problem when ablating liquid paint.

The possibility of improving precision by utilising an internal standard was investigated. This was an attempt to compensate for changes in sample transport, the ablation process or atomisation and excitation processes in the plasma. It was found that using titanium as an internal standard produced the most significant improvement in precision as follows;

Al/Ti	5.0 %RSD
Fe/Ti	21.0 %RSD
Si/Ti	11.0 %RSD
Zn/Ti	10.0 %RSD

This data shows that internal standardisation can improve precision. Naturally, choosing the most appropriate element requires consideration and titanium may not be the best choice. Of the elements considered in this study titanium gave the most significant improvement in precision.

Internal standardisation offered improved precision for this solid material and it has been shown earlier that similar improvements were obtained when considering dried paint films. Consequently, when ablating solids internal standardisation may be necessary to achieve satisfactory reproducibility.

5.3.5 Comparative Studies

A comparative study of three polymeric materials was performed. Samples of a decorative white PVC, a synthetic rubber and polypropylene were used.

Three different time studies were recorded, one for each sample. The single Q-switched laser shot used was fired at different times in the time studies. Consequently, when all three were overlaid, three distinct peaks may be observed at different points along the time axis, each corresponding to a different sample. All the previously described optimised conditions were used.

A second comparative study was undertaken, looking more closely at the white PVC sample. This laminar material had a very shiny, decorative upper layer while below this was a very rough aerated surface. Both surfaces were examined by firing 4 Q-switched laser shots at each surface without moving the sample between shots.

5.3.5.1 Results

The time studies for aluminium, lead and titanium in the PVC, synthetic rubber and polypropylene are given in figure 84. These results show distinct differences between the samples. For example, the levels of titanium are by far the highest in the white PVC. It appears that titanium dioxide may have been used as a whitener in this material as it is in paints.

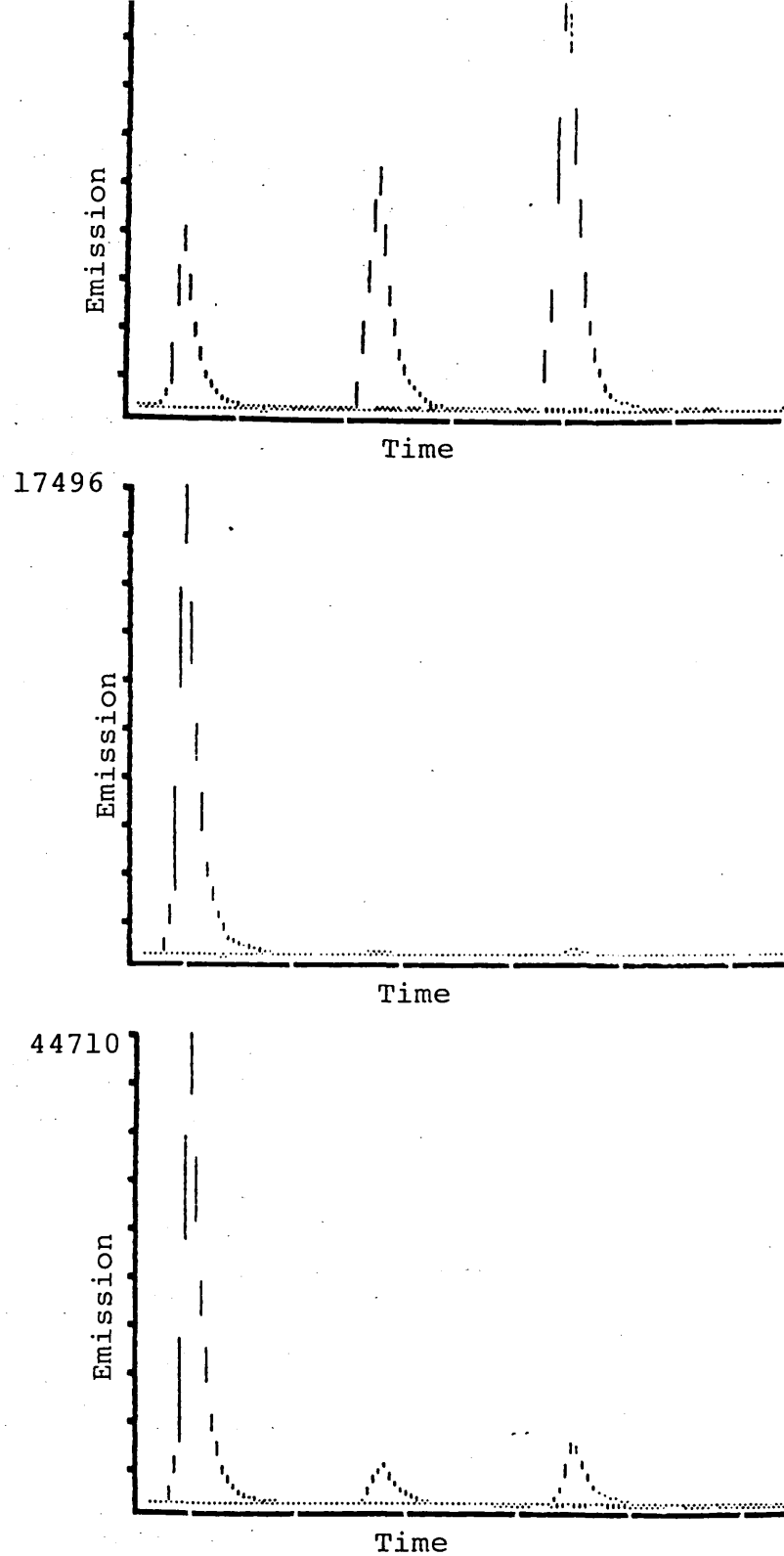


Figure 84. Emission Time Profiles During Laser Ablation of Polymeric Materials. Data are given for Aluminium (upper), Lead (middle) and Titanium (lower) in PVC (left peak), Synthetic Rubber (middle peak) and Polypropylene (right peak). The Time Axis is 120s Long and Maximum Emission Intensities are given on the Y-axis.

Closer examination of the PVC sample revealed a striking difference between the surfaces (see figure 85). A relatively high concentration of lead was found in the upper decorative surface.

5.3.5.2 Discussion

As with the comparative studies of paints, this work revealed differences between polymeric materials. Such information is obtained for upto 34 elements in a matter of minutes, although as solid materials, precision is worse than in paints. Examination of the four consecutive shots at the PVC sample clearly indicated erosion of analyte at the point of laser interaction.

The differences between the upper, decorative layer and the lower rough layer are also very interesting. A microsampling technique such as laser ablation is the only way to obtain such data. A traditional bulk analysis by wet digestion would not reveal this type of information.

5.3.6 An Application

Two sports racquets were examined to determine if their carbon fibre frames had received additions of boron as claimed by the manufacturers. Small pieces were cut from the shafts of both racquets and each piece examined by laser ablation ICP.

The inner surfaces of the test pieces were

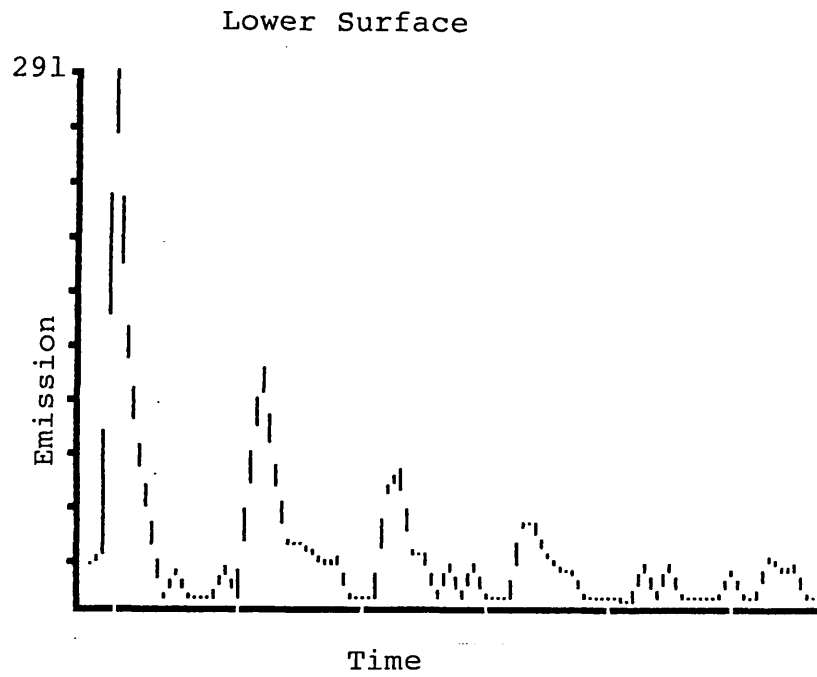
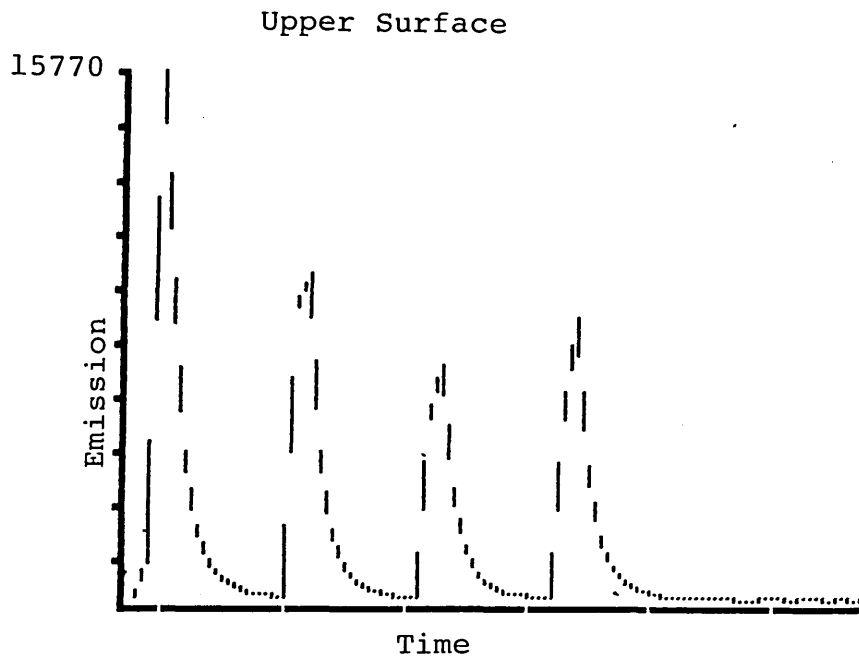


Figure 85. Emission Time Profiles During Laser Ablation of PVC. The Results Show the Peaks for Four Consecutive Q-Switched Laser Shots at the Upper Decorative Surface (upper diagram) and the Lower Surface (lower diagram). The Time Axis is 120s Long and Maximum Emission Intensities are given on the Y-axis.

ablated using 3 consecutive Q-switched shots at 70J and 10Hz. The emission intensity was measured at the boron line (249.77nm).

5.3.6.1 Results

The chart recordings for the three laser shots on each test piece are given in figure 86.

5.3.6.2 Discussion

The emission peaks from the badminton racquet are relatively small and agree closely with those obtained from spectroscopic grade graphite. This implies that boron is present as a contaminant only.

The squash racquet shows relatively intense emission from boron. Although the precision of the three measurements is not good, the implication is that the squash racquet has been treated with boron.

This result was achieved in a matter of minutes. Conventional analysis would have been laborious and taken at least one day for sample preparation alone.

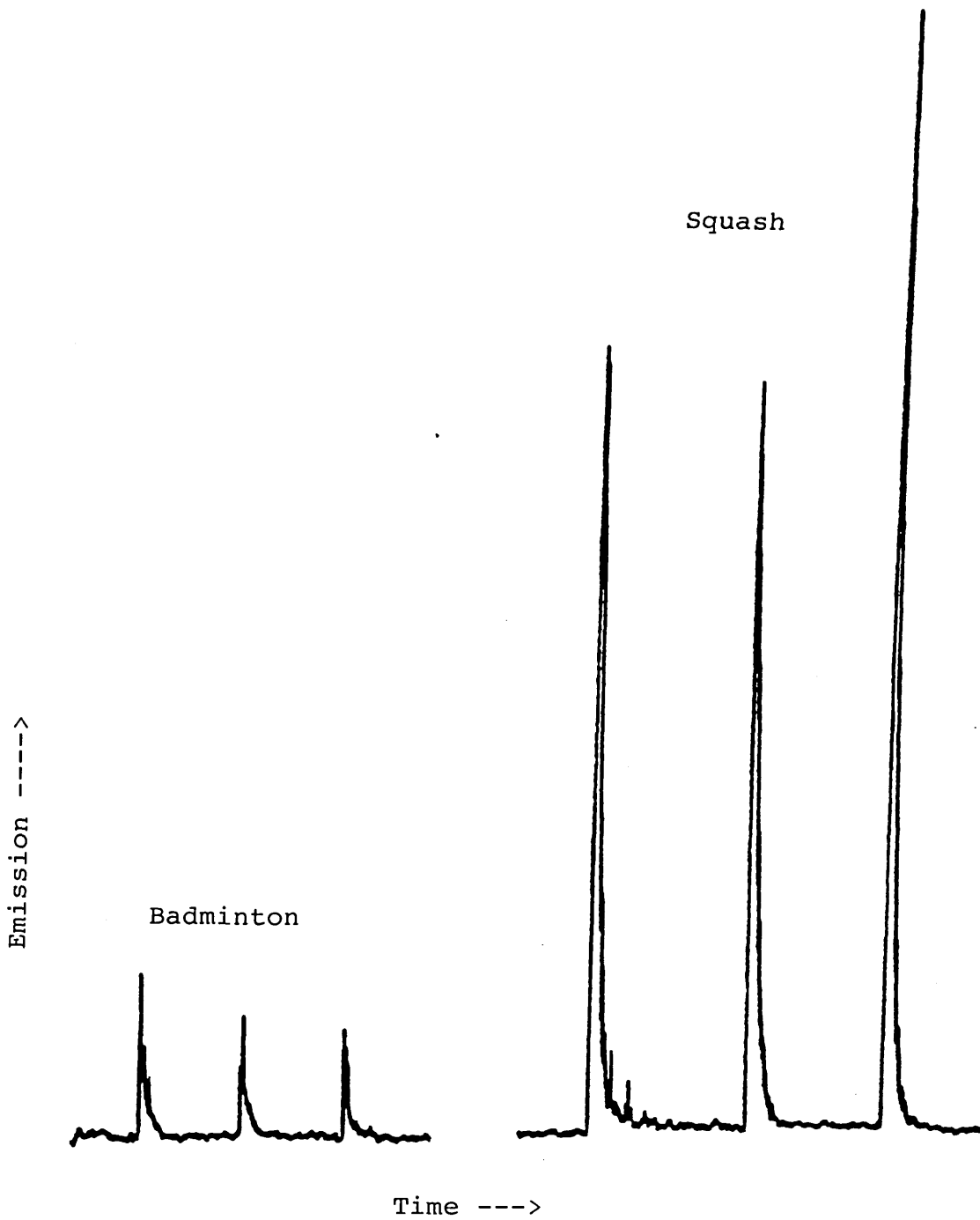


Figure 86. Emission Signals Generated by Long Pulsed Laser Ablation of Samples of Two Sports Racquets.

5.4 CONCLUDING REMARKS

This work has demonstrated that the technique of laser ablation ICP is suitable for measurements of paints and polymeric materials. Useful qualitative data can be obtained in very short times. The technique also provides information on spatial distributions of analytes which a conventional bulk analysis would not.

Various operating conditions were examined and optimised. The optimum conditions are in close agreement with those for metallurgical samples suggesting that the operating conditions may not be sample dependent.

Precision for liquid paint samples is good and represents some of the lowest RSD values reported for laser ablation studies. This is attributed to a combination of good homogeneity because the sample is liquid and viscosity effects. Liquids of lower viscosity would be more likely to spatter inside the ablation chamber leaving less sample material to be transported to the ICP. This was observed for aqueous standard solutions (see chapter 6).

Precision for solid polymers is relatively poor but may be improved by utilising a suitable internal standard. Again, it is a very simple matter to produce comparative qualitative data on such samples.

This work formed the basis of a publication [138] which was the first to consider laser ablation of paints and polymers for ICP spectrometry.

CHAPTER SIX

LASER ABLATION OF AQUEOUS SOLUTIONS

AND CALIBRATION STUDIES

6.0 INTRODUCTION

When considering the technique of laser ablation ICP spectrometry, the ultimate goal is to be able to analyse unknown samples with accuracy and precision. This introduces the requirement of calibration.

Calibration studies by laser ablation ICP have been performed by most research groups. Generally, these studies have utilised certified reference materials appropriate for the sample to be analysed. This has resulted in the almost exclusive examination of metallurgical and geological reference materials [84-90].

Generally, emission intensity for a given analyte is plotted against the certified reference concentration of the analyte. Some workers have reported improvements when using internal standards [86,87] both in terms of linearity and precision.

A major attraction of laser ablation is the ability to analyse solid samples directly, avoiding time consuming sample preparation. However, a suitable range of solid calibration standards is almost impossible to find, even for metallurgical analysis. Consequently researchers strive to achieve a situation where solid samples may be accurately analysed against a range of aqueous calibration standards.

Thompson [141] has considered the analysis of solid samples after calibration by conventional solutions nebulisation. The success of this study

relied on a lack of matrix effects associated with the sample material mobilised by laser ablation. However matrix effects were observed but it was proposed that suitable correction factors may be applicable to convert an aqueous analyte response to laser ablation conditions.

Due to insufficient time, the analysis of solid after aqueous calibration was not examined. However, the feasibility of ablating aqueous standards for calibration was studied. The ablation of liquids by laser radiation has been reported [142] and forms the basis of Laser Induced Breakdown Spectroscopy.

Calibration studies have also been performed using the electrothermal vaporisation facility of the ablation chamber described. This allowed direct comparison of laser ablation with ETV.

6.1 CALIBRATION STUDIES

For laser ablation measurements of synthetic standard solutions, the solution may be pipetted into the sample cup and ablated directly. Alternatively, it may be dried and the residue on the surface of the graphite sample cup ablated.

Ablation of dried residues increases the time taken to make a measurement by virtue of the electrothermal drying required. Furthermore, the most prominent laser interaction is that with the graphite cup. This is likely to produce significant amounts of particular graphite which may disturb the plasma and as the area of interaction is relatively small, the amount of analyte ablated will also be small.

Direct ablation of solutions is likely to result in larger masses of analyte being mobilised for transport to the plasma. This is particularly so for refractories which form carbides when dried on graphite surfaces. This improved mobilisation efficiency is due to the entire liquid aliquot being sampled by the laser rather than a small area of a residue. This was proven

experimentally as a 30 microlitre aliquot of deionised water was entirely eroded by a single Q-switched laser shot leaving the sample cup empty. Clearly, the entire 30 microlitres had not reached the plasma as some of the larger droplets condensed out on the sample chamber walls but a larger mass of analyte was available for laser ablation.

Considering that this degree of erosion was not demonstrated by wet paint samples, the above observation suggests that the viscosity of liquid samples plays a significant role in the ablation process.

One further consideration when ablating dried residues was contamination of the cups themselves. It was found that ablating an empty cup produced significant emission intensity for many elements particularly iron. Consequently, all further work was performed using direct ablation of solutions.

The Jarrell Ash ICAP 9000 system was used for this work. All operating conditions and apparatus were as described in earlier chapters. All synthetic standard solutions were purchased from BDH of Poole UK. These solutions were single element 1000mg/L solutions which were diluted with deionised water as required.

6.1.1 The Effect of Ablation Period

As with previous sample types, the effect of ablation period was investigated when ablating synthetic

aqueous standards. The standard used was a 250mg/L solution of cadmium, copper, lead and zirconium.

Prior to a measurement being made, the graphite sample cup was cleaned in-situ. With the ablation chamber on-line, the cup was ablated repetitively in the Q-switched mode for 25s. This was sufficient to remove most of the surface contamination.

A 30 microlitre aliquot of the standard solution was pipetted into the cleaned sample cup and the chamber placed on-line. The sample was then ablated using the laser in the Q-switched mode at 70J and 10Hz. All other ICP and laser operating conditions have been given earlier. This experiment was conducted five times using a single shot, 1s, 2s, 5s and 10s repetitive firing. Each experiment utilised a new, laser cleaned sample cup and a fresh standard aliquot. An integration time of 25s was used to ensure that the entire analytical peak was measured and the laser was fired as the exposure light illuminated on the spectrometer.

6.1.1.1 Results

It was observed that after firing of all laser shots, the sample cup was empty. Even a single Q-switched shot was sufficient to displace the 30 microlitre sample from its cup. However, some of the sample had spattered onto the walls of the ablation chamber so ablation efficiency was not 100%.

The integrated emission intensities less plasma

background intensities are given below in table 25.

	lshot	1s	2s	5s	10s
Cd	327	974	1567	2794	1741
Cu	804	2415	3750	4702	3414
Pb	623	2312	4545	6729	4606
Zr	819	2536	5755	8371	7072

Table 25. Emission Intensities for Aqueous Standard as a Function of Ablation Period

The above data is shown graphically in figure 87.

6.1.1.2 Discussion

As with metallurgical and polymeric samples, ablation period has a pronounced effect on emission intensity of aqueous solution. Increasing the ablation period increases emission intensity and hence analytical sensitivity, but only to a point. Emission intensity is seen to decrease at ablation periods longer than 5s. This is due to the sample being completely removed from the cup and any further ablation interacting with the graphite cup only. Hence, rather than forming a plateau as with metals and polymers the curve shows a marked decrease in intensity.

Maximum sensitivity may be achieved by ablating for upto 5s repetitively for a 30 microlitre sample.

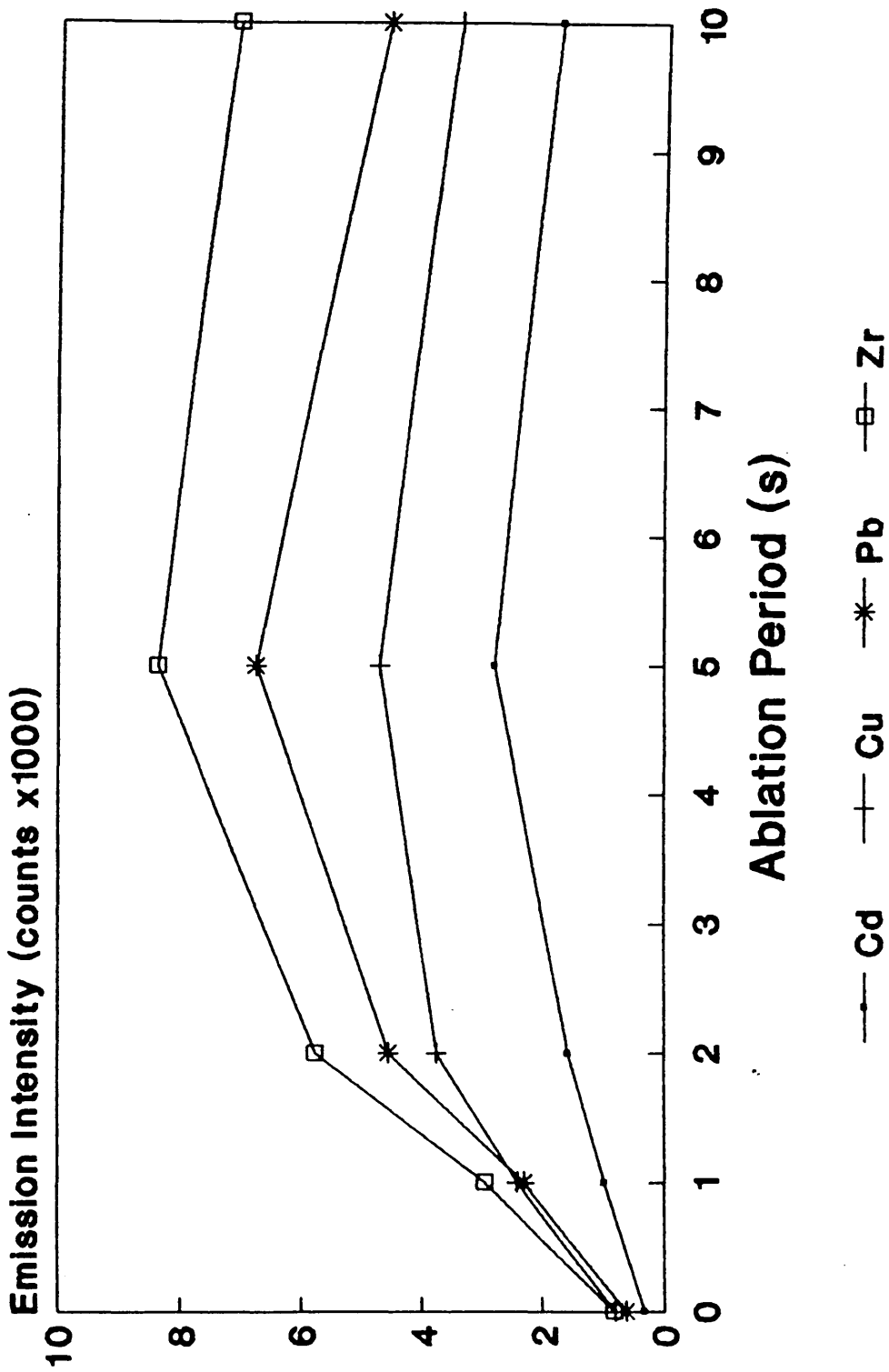


Figure 87. Emission Intensity as a Function of Ablation Period for Aqueous Solutions. The Sample Solution was at a Concentration of 250mg/L for the Four Elements of Interest.

However, some of this 5s ablation period samples the empty sample cup.

6.1.2 Simple Two Point Calibration

This initial calibration study relied on the well known property of ICP's that calibration curves are linear over 4-6 orders of magnitude. A simple two point calibration was used from 0-100mg/L and linearity between these points was assumed.

Deionised water was used as the lower standard and a solution containing 100mg/L aluminium, calcium, chromium, potassium, sodium and nickel was used as the top standard.

A sample cup was placed into the ablation chamber in the usual way. This was then cleaned by repetitive ablation of the sample cup for 25s. This process used Q-switched laser shots at 70J lamp energy and 10Hz. Once "clean", 30 microlitres of deionised water was pipetted into the cup and the chamber turned on-line with the ICP. This sample was then ablated repetitively for 5s using the Q-switched mode at 70J and 10Hz. The resultant emission signal was integrated for 25s. This blank value was obtained in triplicate.

The sample cup was replaced and the replacement cup cleaned. The above procedure was repeated five times using the 100mg/L standard.

This was sufficient to produce calibration curves but three samples were also examined. Acid

digests of a synthetic rubber, PVC and brilliant white gloss paint were used as samples and analysed using the above procedure in triplicate. A new sample cup was used for each sample solution.

Three samples were prepared for analysis, 0.2088g of paint, 0.3266g of PVC and 0.1708g of synthetic rubber were digested. Each was subjected to microwave digestion utilising Aristar grade sulphuric acid and hydrogen peroxide. The paint digest was diluted to 25ml with deionised water and the other samples diluted to 50ml.

Examination of the calibration data showed that of the six elements examined only aluminium and chromium had produced signals of any significance. Consequently, it is the data for these elements that will be considered.

6.1.2.1 Results

The raw emission intensity data for aluminium and chromium are given below in table 26.

The resultant calibration curves using the mean values for the blank and 100mg/L solution are shown in figure 88.

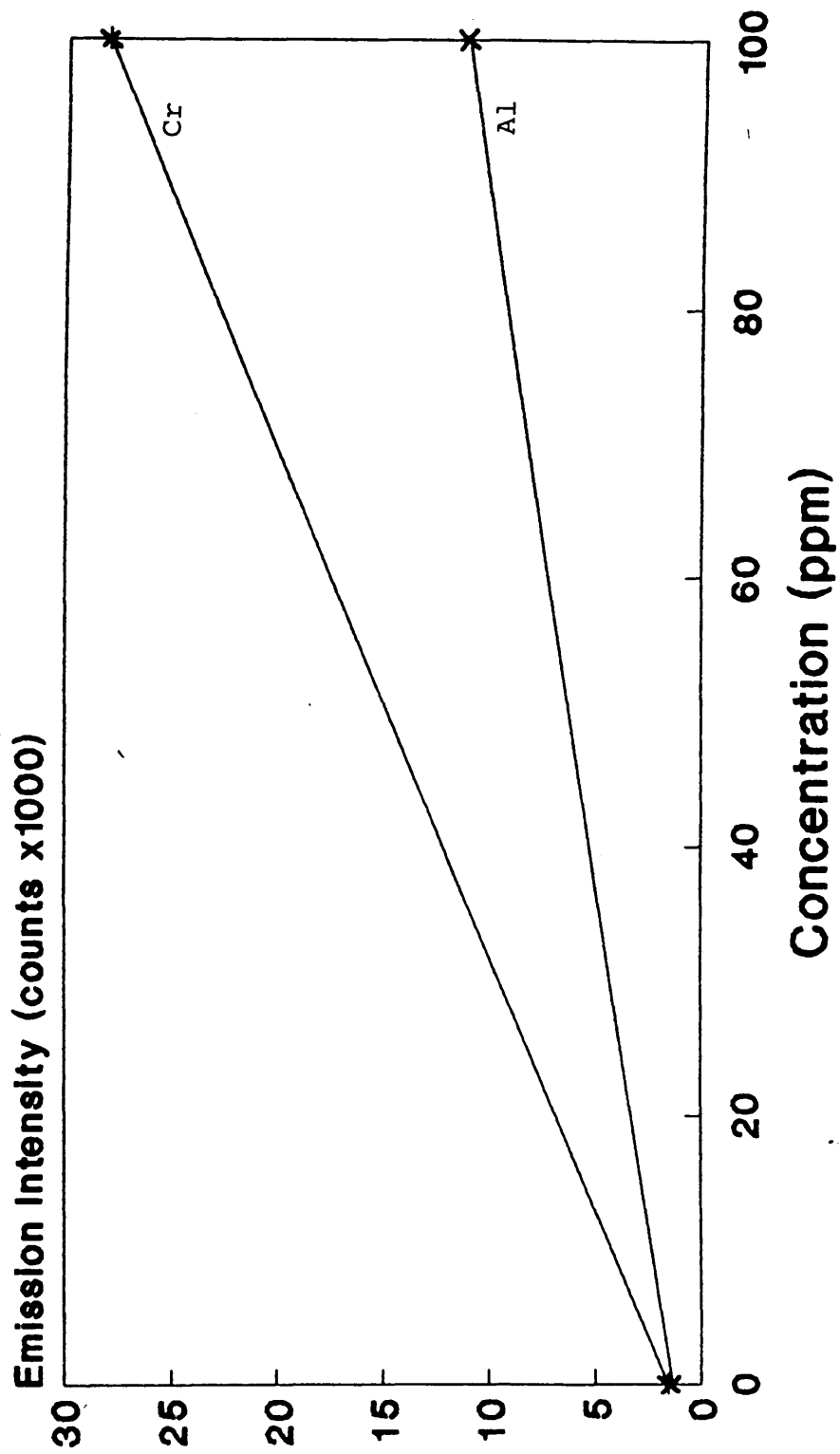


Figure 88. Two Point Aqueous Calibration for Chromium and Aluminium.

	<u>Emission Intensity (counts)</u>			
	<u>Aluminium</u>		<u>Chromium</u>	
	Blank	100mg/L	Blank	100mg/L
1	1410	10011	1510	23936
2	1347	12172	1688	32498
3	1244	13794	1398	37749
4		10293		22198
5		9721		24247
Mean	1334	11198	1532	28126
%RSD		14		21

Table 26. Emission Intensity Data for Two Point Calibration Curves

The calibration lines are described by the following equations;

$$\text{Al :- } y = 98.64x + 1334$$

$$\text{Cr :- } y = 265.94x + 1532$$

The emission intensity data for the sample solutions are given below in tables 27 and 28 for aluminium and chromium respectively. All concentration values are given in mg/L.

Aluminium:-

sample	Rubber		PVC		Paint	
	Counts	Conc	Counts	Conc	Counts	Conc
1	15702	145.7	1406	ND	14068	129.1
2	10827	96.2	1516	ND	10757	95.5
3	13638	124.7	1475	ND	8634	74.0
Mean	13389	122	1466	ND	11153	100
Result(mg/L)	122 ± 20		Not Detected		100 ± 23	

Table 27. Intensity Data and Derived Concentrations of Aluminium in Rubber PVC and Paint.

Chromium:-

sample	Rubber		PVC		Paint	
	Counts	Conc	Counts	Conc	Counts	Conc
1	3131	6.0	1180	ND	1716	ND
2	1797	1.0	1415	ND	1567	ND
3	2100	2.1	1314	ND	1576	ND
Mean	2343	3.0	1303	ND	1620	ND
Result(mg/L)	3.0 ± 2		Not Detected		Not Detected	

Table 28. Intensity Data and Derived Concentrations of Chromium in Rubber PVC and Paint.

ND = Not Detected.

Confidence limits for the above results are one standard deviation.

The above concentration values are derived by calculation using the mean intensity values in the above equations.

Having obtained these concentration values by laser ablation, the sample solutions were analysed by conventional solutions nebulisation. The results of laser ablation and conventional analysis are given below in table 29, the latter are given in parentheses. All values in mg/L.

	Synthetic Rubber	PVC	Paint
Al	122 (110)	ND (1.5)	100 (130)
Cr	3 (2.4)	ND (ND)	ND (0.4)

Table 29. Results Obtained by Laser Ablation and Analysis by Conventional Solutions Nebulisation.

6.1.2.2 Discussion

ICP calibration curves are linear over several orders of magnitude. Consequently, a two point calibration from zero to 100mg/L should be analytically valid. The above calibration and analysis produced results which are in reasonable agreement with those obtained by conventional ICP analysis.

Although chromium was not detected in the samples of PVC and paint by laser ablation, the result for rubber is in good agreement with that obtained by conventional analysis. The results suggest that

concentrations of approximately 3mg/L are the lowest detectable.

Significant levels of aluminium were present in the samples and the results show good agreement with conventional results. Precision of replicate measurements is a problem and if it could be improved, the data suggests that greater accuracy could be achieved and the confidence limits on the results could be narrower.

The relatively poor precision is due to two main characteristics of the measurement. Firstly, the 5s repetitive laser firing was controlled by throwing a switch on the lasers remote control to "repetitive" for 5s then throwing it back to "single shot". In the latter situation the "fire" button needed to be pressed to produce a laser shot. The measurement of the 5s ablation period relied on a digital stop watch. The inevitable variations in ablation period around the nominal 5s would clearly introduce sampling errors. Secondly, the standards and samples have relatively low viscosity and laser ablation spatters all the sample from its cup (see section 6.1.4). Consequently, ablation and sample transport efficiencies will vary from sample to sample.

A further consideration is the level of contamination in the sample cup. Since a single Q-switched shot is sufficient to spatter all 30 microlitres of sample from the cup, most of a 5s ablation

period interacts with the cup and not the sample.

Considering these sources of error the data produced by laser ablation is in surprisingly good agreement with conventional analysis.

6.1.3 Further Calibration Studies

Two further calibration studies were performed. The first considered relatively volatile elements (cadmium, lead and zinc) in the range 1,10 and 100mg/L. A 1000mg/L standard was used for cadmium only. This experiment considered the emission intensities for increasing concentration of analyte but further examined the effects of ablation period by calibrating using 2s and 5s ablation periods.

The second study considered refractory elements (titanium, aluminium and chromium) in the range 0, 50, 100, 500 and 1000mg/L. Several samples were also measured to examine the accuracy of analysis by laser ablation.

A range of multi-element calibration solutions were prepared from BDH stock solutions. Standards of 1, 10 and 100mg/L cadmium, lead and zinc were made up by dilution of the stock with deionised water. Thirty microlitre aliquots were dispensed into laser cleaned sample cups and ablated for a period of 5s using Q-switched mode, at 70J and 10Hz. Each solution was measured once only in a new laser cleaned sample cup.

Having performed a calibration using a 5s ablation period, the above procedure was repeated using a 2s ablation period. Again, only single measurements were made for each solution.

Integration times of 25s were used as this was just sufficient to integrate the whole transient peak. The raw data produced are given below in table 30.

The calibration study of refractory elements utilised standard solutions of 50, 100, 500 and 1000mg/L titanium, aluminium and chromium. Again, 30 microlitre aliquots were used in laser cleaned cups but the measurement of each solution was made in triplicate. Furthermore, before each standard solution a "blank" was obtained by ablating a 30 microlitre aliquot of deionised water. All measurements were made using a 5s ablation period in Q-switched mode at 70J and 10Hz. The raw data are given below in table 31.

After calibration five blank aliquots were ablated to determine limits of detection.

6.1.3.1 Results

The raw data for cadmium, lead and zinc are tabulated below, and shown graphically in figures 89-91 respectively.

Conc (mg/L)	Emission Intensity (counts)					
	Cd		Pb		Zn	
	2s	5s	2s	5s	2s	5s
1	186	157	846	776	495	440
10	534	495	846	1353	2875	3109
100	6212	5834	5436	4644	21000	28680
1000	45540	67910	--	--	---	---

Table 30. Calibration Data for Volatile Elements.

The raw data for titanium, aluminium and chromium are given in table 31 overleaf and shown graphically in figures 92-94 respectively.

The calibration curves in figures 92-94 inclusive are plots of concentration versus mean minus blank intensities.

A series of samples were ablated to relate the emission intensity to the above calibrations. The data for the refractory elements are described by the following linear equations;

$$\text{Al:- } y = 110.907x + 0$$

$$\text{Correlation coefficient} = 0.9809$$

$$\text{Cr:- } y = 328.672x + 0$$

$$\text{Correlation coefficient} = 0.9961$$

$$\text{Ti:- } y = 665.107x + 0$$

$$\text{Correlation coefficient} = 0.9931$$

Element and Conc (mg/L)	Emission Intensity (counts)			Mean (M) (counts)	Blank (B) (counts)	M-B (counts)
	1	2	3			
Ti 0	3621	4398	4471	4163	4163	0
50	41891	26767	36920	35193	4720	30473
100	54760	83520	49070	62450	3995	58455
500	181400	658200	409300	416300	17719	398581
1000	615400	648200	668800	644133	11095	633038
Al 0	1039	965	1298	1101	1101	0
50	7137	4788	5992	5972	1164	4808
100	8632	13380	8494	10169	1098	9071
500	29870	107600	71690	69720	2745	66966
1000	100100	110800	112800	107900	2511	105389
Cr 0	2731	2492	2515	2579	2579	0
50	19550	27969	22748	23422	2584	20838
100	55770	48780	28480	44343	5167	39176
500	79250	270800	155800	168617	5983	162634
1000	200600	205400	209000	205000	7931	197069

Table 31. Raw Data for Titanium, Aluminium and Chromium.

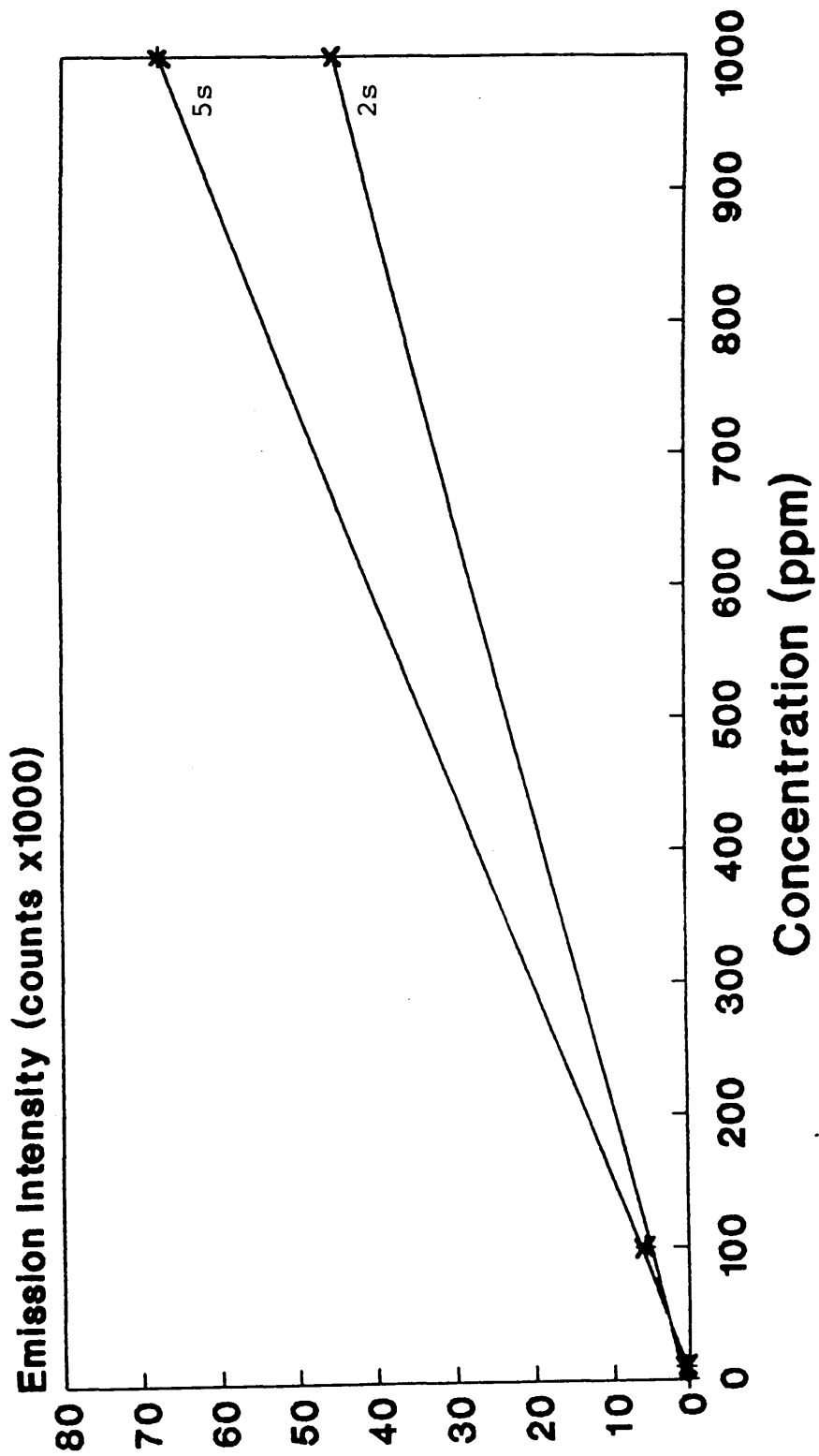


Figure 89. Aqueous Calibration for Cadmium using 2s and 5s Ablation Periods.

See text for further details.

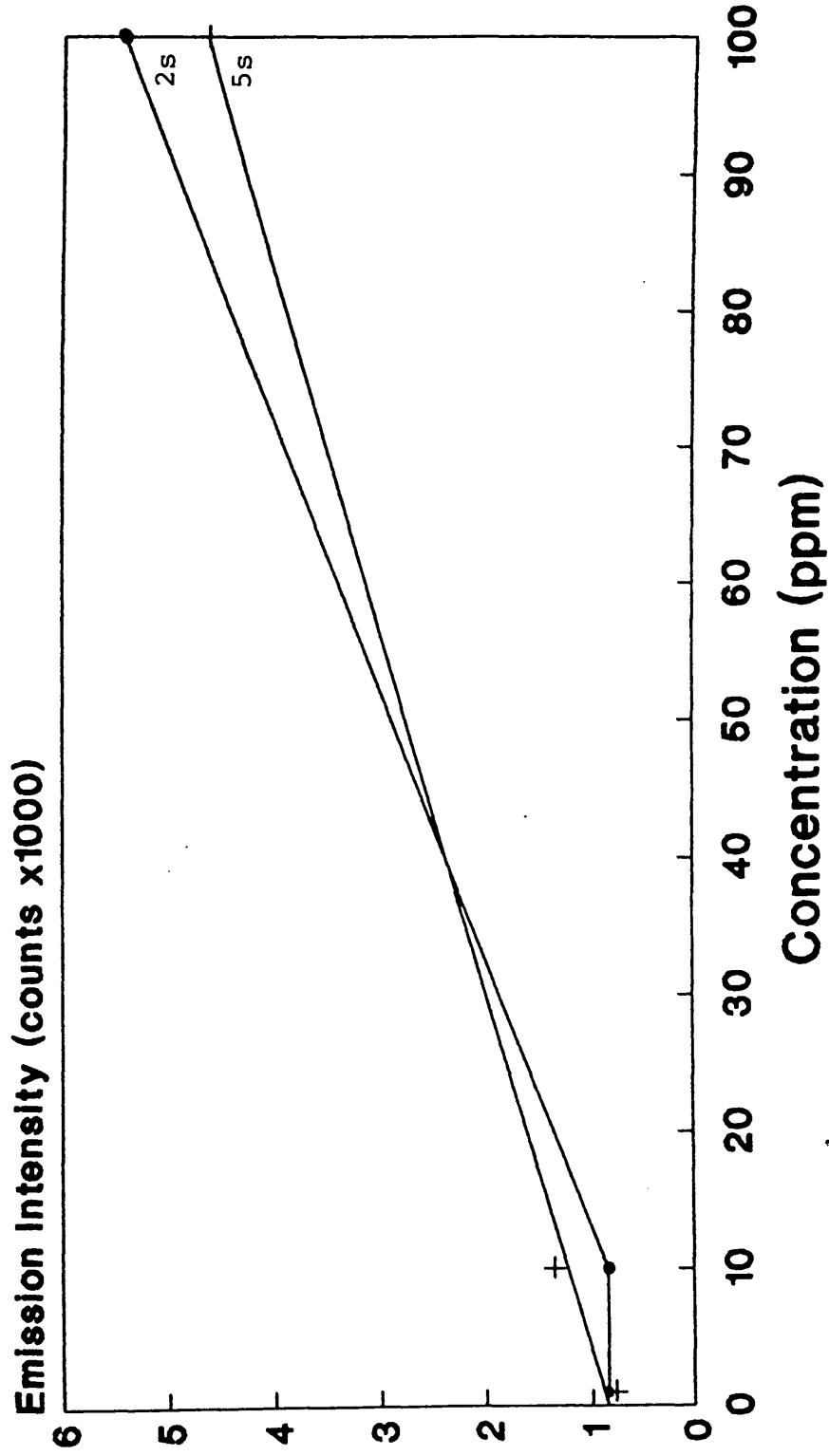


Figure 90. Aqueous Calibration for Lead using 2s and 5s Ablation Periods.

See text for further details.

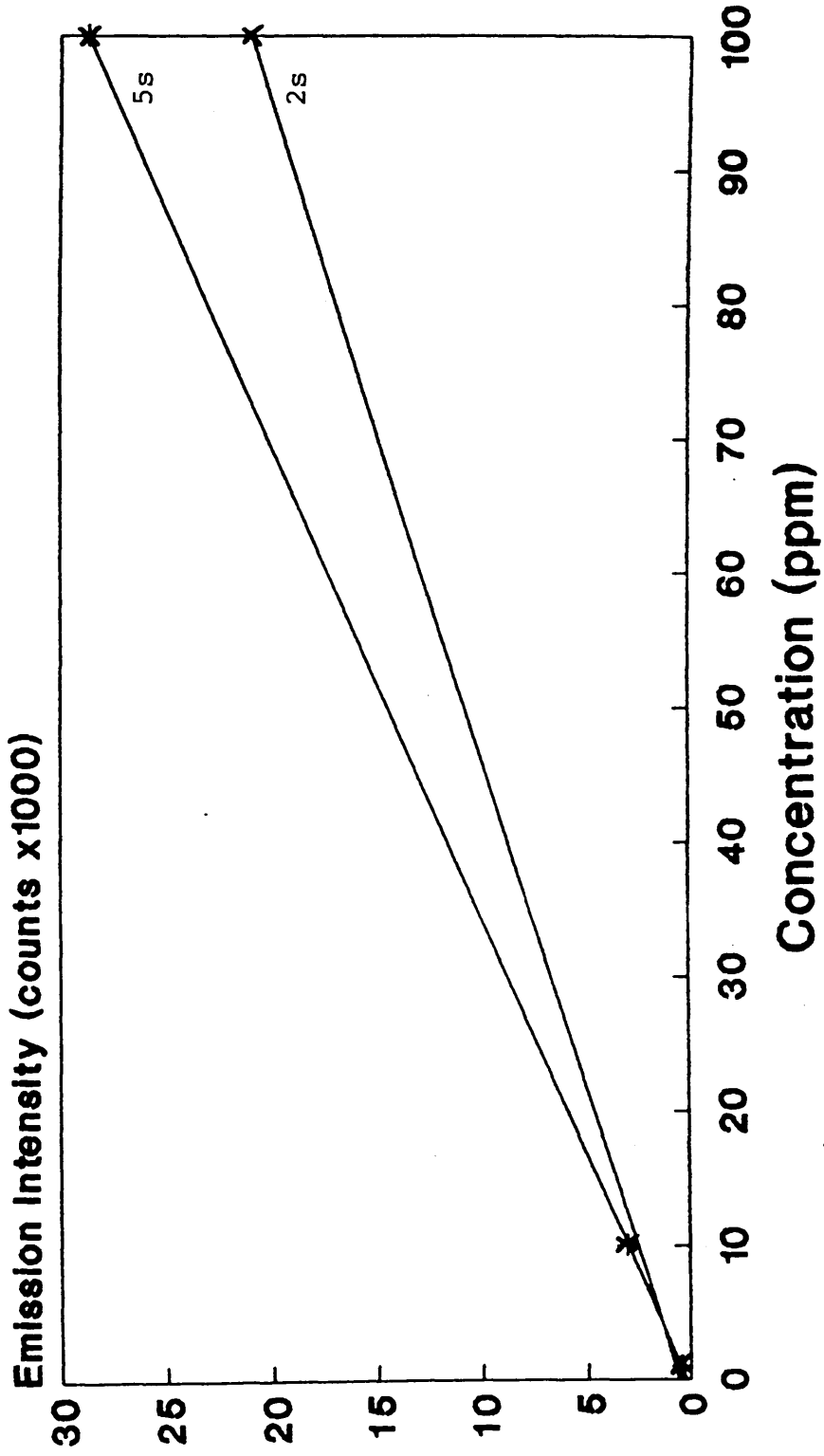


Figure 91. Aqueous Calibration for Zinc using 2s and 5s Ablation Periods.

See text for further details.

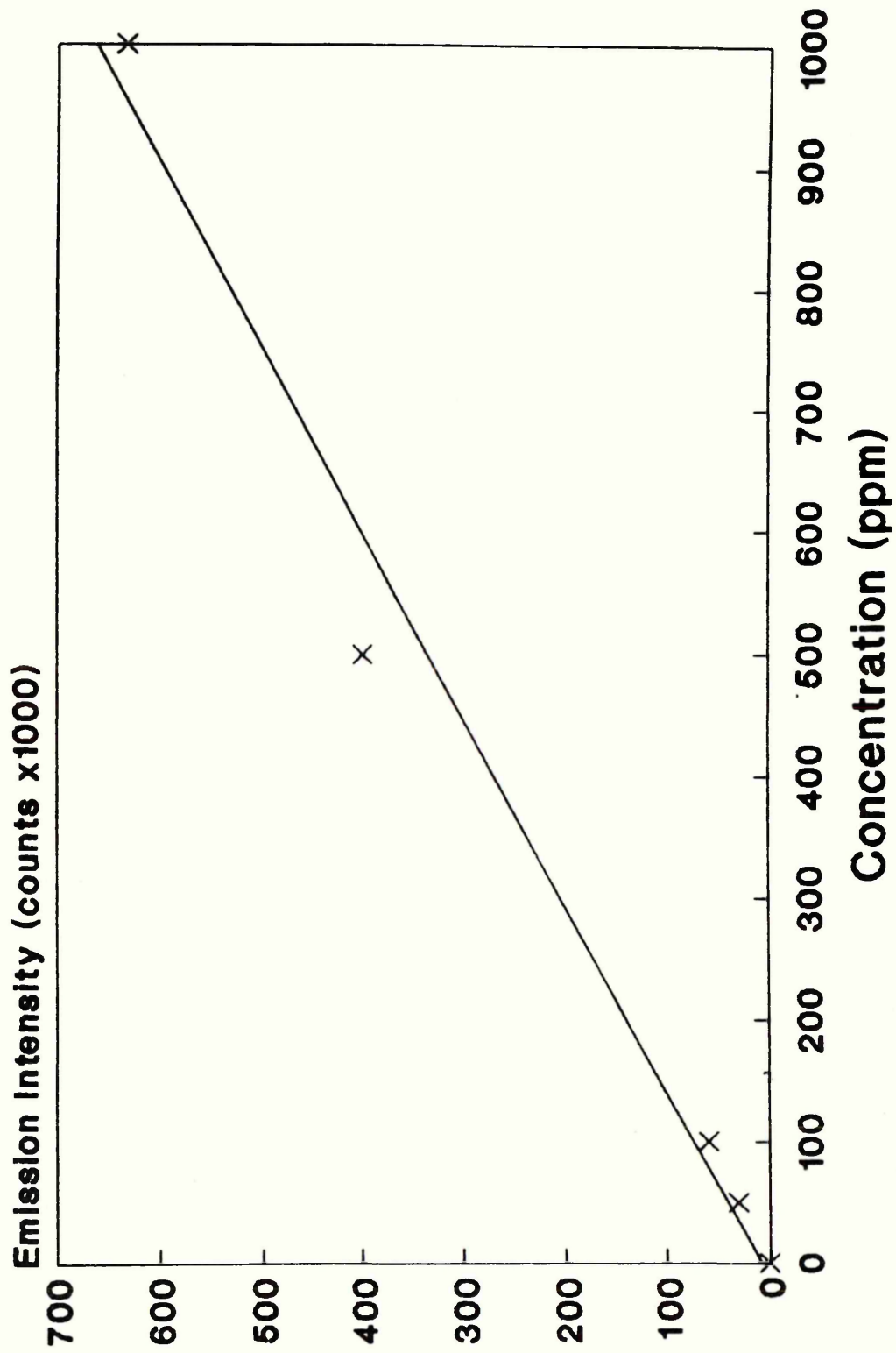


Figure 92. Calibration Graph for Titanium by Laser Ablation of Aqueous Standards.

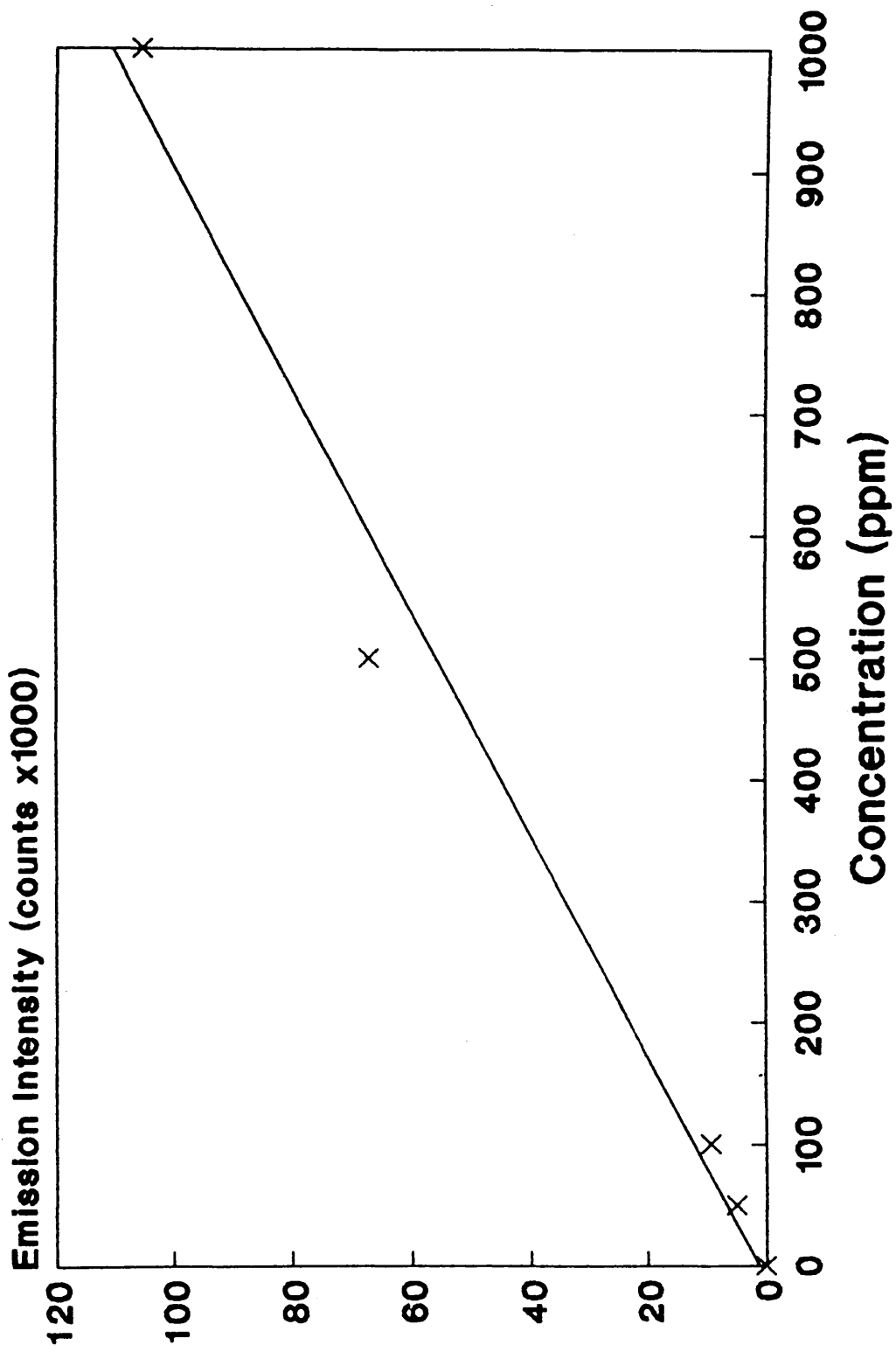


Figure 93. Calibration Graph for Aluminum by Laser Ablation of Aqueous Standards.

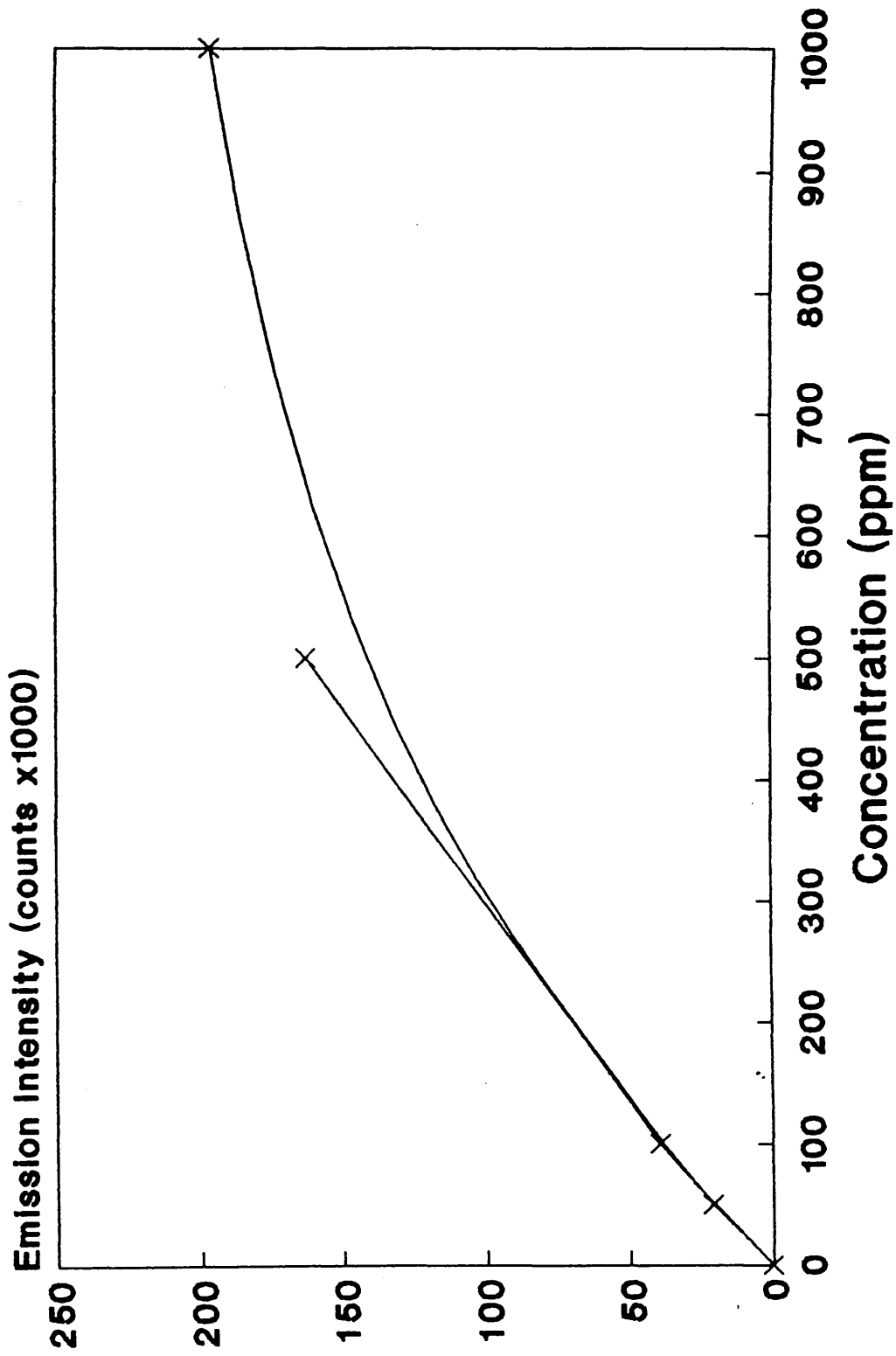


Figure 94. Calibration Graph for Chromium by Laser Ablation of Aqueous Standards.

These equations describe straight lines which pass through the origin. That for chromium considers only the linear portion of the graph ie upto 500mg/L.

The sample intensities (minus blank values) are given below:

	Al	Cr	Ti
PVC	241	3703	41407
Rubber	10760	407	11671
Paint	294033	4093	Too High

The above emission intensity data may be used to determine analyte concentration utilising the above linear equations. The results are tabulated below:

	Al (mg/L)	Cr (mg/L)	Ti (mg/L)
PVC	ND (1.5)	11 (0.1)	62 (81)
Rubber	97 (113)	ND (0.1)	18 (20)
Paint	2700 (133)	12 (0.4)	-- --

The values in parentheses are those obtained by conventional solutions analysis.

6.1.3.2 Discussion

The investigation of ablation period revealed that an increase in sensitivity can be achieved by using a 5s ablation period rather than 2s. It was discussed earlier that a single Q-switched shot was

sufficient to spatter a 30 microlitre aliquot completely leaving the sample cup empty. Consequently, longer ablation periods interact with the sample cup. Since the results show that a 5s ablation period improves sensitivity, this suggests that some of the analyte is associated with the graphite sample cup.

Electrographite is a porous material and it is likely that the sample is partially absorbed into the cups surface. This fraction of analyte is ablated along with the graphite during the longer ablation periods.

The refractory elements aluminium, chromium and titanium are particularly appropriate for laser ablation. Aluminium and titanium demonstrate linearity upto 1000mg/L while the chromium data suggests some curvature at concentrations higher than 500mg/L. Very low concentrations would be difficult to determine using the system described. The lowest concentrations that may be expected to be measurable are approximately 5mg/L Ti, 10mg/L Al and 5mg/L Cr. However, detection limits were found to be 1.7mg/L, 2.6mg/L and 0.9mg/L respectively.

Some of the above results obtained by laser ablation are in good agreement with results obtained by conventional solutions nebulisation eg titanium and aluminium in rubber. However, some are not. Reasons for this should be the subject of further investigation.

6.1.4 Precision Study

The replicate measurements reported above for aqueous standards show relatively poor precision. This may be due to the small number of measurements made ie three. Consequently, precision was studied in a litte more detail by performing nine measurements.

This experiment utilised a multi-element standard containing cadmium, copper, lead and zirconium all at 100mg/L. A 30 microlitre aliquot was pipetted into a laser cleaned sample cup and ablated for 5s using Q-switched mode, 70J lamp energy and 10Hz frequency. The emission intensity was integrated for a period of 25s. This procedure was repeated nine times using a new sample cup for each determination.

The intensity data is presented in table 32 with the resultant mean, standard deviation (S.D.) and precision (%RSD) values.

Clearly, laser ablation measurements of aqueous solutions under the conditions described are relatively imprecise, the most likely reason for this is the method used to control the 5s repetitive ablation period ie by manually throwing a switch and using a stop watch. A second contributory factor is believed to be the low viscosity of the solutions. All of the sample is removed from the cup, consequently the laser spends some time sampling the cup itself.

	Emission intensity (counts)			
	Cd	Cu	Pb	Zr
1	6900	19021	5442	17917
2	4677	17159	3261	12366
3	8043	22863	6322	21427
4	6252	18772	4868	15884
5	4661	15983	3451	12066
6	5377	17444	3987	13342
7	4622	15265	3476	12229
8	4235	15545	3066	11332
9	3783	12409	2868	10259
MEAN	5394	17162	4082	14091
S.D.	1317	2765	1128	3417
%RSD	24	16	28	24

Table 32. Precision Study Data.

The precision data is also presented in figure 95. This gives a very clear indication that the trends for Cd and Pb are very similar. The implication is that the use of an internal standard may improve precision. The trends for Cu and Zr show dissimilarities but internal standardisation may still offer improved precision.

Precisions were recalculated using the Cd/Pb ratio and the Cu/Zr ratio. The precision for Cd using Pb as internal standard improved from 24% to 4% RSD while that for Cu using Zr improved from 16% to 9% RSD.

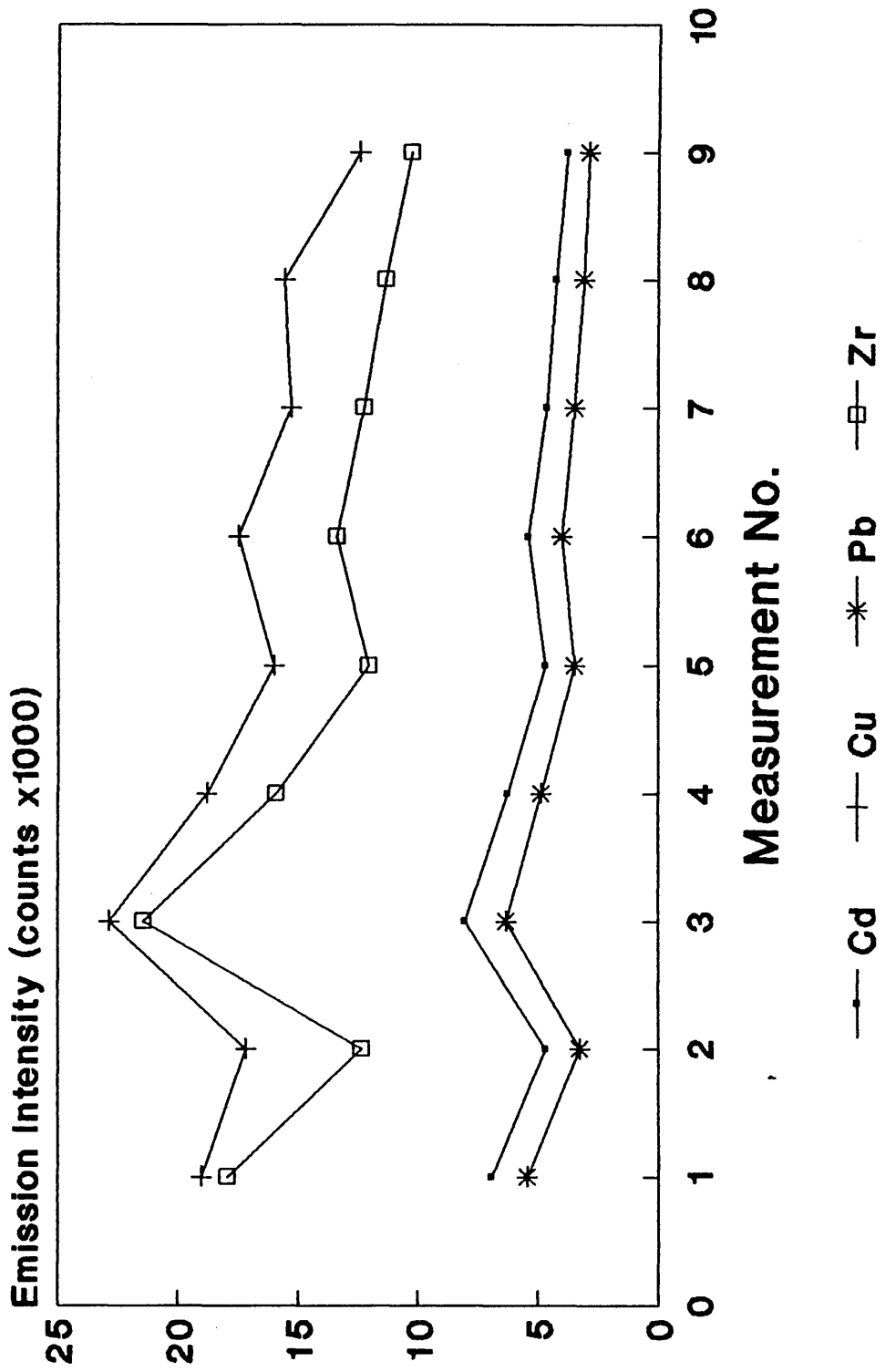


Figure 95. Precision Study Data.

As with measurements made on polypropylene, the use of internal standardisation offers significant improvements to analytical precision. But careful choice of the most appropriate internal standard is required. Cadmium and lead appear to be well suited probably because they have similar laser sampling and spattering characteristics. When considering precision, this research has shown that metals, polymers and aqueous standards exhibit poor precision unless internal standardisation is used. But paints show good precision. Metals and polymers are likely to exhibit heterogeneity which could result in poor precision but aqueous standards and paints are more likely to be homogeneous. Since aqueous standards exhibit poor precision and paints show good precision, it seems likely that the ablation process itself also has a significant effect on precision. It is believed that the viscosity of paint plays a major role resulting in improved precision. The interaction of laser radiation with solids has been discussed earlier but liquids such as the aqueous standards present a different situation.

A laser pulse incident upon a liquid has a characteristically strong electric field which induces dielectric breakdown of the medium. A spark is produced and shock waves emanate from the focal volume. This forms the basis of Laser Induced Breakdown Spectroscopy which has been used for the analysis of liquids [142].

Ready also considered interaction of laser

radiation with liquids [143]. When discussing a variety of intensity-dependent phenomena that occur when lasers are focused into liquids, he concluded that these phenomena can include dielectric breakdown, plasma production and generation of high pressure acoustic waves with ejection of the liquid from its container.

This latter effect was observed during studies with aqueous standards (see section 6.1) and it is believed to be a significant contribution to imprecision.

However, more viscous liquids such as paints are felt to be less susceptible to these pressure waves and consequently are not ejected from the sample containers. When comparing the ablation of paints with that of aqueous solutions, there are differing processes occurring. Internal standardisation needs to be used for aqueous solutions as it compensates for these differences in the laser sampling process.

6.2 Laser Ablation and ETV Studies

Sample introduction has been described as the Achilles Heel of atomic spectroscopy [144] due to a significant weakness of conventional solutions nebulisation. That is poor sample transport efficiency.

Pneumatic nebulisation in atomic absorption spectroscopy may be expected to have an efficiency of 10%. In ICP spectroscopy a typical value is 1% [144]. Consequently, 99% of the analyte solution runs to waste. However, this conventional method of sample introduction does offer simplicity and reliability and lends itself to the majority of analyses where sample dissolution is required to provide suitable sampling statistics.

Electrothermal vaporisation has been investigated by many research groups as a sample introduction device for ICP showing sample transport efficiencies to be significantly higher. Two mechanisms that can inhibit transport of material to the plasma are the formation of non volatile carbides on the furnace walls and the deposition of volatile materials on the walls of the transport tubing [139,144].

Various transport efficiencies have been reported for ETV-ICP systems. A range of 5% to 45% has been reported for cadmium [140]. Park and co-workers [145] have described an ETV device designed specifically for sample introduction to an ICP. This design is claimed to provide transport efficiencies greater than

80%. However, most previously reported devices are less than 20% efficient [145].

Sample transport efficiencies associated with laser ablation ICP analysis are not well documented. Consequently, a series of experiments were conducted in an attempt to compare the transport efficiencies of laser ablation and ETV for this system. This was done by relating emission signals produced by laser ablation to those produced by ETV.

Initially, several calibration curves were generated by ETV. A range of multi-element standards were used containing aluminium, chromium, iron, zinc and titanium at concentrations of 50, 100, 500 and 1000mg/L. Aliquots of 5 microlitres were dispensed into new sample cups which were subjected to a high temperature cycle. A power setting of 2 was used on the furnace power supply along with a 20s ramp and 30s hold time. An integration time of 26s was used.

The furnace power supply was capable of delivering higher powers than that used to generate the ETV signal. The power setting of 2 was half the maximum value. It was felt that higher powers would have destroyed the graphite components in the sample chamber.

For every new sample cup used a blank value was determined by running a 5 microlitre aliquot of deionised water. The appropriate standard was then determined. All the intensity data are given in section 6.2.1.

These calibrations were then repeated using laser ablation. In this case, 30 microlitre aliquots were used. The laser was fired repetitively for 5s using Q-switched mode, 70J lamp energy and a frequency of 10Hz. Again, a blank value was obtained before each standard by ablating a 30 microlitre aliquot of deionised water. The intensity data is given in the following section.

6.2.1 Results

The intensity data for the ETV study is given below in table 33. These values correspond to the signal less the blank value measured immediately before the standard. This is an attempt to compensate for any contamination of the sample cups.

Mass ug	Conc mg/L	Al	Cr	Fe	Zn	Ti
0	0	0	0	0	0	0
0.25	50	78	973	503	64	608
0.5	100	-8	-28	910	264	-743
2.5	500	148	1944	9770	2539	278
5.0	1000	1637	1914	18120	5561	137

Table 33. Intensity Data for the ETV Calibration Study.

Of the above elements, only iron and zinc produced linear calibration curves (figures 96,97). The remaining

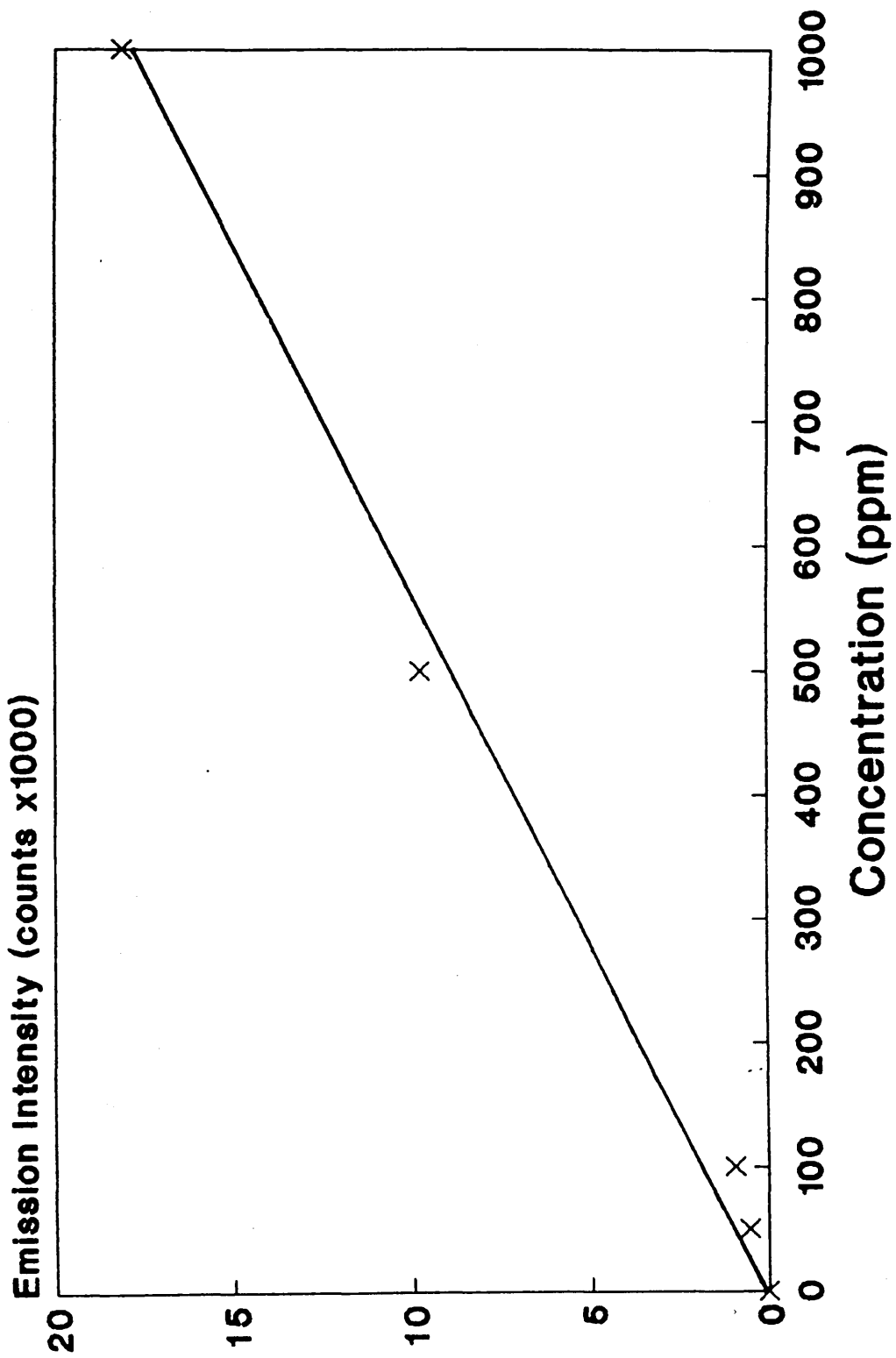


Figure 96. Aqueous Calibration for Iron by Electrothermal Vaporisation.

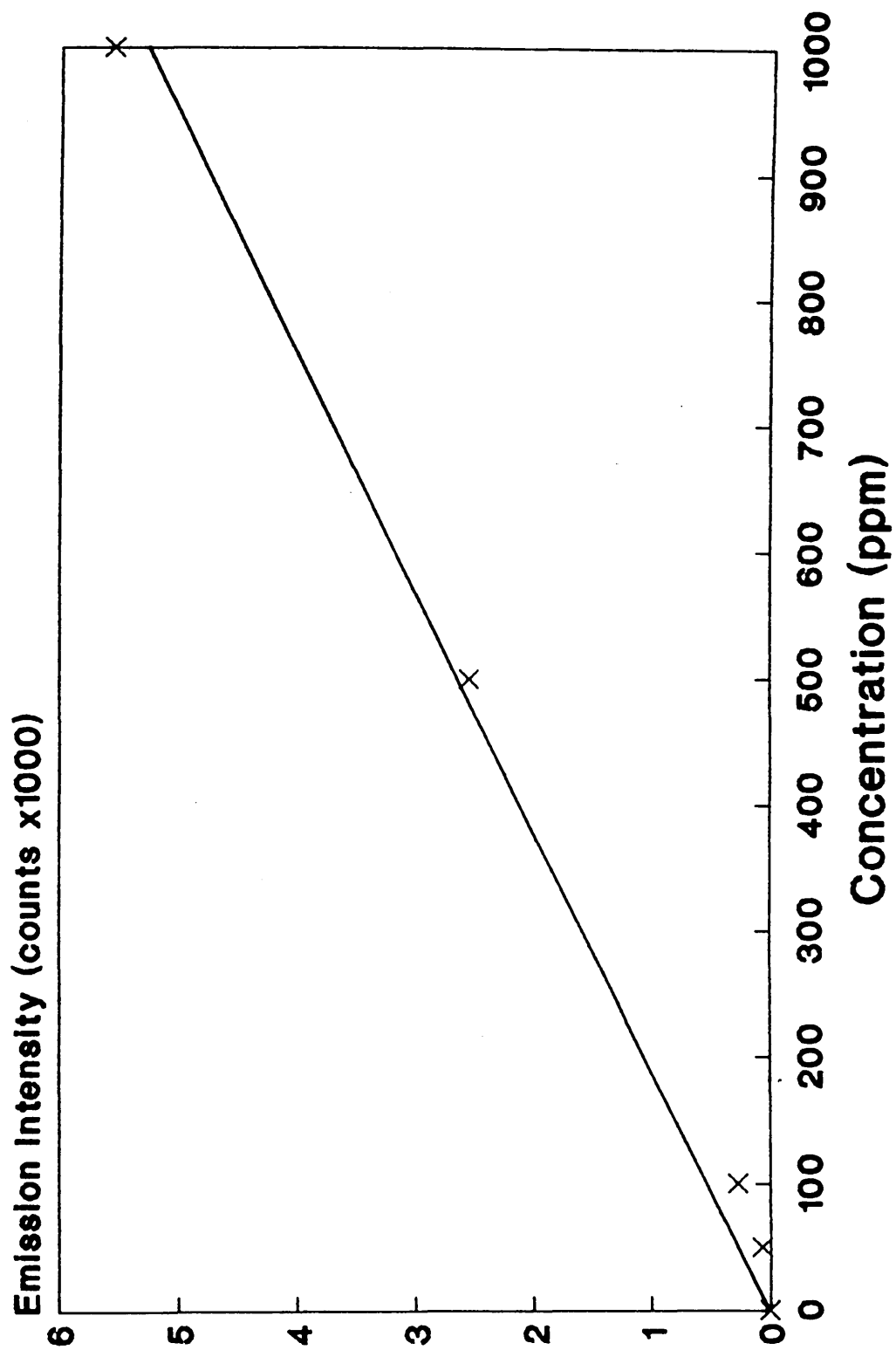


Figure 97. Aqueous Calibration for Zinc by Electrothermal Vaporisation.

elements produce little or no signal at all. These refractory elements will form stable carbides with the electrographite cup and as the temperature achieved within the furnace is insufficient to dissociate these compounds the analyte remains on the cup. Such elements are inappropriate for ETV analysis with the equipment used [139,144].

The above data were obtained from 5 microlitre aliquots of standard solution. As indicated in the table, intensity may be plotted as a function of mass of analyte since the concentration and volume of standard used are known. Hence, signals generated by laser ablation may be related to the above data.

The data for the laser ablation study are given below in table 34. Again, the blank values have been subtracted.

Mass ug	Conc mg/L	Al	Cr	Fe	Zn	Ti
0	0	0	0	0	0	0
1.5	50	1895	1984	7245	6783	7918
3.0	100	4042	4567	16547	11065	17569
15	500	21867	16920	52459	50945	79156
30	1000	42017	43504	122060	116917	184453

Table 34. Intensity Data for the Laser Ablation Calibration Study. See text for further details.

As expected all the above produce linear calibration curves. Those for aluminium and titanium are shown in figure 98. The calibration curve for chromium lies almost exactly on that for aluminium and has been omitted for clarity.

The laser ablation data reveals two important points. Firstly, relatively intense emission is obtained from the refractory elements that were immeasurable by ETV and secondly the emission from iron and zinc are significantly higher than when determined by ETV.

The data produced by laser ablation is based on a 30 microlitre sample whereas that for ETV was 5 microlitres. To compare similar analyte masses the laser ablation intensities must be divided by six. This corrected data are shown in table 35 and graphically in figure 99 for iron and figure 100 for zinc.

Mass ug	Zn		Fe	
	ETV	LA	ETV	LA
0	0	0	0	0
0.25	64	1130	503	7245
0.50	264	1844	910	16547
2.50	2539	8491	9770	52459
5.00	5561	19489	18120	122060

Table 35. Relative Intensities Based on a 5 Microlitre Sample. See text for experimental details.

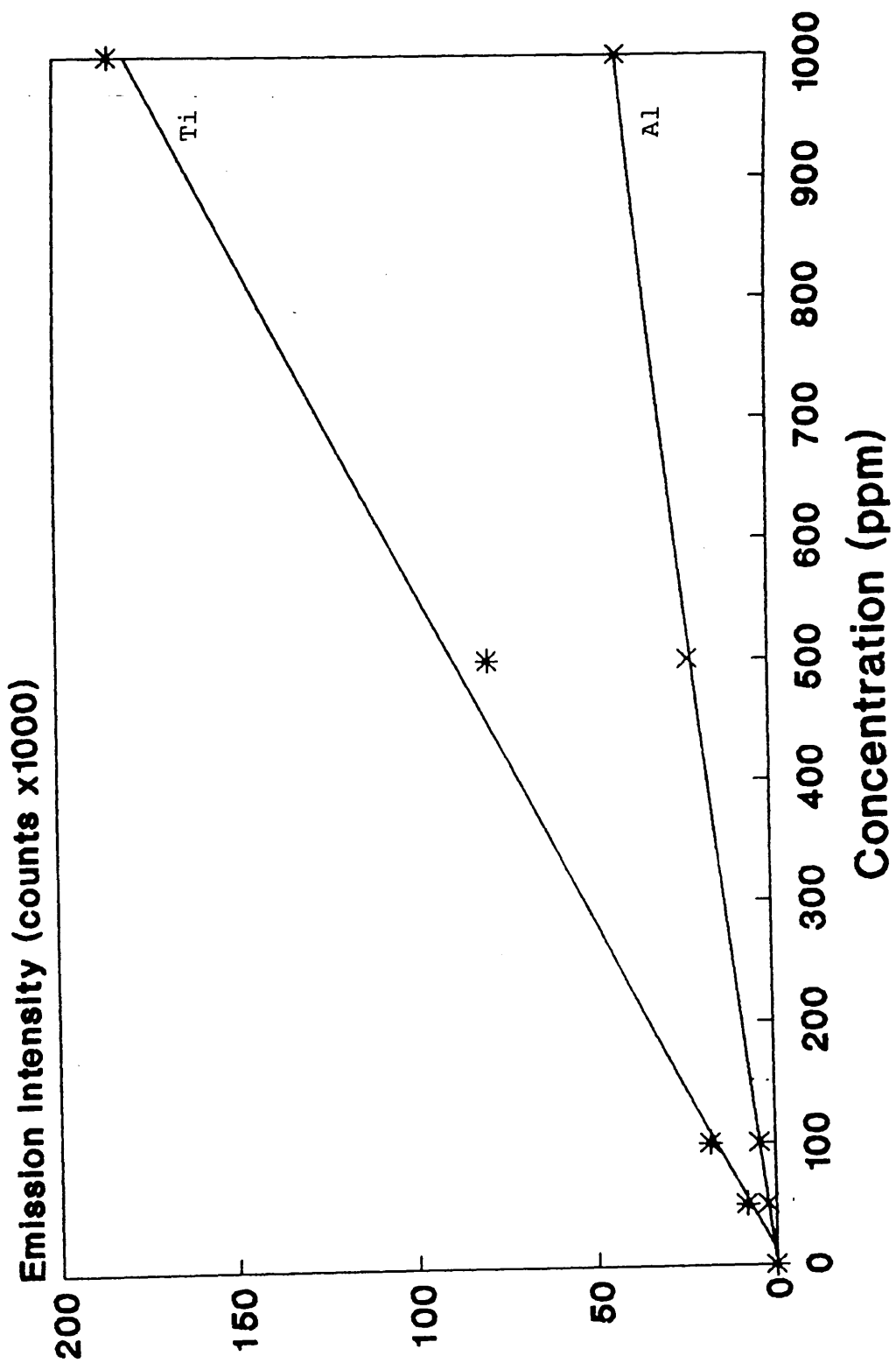


Figure 98. Aqueous Calibration by Laser Ablation for Titanium and Aluminium.

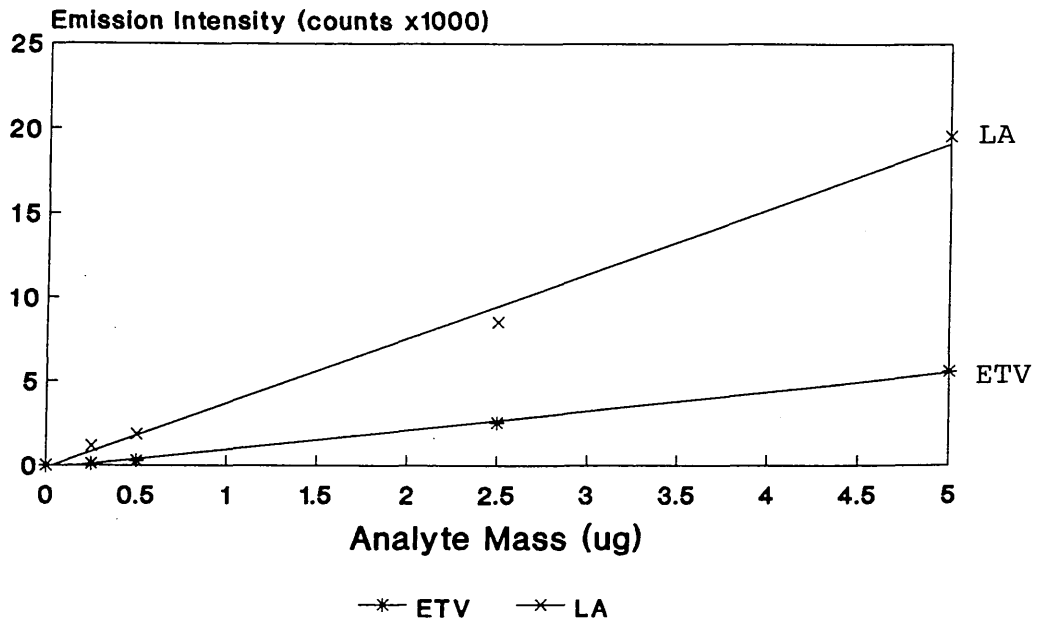


Figure 100. Comparison of LA and ETV Calibration Curves for Zn.

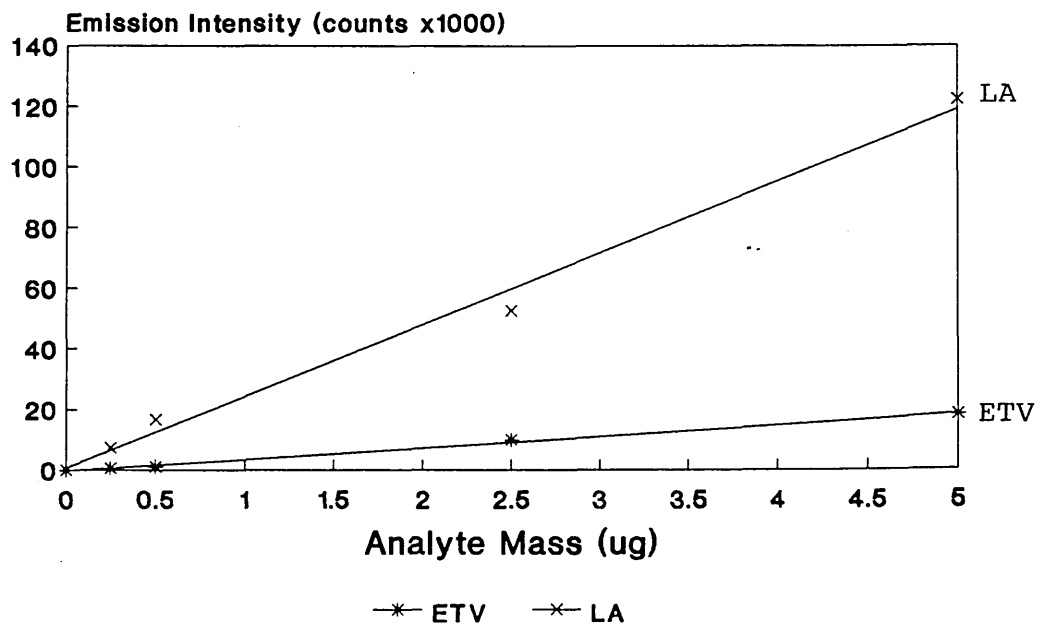


Figure 99. Comparison of LA and ETV Calibration Curves for Fe.

Examination of this data shows that laser ablation offers improved sensitivity for Zn and Fe compared with ETV. This is due to a larger mass of analyte reaching the plasma as a consequence of improved sample transport efficiency.

Furnace design clearly has an effect on transport efficiency when using ETV as a sample introduction device for ICP. Other major factors are pre-vaporisation losses of analyte, deposition of analyte during transport to the plasma and the formation of stable, refractory carbides [139]. Consequently, even when using devices specifically designed for such an application, transport efficiencies can be low.

The calibration curves shown in figures 99 and 100 were used to calculate the sensitivity for both elements by laser ablation and ETV. The sensitivity is defined as the gradient of the calibration curve. Sensitivities for zinc were 19.5 counts per mg/L by laser ablation and 5.6 counts per mg/L by ETV. Hence, laser ablation is 3.5 times more sensitive than ETV for zinc. Sensitivities for iron were 122.1 counts per mg/L by laser ablation and 18.1 counts per mg/L by ETV. Hence, laser ablation is 6.7 times more sensitive than ETV for iron.

6.2.2 Discussion

This study has shown that the ETV device used is not capable of producing ETV signals for refractory elements as they form stable carbides [139]. Of the elements examined, only iron and zinc produce acceptable calibration data.

Laser ablation produced linear calibration data for all five elements studied, including the refractories and demonstrated a marked improvement in sensitivity for iron and zinc when compared with ETV (see figure 99,100).

Clearly, laser ablation of liquids is a viable option for calibration purposes. It remains to be seen if such calibrations are suitable for the direct analysis of solids by laser ablation. This area requires further investigation.

CHAPTER SEVEN

CONCLUSIONS AND FUTURE WORK

7.0 CONCLUSIONS AND FUTURE WORK

Research has shown that the experimental facilities used were suitable for the introduction of samples to an ICP by laser ablation. Many of the operating conditions were optimised and the significance of parameters such as focusing distance and mode of laser operation were discovered. The Q-switched mode of laser operation was preferred for best sensitivity.

The examination of metallurgical samples provided rapid qualitative data, although precision was poor due to sample heterogeneity. Electrothermal melting of samples to fuse several turnings made ablation much simpler without having to align the laser on an individual turning. However, since this process removed many of the volatile elements the technique was more amenable to refractory elements.

Laser ablation was applied to paints and polymers for the first time. This proved successful and provided qualitative and semi-quantitative data. Furthermore, information on analyte distribution was made available which traditional bulk analysis would not reveal. Operating conditions were found to be sample independent but precision was far superior to metallurgical samples. One to four percent relative standard deviation was obtained which ranks among the best precision reported for laser ablation ICP studies.

It also proved possible to apply laser ablation to aqueous solutions. The extended linear range

associated with conventional nebulisation also characterises laser ablation. Precision was poor mainly due to the methods of controlling the ablation period and the production of acoustic pressure waves within the solution sample which results in extensive spattering of the sample. Linear calibrations were easily achieved and analysis by laser ablation has produced some results which show good agreement with those obtained by conventional ICP analysis. However, poor precision results in relatively inferior detection limits.

Further work may include the following. The experimental facilities may be improved by mounting the ablation chamber on an X-Y-Z stage for accurate positioning. Add to this a camera and a coaxial HeNe laser to assist positioning and the need to fuse samples is negated. Individual turnings may then be ablated and fine positioning of the sample under the laser is possible.

The electrothermal heating capability of the system described may be used to investigate laser ablation of molten samples. Although unsuitable for volatile elements, precision for refractory elements may be improved as a consequence of the fluidity of the molten material. This may be applicable to the steel making industry.

Shortening the distance between the sample chamber and ICP will improve sample transport efficiencies as would optimisation of chamber geometry and the use of pyrolytically coated sample cups.

Generating harmonics of the 1064nm laser wavelength would allow the study of alternative wavelengths. Mass spectroscopic detection would improve sensitivity and facilitate dating of archeological objects by studying the carbon-12 carbon-14 ratio.

Computer control of the laser is likely to improve precision of measurements of aqueous solutions by accurately controlling the ablation period.

Experimentally, simplex optimisation of laser operating conditions should be considered to confirm or otherwise the conditions arrived at by univariate optimisation.

Precision for aqueous solutions needs further consideration. Internal standardisation provides slight improvements but the use of a more viscous medium such as glycerol to help overcome the effects of acoustic pressure waves warrants investigation.

Standard additions experiments should be performed to investigate the presence of matrix effects which may prevent the analysis of solids using aqueous calibration. Spiked recovery experiments would support this.

Precision for paint samples may be improved by using longer ablation periods ie greater than 10s. This possibility needs investigating as the integration of a steady state signal may be beneficial. However it may simply result in analyte erosion.

Alternative sample cups of higher purity such as teflon and tantalum are desirable. This would result

in lower blank intensities, which in conjunction with improved precision would result in improved detection limits.

The technique of laser ablation ICP is capable of generating useful analytical data, some of which can not be obtained by conventional bulk analysis. Although commercial laser ablation ICP mass spectrometry systems are available, it remains a highly specialised technique requiring further investigation. It may then be possible to produce accurate quantitative analysis of solid samples while avoiding lengthy sample dissolution techniques.

REFERENCES

1. Bisson, W.J. & Dennen, W.H., *Science*, 1962, 135, 921.
2. Melvill, T., *Essays and Observations, Physical and Literary*, Edinburgh, 1756, 2, 12-90.
3. Wollaston, W.H., *Phil. Trans.*, 1802, 92, 365-380.
4. Fraunhofer, J., *Ann. Physik (Gilbert's Ann.)*, 1817, 56, 264-313.
5. Talbot, H.F., *Edinburgh J. Sci. (Brewster's)*, 1826, 5, 77.
6. Brewster, D., *Trans. Roy. Soc. (Edinburgh)*, 1823, 9, 433.
7. Roscoe, Sir H., *Trans. Chem. Soc. London*, 1900, 77, 513.
8. Simmler, R.T., *Jahresber. d. Naturforsch. Ges. Graubundens (1859-1860)*, N.F.6, 194-218 (1861).
9. Champion, P., Pellet, H. & Grenier, M., *Compt. Rend.*, 1873, 76, 707-711.
10. Gouy, A., *Ann. Chim. Phys. (5)*, 1879, 18, 5-101.
11. Lundegardh, H., *Arkiv. Kemi. Min. Geol.*, 1928, 10A, No.1.
12. Lundegardh, H., *Z. Physik*, 1930, 66, 109-118.
13. Lundegardh, H., *Lantbruks-Hogsk. Ann.*, 1936, 3, 49.
14. Jansen, W.H., Heyes, J. & Richter, C., *Z. Physik. Chem. (Leipzig)*, 1935, 174A, 291-300.
15. Waibel, F., *Wiss. Veroffentl. Siemens-Werken*, 1935, 14, 32-40.
16. Schuhknecht, W., *Angew. Chem.*, 1937, 50, 299-301.
17. Pratt, P.F. & Larson, W.E., *Anal. Chem.*, 1949, 21, 1296.
18. Ivanov, D.N., *Pochvovedenie*, 1953, No.1, 61-66.
19. Lundegardh, H., *Die Blattanalyse*, Gustav Fischer, Jena 1945 (Transl. by R.L. Mitchell, *Leaf Analysis*, Hilger, London, 1951).
20. Barnes, R.B., et al, *Ind. Eng. Chem., Anal: Ed.*, 1945, 17, 605-611.
21. Gilbert, P.T., *Am. Soc. Testing Materials, Spec. Tech. Publ.*, 1960, 269, 73-156.
22. Knutson, K.E., *Analyst*, 1957, 82, 241-254.
23. Fassel, V.A., et al, *Spectrochim. Acta*, 1962, 18, 1127.
24. Rauterburg, E. & Knippenberg, E., *Angew. Chem.*, 1940, 53, 477-479.
25. Straubel, H., *Naturwissenschaften*, 1953, 40, 337.

26. Dunken,H., et al, Spectrochim. Acta, 1964,20,1531.
27. Babat,G.I., Vestn. Elektroprom., No.2,p.1;
No.3,p.2 (1942).
28. Babat,G.I., J. Inst. Elect. Eng., 1947,94,27.
29. Reed,T.B., J. Appl. Phys., 1961,32,821.
30. Reed,T.B., J. Appl. Phys., 1961,32,2534.
31. Reed,T.B., Int. Sci. Technol., 1962,6,42.
32. Greenfield,S., et al, Analyst, 1964,89,713.
33. Greenfield,S., et al, Anal. Chim. Acta, 1975,74,225.
34. Wendt,R.H. & Fassel,V.A., Anal. Chem., 1965,37,920.
35. Dickinson,G.W. & Fassel, V.A., Anal. Chem.,
1969,41,1021.
36. Fassel,V.A., Proc. 16th Coll. Spectr. Int.,
Heidelberg 1971, Plenary lectures and reports,
Adam Hilger, London, 1972, p.63.
37. Boumans,P.W.J.M. & de Boer,F.J., Spectrochim.
Acta, 1972,27B,391.
38. Fassel,V.A. & Kniseley,R.N., Anal. Chem., 1974,
46,1110A,1155A.
39. Boumans,P.W.J.M. & de Boer,F.J., Spectrochim.
Acta, 1975,30B,309.
40. Scott,R.H., et al, Anal. Chem., 1974,46,75.
41. Mermet,J.M., C.R. Acad. Sci. Ser., 1975,B281,273.
42. Ohls,K.D., Golightly,D.W. & Montaser,A.,
"Mixed Gas, Molecular Gas and Helium Inductively
Coupled Plasmas Operated at Atmospheric and Reduced
Pressures", in Inductively Coupled Plasmas in
Analytical Atomic Spectrometry, Montaser,A. and
Golightly,D.W., eds., Ch.15, VCH Publishers.
43. Koirtyohann,S.R., et al, Anal. Chem., 1980,52,1965.
44. Greenfield,S., et al, Talanta, 1976,23,1.
45. Barnes,R.M., C.R.C. Crit. Rev. Anal. Chem.,1978,7,203.
46. Hasegawa,T. & Haraguchi,H., "Fundamental Properties
of Inductively Coupled Plasmas", in Inductively
Coupled Plasmas in Analytical Atomic Spectrometry,
Montaser,A. & Golightly,D.W., eds., Ch.8, VCH
Publishers.

47. Thorne, A.P., "Spectrophysics", Chapman and Hall, London, 1974.
48. Houk, R.S., et al, Appl. Spectrosc., 1983, 37, 425.
49. Griem, H.R., "Plasma Spectroscopy", McGraw-Hill, New York, 1964.
50. Mermet, J.M., C.R. Acad. Sci. Ser., 1975, B281, 273.
51. Boumans, P.W.J.M. & de Boer, F.J., Spectrochim. Acta, 1977, 32B, 365.
52. Uchida, H., et al, Spectrochim. Acta, 1980, 35B, 881.
53. Larson, G.F. & Fassel, V.A., Appl. Spectrosc., 1979, 33, 592.
54. Hasegawa, T. & Haraguchi, H., Spectrochim. Acta, 1985, 40B, 1505.
55. Hasegawa, T. & Haraguchi, H., Spectrochim. Acta, 1985, 40B, 1067.
56. Boumans, P.W.J.M., "Inductively Coupled Plasmas" in Inductively Coupled Plasma Emission Spectroscopy, Part 1, Boumans, P.W.J.M., ed., Ch.3, p.86, John Wiley & Sons, U.S.A., 1987.
57. Browner, R.F. & Boorn, A.W., Anal. Chem., 1984, 56(7), 786A.
58. Babington, R.S., U.S. Patent 3,421,692, 1969.
59. Anderson, H., et al, in Developments in Atomic Plasma Spectrochemical Analysis, Barnes, R.M., ed., Heyden, London, 1981, pp.251-277.
60. Olsen, K.W., et al, Anal. Chem., 1977, 49, 632.
61. Scott, R.H., et al, Anal. Chem., 1974, 46, 75.
62. Salin, E.D. & Horlick, G., Anal. Chem., 1979, 51, 2284.
63. Kirkbright, G.F. & Walton, S.J., Analyst, 1982, 107, 276.
64. Zhang Li-Xing et al, Appl. Spectrosc., 1983, 37, 250.
65. Ohls, K. & Sommer, D., Fresenius Z. Anal. Chem., 1980, 304, 97.
66. Ohls, K. & Sommer, D., Proc. Int. Winter Conf., 1981, 321.
67. Abdullah, M. et al, Spectrochim. Acta, 1984, 39B, 1129.
68. Pettit, W.E. & Horlick, G., Spectrochim. Acta, 1986, 41B, 699.
69. Shao, Y. & Horlick, G., Appl. Spectrosc., 1986, 40, 386.

70. McLeod, C.W. et al, *Spectrochim. Acta*, 1986, 41B, 63.
71. Page, A.G. et al, *Spectrochim. Acta*, 1984, 39B, 551.
72. Blakemore, W.M. et al, *Anal. Chem.*, 1984, 56, 1376.
73. Tikkanen, M.W. & Niemcsyk, T.M., *Anal. Chem.*, 1984, 56, 1997.
74. Hull, D.R. & Horlick, G., *Spectrochim. Acta*, 1984, 39B, 843.
75. Jones, J.L. et al, *Appl. Spectrosc.*, 1971, 25, 628.
76. Farnsworth, P.B. & Hieftje, G.M., *Anal. Chem.*, 1983, 55, 1414.
77. Scott, R.H., *Spectrochim. Acta*, 1978, 33B, 123.
78. Marks, J.Y. et al, *Spectrochim. Acta*, 1983, 38B, 107.
79. Beaty, J.S. & Belmore, R.J., *Test. Eval.*, 1984, 12, 212.
80. Aziz, A. et al, *Spectrochim. Acta*, 1984, 39B, 1091.
81. Golightly, D.W. & Montaser, A., Paper no.36, Winter Conference on Plasma Spectrochemistry, Kailua-Kona, Hawaii, 1986.
82. Kantor, T. et al, *Talanta*, 1976, 23, 585.
83. Laqua, K., "Analytical Spectroscopy using Laser Atomisers" in *Analytical Laser Spectroscopy*, Omenetto, N., ed., Chemical Analysis Series, Vol.50, Wiley-Interscience, New York, pp.47-118.
84. Ishizuka, T. & Uwamino, Y., *Spectrochim. Acta*, 1983, 38B, 519.
85. Abercrombie, F.N. et al, in "Applications of Inductively Coupled Plasmas to Emission Spectroscopy", Barnes, R.M., ed., Franklin Institute Press, Philadelphia, 1978, pp.121-145.
86. Carr, J.W. & Horlick, G., *Spectrochim. Acta*, 1982, 37B, 1.
87. Thompson, M. et al, *Analyst*, 1981, 106, 32.
88. Mitchell, P.G. et al, *Appl. Spectrosc.*, 1987, 41(1), 141.
89. Cremers, D.A. et al, SPIE Vol.540, Southwest Conference on Optics, 1985, pp.542-546.
90. Thompson, M. et al, *J. Anal. At. Spectrom.*, 1988, 3, 1133.
91. Hale, M. et al, *J. Geochem. Explor.*, 1984, 21, 361.
92. Chenery, S. et al, *Anal. Proc.*, 1988, 25, 68.
93. Thompson, M. et al, *J. Anal. At. Spectrom.*, 1989, 4, 11.
94. Thompson, M. et al, *J. Anal. At. Spectrom.*, 1990, 5, 49.

95. Thompson, M. et al, *J. Anal. At. Spectrom.*, 1988, 3, 1133.
96. Gray, A.L., *Analyst*, 1985, 110, 551.
97. Tye, C. et al, *Int. Lab.*, 1987, 12, 34.
98. Arrowsmith, P. & Hughes, S.K., *App. Spec.*, 1988, 42, 1231.
99. Arrowsmith, P., *Anal. Chem.*, 1987, 59, 1437.
100. Greenfield, S. & Hutton, T.P., *ICP Inf. Newsl.*, 1980, 6, 267.
101. Dagnall, R.M. et al, *Anal. Chim. Acta*, 1971, 54, 397.
102. Mohamed, N. et al, *Appl. Spectrosc.*, 1981, 35, 153.
103. Ebdon, L. & Cave, M.R., *Analyst*, 1982, 107, 172.
104. Townes, C.H. & Schawlow, A.L., *Phys. Rev.*, 1958, 112, 1940-1949.
105. Maiman, T.H., *Nature*, 1960, 187, 493.
106. Faller, J.F. & Wampler, E.J., *Sci. Am.*, 1970, 38.
107. Yeh, Y. & Cummings, H.Z., *Appl. Phys. Lett.*, 1964, 4, 176.
108. Winefordner, J.D. & Vickers, T.J., *Anal. Chem.*, 1964, 36, 161.
109. Webb, J.P., *Anal. Chem.*, 1972, 44, 30A.
110. Allkins, J.R., *Anal. Chem.*, 1975, 47, 752A.
111. Falk, H. et al, *Spectrochimica Acta*, 1988, 43B, 1101.
112. Omenetto, N. et al, *Spectrochimica Acta*, 1988, 43B, 1111.
113. Bolshov, M.A. et al, *Spectrochimica Acta*, 1988, 43B, 519.
114. Dittrich, K. & Stark, H.J., *J. Anal. At. Spectrom.*, 1987, 2, 63.
115. Omenetto, N. et al, *Spectrochim. Acta*, 1987, 42B(6), 807.
116. Bolshov, M.A. et al, *Spectrochim. Acta*, 1981, 36B, 1143.
117. Berthoud, T. et al, *Appl. Spectrosc.*, 1987, 41(5), 913.
118. Tremblay, M.E. et al, *Anal. Chim. Acta.*, 1987, 199, 111.
119. Preli, F.R. et al, *Spectrochim. Acta*, 1988, 43B, 501.
120. Conzemius, R.J. & Capellen, *Int. J. Mass Spectro. Ion Phys.*, 1980, 34, 197.
121. Mayo, S. et al, *Anal. Chem.*, 1982, 54, 553.
122. Hercules, D.M., *Anal. Chem.*, 1982, 54(2), 280A.
123. Sekreta, E. et al, *Spectrochim. Acta*, 1988, 43B, 679.
124. Humphries, M.R., *Chem. in Brit.*, 1989, 25(2), 165.
125. Green, R.B. et al, *Appl. Phys. Lett.*, 1976, 29, 727.
126. Green, R.B. et al, *J. Am. Chem. Soc.*, 1976, 98, 8517.
127. Mallard, W.G. et al, *J. Chem. Phys.*, 1982, 76, 3483.

128. Rockney, B.H. et al, *Chem. Phys. Lett.*, 1982, 87, 141.
129. Smyth, K.C. & Mallard, W.G., *J. Chem. Phys.*, 1982, 77, 1779.
130. Schenck, P.K. et al, *J. Chem. Phys.*, 1978, 69, 5147.
131. Axner, O. et al, *Appl. Spectrosc.*, 1987, 41(1), 19.
132. Travis, J.C. et al, *Prog. Analyt. Atom. Spectrosc.*, 1984, 7, 199.
133. Mossotti, V.G. et al, *Spectrochim. Acta*, 1967, 23B, 197.
134. Kantor, T. et al, *Talanta*, 1976, 23, 585.
135. Omenetto, N., *Analytical Laser Spectroscopy*, John Wiley & Sons, 1979.
136. Ready, J.F., *Effects of High Power Laser Radiation*, Ch. 4, Academic Press, 1971.
137. Marshall, J. et al, *J. Anal. At. Spectrom.*, 1989, 4, 251R.
138. Booth, P.K. & McLeod, C.W., *Mikrochim. Acta*, 1989 III, 3-6, 283.
139. Matusiewicz, H., *J. Anal. At. Spectrom.*, 1986, 1, 171.
140. Millard, D.L. et al, *Analyst*, 1980, 105, 502.
141. Thompson, M. et al, *J. Anal. At. Spectrom.*, 1989, 4, 11.
142. Cremers, D.A. et al, *Appl. Spectrosc.*, 1984, 38(5), 721.
143. Ready, J.F., *Effects of High Power Laser Radiation*, Chapter 6, Academic Press, 1971.
144. Browner, R.F. & Boorn, A.W., *Anal. Chem.*, 1984, 56(7), 786A
145. Park, C.J. et al, *Can. J. Spectrosc.*, 1987, 32(2), 29.
146. Arrowsmith, P., *Anal. Chem.*, 1987, 59, 1437.
147. Arrowsmith, P. & Hughes, S.K., *Appl. Spectrosc.*, 1988, 42(7), 1231.
148. Chenery, S. et al, *Anal. Proc.*, 1988, 25, 68.
149. Routh, M.W. & Tikkanen, M.W., *Inductively Coupled Plasmas in Analytical Atomic Spectroscopy*, Eds. Montaser & Golightly, Chapter 12, VCH Publishers, 1987.
150. Thompson, M., as ref. 149, Chapter 5.

BIBLIOGRAPHY

1. O'Shea, D.C. et al, Introduction to Lasers and Their Applications, Addison Wesley Publishing Co., 1977.
2. Omenetto, N. (Ed.), Analytical Laser Spectroscopy, John Wiley and Sons Inc., 1979.
3. Ready, J.F., Effects of High Power Laser Radiation, Academic Press, N.Y., 1971.
4. Wilson, J. and Hawkes, J.F.B., Lasers Principles and Applications, Prentice Hall (UK) Ltd., 1987.
5. Montaser, A. and Golightly, D.W. (Eds.), Inductively Coupled Plasmas in Analytical Atomic Spectrometry, VCH Publishers Inc., 1987.